Titre: Title:	Self-healing of fibre reinforced concretes containing various admixtures under laboratory and outdoor conditions
Auteur: Author:	Kim-Séang Lauch
Date:	2021
Type:	Mémoire ou thèse / Dissertation or Thesis
Référence: Citation:	Lauch, K.-S. (2021). Self-healing of fibre reinforced concretes containing various admixtures under laboratory and outdoor conditions [Ph.D. thesis, Polytechnique Montréal]. PolyPublie. https://publications.polymtl.ca/9143/

Document en libre accès dans PolyPublie
Open Access document in PolyPublie

URL de PolyPublie: PolyPublie URL:	https://publications.polymtl.ca/9143/
Directeurs de recherche: Advisors:	Jean-Philippe Charron
Programme: Program:	Génie civil

POLYTECHNIQUE MONTRÉAL

affiliée à l'Université de Montréal

Self-healing of fibre reinforced concretes containing various admixtures under laboratory and outdoor conditions

KIM-SÉANG LAUCH

Département des Génies Civil, Géologique et des Mines

Thèse présentée en vue de l'obtention du diplôme de *Philosophiæ Doctor*

Génie Civil

Août 2021

POLYTECHNIQUE MONTRÉAL

affiliée à l'Université de Montréal

Cette thèse intitulée :

Self-healing of fibre reinforced concretes containing various admixtures under laboratory and outdoor conditions

Présentée par **Kim-Séang LAUCH**

en vue de l'obtention du diplôme de *Philosophiæ Doctor*

a été dûment acceptée par le jury d'examen constitué de :

Pierre LEGER, président

Jean-Philippe CHARRON, membre et directeur de recherche

Claudiane OUELLET-PLAMONDON, membre

Marta ROIG-FLORES, membre

DÉDICACE

À la mémoire de Kong et Ma,

REMERCIEMENTS

1.59 m³ de béton produit, 177 prismes et 169 cylindres manipulés, 3124 heures de mesures de perméabilité, 299 essais de flexion et 391 heures de rédaction et de révision plus tard... voilà qu'il ne me reste plus qu'à écrire cette dernière section, et non la moindre, de cette thèse. Derrière ces nombres conséquents, se cache évidemment plus d'une personne. J'ai eu la chance d'avoir été bien entourée pendant ces quatre années de doctorat et je voudrais exprimer ma gratitude à toutes les personnes qui m'ont aidée de près ou de loin à réaliser ce projet.

> Moins que d'autres, je ne savais si le but de notre vie avait un sens. Mais je savais, plus que quiconque, qu'elle avait une valeur. Par elle-même, directement, hors de toute réussite ou déroute. Cette valeur venait du combat […]. Moi je me battais contre moi pour gagner pas à pas un visage.

En premier lieu, je voudrais profondément remercier mon directeur de recherche, Jean-Philippe Charron et son associée de recherche Clélia Desmettre.

Depuis ce cours de Techniques du béton suivi en 2013 lors d'un programme d'échange international, Jean-Philippe m'a marquée par la qualité de son enseignement et sa passion pour le béton. Il a suscité mon intérêt pour la recherche dans ce domaine, orientant ainsi le début de ma carrière professionnelle. Je n'aurais pas pu imaginer un meilleur directeur de recherche pour me guider, me conseiller, partager son expertise, m'encourager et me soutenir tout au long de ce doctorat. Merci pour votre bienveillance.

J'ai également été bien accompagnée par Clélia pour le travail quotidien. Clélia, merci d'avoir toujours pris le temps pour moi, pour répondre à mes questions, pour m'aider avec le dispositif de perméabilité et pour réviser les nombreuses versions préliminaires de mes articles. J'ai grandement bénéficié de ton aide précieuse, tes conseils avisés et tes réflexions enrichissantes. Merci pour les nombreux trajets à Québec, à Sherbrooke et ailleurs, merci pour ces moments de partage hors Polytechnique. Enfin, un grand merci de m'avoir soutenue à travers les épreuves.

> Mais ce visage-là était tout sauf donné par avance […]. Il devait être conquis tout au bout du contre, à travers le contre et par lui.

> Lorsqu'on me demandait ce que j'espérais trouver en Extrême-Amont, cette question banale posée mille fois, je répondais maintenant : « J'espère trouver mon visage ».

> Et je le verrai, comme je vous vois devant moi, comme on se regarde dans un miroir enfin exact. Je verrai ce visage que je me suis fait tout au long de ma vie, juste avant de mourir. Ce sera ma récompense.
>
> π Pietro Della Rocca, *La Horde du Contrevent* – Alain Damasio

Kim-Séang LAUCH

15 juillet 2021

RÉSUMÉ

Les fissures présentes dans le béton, qui sont inévitables, accélèrent la pénétration d'agents agressifs comme le CO_2 ou les chlorures, causant des dégradations et réduisant ainsi la durabilité des structures. En Amérique du Nord, 40% des ponts sont dans un état déficient et des milliards de dollars sont investis chaque année pour leur réparation. Des bétons avec des propriétés auto-cicatrisantes constituent une solution prometteuse aux problèmes de durabilité et de sécurité des structures de plus en plus préoccupants.

Ce projet de recherche a pour but d'évaluer la capacité d'auto-cicatrisation de bétons contenant différents agents cicatrisants (ajout cristallin AC, agent expansif CSA, polymère superabsorbant SAP et combinaisons de deux ajouts AC+SAP et AC+CSA), exposés dans des conditions de laboratoire (immersion sous eau, cycles de mouillage/séchage, air pendant 3 mois, écoulement d'eau continu pendant 1 semaine) et en condition réelle à l'extérieur (pendant 1 an à Montréal). La cicatrisation a été évaluée par des mesures de perméabilité à l'eau, de regain mécanique, d'observations visuelles et d'analyses de la microstructure (MEB-EDS) sur le même spécimen.

Les résultats du Programme Expérimental 1 ont démontré la robustesse (répétabilité et fiabilité) du nouveau dispositif de perméabilité à l'eau développé pour des prismes présentant une fissure de flexion. Le coefficient de perméabilité s'est avéré être le paramètre le plus sensible à la fissuration et donc idéal pour évaluer l'évolution de la cicatrisation.

Concernant le Programme Expérimental 2, les résultats ont mis en évidence l'impact majeur de la condition d'exposition, que ce soit au niveau des mesures de perméabilité, des regains mécaniques et de la microstructure. Les résultats de perméabilité ont montré une cicatrisation rapide au début sous eau, suivie d'une stabilisation. Dans les autres expositions, l'évolution de la cicatrisation était plus progressive. En termes de Healing Ratios (*HR*), les cycles de mouillage/séchage ont permis de mieux cicatriser en moyenne (*HR* = 93%) que sous eau (*HR* = 84%). Dans l'air et sous écoulement continu d'eau, des Healing Ratios de 46% et 71% en moyenne ont respectivement été obtenus. Contrairement à ce qui était attendu, l'écoulement continu n'a pas montré d'accélération significative de la cicatrisation par rapport à l'immersion sous eau. Après 1 an d'exposition extérieure, les prismes ont atteint un *HR* moyen de 71%. Des équivalences de temps entre les cycles de mouillage/séchage et la condition extérieure ont pu être établies. Les résultats de regains

mécaniques ont mis en évidence la condition extérieure par rapport aux expositions en laboratoire. En moyenne, les regains de résistance en cycles de mouillage/séchage étaient légèrement supérieurs à ceux obtenus en immersion sous eau (99% contre 95%). Par contre, les regains obtenus pour les prismes à l'extérieur ont atteint 109% en moyenne.

En ce qui concerne l'effet des ajouts, celui-ci était en revanche moins marqué sur l'ensemble des mesures (perméabilité, mécanique et microstructure). Néanmoins, le mélange contenant du SAP a présenté globalement les meilleures performances aux niveaux durabilité et mécanique. De plus, les deux combinaisons AC+SAP et AC+CSA n'ont pas présenté de synergie particulière.

Les résultats obtenus dans cette thèse ont montré que le regain mécanique n'était pas corrélé à l'état de cicatrisation en termes de perméabilité à l'eau. Ces différentes performances s'expliquent par la microstructure. Le Healing Ratio semble lié à la densité des produits de cicatrisation, tandis que le regain mécanique serait influencé par le type de produits et leur répartition à l'intérieur des fissures. Sous eau, de l'ettringite et de la calcite ont été observées principalement au niveau des surfaces extérieures de la fissure. De même, en mouillage/séchage, des cristaux denses de calcite et vatérite ont été trouvés surtout aux surfaces de la fissure. Finalement, dans les prismes exposés à l'extérieur, de larges cristaux de calcite ont été observés à l'intérieur de la fissure et moins aux surfaces.

Enfin, dans le Programme Expérimental 3, la capacité de cicatrisation du mélange AC+CSA sous des chargements répétés a été étudiée. Deux phénomènes interviennent avec des effets opposés : la cicatrisation en cycles de mouillage/séchage et l'endommagement lors des rechargements. L'importance du niveau d'endommagement (rechargement sans ouvrir davantage la fissure et rechargement en augmentant l'ouverture de fissure) dicte lequel des phénomènes aura le plus d'ampleur. Dans le premier cas, l'effet de la cicatrisation l'emporte sur celui de l'endommagement. Dans le second cas, c'est l'endommagement qui est supérieur à la cicatrisation. Mais dans tous les cas, la cicatrisation se produit toujours après chaque rechargement.

En conclusion, les bétons avec ajouts ont présenté une cicatrisation modérée à élevée, même en condition réelle. L'utilisation de ces ajouts est plus économique et plus facilement applicable en industrie par rapport à d'autres approches de cicatrisation. Pour évaluer adéquatement le potentiel de cicatrisation de différents agents cicatrisants, il est recommandé de réaliser des essais à la fois de durabilité et mécaniques sur le même spécimen.

ABSTRACT

The presence of cracks in concrete, which are inevitable, accelerates the penetration of aggressive agents such as CO_2 or chlorides, causing deteriorations and hence reducing the durability of the structures. In North America, 40% of concrete bridges present some degradation and billions of dollars are spent every year for their repair and maintenance. As the durability and safety of structures are raising concerns, concretes with self-healing capacities are a promising solution in line with sustainable development.

This research project aims to evaluate the self-healing capacity of concretes containing various admixtures (crystalline admixture CA, expansive agent CSA, superabsorbent polymer SAP and combinations of two agents CA+SAP and CA+CSA), exposed in different laboratory (water immersion, wet/dry cycles, ambient air for 3 months, continuous water flow for 1 week) and long-term outdoor (1 year in Montreal climate) conditions. The self-healing capacity was assessed through water permeability measures, mechanical recovery evaluations, visual observations of crack closure and microscopic analyses (SEM-EDS) on the same specimen.

Results from Experimental Program 1 demonstrated the robustness (repeatability and reliability) of the new water permeability set-up developed for prisms with a flexural crack. The permeability coefficient was found the most sensitive parameter to cracking and is thus ideal for evaluating the evolution of self-healing.

Results from Experimental Program 2 highlighted the major impact of the exposure condition, which was noticeable through water permeability measures, mechanical recovery and microstructure. Permeability results showed that healing kinetics under water immersion were quick at the beginning and then stabilised. In the other expositions, the evolution of healing was more progressive. In terms of Healing Ratios (*HR*), wet/dry cycles were the most favourable condition (average *HR* = 93%) compared to water immersion (average *HR* = 84%). In air and under continuous water flow, average *HR* = 46% and 71% were obtained respectively. Contrary to what was expected, the continuous water flow did not particularly accelerate healing compared to water immersion. After 1 year in outdoor exposure, the prisms reached a *HR* = 71% in average. Time equivalence between wet/dry cycles and outdoor exposure could be established. Mechanical recovery results pointed out the effect of the outdoor exposure compared to the laboratory

conditions. In average, Strength Regains (*SR*) in wet/dry cycles were slightly superior to those obtained in water immersion (99% vs 95%). In contrast, the prisms exposed in outdoor condition reached *SR* = 109% in average.

The impact of the self-healing agents was less distinct in all types of measurements (permeability, mechanical recovery, microstructure). However, the mix containing SAP presented overall the best healing performance in terms of durability and mechanical properties. The combinations of CA+SAP and CA+CSA did not present any synergetic effect.

The results obtained in this thesis showed that the Strength Regain was not correlated to the healing state in terms of water permeability. These different performances are explained by the microstructure of the healing products. Healing Ratio may be linked to the density of the products, while Strength Regain may be governed by the type of products and their distribution inside the crack. Under water immersion, ettringite and calcite were observed mainly at the external crack surfaces. In wet/dry cycles, dense crystals of calcite and vaterite were also found mainly at the external crack surfaces. In outdoor exposure, large calcite crystals were more observed inside the crack in depth compared to the surfaces.

Lastly, the self-healing capacity of CA+CSA mix under repeated reloading was studied in Experimental Program 3. Two phenomena occur with opposite effects: healing in wet/dry cycles and damage during reloading. The magnitude of the reloading (reloading to the same crack width and reloading with increasing the crack opening) determines the dominant phenomenon. In the first case, healing outweighs damage. In the second case, the damage effect is superior to the healing effect. But in both cases, self-healing always occurs after each reloading.

In conclusion, a moderate to high healing in concretes containing various admixtures has been demonstrated, even in real outdoor exposition. Use of these self-healing agents is cheaper and easier to implement in the industry than other self-healing approaches. To adequately assess the self-healing potential of different healing agents, performing both durability and mechanical tests on the same specimen is recommended.

TABLE OF CONTENTS

LIST OF TABLES

LIST OF FIGURES

LIST OF SYMBOLS AND ABBREVIATIONS

Symbols

A Cross-section of the prism exposed to the water flow (m²)

A, A_i, A_f Crack area at the surface, initial or final crack area after healing (mm²)

b Length of the crack in Poiseuille's law (m)

d Flow path length of the crack in Poiseuille's law (m)

γ Weighting factor for the fibres analyses (-)

$\Delta h/L$ Applied pressure gradient (-)

$\Delta P, \Delta p$ Pressure gradient (kPa or Pa)

E_c Young's modulus (MPa or GPa)

ε Deformation (-)

$\varepsilon\text{-}\sigma$ Stress-strain curve

f_c Compressive strength (MPa)

ζ Reduction factor considering roughness of the crack (-)

θ Orientation angle of fibre (°)

K, K_w, K_{wi} (Water) permeability coefficient, initial water permeability coefficient (m/s)

$K_{pre\text{-}load}$ Stiffness at pre-cracking (MPa/mm)

$K_{pre\text{-}load,\ ref}$ Stiffness at pre-cracking of a reference uncracked specimen (MPa/mm)

K_{reload} Stiffness at reloading (MPa/mm)

$K_{reload,\ ref}$ Stiffness at reloading of a reference uncracked specimen (MPa/mm)

l_f Length of fibre (mm)

L_i Initial crack length at the surface from the tip to the notch root (mm)

μ Dynamic viscosity (Pa.s)

μ	Average
P	Load (N)
P-COD	Load-COD curve
Q	Flow rate (m³/s)
$Q_{measured}$	Flow rate measured (m³/s)
$Q_{Poiseuille}$	Flow rate determined with Poiseuille's law (m³/s)
R^2	Coefficient of determination (-)
Re	Reynolds number (-)
ρ	Density of fibres (fibres/cm²)
σ-COD	Stress-COD curve
σ	Stress (MPa)
σ	Standard deviation
σ_{max}	Maximal flexural stress at pre-cracking (MPa)
$\sigma_{pre\text{-}load}$	Stress at pre-cracking (MPa)
$\sigma_{pre\text{-}load,max}$	Maximal flexural stress at pre-cracking (MPa)
$\sigma_{pre\text{-}load,ref}$	Stress at pre-cracking from a reference uncracked specimen (MPa)
σ_{reload}	Stress at reloading (MPa)
$\sigma_{reload,max}$	Maximal flexural stress at reloading (MPa)
$\sigma_{reload,ref}$	Stress at reloading from a reference uncracked specimen (MPa)
σ_{unload}	Flexural stress before unloading (MPa)
ϕ	Diameter of a cylindrical specimen (mm)
ϕ_f	Diameter of fibre (mm)
w, w_i	Crack width at the surface (at the notch root or between the notch root and the tip), initial crack width before healing (mm)

w/b	Water to binder ratio (-)
w/c	Water to cement ratio (-)
w_{eq}	Equivalent crack width (mm)
%-m_{cement}	Percentage by mass of cement
%-vol	Percentage by volume of concrete

Chemical abbreviations

Al	Aluminium
$Al_2(SO_4)_3$	Aluminium sulphate
Ca	Calcium
$Ca(OH)_2$	Calcium hydroxide or portlandite
Ca^{++}	Calcium ion
$CaCO_3$	Calcium carbonate
CaO	Calcium oxide
C-A-S-H	Calcium aluminate silicate hydrates
CO_2	Carbon dioxide
CO_3^{--}	Carbonate ion
C-S-H	Calcium silicate hydrates
MgO	Magnesium oxide
Na_2SO_3	Sodium sulphite
NaCl	Sodium chloride
S	Sulphur
Si	Silicon

Abbreviations

AC   *Ajout cristallin*

Avg   Average

BFS   Blast-furnace slag

CA   Crystalline admixture

CA+CSA   Combination of CA and CSA

CA+SAP   Combination of CA and SAP

CMOD   Crack mouth opening displacement measured at the extensometer (mm)

$CMOD_{max}$ Limit of CMOD for reloading to 0.9 mm

CMOD+0.2   Reloading up to an additional 0.2 mm

COD   Crack opening displacement = CMOD

COV   Coefficient of variation

CR   Closing Ratio (-)

CSA   Calcium sulfoaluminate-based expansive agent (*agent expansif à base de CSA*)

ECC   Engineered cementitious composites

EDS   Energy-dispersive X-ray spectroscopy (*spectroscopie à dispersion d'énergie*)

FA   Fly ash

FRC(C)   Fibre reinforced concrete/cementitious composite

GUb-SF   General Use blended cement with silica fume

HPC   High performance concrete

HPFRC(C)   High performance fibre reinforced concrete/cementitious composite

HR   Healing Ratio (-)

LCA   Life cycle assessment

LVDT   Linear variable displacement transducer

LWA	Lightweight aggregates
MEB	*Microscope électronique à balayage*
NA	Value not available
NSC	Normal strength concrete
PE	Polyethylene
PP	Polypropylene
PVA	Polyvinyl alcohol
RF	Resonant frequency
RH	Relative humidity
SAP	Superabsorbent polymer (*polymère superabsorbant*)
SCMs	Supplementary cementitious materials
SEM	Scanning electron microscopy
SF	Silica fume
SI	Sealing Index (equivalent to Closing Ratio)
SP	Superplasticiser
SR	Strength Regain (-)
TGA	Thermogravimetric analysis
UHPC	Ultra high performance concrete
UHPFRC	Ultra high performance fibre reinforced concrete
UPV	Ultrasonic pulse velocity
XRD	X-ray powder diffraction

LIST OF APPENDICES

CHAPTER 1   INTRODUCTION

1.1 Context

Most reinforced concrete structures prematurely reach the end of their service life because of gradual degradations caused by the environment. In North America, 40% of bridges show some form of degradation (Lachemi et al., 2007) and about 20 billion dollars are spent each year for maintenance, repair or replacement of deteriorating structures (Li & Herbert, 2012). In Quebec (Canada), 25% of Quebec Ministry of Transportation bridges suffer from various disorders such as rebar corrosion and concrete cracking and require major repairs (Quebec Ministry of Transport, 2019), bridge upgrade investment being of the order of $2634 million per year (Quebec Ministry of Transport, 2013). In Europe, 50% of the annual construction budget is spent on maintenance and repair of existing structures (Cailleux & Pollet, 2009).

Most reinforced concrete structures are designed to present small cracks in service condition according to the requirements of the design codes CSA A23.3 and CSA S6 (Canadian Standards Association, 2014, 2019). However, their presence accelerates the penetration of aggressive agents such as CO_2 or chlorides and hence reduce the durability of the structures (Ghosh, 2009). As the durability and safety of structures are raising concerns, concretes with self-healing capabilities of cracks are a promising solution in line with sustainable development. Such construction materials could not only increase the service life of bridges, but also cut down the huge costs of maintenance and repair, and reduce the traffic and disturbances around construction sites for the road users.

Given durability issues experienced by reinforced concrete structures, research on self-healing concretes has been largely and more thoroughly studied in the last decade. For instance, the number of publications on that topic increased tenfold between 2010 and 2020 (from 25 to 233 papers)[1]. It is now well known that cementitious materials have an intrinsic self-healing capacity (autogenous healing) that can only heal very small cracks (0.01 to 0.1 mm) (De Belie et al., 2018). However, cracks present in concrete structures in practice are often wider. In the Canadian standards (Canadian Standards Association, 2014, 2019), the crack width limits allowed are 0.25 mm for

---

[1] Data from Web of Science with the words "self healing concrete" as topic, accessed date: 02/02/2021

highway bridges (CSA S6) and 0.3 mm for other structures exposed to outdoor environment (CSA A23.3). In the Eurocode 2 (European Committee for Standardization, 2004), the maximal crack width for outdoor exposition classes is also 0.3 mm. Therefore, different self-healing approaches have been developed to enhance the self-healing capacity of concrete for larger cracks, such as the introduction of bacteria, microcapsules, vascular systems and mineral admixtures in concrete (De Belie et al., 2018). However, there exists no consensus yet regarding the best self-healing approach. For lower costs, ease of implementation and availability in the market, the use of crystalline admixture (CA), expansive agent (CSA) and superabsorbent polymer (SAP) has been chosen in this project. Crystalline admixtures are a type of concrete permeability reducing admixtures, while calcium sulfoaluminate (CSA)-based expansive agents are a type of shrinkage-reducing admixtures. Superabsorbent polymers are cross-linked polymers traditionally used for internal curing in concrete as they can absorb and release water.

Interest in these admixtures as self-healing agents in concrete has increased this last decade. The self-healing potential of CA has been largely studied (Cuenca et al., 2018; Ferrara et al., 2014b; Roig-Flores et al., 2016; Sisomphon et al., 2012), but its beneficial effect to enhance self-healing is not unanimous yet. The use of CSA generally increases the self-healing capacity of concrete (Jiang et al., 2015; Park & Choi, 2021) and also presented a synergetic effect when combined with CA (Sisomphon et al., 2013). In general, water immersion is required for both CA and CSA to favour self-healing. The beneficial effect of SAP for self-healing has been demonstrated in water and wet/dry exposures (Deng & Liao, 2018; Gruyaert et al., 2016; Hong et al., 2020), but also in humid environment (Deng & Liao, 2018; Snoeck et al., 2014b). Besides, the addition of SAP to other self-healing agents accelerated self-healing (Li et al., 2020a; Park & Choi, 2018). In addition to the admixtures alone CA, CSA and SAP, the combinations of CA+CSA and CA+SAP will be studied in this project as well to maximise the self-healing capacity.

Several aspects can explain the variation of self-healing capacities found in literature. First, the mineral admixtures (CA and CSA), which are proprietary materials developed originally for other purposes, can present different compositions, particularly in the case of crystalline admixtures. The many types, shapes and sizes of SAP also influence the self-healing results.

Moreover, as there exists no standard yet to evaluate self-healing in concrete, a wide range of different testing methods (visual, transport or mechanical properties, analysis of healing products),

specimens (form, dimensions, type of crack) and parameters (age of pre-cracking, crack width, healing condition and duration) are used in literature (Ferrara et al., 2018). In general, researchers only measure surface crack closing and either a transport property (permeability, absorption, diffusion) or a mechanical recovery. Besides, among those who studied both durability and mechanical properties, they used different types of specimens, which means different cracks. For example, split cylinders (linear crack) are often used for water permeability test, alongside prisms subjected to bending (flexural crack) to assess mechanical recovery (Buller et al., 2019; Snoeck et al., 2014b). In that case, the evaluated durability and mechanical properties could not be correlated. The assessment of both properties on the same specimen (same crack) has rarely been carried out and would enable a direct comparison between a healing state with a mechanical regain.

Furthermore, while most studies investigated laboratory expositions (water immersion, wet/dry cycles, humid chamber), very few studied self-healing in real outdoor condition. While water immersion is generally considered the most favourable exposition for self-healing (De Belie et al., 2018), the healing process needs to be examined in a realistic condition involving a wide range of temperatures and precipitations.

In addition, cracks of structures are rarely dormant (constant width). Subjected to repeated thermal, chemical and mechanical loadings, crack openings vary (active cracks) and may gradually get wider. Few researchers studied the self-healing capacity of concretes after repeated cracking and healing cycles (Alghamri & Al-Tabbaa, 2020; Cuenca et al., 2018; Herbert & Li, 2013; Sahmaran et al., 2015; Snoeck & De Belie, 2016). While they observed repeated healing via surface crack closure or mechanical tests, none of these studies determined a durability property. This needs to be addressed as well to contribute to the advancement of self-healing concrete research.

Therefore, this project has been launched to address the aforementioned issued regarding the self-healing agents, the testing methods, the exposure conditions and the repeated reloading. This research project being one of the first dedicated solely on self-healing concrete at Polytechnique Montreal, the general methodology consisted in studying a large range of materials, testing methods and exposure conditions to provide insights on the best paths to follow in future projects.

1.2 Objectives

The general objective of this research project was to evaluate the self-healing capacity of concrete containing various admixtures (crystalline admixture CA, expansive agent CSA, superabsorbent polymer SAP) alone and in combinations (CA+SAP and CA+CSA) under several exposure conditions via a thorough characterisation.

The four following specific objectives were set to achieve the main one. The first three objectives were associated to an experimental program.

1. Develop and validate a new water permeability set-up adapted to concrete prisms with a flexural crack;

2. Evaluate the self-healing potential of concrete containing various admixtures under laboratory (water immersion, wet/dry cycles, air, water flow) and outdoor expositions with several characterisation methods (water permeability, mechanical recovery and microstructure analyses);

3. Evaluate the self-healing potential of concrete under repeated reloading;

4. Establish performance of concrete compositions, exposure conditions and experimental methods to improve and measure the self-healing capacity of concrete and deepen fundamental understanding of the phenomenon.

It must be noted that this thesis mainly concerns specific objectives 1, 2 and 4, which have been the subject of three scientific articles. This thesis contains only the preliminary results related to the third objective since activities are still ongoing. A fourth scientific paper will be written with complete results beyond the scope of this thesis.

1.3 General methodology

The research project was divided into three experimental programs to reach objectives 1 to 3 specifically and gathers the new knowledge and understanding to answer objective 4. These experimental programs are briefly introduced here and will be detailed thoroughly in **Chapter 3**.

Experimental Program 1: Development of a new water permeability set-up

This first experimental program aims to develop and validate a new water permeability set-up for fibre reinforced concrete (FRC) prisms having a single flexural macrocrack that can be reloaded to compare the self-healing potential of different self-healing agents with durability and mechanical measurements. The set-up was adapted from the water permeability device previously developed at Polytechnique Montreal for concrete tie-specimens (Desmettre & Charron, 2011) and validated on a FRC control mix with specimens kept under water immersion for 25 days. The set-up validation included the evaluation of the measurement repeatability and the influence of the pressure gradient on the water permeability coefficient. Additional correlations before (between initial mechanical behaviour, crack characteristics and permeability) and after healing (between crack characteristics and permeability) were analysed.

Experimental Program 2: Evaluation of the self-healing potential with various admixtures under laboratory and outdoor expositions

The second experimental program addresses the evaluation of the self-healing potential of FRC containing various admixtures and subjected to laboratory and outdoor expositions. Six FRC mixes were produced (control, CA, CSA, SAP, CA+SAP and CA+CSA). After pre-cracking at 28 days, the specimens were exposed in water immersion, wet/dry cycles and air for 3 months, water flow for 1 week and outside for 1 year. Self-healing was assessed by water permeability measures, mechanical recovery evaluation, macroscopic observations of the healed cracks and microscopic (SEM-EDS) analyses of the healing products in the cracks.

Experimental Program 3: Evaluation of the self-healing potential under repeated reloading

In this last experimental program, two FRC mixes (control and CA+CSA) were made to evaluate their self-healing potential under repeated cracking and healing cycles. After pre-cracking at 28 days, the specimens were exposed in wet/dry cycles for 14 days. They were then reloaded and placed in wet/dry cycles again for 14 days before reloading a second time. After a third period of healing, they were reloaded until failure. Water permeability was measured each time before and after reloading. Macroscopic observations were also carried out at the same times. Due to delays attributed to COVID-19, only the CA+CSA mix was tested and preliminary analyses are shown in this thesis. The control mix will be tested beyond the scope of this thesis.

1.4 Scope and impact

First, this research project will enable to accurately assess the self-healing potential of concrete with both durability and mechanical measurements conducted on the same specimen. Only one other study evaluated both properties on the same specimen but the results were not conclusive.

Moreover, the cracks induced in prisms are flexural cracks, which are more representative of the types of cracks found in structures. Consequently, this research will help to better compare the self-healing performance of concretes with various admixtures (crystalline admixture, expansive agent, superabsorbent polymer) and their potential synergy, in several laboratory and more realistic conditions (outdoor exposure and repeated loadings) with an innovative testing procedure. Comparing laboratory and outdoor expositions will enable to identify the accelerated condition in laboratory that can best simulate the long-term outdoor exposition experienced by concrete structures during their service life. Lastly, water permeability and mechanical recovery measurements will be combined with microstructure analysis to deepen the understanding of the healing process in each exposition.

Therefore, the results from this thesis will definitely contribute to research on self-healing concrete, by proposing a novel methodology to evaluate thoroughly the self-healing capacity, investigating more realistic conditions (long-term outdoor exposure and repeated reloading) and providing explanations of the healing process at macro- and microscopic scales.

More generally, this research is in line with a sustainable development approach to extend the durability of reinforced concrete structures. Self-healing concretes containing admixtures that are already available in the market help to meet the need of more durable structures. While their initial cost is slightly higher than a standard concrete, their total life cycle cost will be lower in the end. The enormous maintenance and repair costs of concrete structures will be reduced and the disturbance from construction works will decrease as well, thus improving the quality of life of users. Many civil engineering infrastructures could benefit from the use of self-healing concrete, such as bridges, water tanks, dams, industrial floors and docks.

Finally, a quote from Erik Schlangen and Christopher Joseph sums up the relevance of this research project: *"The durability issues associated with concrete are significant and are not going to reduce in the near future, unless materials with rejuvenating healing abilities are researched, developed and promoted"* (Schlangen & Joseph, 2009).

1.5 Original contributions

The experimental programs of this research project have been elaborated based on the lacks of knowledge in literature highlighted in the introduction and detailed further in **Chapter 2**.

Hence, this research project brings the following original contributions:

1. A new water permeability set-up adapted to prisms presenting a flexural crack found in structures that can be reloaded so that durability and mechanical properties can be evaluated on the same healed specimen;

2. New correlations obtained with several characterisation methods: water permeability, mechanical recovery and microstructure on healed concrete prisms;

3. Study of various combinations of admixtures (crystalline admixture with expansive agent or superabsorbent polymer) that could have a synergetic healing effect under various exposure conditions;

4. Evaluation of self-healing concrete in a long-term outdoor exposure in a northern climate;

5. Evaluation of self-healing concrete under repeated mechanical reloading experienced by many reinforced concrete structures.

Most of these original contributions were included in three scientific articles that are or will be published in international peer-reviewed journals. The original contributions of each article are described hereafter.

Article 1

- **Title:** New water permeability set-up and factors affecting concrete self-healing;

- **Journal:** *Construction and Building Materials*, published online on the 17th of May 2021.

- **Original contributions:**

  1. Presentation and validation of the new water permeability set-up;

  2. Sensitivity of cracking between initial flexural behaviour, crack characteristics and water permeability coefficient;

  3. Evaluation of the influence of the pressure gradient on the water permeability results;

  4. Discussion of the more relevant parameters for self-healing evaluation, based on surface crack closure (Closing Ratio) and water permeability measures (Healing Ratio);

  5. Correlations of self-healing with the initial crack parameters (crack geometry and water permeability coefficient).

Article 2

- **Title:** Self-healing of concrete containing different admixtures under laboratory and outdoor expositions – Part 1: water permeability;

- **Journal:** *Cement and Concrete Composites*, submitted on the 5th of July 2021.

- **Original contributions:**

  1. Evolution of self-healing of different admixtures and combinations (CA, CSA, SAP, CA+SAP and CA+CSA);

2. Evolution of self-healing in different expositions, including outdoor for 1 year, so that comparison between accelerated laboratory and long-term realistic expositions can be made;

3. Correlations between self-healing and microstructure.

Article 3

- **Title:** Self-healing of concrete containing different admixtures under laboratory and outdoor expositions – Part 2: mechanical behaviour;

- **Journal:** *Cement and Concrete Composites*, submitted on the 5th of July 2021.

- **Original contributions:**

    1. Impact of fibres orientation and density on the initial mechanical behaviour to isolate the effect of the self-healing agents;

    2. Mechanical recovery (strength and stiffness regains) of concrete containing different admixtures (CA, CSA, SAP, CA+SAP and CA+CSA) healed in different expositions, including outdoor for 1 year;

    3. Correlations between the permeability reduction due to self-healing, the resulting mechanical recovery and microstructure (self-healing products).

1.6 Structure of this thesis

This thesis is organised into 9 chapters (**Figure 1.1**). After this present introduction (**Chapter 1**), an overview of self-healing concrete will be presented in **Chapter 2**, and the lacks in literature will be highlighted. Then, the detailed methodology of this research project will be explained in **Chapter 3**, specifying the experimental programs and the testing methods. The relevance of the experimental works will also be emphasised. **Chapter 4**, **Chapter 5** and **Chapter 6** correspond to the three scientific articles, published or submitted for publication, describing the results of Experimental Programs 1 and 2. Complementary studies, including a preliminary analysis of the results of Experimental Program 3, will be presented in **Chapter 7**. Then, a general discussion about the new knowledge and understanding gathered from the research project will be presented in **Chapter 8**. Lastly, the conclusions and recommendations will be given in **Chapter 9**.

INTRODUCTION	**CHAPTER 1** Context, objectives
LITERATURE REVIEW	**CHAPTER 2** Self-healing concrete
METHODOLOGY	**CHAPTER 3** Description of the experimental programs
EXPERIMENTAL PROGRAM 1 New water permeability set-up	**CHAPTER 4** Article 1 – Published in *Construction and Building Materials*
EXPERIMENTAL PROGRAM 2 Self-healing with various admixtures under laboratory and outdoor expositions	**CHAPTER 5** Article 2 – Submitted to *Cement and Concrete Composites*
	CHAPTER 6 Article 3 – Submitted to *Cement and Concrete Composites*
COMPLEMENTARY STUDIES SAP mix, concrete strength, fibres analyses, mechanical recovery	**CHAPTER 7** Complementary studies and Experimental Program 3
EXPERIMENTAL PROGRAM 3 Self-healing under repeated reloading	
DISCUSSION	**CHAPTER 8** Scientific discussion and practical considerations
CONCLUSIONS AND RECOMMENDATIONS	**CHAPTER 9** Conclusions and recommendations for further research

Figure 1.1. Schematic structure of this thesis

CHAPTER 2   LITERATURE REVIEW OF SELF-HEALING CONCRETE

2.1 Self-healing in concrete

Although the phenomenon of self-healing in concrete has been reported for the first time by the French Academy of Sciences in 1836 in water-retaining structures (Hearn, 1998), the subject has only been largely and more thoroughly studied in the last decade. Interest in this research area has increased exponentially since the first *International Conference on Self-Healing Materials* in 2007, as it can be seen from the number of publications in **Figure 2.1**. This trend coincides with the growing interest of durable materials to repair or replace concrete structures showing durability issues.
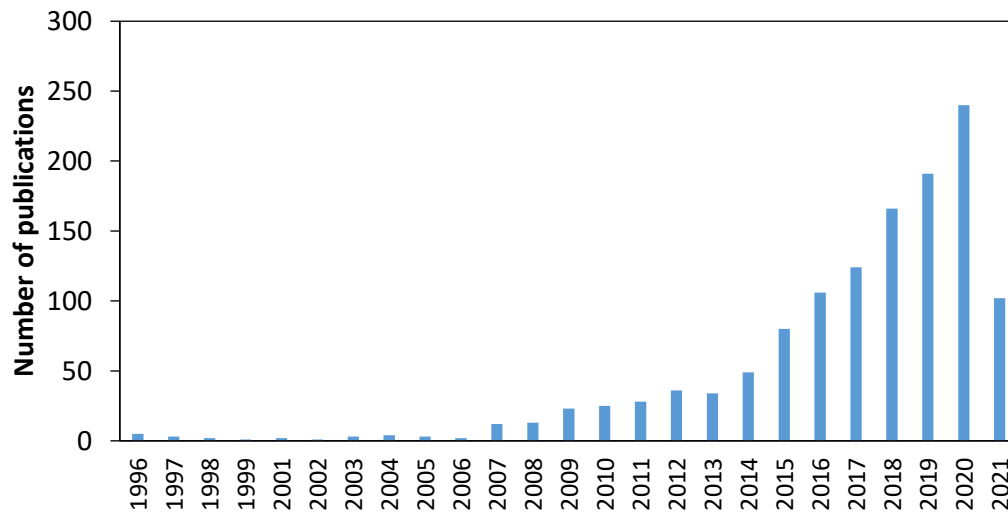
Figure 2.1. Number of publications per year with "*self-healing concrete*" as topic, data from Web of Science, accessed date: 02/06/2021

Even though more and more papers about self-healing concrete are published every year, this research area is not mature yet. This literature review will first describe the healing processes (definitions and kinetics) and the influencing parameters. Then, the methods to evaluate self-healing as well as different self-healing approaches will be reviewed, before describing in more details the tests and self-healing agents used in this project. The review will end with discussions highlighting the lacks of knowledge and understanding of self-healing concrete.

2.1.1 Autogenous healing vs autonomous healing

According to the RILEM state-of-the-art report of *Self-Healing Phenomena in Cementitious-Based Materials* (de Rooij et al., 2013), **self-healing** is defined as: *"any process by the material itself involving the recovery and hence improvement of a performance after an earlier action that had reduced the performance of the material".*

The report distinguishes two types of self-healing:

- **Autogenic (autogenous) healing:** *"when the recovery process uses materials components that could otherwise also be present when not specifically designed for self-healing (own generic materials)"*;

- **Autonomic (autonomous) healing:** *"when the recovery process uses materials components that would otherwise not be found in the material (engineered additions)"*.

The difference between the two types of self-healing comes from the fact that cementitious materials already have an intrinsic self-healing capacity (autogenous healing). In this case, the main mechanisms in presence of water are continuing hydration of unhydrated cement grains (especially at early age) and calcium carbonate precipitation (more at later age) due to the reaction between calcium ions Ca^{++} present in the concrete matrix and carbonate ions CO_3^{--} available from carbon dioxide in the air (De Belie et al., 2018; Edvardsen, 1999). Loose particles could also contribute to the crack sealing. It is now known that autogenous healing of concrete is only efficient to heal very small cracks (10 to 100 µm) and is not reliable to achieve significant healing effects (De Belie et al., 2018).

That is why different engineered approaches (autonomous healing) have been developed and investigated, such as the use of bacteria, encapsulated chemical agents, mineral admixtures, superabsorbent polymers, vascular systems, etc. While the use of mineral admixtures (expansive agents for example) or superabsorbent polymers (SAPs) were regarded initially as autonomous processes (de Rooij et al., 2013), they have now been considered as stimulated autogenous approaches in recent reviews (De Belie et al., 2018; Ferrara et al., 2018), where autonomous healing only concerns encapsulated methods (micro- and macrocapsules, vascular systems) and bacteria (encapsulated or not). This is explained by the fact that encapsulation is a fully autonomic approach, because the self-healing approach is independent from the mix composition and

environment as cracking triggers the mechanism, in contrast to the other approaches that need water to react with the cementitious matrix and heal the crack (stimulated autogenous healing). Bacteria also need contact with water, but the cementitious matrix is not the only source for precipitation of calcium carbonate (Snoeck, 2015).

In **Section 2.4**, the self-healing approaches will be presented by category, with or without encapsulation, rather than by autogenous or autonomous processes.

2.1.2 Self-sealing vs self-healing

The RILEM state-of-the-art report (de Rooij et al., 2013) also distinguishes the terms "**self-sealing**" and "**self-healing**". Self-sealing is defined as a recovery of durability properties, while self-healing includes a recovery of mechanical properties. In this regard, Snoeck (2015) reported that self-sealing was usually measured by water or air permeability test.

However, the term "crack sealing" has often been used to describe the surface crack closure (Borg et al., 2018; Cuenca et al., 2018; Ferrara et al., 2016a), while "crack healing" was often used with evaluation of water permeability (Azarsa et al., 2019; Li et al., 2020a; Park & Choi, 2018; Roig-Flores et al., 2016; Sisomphon et al., 2012). The latter references did not determine mechanical recovery.

Hence in this project, the term "self-sealing" will also be preferred for surface crack closure, while "self-healing" will refer to the durability and/or mechanical recoveries. An exception to these definitions concerns the SAP, for which the mechanism consists first in self-sealing (swelling of SAP upon ingress of water that blocks the crack), and then promotion of self-healing (releasing of water by SAP to react and heal the crack). Further information will be provided in **Section 2.4.4**.

2.1.3 Self-healing kinetics

The self-healing process is characterised by a particular kinetics: a rapid healing rate at the process initiation then a gradual slowdown of the process with time. This kinetics can easily be observed with the evolution of air (Gagné & Argouges, 2012; Wang et al., 2018) or water (Edvardsen, 1999; Escoffres et al., 2018; Park & Choi, 2018; Reinhardt & Jooss, 2003; Sisomphon et al., 2012) permeability results, though same sort of kinetics were also observed for the evolution of crack

closure (Sisomphon et al., 2012), Resonant Frequency (non-destructive testing) (Yang et al., 2009) or the thickness of the healing products (Homma et al., 2009).

Figure 2.2 shows examples of self-healing kinetics in the form of normalised flow rate or permeability reduction of specimens pre-cracked at 28 days, subjected to continuous water flow (**Figure 2.2a**, $w = 0.05 – 0.15$ mm) or kept immersed in water (**Figure 2.2b**, $w = 0.10 – 0.40$ mm). Although continuous water flow test accelerated self-healing compared to still water immersion, the kinetics are similar.

a)   b)
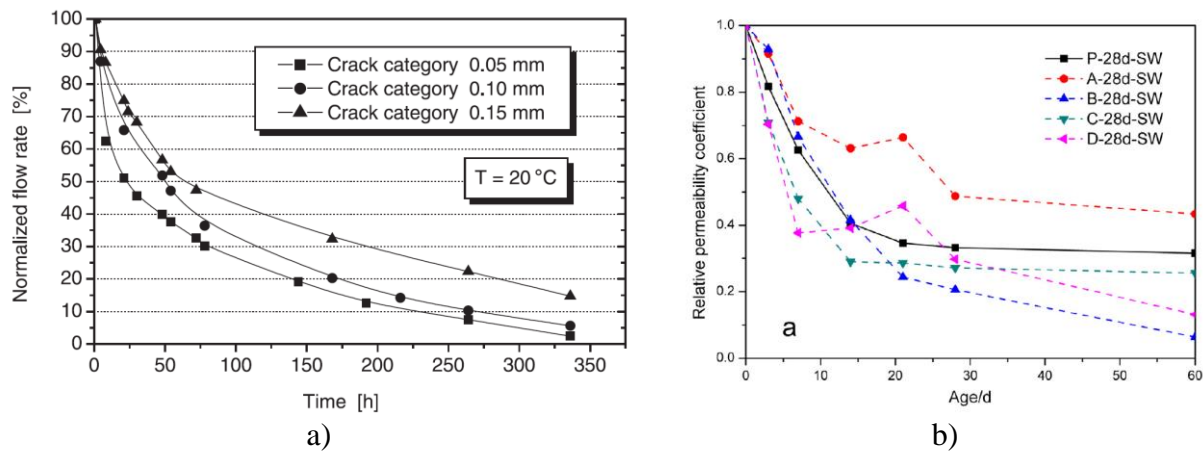
Figure 2.2. Examples of self-healing kinetics for a) continuous water flow test (Reinhardt & Jooss, 2003) and b) immersion in water (Jiang et al., 2015)

This kinetics can be explained by the main self-healing mechanisms previously mentioned: ongoing cement hydration at early age and carbonation at later age. In the first case, hydration of cement occurs with a short accelerated phase (several hours/days) followed by a long deceleration period (several months/years). In the second case, the mechanism of calcium carbonate precipitation comprises two phases, described by Edvardsen (1999). First, precipitation of $CaCO_3$ happens rapidly as calcium ions Ca^{++} are readily available at the concrete surface (surface-controlled phase as in **Figure 2.3a**), then the process is controlled by the diffusion phase during which the calcium ions diffuse through the matrix and the $CaCO_3$ layer (**Figure 2.3b**), which is a slower process. In addition, the progressive closing of the crack also slows down the penetration of reactants (CO_2 and water) (Gagné & Argouges, 2012).

Surface controlled   Diffusion controlled

a)   b)
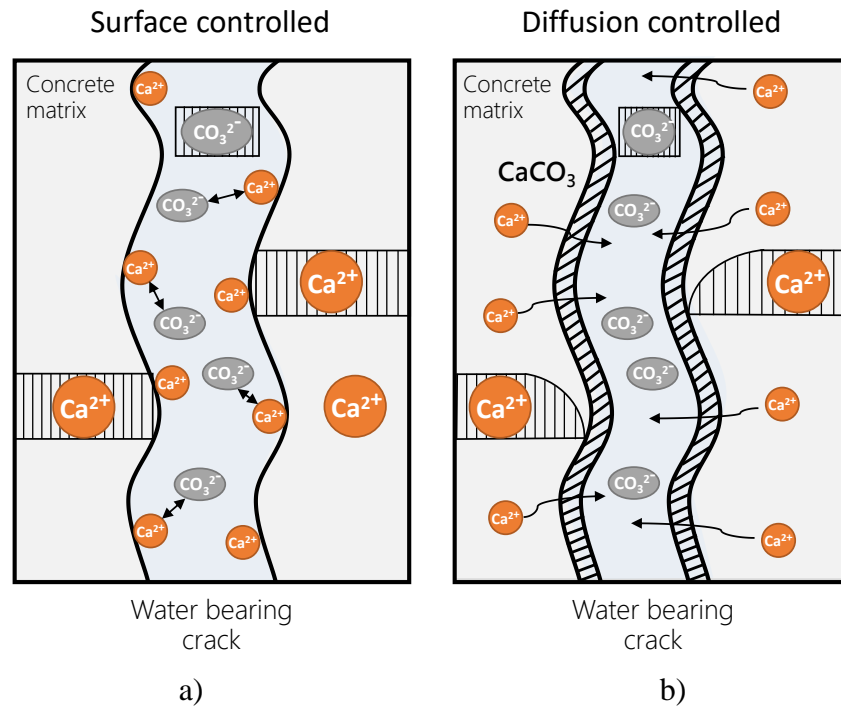
Figure 2.3. Mechanism of healing by carbonation: a) surface-controlled and b) diffusion-controlled phases, redrawn after (Edvardsen, 1999)

When different self-healing agents are used, such as silica-based component, chemical expansive, swelling and crystalline materials (respectively A, B, C and D in **Figure 2.2b**), the kinetics follows the same trend as well.

2.2 Parameters influencing autonomous healing

2.2.1 Cracking

2.2.1.1 Crack width

Crack width is ineluctably one of the most important factors of self-healing (Edvardsen, 1999). The narrower the crack, the faster it will heal, regardless of the self-healing process, as it can be seen from previous **Figure 2.2a**. As it will be shown further, the use of fibres is very effective to control and limit the crack widths, hence facilitating complete healing of the cracks.

However, it has also been observed that very narrow cracks will not always heal faster (Nanayakkara, 2003). Ismail (2006) found a slower healing in terms of flow rate reduction for a

crack width of 78 μm compared to one of 117 μm after 1 month in humid chamber, which could be due to the lower penetration of water and CO_2 in the thinner crack. Gagné and Argouges (2012) also mentioned this slower diffusion of external reactants into the crack to continue self-healing.

2.2.1.2 Age of cracking

The concrete maturity at cracking has a large impact on the self-healing process. If cracked at early age, concretes will necessarily contain more unhydrated cementitious particles and thus self-healing via ongoing hydration will occur, forming new C-S-H gel (De Belie et al., 2018). On the other hand, self-healing via $CaCO_3$ formation will occur more in concretes cracked at later age. In general, early age cracks heal quicker than later age ones.

2.2.1.3 Dormant or active crack

Most studies investigated self-healing of a dormant crack, for which the width does not vary (pre-cracked once and maybe reloading to failure). But in real life, many concrete structures are subjected to cyclic loading, creating active cracks with varying width.

While some researchers examined the self-healing capacity of cracks under repeated reloading with healing periods in between (Alghamri & Al-Tabbaa, 2020; Cuenca et al., 2018; Herbert & Li, 2013; Sahmaran et al., 2015; Snoeck & De Belie, 2016), very few studied self-healing of cracks under loading. This has been first investigated by Edvardsen (1999), who measured water permeability of an active crack (12h $w_{min} = 0.2$ mm/12h $w_{max} = 0.26$ mm cycles for 1 month). She found that the crack could heal, with a similar kinetics trend, but slower than a dormant crack of similar width. Later, Desmettre and Charron (2011) developed a new water permeability device that enables to measure water permeability of multicracked concrete tie-specimens under static, constant (Desmettre & Charron, 2012) and cyclic loadings, at higher frequency (Desmettre & Charron, 2013). They observed that cyclic loading was more favourable for self-healing than constant loading for the fibre reinforced concrete (FRC) in comparison to the normal strength concrete (NSC), as it can be seen from **Figure 2.4a** and **Figure 2.4b** respectively. This observation was explained by the fact that cyclic loading was creating microcracks progressively in FRC, promoting a quick healing on new crack surfaces, while it was widening the macrocrack already present in NSC, with less new cracks surfaces.
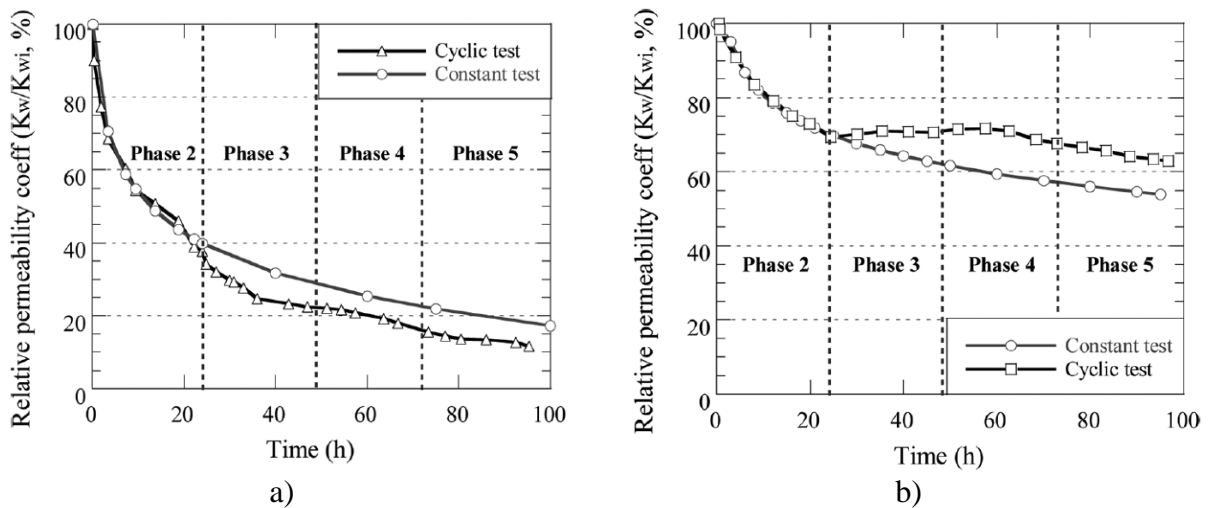
Figure 2.4. Evolution of relative permeability coefficient of concrete tie-specimens under cyclic or constant loads for a) FRC and b) NSC (Desmettre & Charron, 2013)

2.2.2 Mix composition

2.2.2.1 Water to cement ratio (w/c)

Concretes with lower w/c ratios contain a higher amount of anhydrous cement, hence probably increasing its self-healing capacity from hydration products. However, contrary to what one may think, the impact of water to cement ratio on self-healing is not straightforward.

For mature concretes, the impact of w/c seems minor (Gagné & Argouges, 2012; Lauer & Slate, 1956). Gagné and Argouges (2012) studied air permeability through mortars pre-cracked at 28 days and at 6 months, healed in humid chamber, with w/c of 0.35, 0.45 and 0.60. They did not find any significant effect of the w/c.

For early age cracks, the impact of w/c seems greater but not as expected. Lauer and Slate (1956) obtained higher healing in terms of tensile strength recovery, when increasing w/c for cement pastes pre-cracked at 1 day and healed in water (**Figure 2.5**). More recently, Rajczakowska et al. (2019) compared an ultra high performance concrete (UHPC with w/c = 0.22 and 1000 kg/m³ of cement) with a high performance concrete (HPC with w/c = 0.45 and 675 kg/m³ of cement) pre-cracked at 1 day and healed in water for 21 days. They also found higher self-healing efficiency for HPC compared to UHPC, via UPV, crack closure and flexural recovery tests. This could be explained by the very dense and impermeable matrix of the UHPC that surrounds the anhydrous

grains, hindering the healing process. Moreover, the rapid reaction of unhydrated cement in contact with water may result in an impermeable membrane of healing products around the grain, which prevents access to the necessary ions (Ca and Si) for further healing.
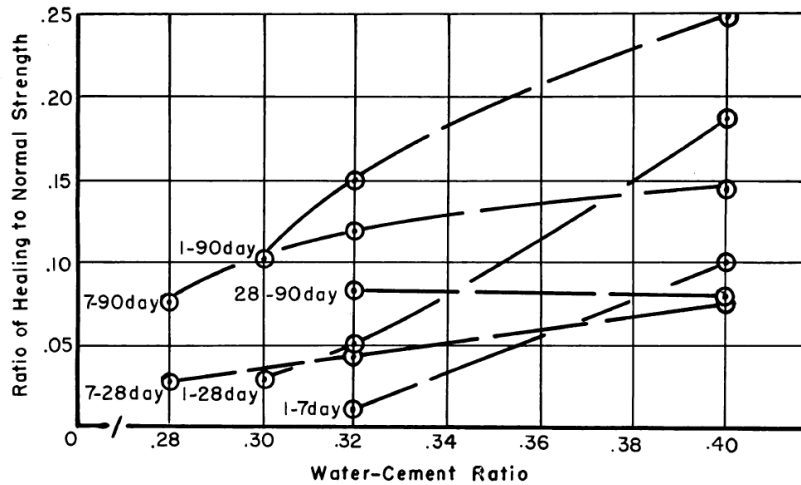
Figure 2.5. Impact of w/c on the strength recovery (notation: 1-7day = pre-cracked at 1 day, healed in water and reloaded at 7 days) (Lauer & Slate, 1956)

2.2.2.2 Fibres

The presence of fibres has a significant impact on the self-healing process as it controls cracking. Fibres enable to generate finer cracking, which favours self-healing (**Section 2.2.1.1**). A review on self-healing of fibre reinforced cementitious composites (FRCC) can be found in (Cuenca & Ferrara, 2017).

Different types of concretes (or cementitious composites), with various compositions as well as types and dosages of fibres, are summarised in **Table 2.1**. In all cases, self-healing has been demonstrated in presence of fibres.

A low (0.2 – 0.3%-vol) to moderate (0.5 – 1%-vol) amount of macrofibres enables the fibre reinforced concrete (FRC) to feature a tensile strain-softening behaviour that helps to control the formed macrocrack before failure. That is why some researchers used such limited dosage to have a reliable post-cracking phase, alternatively to internal reinforcement or external strengthening. The beneficial effect of fibres on self-healing has also been highlighted with water permeability test (Desmettre & Charron, 2012; Escoffres et al., 2018).

When adding higher dosages of microfibres (1 – 2%-vol), materials, called high performance fibre reinforced concrete (HPFRC) can feature a tensile strain-hardening behaviour and stable multiple microcrack formation. However, if the fibres are poorly oriented, the materials may show a strain-softening behaviour instead. Good and poor fibres orientations in HPFRC prisms exposed in various environments were studied by (Ferrara et al., 2016a, 2016b; Ferrara et al., 2017) in terms of crack closing and mechanical recovery. They obtained larger self-healing for HPFRC with both fibres orientations compared to normal strength concrete (NSC).

Increasing even more the cement content and fibres dosage (> 2%) leads to ultra high performance fibre reinforced concrete (UHPFRC), which typically contains a high amount of cement and pozzolanic materials, providing a very dense and impermeable matrix (compressive strength > 120 MPa). A very high self-healing capacity was clearly demonstrated for UHPFRC with water and glycol permeability test (Charron et al., 2008) and chloride penetration test (Negrini et al., 2019). For information, Negrini et al. (2019) could not use their water permeability test with UHPFRC because water did not penetrate in the cracks, even at high pressure gradient.

Lastly, Engineered Cementitious Composites (ECC), characterised by a high tensile ductility, were first developed by Li and coworkers (Li, 2003; Li et al., 2002), purposely to restrict crack width (≤ 60 µm) and promote autogenous healing (Van Tittelboom & De Belie, 2013). ECC typically contains a high amount of fly ash (FA) and 2% of oil-coated micro polyvinyl alcohol (PVA) fibres (Snoeck & De Belie, 2016). Self-healing of ECC has been confirmed in various environmental conditions (Li & Li, 2011) and even in a long-term outdoor exposure (Herbert & Li, 2013).

Table 2.1. Categories of fibre reinforced concretes

Type of concrete	Composition	Mechanical behaviour	Dosage (in volume)	Size	Type
FRC	Cementitious /pozzolanic materials	- Strain-softening behaviour - Single macrocrack - $f_c = 20 – 60$ MPa	0.2 – 0.3% 0.5 – 1%	Macro	Steel
HPFRC	Cementitious /pozzolanic materials	- Strain-hardening behaviour - Multiple microcracks - $f_c = 70 – 110$ MPa	1 – 2%	Micro	Steel
UHPFRC	High amount of cement and pozzolanic materials	- Strain-hardening behaviour - Multiple microcracks - $f_c > 120$ MPa	> 2%	Micro	Steel
ECC	High amount of FA	- Strain-hardening behaviour - Multiple microcracks (≤ 60 µm) - $f_c = 35 – 60$ MPa - High tensile ductility (strain capacity of 5%)	2%	Micro	Coated PVA

Though steel fibres are mostly mentioned in **Table 2.1**, the effect of different types of fibres on the self-healing capacity has been studied. FRC with synthetic fibres, such as polypropylene (PP), polyethylene (PE) or polyvinyl alcohol (PVA), showed higher self-healing than steel fibres because they act as nucleation sites for healing products (Homma et al., 2009; Nishiwaki et al., 2012). Furthermore, natural vegetable fibres also enhance self-healing as they absorb water and can act as water reservoirs (Ferrara et al., 2014a).

Finally, a synergy between fibres and self-healing approaches may be promising, as stated by Cuenca and Ferrara (2017). Research combining fibres and self-healing agents will be discussed further in **Section 2.4**.

2.2.2.3 Supplementary cementitious materials (SCMs)

The use of supplementary cementitious materials (SCMs) or mineral additions, e.g. blast-furnace slag (BFS), fly ash (FA) and silica fume (SF), has become common in concrete because of economical and ecological reasons. These mineral additions impact the hydration kinetics, the material properties and the self-healing capacity as well (De Belie et al., 2018). On one hand, they can enhance self-healing via continued hydration, especially at later age because of the slower

hydration of these SCMs. BFS is reported to have more self-healing capacity than FA as slag has additional latent hydraulic activity. On the other hand, because of their pozzolanic reaction, they consume portlandite to produce C-S-H, leading to less calcium ions for self-healing via carbonation. The influence of SF has been less studied, but they usually lead to high self-healing performance, as seen via surface crack closure (Borg et al., 2018; Jaroenratanapirom & Sahamitmongkol, 2011) or via isothermal calorimetry measures (Park & Choi, 2019).

2.2.3 Healing condition

Because water is considered essential for self-healing, the impact of water properties has been studied and are presented hereafter. Furthermore, the second section will present the influence of exposure conditions and durations.

2.2.3.1 Water properties

Self-healing capacity is influenced by the following properties of the water healing condition (under water immersion or continuous water flow):

- Alkalinity: alkaline water (high pH) accelerates self-healing as calcium carbonate formation is favoured (Edvardsen, 1999; Huang & Ye, 2015);

- Temperature: high temperature favours self-healing (Desmettre, 2011; Reinhardt & Jooss, 2003);

- Pressure gradient: the effect of pressure gradient on self-healing is not well known yet. Its influence on the water permeability coefficient (K_w) has been studied in a few studies and it can be assumed the same on the self-healing capacity measured with K_w. While Desmettre and Charron (2011) found negligible impact of the pressure gradient (25, 50 and 100 kPa) on the water permeability coefficient of tie-specimens under load, Shin et al. (2017) observed lower permeability coefficients when increasing pressure gradient (from 150 to 700 mm of water head, equivalent to 1.5 to 7 kPa) in split cylinders for crack width above 0.3 mm. Below this crack width, the permeability is less influenced by the pressure gradient, as seen in **Figure 2.6a**.

- Water renewal: renewing frequently the water from basins where specimens are stored during the healing period has a negative impact on self-healing. Sisomphon et al. (2012) replaced water ever 7 days, causing some water permeability increases, particularly in the first 14 days, as seen in **Figure 2.6b**. They assumed that some healing products formed at early age could be dissolved under fresh water exposure. Jiang et al. (2015) also observed similar permeability increases for specimens healed under flowing water (water replaced every 12h), explaining that ions for self-healing may be drained away.

a)   b)
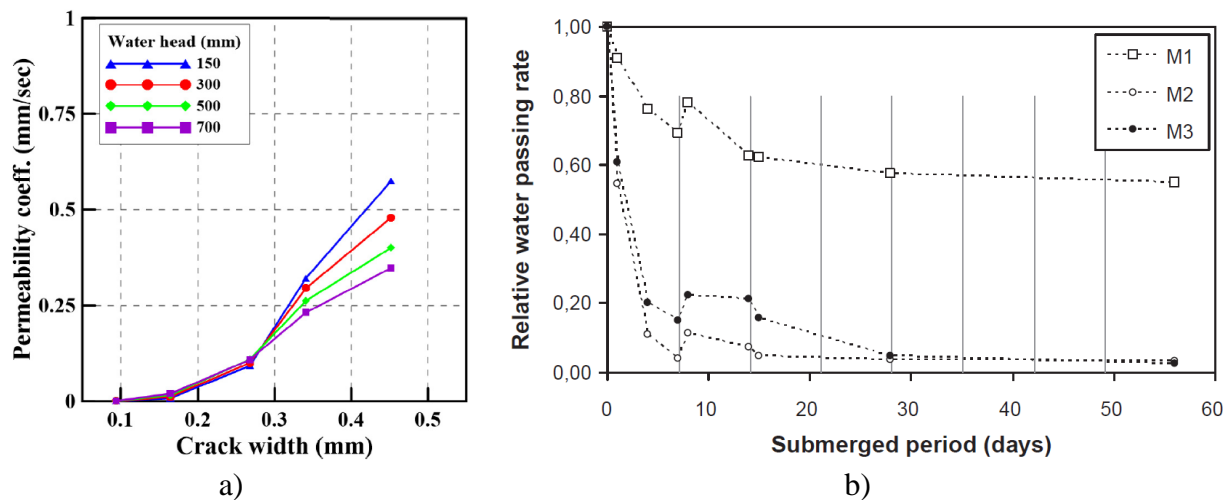
Figure 2.6. Impact of some water properties on self-healing: a) impact of water pressure gradient (water head) on the permeability coefficient (Shin et al., 2017) and b) impact of frequent renewal of water on the water flow (Sisomphon et al., 2012)

2.2.3.2   Exposition and duration

Table 2.2 lists references corresponding to the most frequent expositions as well as their duration considered in research projects dedicated to self-healing. These references mainly concern studies on concretes containing CA, CSA and SAP, the three admixtures that were selected in this thesis. **Table 2.2** also gives information on the method used to evaluate self-healing (via visual crack closure, durability property or mechanical recovery measurement). These testing methods will be discussed in **Section 2.3**.

While most studies only investigated the water exposition (with or without renewal, continuous water flow, sometimes with distilled water or NaCl), several researchers also examined wet/dry

cycles (the wet and dry periods changed study from study) and humid conditions (usually 60% and ≥ 90% of relative humidity RH). Few exposed specimens outside in a realistic condition, or in water contact or controlled air (supposedly RH < 50%) expositions. **Figure 2.7** shows examples of crack healing after 42 days in different expositions from (Roig-Flores et al., 2015). They pointed out the importance of the presence of liquid water to achieve some healing, while air exposure is considered the worst condition for self-healing.

The duration of healing usually ranged from 20 days to 3 months in laboratory conditions, with shorter periods (several minutes to some days) for the continuous water flow test. Realistic outdoor exposure often lasts 1 year.

Table 2.2. List of references in literature (non exhaustive) investigating different healing conditions and evaluated properties

Exposit-ion	References	Duration	Evaluation of self-healing		
			Crack closure	Durability property	Mechanical recovery
Water immers-ion (with or without renewal)	(Sisomphon et al., 2012)	56 days	X	X	
	(Sisomphon et al., 2013)	28 days			X
	(Ferrara et al., 2014b)	1 year			X
	(Roig-Flores et al., 2015) 15°C	42 days	X	X	
	(Roig-Flores et al., 2016) 30°C	42 days	X	X	
	(Escoffres et al., 2018) beams	28 days			X
	(Cuenca et al., 2018)	1 year	X		
	(Wang et al., 2018)	28 days	X	X	
	(Borg et al., 2018) distilled water	3 months	X		
	(Borg et al., 2018) NaCl	3 months	X		
	(Park & Choi, 2018)	56 days	X	X	
	(Park & Choi, 2021)	21 days		X	
	(Li et al., 2020b)	56 days	X	X	X
	(Jiang et al., 2015)	58 days	X	X	
	(Buller et al., 2019)	56 days	X	X	X
	(Sherir et al., 2017a)	1 year			X
	(Hong & Choi, 2017)	28 days		X	

Table 2.2. List of references in literature (non exhaustive) investigating different healing conditions and evaluated properties (cont.)

Continuous water flow test	(Escoffres et al., 2018) tie-specimens	7 days		X	X
	(Azarsa et al., 2019)	4 days		X	
	(Snoeck et al., 2014b)	30 days		X	
	(Lee et al., 2016) NaCl	7 days		X	
	(Hong & Choi, 2017) distilled water	13 min		X	
	(Li et al., 2020a)	22 days		X	
Water contact	(Roig-Flores et al., 2015) 2 cm layer of water on top	42 days	X	X	
	(Van Tittelboom et al., 2016) 1 week air then spraying water 4 times/day for the last 6 weeks	7 weeks	X	X	X
Humid chamber	(Ferrara et al., 2014b) summer/winter cycles (50°C 90% RH and 5°C 95% RH)	4 weeks			X
	(Roig-Flores et al., 2015) 20°C 95% RH	42 days	X	X	
	(Snoeck et al., 2014b) RH > 90% and = 60%	28 days			X
	(Snoeck & De Belie, 2016) RH > 90% and = 60%	28 days	X		X
	(Deng & Liao, 2018) RH cycles 24h 95% RH/24h 60% RH Constant 95% RH	20 days		X	X
	(Roig-Flores et al., 2016) 3.5 days wet/3.5 days dry	42 days	X	X	
	(Cuenca et al., 2018) 4 days wet/3 days outdoor	1 year	X		
	(Borg et al., 2018) 12h wet (distilled water)/12h dry 12h wet (NaCl)/12h dry	3 months	X		
	(Jiang et al., 2015) 1 day wet/1 day dry	58 days	X	X	
	(Snoeck et al., 2014b) 1 day wet/1 day dry	28 days			X
	(Snoeck & De Belie, 2016) 12h wet/12h dry	28 days	X		X

Table 2.2. List of references in literature (non exhaustive) investigating different healing conditions and evaluated properties (cont.)

	(Gruyaert et al., 2016) 12h wet/12h dry	28 days		X	
	(Hong et al., 2020) 1h wet/47h dry	28 days	X	X	X
Control-led air	(Sisomphon et al., 2013)	28 days			X
	(Roig-Flores et al., 2015) 17°C 40% RH	42 days	X	X	
	(Escoffres et al., 2018) beams	28 days			X
Outdoor	(Ferrara et al., 2014b) Milan	1 year			X
	(Cuenca et al., 2018) Milan	1 year	X		
	(Borg et al., 2018) Malta	3 months	X		
	(Sherir et al., 2017a) Toronto	1 year			X
	(Ferrara et al., 2016a; Ferrara et al., 2017) Milan	2 years	X		X
	(Herbert & Li, 2013) Michigan	1 year			X
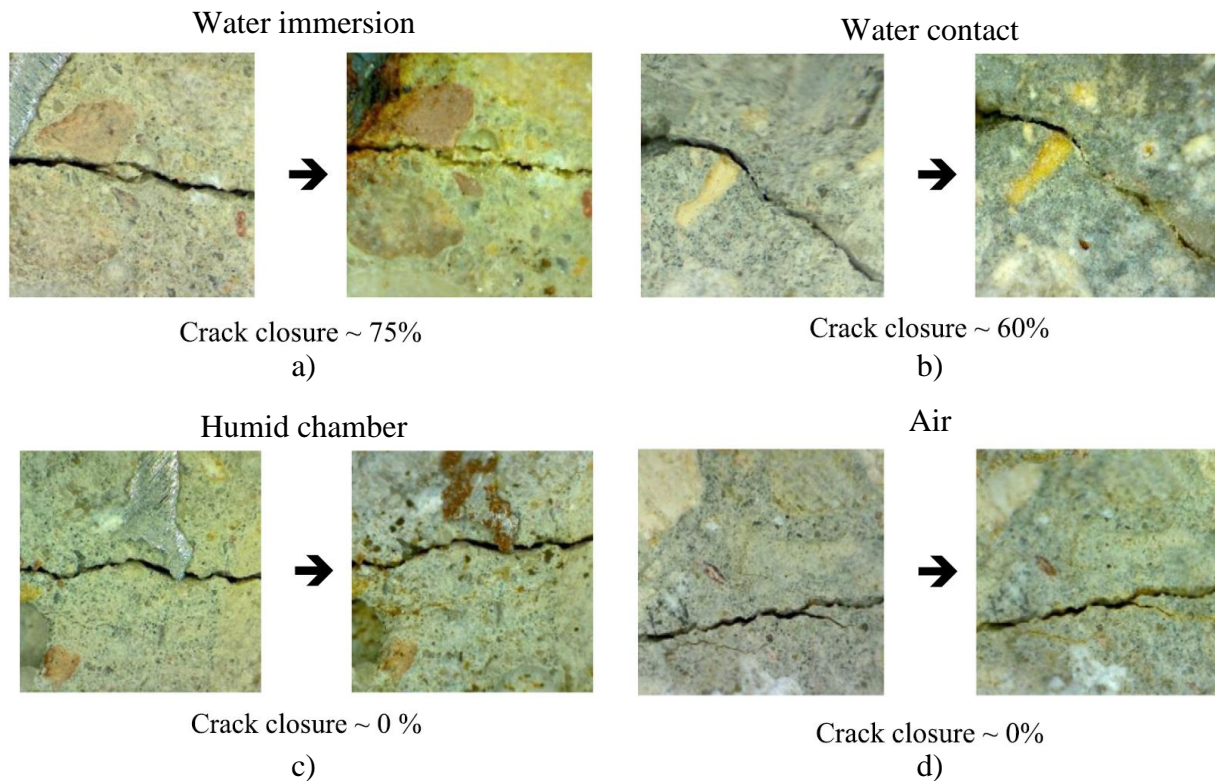
Figure 2.7. Pictures of cracks before and after healing for the control mix in a) water immersion, b) water contact, c) humid chamber and d) air (Roig-Flores et al., 2015)

Furthermore, as highlighted by Li and Herbert (2012) and shown in **Table 2.2**, there is a lack in research of self-healing under field conditions. While self-healing approaches can be promising in controlled laboratory conditions, they may not be as efficient under long-term outdoor expositions, involving a wide and random range of temperatures and precipitations.

Herbert and Li (2013) were the first to study ECC samples exposed outdoor for 1 year. They evaluated the self-healing capacity of ECC specimens via uniaxial tensile and Resonant Frequency (RF) tests and observed recoveries of these properties, even after multiple reloading. They noticed some influence of the temperature and amount of precipitations outside. Ferrara et al. (2014b) exposed concrete specimens outdoor for 1 year and found very limited mechanical recovery and a moderate crack closing. However, the addition of crystalline admixture (CA) improved the mechanical performance. The beneficial effect of CA in outdoor exposure had also been reported by (Borg et al., 2018; Cuenca et al., 2018). Ferrara et al. (Ferrara et al., 2016a; Ferrara et al., 2017) also evaluated crack closing and strength recovery via 4-point bending and UPV tests of HPFRCC specimens exposed outdoor up to 2 years. They observed that a significant crack closure (60 – 80%) was necessary to reach any appreciable mechanical recovery. Finally, Sherir et al. (2017a) obtained enhanced compressive and flexural strength recoveries for ECC specimens containing an MgO-based expansive agent exposed outdoor for 1 year.

2.3 Testing methods to evaluate self-healing

2.3.1 General methodology and overview of different testing methods

There exists no standard method to evaluate self-healing yet, but the general methodology often used is illustrated in **Figure 2.8**. After pre-cracking, the initial properties considered in the study are evaluated before healing, so that the evolution of these properties during and after the healing period can be determined. A comprehensive state-of-the-art on self-healing characterisation methods was published by Ferrara et al. (2018). The numbers between brackets indicated in **Figure 2.8** correspond to the sections where the method is detailed.

The properties that can be evaluated are divided into 3 categories: crack closure measurement, recovery of durability properties or of mechanical properties. Additional microscopic analyses of

the healing products can also be carried out. **Table 2.3** shows a review of the most common testing methods corresponding to the 3 types of measurements.
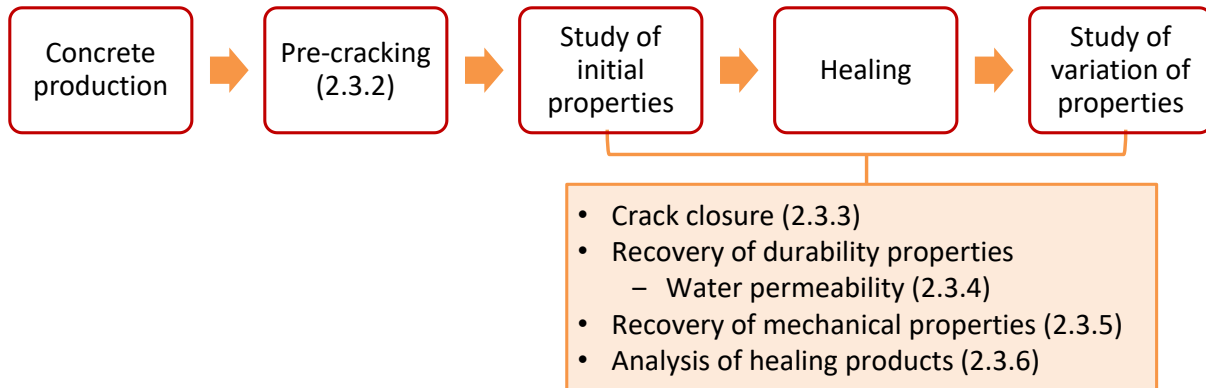
Figure 2.8. General methodology used to evaluate self-healing

Table 2.3. Review of the most common testing methods to evaluate self-healing, summarised from (Ferrara et al., 2018)

Category	Examples	Advantages	Disadvantages	Comments
Crack closure	Light microscopy on concrete surface	Cheap and easy to perform	No information of the interior of the crack	Must not be used alone (risk of overestimation), for supporting other tests
	Tomography	Visualisation of the whole crack volume	- Hazardous because of radiation - Expensive equipment	Great internal crack evaluation but disadvantages lead to make it less accessible
Durability properties	Water permeability	Easy to perform	More complex to implement than mechanical tests	Straightforward evaluation of the whole crack
	Gas permeability	More sensitive to cracking than water permeability	- More difficult to perform - Very sensitive to composition	Straightforward evaluation of the whole crack

Table 2.3. Review of the most common testing methods to evaluate self-healing, summarised from (Ferrara et al., 2018) (cont.)

	Sorptivity	Easy to perform	- Need reference uncracked samples - Reliability problem - Calculation of sorptivity index questionable	Not ideal to assess self-healing (problems with partial healing and SAP)
Mechanical recovery	Mechanical test (same as pre-cracking)	Same as pre-cracking method	Destructive	Need further analysis and interpretation of the results
	UPV	Non-destructive and thus in situ application	Many disruptive effects due to variability in the coupling between sensors and surface	Indirect evaluation of mechanical properties

Overall, visual measurements of the cracks at the surface are intuitive and the easiest way to observe self-healing process via crack closing. With light microscopy (optical, digital or stereo), one can take a picture of the crack and measure its width and area. However, these measures at the surface do not give any information about healing inside the cracks. The use of tomography allows to visualise the whole crack volume, but it represents an expensive equipment that comprises health and safety hazards, which makes this method of limited application.

Then, the methods based on transport or durability properties constitute a direct way to characterise the cracks. Water and gas permeability as well as sorptivity capacity are often examined. Water absorption test is also easy to perform, but it has been demonstrated that it was prone to application errors (operator sensitivity, quality of waterproofing) (Litina et al., 2021; Van Mullem et al., 2020a). As stated by Mengel et al. (2020) in a recent review about water transport through cracked concrete, permeation is the major transport mechanism through cracked concrete. It controls water transport by several orders of magnitude compared to diffusion and capillary suction. Permeability tests are thus more adequate to characterise the self-healing evolution in cracks.

Finally, mechanical recovery has also been assessed and constitutes the third category (**Table 2.3**). Mechanical regain is necessarily evaluated with the same test used during pre-cracking or with

non-destructive tests such as Ultrasonic Pulse Velocity (UPV). Specimens are reloaded several times or until failure at different times and at the end of the healing period. These mechanical tests are destructive, which means that different specimens have to be used if one wishes to determine the evolution of strength in time. UPV tests are non-destructive, which makes them applicable on a structure, but they constitute an indirect evaluation of the mechanical properties and are subject to many disruptive effects that can alter the confidence in the results.

Now that the general testing methods to evaluate healing were described, the next sections will focus on pre-cracking (**Section 2.3.2**), surface crack closure (**Section 2.3.3**), water permeability (**Section 2.3.4**) and mechanical recovery via destructive tests (**Section 2.3.5**), as they are more related to the experimental program of this project. Lastly, information about the analysis of the healing products will be presented in **Section 2.3.6**.

2.3.2 Pre-cracking of specimens

Several methods are used for pre-cracking specimens according to the type of concrete. Each method produces different cracking patterns. The most common methods are summarised in **Table 2.4**. For plain and fibre reinforced (FRC) concretes, the most frequent tests are tensile splitting and 3-point bending tests due to their simplicity and formation of one single macrocrack in specimens with a good control of the crack width. These methods are used for concrete with a low to moderate amount of fibres or reinforcing bars. Direct tensile and 4-point bending tests are used on HPFRC to study the effect of multiple microcracks, which is a characteristic of these strain-hardening materials.

Flexural cracks, with a varying opening along their length (widest at the crack mouth to null at the tip) obtained with bending tests, are typically found in beams and plate elements. In contrast, linear cracks, which have a constant width lengthwise are obtained from direct and splitting tensile tests. They are less encountered in the structures, but may represent the cracks in concrete cover where the stress gradient is nearly uniform (Desmettre & Charron, 2011).

Depending on the type of material, the residual crack widths in specimens after pre-cracking ranged from 10 to 400 µm.

Table 2.4. Most common pre-cracking methods, cracking patterns produced and concrete types, summarised from (Ferrara et al., 2018)

Pre-cracking method	Cracking pattern	Concrete type
Compressive test	Multiple cracking	Plain
Direct tensile test	Multiple cracking	HPFRC and UHPFRC
Splitting tensile test	One localised crack	Plain, FRC
3-point bending test	One localised crack	FRC
4-point bending test	Multiple cracking	HPFRC and UHPFRC

Regardless of the pre-cracking method used, variation of the residual crack width between specimens subjected to the same loading condition has been observed. This variation comes from the technique used for monitoring the crack width during pre-cracking, but also from the method used to measure the crack width (Ferrara et al., 2018). This impacts the accuracy and robustness of the evaluation of self-healing and constitutes the first issue to solve before any attempt of methods standardisation according to (Ferrara et al., 2018). A recent round robin test by Van Mullem et al. (2020a), involving 6 laboratories, performed 3-point bending tests on mortar and concrete specimens. With a classic crack width control, they obtained a large scattering in the residual crack widths, with coefficients of variations (COV) varying from 3 to 32% depending on the laboratory. When using an active crack width control technique, the variation between the laboratories decreased greatly and the target crack width of $290 - 310$ µm could be reached for most specimens.

In addition, even a same crack width measured at the surface can lead to different internal cracking pattern (tortuosity, width variation, roughness). Consequently, crack width at the surface is not an ideal parameter to fully describe a crack (Ferrara et al., 2018). The differences inside a crack can be better revealed with a water permeability test. For very similar cracks widths at the surface, Van Mullem et al. (2020a) observed a scattering in the water permeability results, within the same laboratory and between laboratories.

2.3.3 Evaluation of surface crack closure

Surface crack closure can be quantitatively measured with different techniques. The easiest and mostly used one is to periodically measure crack width before, during and after healing, at some constant equidistant points along the crack. Then an average crack width can be calculated for each specimen. In case of linear cracks, the average of different points along the crack and in both faces

of the specimen is taken. For flexural cracks, the considered average crack width from both faces can be either measured at the notch root (Van Mullem et al., 2019) or at mid-height (Namnoum et al., 2021). Then, from crack width measurements, the surface crack area can also be estimated, multiplying widths by their associated lengths (Roig-Flores et al., 2015). A more advanced technique is to perform image analysis, via black pixels (Roig-Flores et al., 2015) or binarisation (Cuenca et al., 2018), as illustrated in **Figure 2.9**, which provided accurate crack measurements.

Figure 2.9. Example of binary image of the crack (Cuenca et al., 2018)

With both techniques, a crack Closing Ratio (*CR*) can be calculated via **Eq. 2.1**, considering either the crack width (Borg et al., 2018; Cuenca et al., 2018; Ferrara et al., 2016a; Hong et al., 2020; Roig-Flores et al., 2016; Wang et al., 2018) or the crack area (Li et al., 2020b; Wang et al., 2018). Instead of *CR*, relative crack results (final crack/initial crack) can be determined (Sisomphon et al., 2012; Snoeck & De Belie, 2016).

$$Closing\ Ratio\ CR\ (\%) = 1 - \frac{final\ crack\ width\ or\ area}{initial\ crack\ width\ or\ area} \tag{2.1}$$

Cuenca et al. (2018) measured the Sealing Index (SI equivalent to Closing Ratio) of specimens exposed in various conditions (water, wet/dry cycles and outdoor) for 1 year. The impact of the exposure condition as well as of the crack width can be seen in **Figure 2.10** on the SI. They concluded that the exposition was the most determinant factor for self-healing, with frequent complete sealing (100%) of the cracks under water immersion and low crack sealing (< 40%) in outdoor. Besides, large cracks (> 0.3 mm) never reached complete sealing even in water exposure. When analysing different expositions, including with NaCl solution to simulate seawater, Borg et

al. (2018) found better and faster healing (in terms of surface crack closure) with increasing the chloride content than in distilled water, probably due to a synergy between healing process and chloride binding. Ferrara et al. (2016a) compared correlations between crack closing measured by image processing or estimated from damage evolution curves with mechanical recovery indexes. They found that a significant crack closure (> 80%) was necessary to have appreciable strength (10 – 20%) and stiffness (2 – 4%) recoveries.
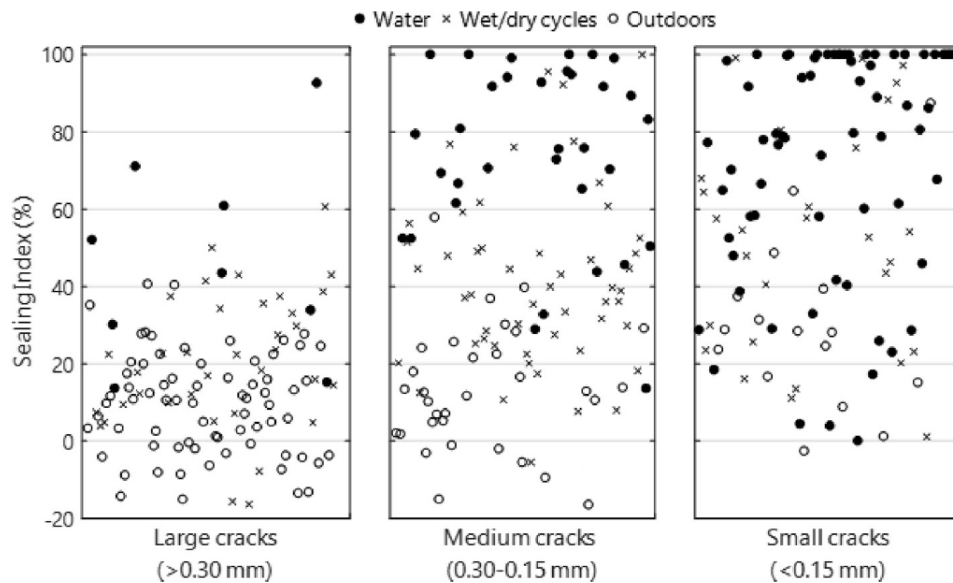
Figure 2.10. Sealing Index (or Closing Ratio) for different crack widths and exposure conditions (Cuenca et al., 2018)

Nevertheless, several researchers mentioned that surface crack closure measurement should not be used alone to assess self-healing, but rather to support other tests such as mechanical or durability ones. Indeed, as analysed by Roig-Flores et al. (2016), visual evaluation of crack closing may lead to overestimation of the healing, compared to Healing Ratios (**Eq. 2.4**) based on water permeability tests (**Figure 2.11**). Park and Choi (2018) also found no correlation between surface crack widths and water permeability results. They sometimes observed no crack closing for specimens that reached zero for the water flow. Li et al. (2020a) also chose not to determine a Closing Ratio because the water flow can be blocked internally by SAP particles while the surface crack width remains unchanged. For these reasons, several authors evaluated self-healing quantitatively with

more reliable techniques and use visual observations of the cracks before and after healing only for qualitative analyses of the self-healing process.
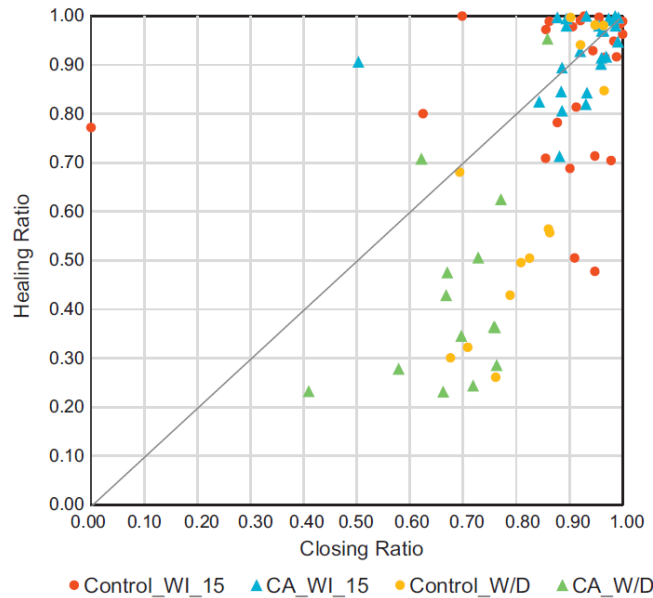
Figure 2.11. Healing Ratio (based on water flow test) vs Closing Ratio (based on crack measurement) for control and CA specimens in different healing expositions (Roig-Flores et al., 2016)

2.3.4 Evaluation of water permeability

Compared to the other testing methods used to assess self-healing, durability tests such as permeability ones give an easy and straightforward characterisation of the whole crack volume. Water permeability had been found to be more sensitive to cracking than chloride permeability (Aldea et al., 1999), as it is proportional to the cube of crack width according to the parallel-plate theory of fluid dynamics (Poiseuille's law) (Tsukamoto & Woener, 1991). As claimed by Picandet et al. (2009), permeability is an intrinsic parameter and constitutes thus a great indicator to evaluate the effects of cracks on concrete durability or performance. Because durability issues in concrete structures are more related to the ingress of liquids and contaminants and because a water permeability device had been previously developed at Polytechnique Montreal, water permeability has been selected in this project to assess self-healing in concrete. In the next sections, different water permeability set-ups and water permeability results will be presented.

2.3.4.1 Water permeability set-ups

Different water permeability set-ups used to evaluate self-healing in literature are reviewed in **Table 2.5** and illustrated in **Figure 2.12**. Van Mullem et al. (2019) also reviewed different configurations while featuring the one developed by Gruyaert et al. (2016). The main set-up parameters are: a) low or high-pressure gradient, by water head or pressure applied directly to the water, and b) measuring inlet flow (water drop), outlet flow (water leak) or both, periodically or continuously. Different specimens and pre-cracking methods are also used, which induces different types of cracks (linear, flexural, artificial).

Disks or cylinders are mostly used for the water permeability tests. While Sisomphon et al. (2012) and Van Tittelboom et al. (2011) worked with linear macrocrack induced by splitting test, Palin et al. (2019) completely split cylinders in halves and then reassembled the specimens. Other researchers also worked with such artificial cracks (Lee et al., 2016; Park & Choi, 2018). During the permeability tests, Sisomphon et al. (2012) and Palin et al. (2019) recorded the outlet flow with a constant water head of 100 mm (1 kPa) (**Figure 2.12a**) or 1000 mm (10 kPa) (**Figure 2.12b**) respectively. The same methodology was also used by (Buller et al., 2019; Hong & Choi, 2017), some with higher pressure gradients (Azarsa et al., 2019; Roig-Flores et al., 2015). On the other hand, Van Tittelboom et al. (2011) measured the inlet flow (drop in water) (**Figure 2.12c**) and considered that a steady state flow has been reached when similar results were obtained during 5 consecutive days. Snoeck et al. (2014b) also used the same set-up.

The aforementioned configurations (cylindrical specimens) are quite simple and many specimens can be tested at the same time. However, linear cracks are less representative of cracks found in structures and artificial cracks from reassembling two separate halves are never ideal (Van Mullem et al., 2019). In addition, such specimens cannot be reloaded to assess mechanical recovery.

Other researchers used in contrast prismatic specimens (**Table 2.5**). Van Tittelboom et al. (2016) evaluated self-healing via visual crack closing, water permeability, 4-point bending tests and acoustic emissions on the same large-scale concrete beams (**Figure 2.12d**). However, they could not draw sound conclusions from the water ingress measurements because of water leakages. They concluded that the set-up was not optimal and needs improvements. Gruyaert et al. (2016) developed a water permeability test that uses prisms with a cast-in hole over their length, which

were pre-cracked by means of a 3-point bending test, creating one flexural macrocrack (**Figure 2.12e**). The hole is sealed at one end and connected to a water reservoir at the other end, where the applied pressure gradient can be easily adjusted (5, 100 and 200 kPa have been tested). They measured the outlet flow that leaked at the bottom of the specimen. Even if this water flow test has been successfully implemented, it requires more specimen preparation and the results depend on the position of the inner hole (Van Mullem et al., 2020a). Besides, the crack width at the connection with the hole can never be exactly known and small particles could block it (Gruyaert et al., 2016).

All these previous studies only measured the inlet or outlet flow through the specimens and assumed a steady state when the value is stabilized. This does not allow to discriminate the effect of pore saturation from the self-healing as they both reduce the flow. With the permeability device developed at Polytechnique Montreal (Desmettre & Charron, 2011) (**Figure 2.12f**), which will be used in this project, both inlet and outlet flows are recorded and a steady-state flow is achieved when both flows are equal. As the pressure gradient is directly applied to the water, it can also be easily adjusted (20, 30, 40, 50 and 100 kPa have been tested). This device was used to measure water permeability on concrete tie-specimens under tensile load and to assess the autogenous healing of concrete under static, constant (Desmettre & Charron, 2012) and cyclic loadings (Desmettre & Charron, 2013), as well as the self-healing capacity of concrete with crystalline admixtures and the impact of fibres (Escoffres et al., 2018). While this device enables to study healing of cracks under representative service conditions (on reinforced concrete containing multiple cracking), the testing method requires a long preparation, followed by a long test duration. This limits the number of specimens and conditions that can be tested.

Table 2.5. Comparison of different water permeability set-ups to evaluate self-healing

Refs	Specimens and pre-cracking	Crack	Pressure gradient[*]	Measurement	Advantages	Disadvantages
(Sisomphon et al., 2012) (1 water tank)	Disks Pre-cracked by splitting	Single tensile macrocrack (uniform width)	1 kPa (water head)	Mass of water passing during 10 min (outlet flow)	- Simple set-up - Many specimens can be tested at the same time	- Crack not representative from structures - Specimens that cannot be reloaded
(Palin et al., 2019) (1 water tank)	Cylinders with grooves Pre-cracked with a vise	In halves and reassembled	10 kPa (water head)	Mass of water passing during 10 min (outlet flow)	- Simple set-up and quick specimen preparation - Many specimens can be tested at the same time	- Artificial crack - Specimens that cannot be reloaded
(Van Tittelboom et al., 2011) (2 water tanks)	Disks Pre-cracked by splitting	Single tensile macrocrack (uniform width)	Not mentioned	Drop in water level at regular time intervals (inlet flow)	- Simple set-up - Many specimens can be tested at the same time	- Crack not representative from structures - Specimens that cannot be reloaded - Can take a very long time to achieve steady state flow
(Van Tittelboom et al., 2016) (1 water tank)	Large-scale concrete beams Pre-cracked by 4-pt bending	Multiple flexural microcracks (variable width)	Not mentioned	Time for water to drop a certain level (inlet flow)	- Realistic cracks - Specimens that can be reloaded	- Not robust, leakages occurred - Can take a very long time

Table 2.5. Comparison of different water permeability set-ups to evaluate self-healing (cont.)

(Gruyaert et al., 2016) (1 water tank)	Prisms with a cast-in hole over the length Pre-cracked by 3-pt bending	Single flexural macrocrack (variable width)	5, 100, 200 kPa (Δp adjustable)	Outlet flow with time	- Realistic crack - Quick measurement - Specimens that could theoretically be reloaded (but not performed)	- Requires more specimen preparation - Not robust, results depend on the position of the cast-in hole in the specimen
(Desmettre & Charron, 2011; Escoffres et al., 2018) (2 water tanks)	Tie-specimens under direct tensile load	Multiple tensile macrocracks (uniform width)	25, 50, 100 kPa (ΔP adjustable)	Inlet and outlet flows with time (+ tensile stress in reinforcement bar)	- Representative cracks found in reinforced concrete cover - Specimens under load (service condition) - Allows varying loading histories - Steady state flow verified when inlet and outlet flows are equal	- Long specimen preparation - Long test duration - Cannot perform multiple tests at the same time

[*]Pressure gradient converted in kPa
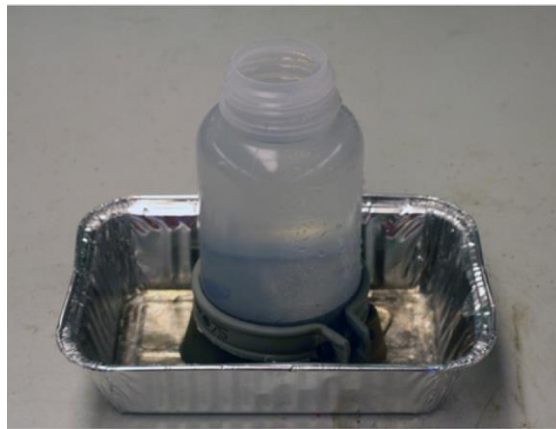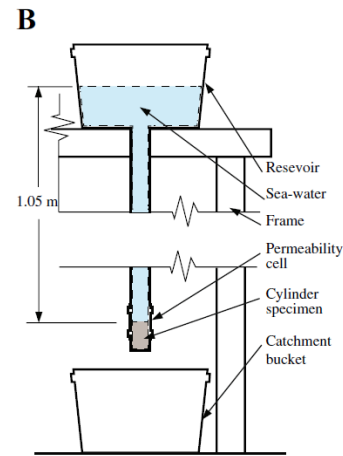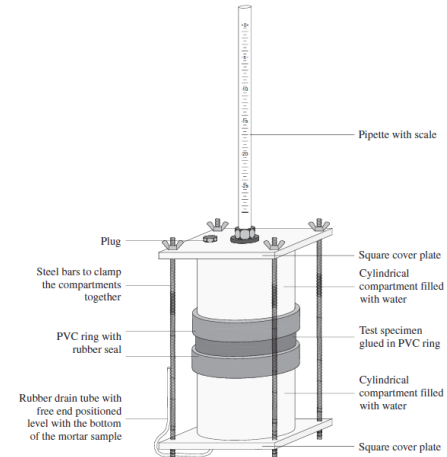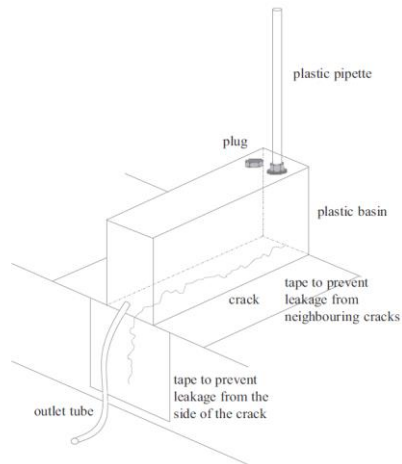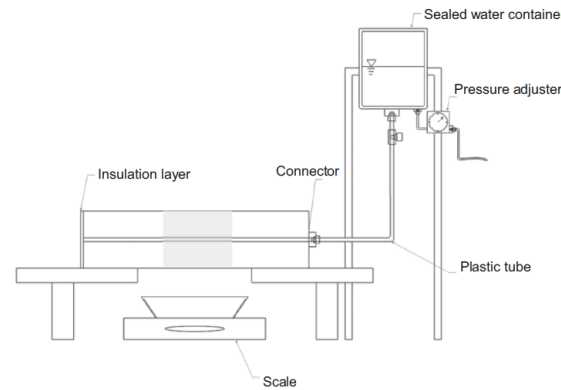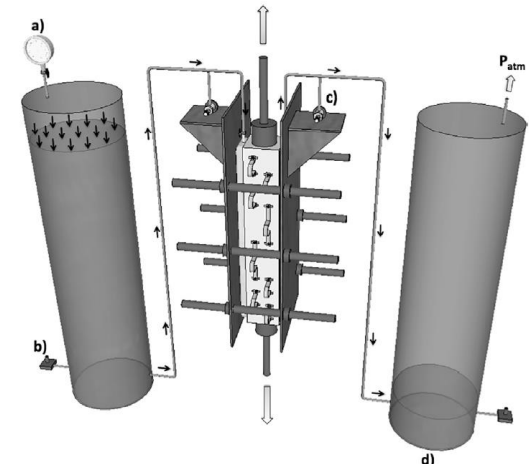
Figure 2.12. Illustrations of the permeability set-ups in literature: a) from (Sisomphon et al., 2012), b) from (Palin et al., 2019), c) from (Van Tittelboom et al., 2011), d) from (Van Tittelboom et al., 2016), e) from (Gruyaert et al., 2016) and f) from (Escoffres et al., 2018)

2.3.4.2   Analysis of the water permeability results

From the permeability test, the flow rate Q (m³/s) going through the specimen can be deduced or directly recorded. This flow rate can be analysed in different ways.

First, in case of one single cracked specimen, the measured water flow rate ($Q_{measured}$) can be described by Poiseuille's law ($Q_{Poiseuille}$). This law represents a flow through two parallel plates that can be multiplied by a reduction factor ζ to take into account the roughness of the crack and the variation of its width (**Eq. 2.2**) (Edvardsen, 1999). In **Eq. 2.2**, Δp (Pa) is the pressure gradient, b (m) is the length of the crack, w (m) is the crack width, μ (Pa s) is the dynamic viscosity and d (m) is the flow path length of the crack. The proportionality between $Q_{measured}$ and w^3 illustrates the significant impact of w on the flow rate. **Eq. 2.2** is useful to study crack characteristics through the variation of factor ζ or to validate some results by verifying the cubic relationship between $Q_{measured}$ and w. However, it does not allow to determine a durability index independent on the testing conditions (pressure gradient and specimen geometry). Such a durability index is useful to compare results from various studies and/or from different testing conditions.

$$Q_{measured} = \zeta\, Q_{Poiseuille} = \zeta \frac{\Delta p\; b\; w^3}{12\, \mu\, d} \tag{2.2}$$

The durability index generally obtained from water permeability test is the permeability coefficient K (m/s), from Darcy's law (**Eq. 2.3**), where $\Delta h/L$ the applied pressure gradient and A (m²) the cross-section exposed to the unidirectional flow.

$$Q_{measured} = K\, A\, \frac{\Delta h}{L} \tag{2.3}$$

Darcy's law is theoretically used to describe a steady incompressible laminar flow through a homogeneous porous medium and implies a proportional relationship between the applied pressure gradient and the flow rate. First, the assumptions of incompressible and laminar flow are generally encountered in case of water permeability tests on concrete. In this study, the Reynolds number (Re) less than 1 (calculation in **Appendix A**) confirms the laminar flow. Secondly, the steady state equilibrium is also verified experimentally during the permeability tests when validating that the inlet and outlet flows are equal. Concerning the assumption of the homogeneity of the porous material, it is more questionable in the case of concrete. It is generally considered that a concrete

matrix uncracked (Breysse & Gérard, 1997) or uniformly cracked (Breysse & Gérard, 1997; Desmettre & Charron, 2011; Escoffres et al., 2018) is homogeneous at a macroscopic scale. But the homogeneous assumption is not well appropriate for one single crack. However, as the permeability coefficient is the only available permeability index, it is thus generally also used to characterise a flow through one single crack (Charron et al., 2007; Gérard et al., 1996; Picandet et al., 2009; Rapoport et al., 2002) and to compare quantitative results from different studies and testing conditions. For these reasons, Darcy's law will also be used in this study. However, as the proportional relationship between the applied pressure gradient and the flow rate could not be perfectly verified in case of one single crack, it is important to verify the impact the pressure gradient on the permeability coefficient to select the adequate experimental procedure. This point will be discussed in more details in **Chapter 4**.

Once the values of Q or K are obtained on a cracked specimen, the self-healing capacity can be deduced from their decrease in time during healing. The self-healing capacity is often evaluated through a Healing Ratio (*HR*), calculated according to **Eq. 2.4** that indicates the percentage of healing (Azarsa et al., 2019; Beglarigale et al., 2021; Buller et al., 2019; Hong & Choi, 2017; Li et al., 2020a; Roig-Flores et al., 2015; Wang et al., 2018). Other studies used instead **Eq. 2.5** to present the percentage of residual flow or permeability (Escoffres et al., 2018; Jiang et al., 2015; Sisomphon et al., 2012).

$$Healing\ Ratio\ HR\ (\%) = 1 - \frac{final\ flow\ rate\ Q\ or\ permeability\ coefficient\ K}{initial\ flow\ rate\ Qi\ or\ permeability\ coefficient\ Ki} \quad \textbf{(2.4)}$$

$$Healing = \frac{final\ flow\ rate\ Q\ or\ permeability\ coefficient\ K}{initial\ flow\ rate\ Qi\ or\ permeability\ coefficient\ Ki} \quad \textbf{(2.5)}$$

Another method consists in determining the evolution of equivalent crack width (w_{eq}) to analyse self-healing from permeability measurements. In that case, **Eq. 2.2** is used to calculate the reduction factor ζ from the initial measured crack width and the associated initial $Q_{measured}$. Then, the evolution of w_{eq} in time can be determined from the evolution of $Q_{measured}$, assuming a constant reduction factor in time. This methodology was used by (Gupta & Biparva, 2015; Park & Choi, 2018) to assess self-healing in concrete with linear cracks and by Van Mullem et al. (2019) for flexural crack. **Figure 2.13** illustrates the application of this methodology by Park and Choi (2018),

who determined the constant reduction factor ζ via regression analysis of the flow rate measured on different specimens (**Figure 2.13a**), and then used it to obtain the results of equivalent crack width in **Figure 2.13b**.

The advantages and drawbacks of both methods (evolution of *HR* or w_{eq} in time) to analyse the self-healing process will be discussed in **Chapter 5**.
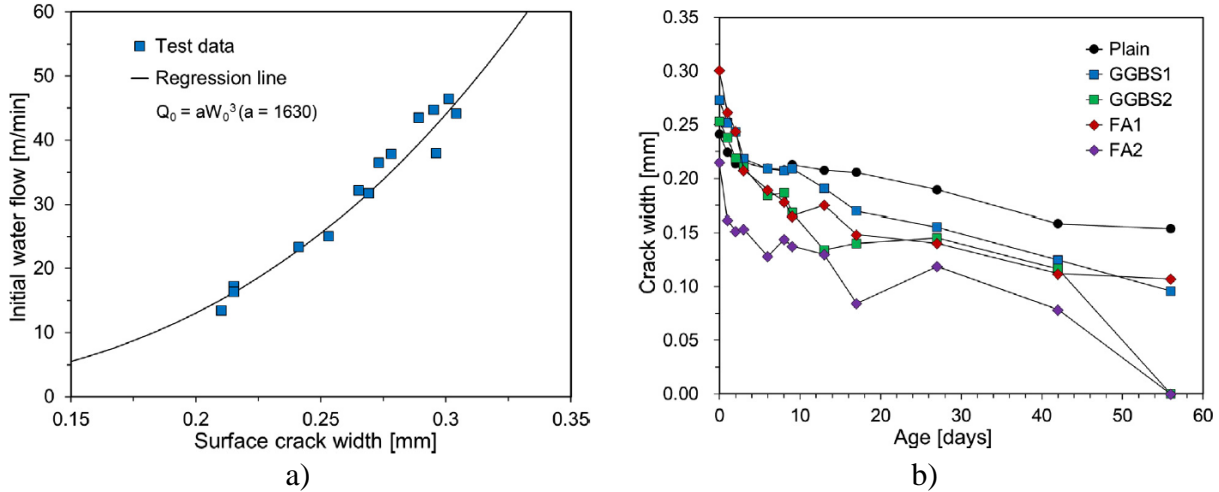
Figure 2.13. Water permeability results from (Park & Choi, 2018): a) relationship between initial water flow and crack width, b) evolution of equivalent crack width

2.3.5 Evaluation of mechanical recovery

Contrary to durability tests, mechanical tests do not give a straightforward evaluation of the cracks and further analysis and interpretation of the results are needed to assess self-healing. Recovery of strength (peak or first cracking), stiffness and deformation capacity can be determined and different ratios or indexes are used. **Table 2.6** indicates the most common indexes considered for strength (in load *P* or in stress σ values) and stiffness (from stress-strain or σ-COD or *P*-COD curves) recoveries when performing bending tests. An example of **Eq. 2.7** is illustrated in **Figure 2.14** for the strength recovery, for better understanding of the parameters.

Table 2.6. Expressions of mechanical recovery indexes frequently used when performing bending tests (p*re-load* and *unload* = from pre-cracking curve, *reload* = from reloading curve, *ref* = from reference unhealed specimen)

Mechanical recovery index		References	Eq.
For strength	$\dfrac{\sigma_{reload}}{\sigma_{pre-load}}$	(Alghamri & Al-Tabbaa, 2020; Escoffres et al., 2018; Snoeck & De Belie, 2016)	**(2.6)**
	$\dfrac{P \text{ or } \sigma_{reload} - P \text{ or } \sigma_{unload}}{P \text{ or } \sigma_{pre-load} - P \text{ or } \sigma_{unload}}$	(Anglani et al., 2020; Buller et al., 2019; Ferrara et al., 2014b; Ferrara et al., 2016b; Snoeck et al., 2014b; Van Tittelboom et al., 2012)	**(2.7)**
	$\dfrac{P_{reload} - P_{reload,ref}}{P_{pre-load,ref} - P_{reload,ref}}$	(Namnoum et al., 2021)	**(2.8)**
For stiffness	$\dfrac{K_{reload}}{K_{pre-load}}$	(Alghamri & Al-Tabbaa, 2020; Van Tittelboom et al., 2012)	**(2.9)**
	$\dfrac{K_{reload} - K_{unload}}{K_{pre-load} - K_{unload}}$	(Buller et al., 2019; Ferrara et al., 2014b; Snoeck & De Belie, 2016)	**(2.10)**
	$\dfrac{K_{reload} - K_{reload,ref}}{K_{pre-load,ref} - K_{reload,ref}}$	(Namnoum et al., 2021)	**(2.11)**
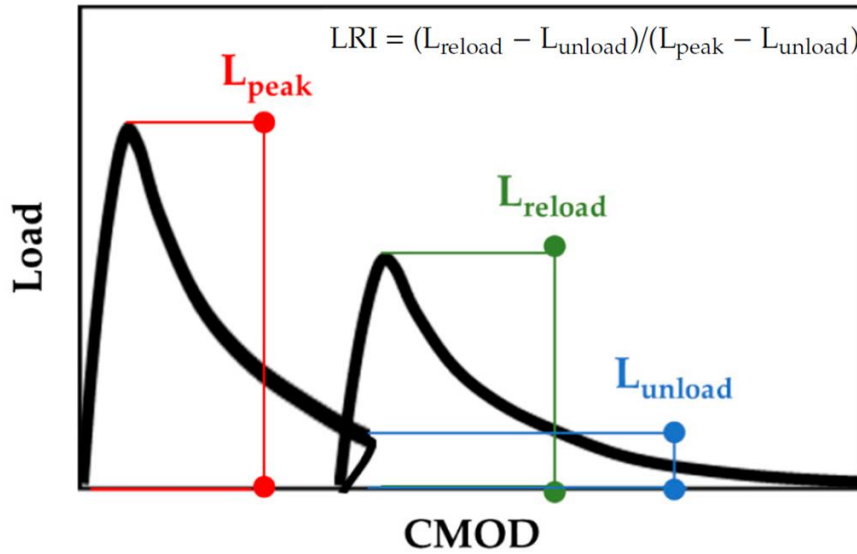
Figure 2.14. Parameters used to determine the Load Recovery Index by (Anglani et al., 2020)

The strength regain was evaluated with **Eq. 2.6** (direct ratio) by Snoeck and De Belie (2016) considering σ for first-cracking, by Escoffres et al. (2018) considering $\sigma_{pre\text{-}load}$ and σ_{reload} at the same COD and by Alghamri and Al-Tabbaa (2020) considering $\sigma_{pre\text{-}load}$ for first-cracking and σ_{reload} at peak. **Eq. 2.7** (ratio with subtraction of unload) was mostly used by (Ferrara et al., 2014b; Ferrara et al., 2016b) and others considering the peak values with σ results (Snoeck et al., 2014b) or with P results (Anglani et al., 2020; Buller et al., 2019; Van Tittelboom et al., 2012), or the first-cracking values in σ (Snoeck et al., 2014b). Lastly, Namnoum et al. (2021) used **Eq. 2.8** considering a reference unhealed specimen undergoing the same curing condition.

The stiffness recovery was calculated with direct ratios (**Eq. 2.9**) by Alghamri and Al-Tabbaa (2020) from stress-strain (σ-ε) curve considering the slopes at peak, and by Van Tittelboom et al. (2012) from σ-COD curve considering the slopes at 40% of the peak. **Eq. 2.10** (same expression as **Eq. 2.7**) was used by Ferrara et al. (2014b) from σ-COD, by Buller et al. (2019) from P-COD and by Snoeck and De Belie (2016) from σ-ε curves. Finally, Namnoum et al. (2021) used **Eq. 2.11** considering a reference unhealed specimen again.

Other researchers considered other characteristics of the mechanical behaviour of healed specimens. They compared the number of cracks formed before and after healing (new cracks) (Deng & Liao, 2018; Sisomphon et al., 2013) or determined index of dissipation energy (Buller et al., 2019).

Besides all these different ratios, a wide range of different loading procedures (and hence cracking states), specimens (shape and dimensions of specimens) and parameters (age of pre-cracking, type of crack, crack width, healing condition) are used in studies, which makes comparison of mechanical recovery indexes in literature difficult. For example, with respect to the studies that used CSA, CA and SAP, strength regain ranged from 27 to 250%, while stiffness regain varied from 40 to 75%. Moreover, a crack with a lower residual strength will probably have a higher mechanical recovery after healing compared to one with a higher residual strength, for which healing products must be very strong to bring a regain.

Therefore, mechanical recovery results should be compared to the ones from reference uncracked specimens that underwent the same condition to adequately assess self-healing.

2.3.6 Analysis of the healing products

Many studies undertook identification of the mineralogy and chemistry of the healing products formed in the cracks. Scanning electron microscopy (SEM) combined with energy-dispersive X-ray analysis (EDS) are mostly used. Besides, X-ray powder diffraction (XRD) and thermogravimetric analysis (TGA) allow accurate identification of the products.

The main healing products found in healed cracks are calcium carbonate (Buller et al., 2019; Cuenca et al., 2018; Deng & Liao, 2018; Escoffres et al., 2018; Gruyaert et al., 2016; Hong et al., 2020; Li et al., 2020a; Li et al., 2020b; Sisomphon et al., 2013; Snoeck & De Belie, 2016; Snoeck et al., 2016; Snoeck et al., 2014b; Wang et al., 2018; Yildirim et al., 2018), mainly in the form of calcite (**Figure 2.15a**). Other polymorphs of $CaCO_3$, aragonite (**Figure 2.15b**) (Escoffres et al., 2018; Wang et al., 2018) and vaterite (**Figure 2.15c**) (Yildirim et al., 2018), have been observed as well. It must be noted that Yildirim et al. (2018) performed TGA and XRD analyses but did not show SEM pictures of vaterite. **Figure 2.15c** (Sevcik et al., 2018) does not come from a study about self-healing concrete. Delayed hydration products such as C-S-H (**Figure 2.15d**) (Ferrara et al., 2017; Hong et al., 2020; Sisomphon et al., 2013), C-A-S-H (**Figure 2.15e**) (Snoeck et al., 2016; Yildirim et al., 2018) and ettringite (**Figure 2.15f**) (Cuenca et al., 2018; Escoffres et al., 2018; Ferrara et al., 2014b; Sisomphon et al., 2013; Wang et al., 2018) are common healing products as well.
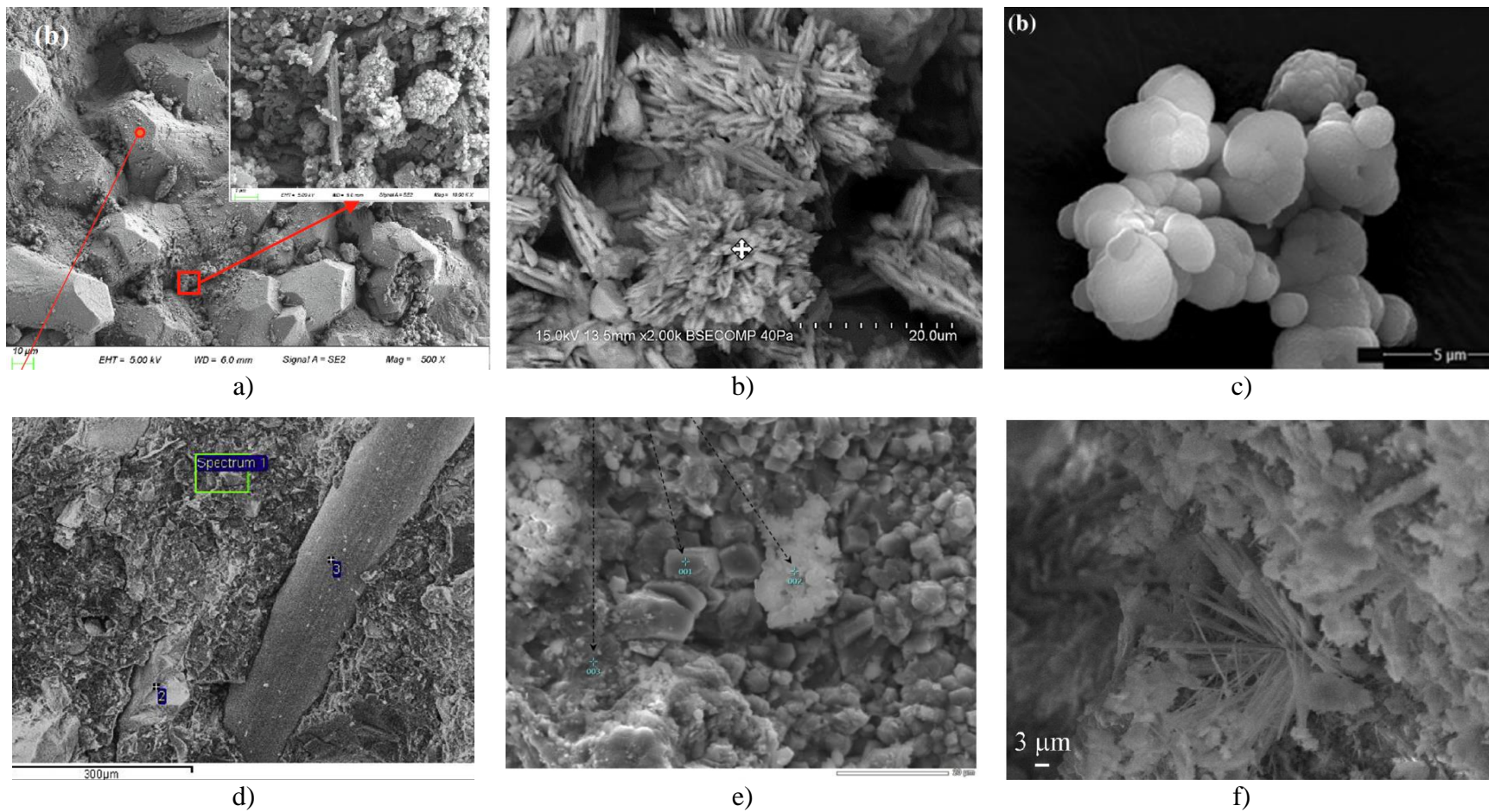
Figure 2.15. Main healing products found in literature: a) calcite (bigger picture) from (Li et al., 2020b), b) aragonite from (Escoffres et al., 2018), c) vaterite from (Sevcik et al., 2018) (not a self-healing study), d) C-S-H (spectrum 1) from (Ferrara et al., 2017), e) C-A-S-H (spot 003) from (Snoeck et al., 2016), and f)) ettringite from (Ferrara et al., 2014b)

The healing products vary according to the exposure condition. For example, Sisomphon et al. (2013) found more $CaCO_3$ and C-S-H in wet/dry cycles, while more ettringite in tap water. In addition, the healing products are influenced by the self-healing agents used. When using CA in concrete, Ferrara et al. (2014b) found typical reaction products with a peak in sulphur for specimens containing CA compared to the control mix (**Figure 2.16**). Cuenca et al. (2018) found acicular products in specimens with CA. Escoffres et al. (2018) found aragonite instead of calcite, with a CA containing magnesium. When using CSA, Park and Choi (2018) observed needle-type hydrates and C-S-H compared to plate-type products (portlandite) in the plain mix. With SAP, Lee et al. (2016) found more portlandite and no calcium carbonate in contrast to (Snoeck et al., 2014b), who mainly observed calcium carbonate in mixes with SAP.

a)   b)
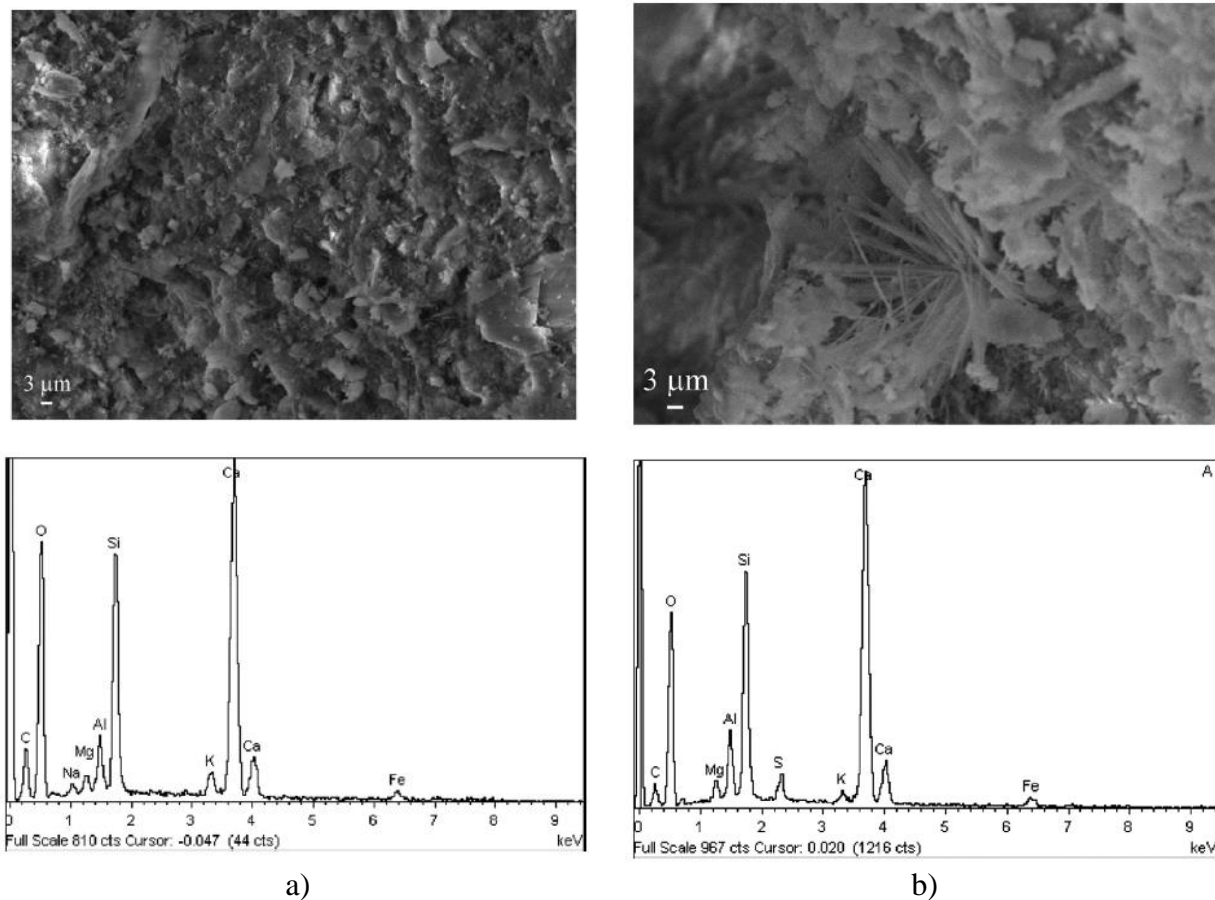
Figure 2.16. Microscopic analyses of concrete specimens immersed in water for 3 months, a) control mix, b) mix with CA (Ferrara et al., 2014b)

In addition to the nature of the healing products, Park and Choi (2021) correlated water flow results with amounts of healing products found with thermogravimetric analysis (TGA). The higher content of the healing products observed, the higher reduction of water flow was measured. They found a strong correlation between the self-healing performance and the total amounts of calcite and M_{70-200}, which includes C-S-H, C-A-H and ettringite (**Figure 2.17**).
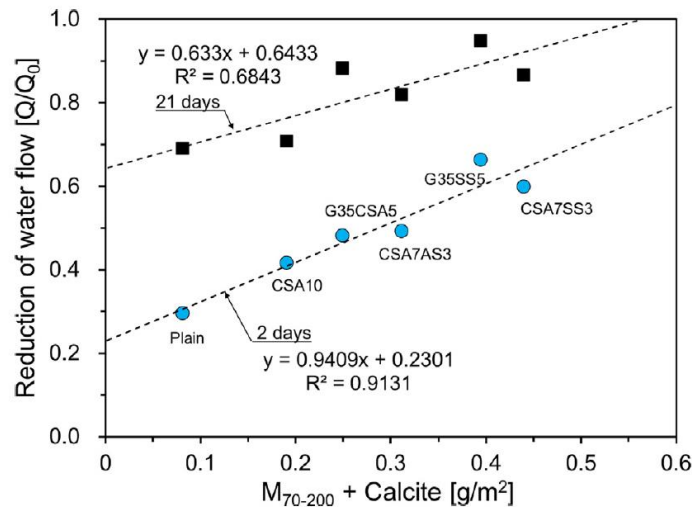
Figure 2.17. Correlations between water flow results and the amount of M_{70-200} + calcite (Park & Choi, 2021)

2.4 Self-healing approaches

2.4.1 Overview of different self-healing approaches

Before focusing on studies using the self-healing agents selected in this project (crystalline admixture, expansive agent and superabsorbent polymer), **Table 2.7** presents a review of the most common self-healing approaches, categorised into non-encapsulated and encapsulated approaches. This table presents the advantages, disadvantages and potential use in practice, as well as reference examples. **Figure 2.18** also illustrates some of these techniques. These self-healing approaches have been reviewed and discussed in previous state-of-the-art papers (De Belie et al., 2018; Li & Herbert, 2012; Van Tittelboom & De Belie, 2013).

Table 2.7. Review of most common self-healing approaches

Category		Examples	Advantages	Disadvantages	Potential use in practice
Non-encapsulated	Mineral additions	SCMs (fly ash or slag) (Van Tittelboom, 2012)	Enhance further hydration	- Not beneficial for calcium carbonate precipitation - Slow hydration kinetics, needs activation to accelerate	Already used in concrete industry
		Crystalline admixture (Ferrara et al., 2016b)	- Promotes crystallisation and can enhance self-healing - Synergy observed if combined with CSA	- Efficiency not unanimous - Needs contact with liquid water - A wide range of different materials under this generic name	Already used in concrete industry
		Expansive agent (CSA) (Sisomphon et al., 2012)	Enhances self-healing via formation of expansive products	Risk of excessive expansion and disintegration if overdose	Already used in concrete industry
	Water reservoir	SAP (Snoeck et al., 2014b)	- Crack mitigation - Immediate self-sealing - Promotes self-healing	Loss of mechanical properties	Readily available
	Fibres	ECC (Herbert & Li, 2013)	Very narrow crack width beneficial for autogenous healing	Very expensive (FRC more economical)	Very interesting but high cost and innovative material, drawbacks for rapid market penetration
	Bacteria	Bacterial solution in expanded clay (Jonkers, 2011)	Enhances self-healing via calcium carbonate precipitation	- Low shelf life - Needs protection - Expensive - Need nutrients	Interesting but still high cost

Table 2.7. Review of most common self-healing approaches (cont.)

Encapsulated	Chemical micro-capsules	Epoxy in organic shells + catalyst (Wang et al., 2013)	Autonomous self-healing upon cracking	- Loss of mechanical properties - Low shelf life - Requires a lot of preparation - Needs a catalyst	Interesting but complex (capsules technology, implementation) and high cost
	Chemical macro-capsules	Polyurethane in glass tubing (Van Mullem et al., 2020a)	Fast autonomous self-healing upon cracking	- Non-pervasive - Requires a lot of preparation	Not pervasive, complex (capsules technology, implementation) and high cost
	Vascular systems	Cyanoacrylate in vascular channels (Selvarajoo et al., 2020)	Healing agent is continuously supplied	- Need human intervention (not autonomous) - Need adequate low viscosity healing agent - Non-pervasive if it's not 3D	Interesting but complex (capsules technology, implementation, healing agent), high cost and not really autonomous
	Bacteria	*B. sphaericus* in melamine shells (Wang et al., 2014)	- Enhances self-healing via calcium carbonate precipitation - Higher viability than non-encapsulated bacteria	- Low shelf life - Needs protection - Expensive - Need nutrients	Interesting but still high cost
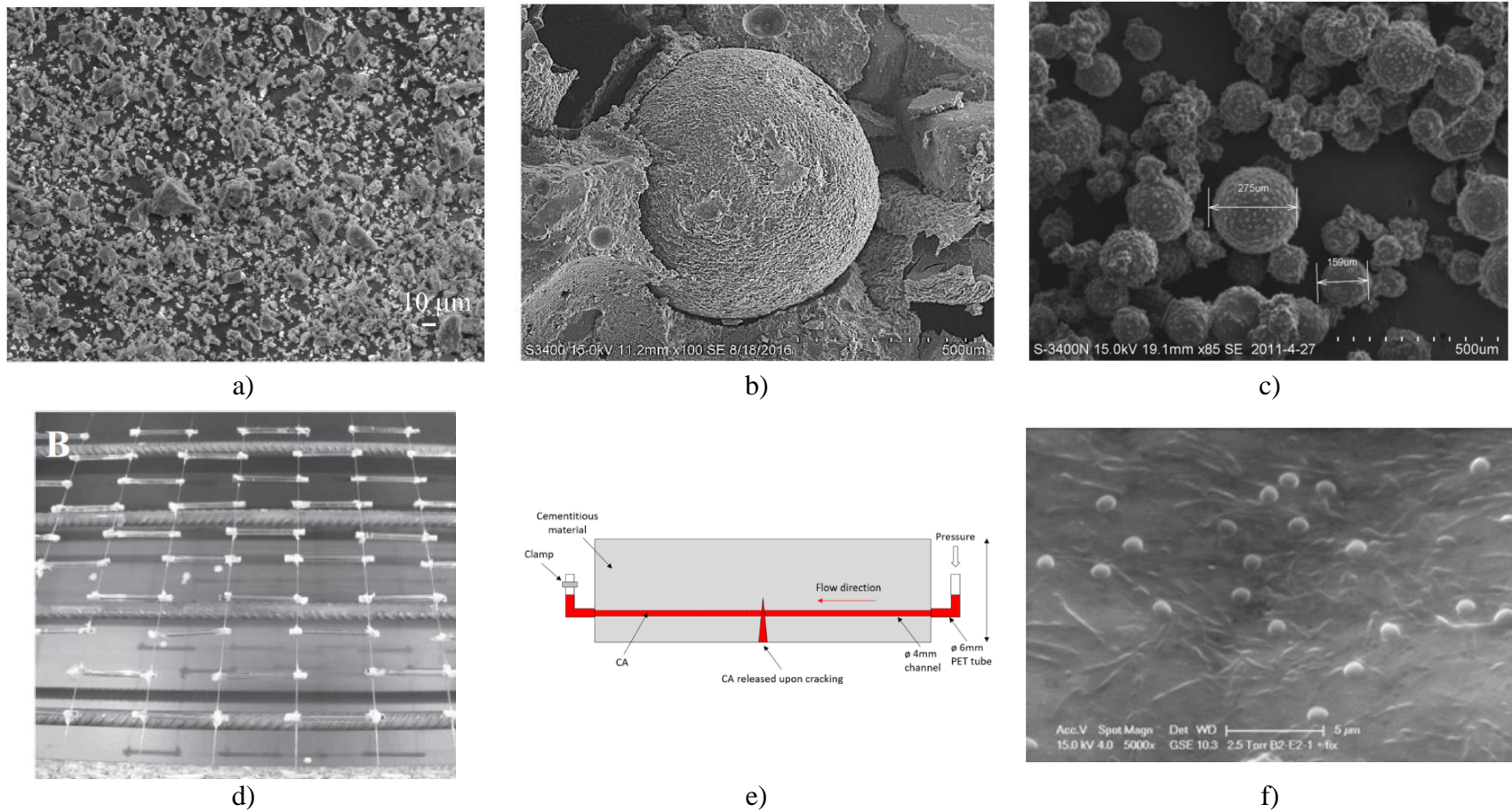
Figure 2.18. Illustrations of different self-healing approaches used in literature: a) crystalline admixture (Ferrara et al., 2014b), b) SAP (Hong & Choi, 2017), c) microcapsules (Wang et al., 2013), d) macrocapsules (Van Tittelboom et al., 2016), e) vascular systems (Selvarajoo et al., 2020) and f) bacteria (Jonkers, 2011)

The first category related to non-encapsulated approaches is easier to implement and cheaper than the encapsulated approaches. Mineral additions, such as supplementary cementitious materials (SCMs), crystalline admixtures (**Figure 2.18a**) and expansive agents are already commonly used in concrete. Crystalline admixtures are permeability reducing admixtures, while expansive agents are shrinkage-reducing admixtures. They stimulate autogenous healing by promoting crystallisation and expansive products in the porous matrix respectively. Another way to boost this self-healing process is to incorporate water reservoirs in the matrix, by means of lightweight aggregates (LWA) or superabsorbent polymers (SAP). SAP are natural or synthetic cross-linked polymers (**Figure 2.18b**) with a high capacity to absorb fluid and have a threefold action in concrete: crack mitigation, immediate self-sealing and promotion of self-healing (De Belie et al., 2018). Finally, as it is usually agreed that narrow cracks can heal better than larger cracks, the use of fibres to restrict crack width in conventional FRC (Desmettre & Charron, 2012) (Escoffres et al., 2018), or to favour multiple microcracking HPFRCC (Ferrara et al., 2017), UHPFRC (Charron et al., 2008; Lo Monte & Ferrara, 2021) or ECC (Herbert & Li, 2013), enhances the self-healing capacity.

The second category, involving either micro- (**Figure 2.18c**) or macrocapsules, have to withstand concrete mixing and casting while staying brittle enough to open upon cracking. A lot of preparation is required to fill the capsules (Anglani et al., 2020; Van Mullem et al., 2020a; Van Tittelboom et al., 2016; Wang et al., 2013) and they can lead to lower mechanical performance (De Belie et al., 2018). Glass tubing (**Figure 2.18d**) and some vascular systems (**Figure 2.18e**) are non-pervasive because they are placed in some locations and not in the whole element. However, one of the main advantages of this category is certainly to prevent the consumption of the healing agent before cracking, unlike mineral additions that are partially consumed during the initial hydration.

In the bacteria-based approach (**Figure 2.18f**), bacteria need protection (capsule, impregnation in LWA or in hydrogels) to survive in the highly alkaline environment and a dense matrix. Nutrients must be supplied and contact with water is needed for microbiologically induced calcite precipitation to occur. At the end, bacteria cells will die when they become embedded by $CaCO_3$ crystals or when all nutrients are consumed (Van Tittelboom & De Belie, 2013).

There is no consensus yet about the best approach in terms of efficiency, cost and implementation (De Belie et al., 2018). Regarding these criteria, the use of mineral admixtures seems favourable. Even if they are partially consumed in the matrix before cracking when in contact with water during

cement hydration, the lower cost and ease of implementation of this approach surpass this drawback, compared to encapsulation techniques and bacteria.

The next sections will thus focus on self-healing studies with crystalline admixtures (**Section 2.4.2**), expansive agents (**Section 2.4.3**) and superabsorbent polymers (**Section 2.4.4**), the self-healing agents used in this project.

2.4.2 Crystalline admixtures (CA)

Crystalline admixtures are hydrophilic permeability reducing admixtures that can resist to hydrostatic pressure. They are commonly used for watertight concrete structures. The term "crystalline admixture" is in fact a commercial label under which a wide range of compositions can be found. According to ACI-212 (2012) report, the general reaction process may follow **Eq. 2.8**, where the crystalline promoter (M_XR_X) reacts with calcium silicate and water to produce modified C-S-H and a pore-blocking precipitate.

$$3\ CaO\text{-}SiO_2 + M_XR_X + H_2O \rightarrow Ca_XSi_XO_XR\text{-}(H_2O)_X + M_XCaR_X\text{-}(H_2O)_X \tag{2.8}$$

Calcium silicate + crystalline + water $\rightarrow$ modified C-S-H + pore-blocking precipitate
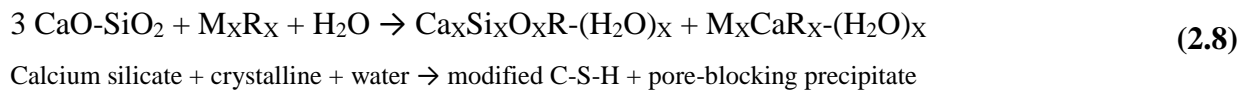
The self-healing capacity of concrete with crystalline admixtures (CA) has been more investigated this past decade. First, Jaroenratanapirom and Sahamitmongkol (2011) found via crack closure measurement that CA (1%-m_{cement} in addition) was only efficient to seal very small cracks (up to 0.05 mm) in mortar specimens under water. More recent studies who measured crack closure also reported that the use of CA was most efficient to seal small cracks (up to 0.15 mm), especially under water but also in outdoor exposure (1%-m_{cement} in replacement) (Borg et al., 2018) and under repeated reloading (0.8%-m_{cement} in addition) (Cuenca et al., 2018).

Sisomphon et al. (2012) found complete crack closure with CA for small cracks (up to 0.2 mm) under water and noticed that an overdose of CA was not necessary (1.5 vs 4%-m_{cement} in replacement were tested). Regarding water permeability (Sisomphon et al., 2012) and mechanical recovery (Sisomphon et al., 2013), the strain-hardening cementitious composites with CA showed the lowest performance, while the combination of CA+CSA showed the highest one. Wet/dry cycles (12h wet/12h dry) were the most favourable exposition for recovery of mechanical properties. It must be noted that they worked with smaller crack widths (0.01 – 0.05 mm)

(Sisomphon et al., 2013). Later, Ferrara et al. studied the self-healing potential of CA (1%-m_{cement} in addition) via flexural tests in ordinary concrete (w/c = 0.63) (Ferrara et al., 2014b) and HPFRCC (w/b = 0.18) (Ferrara et al., 2016b), in different expositions including a long-term outdoor exposition. They determined the mechanical recovery and found a beneficial effect of CA in all conditions compared to the control mix as illustrated in **Figure 2.19**. Efficiency of HPFRCC was superior because of a "chemical pre-stressing" of fibres due to the somewhat expansive reaction provided by CA. They also found less scattering in the healing performance with CA compared to the control mix. This beneficial effect of CA to reduce the variation of the healing process was also reported by (Escoffres et al., 2018; Roig-Flores et al., 2015). Li et al. (2020b) also obtained a much higher self-healing capacity with CA (1.2%-m_{cement} in addition) compared to the control mix, in terms of crack closure, water absorption and recovery of compressive strength.
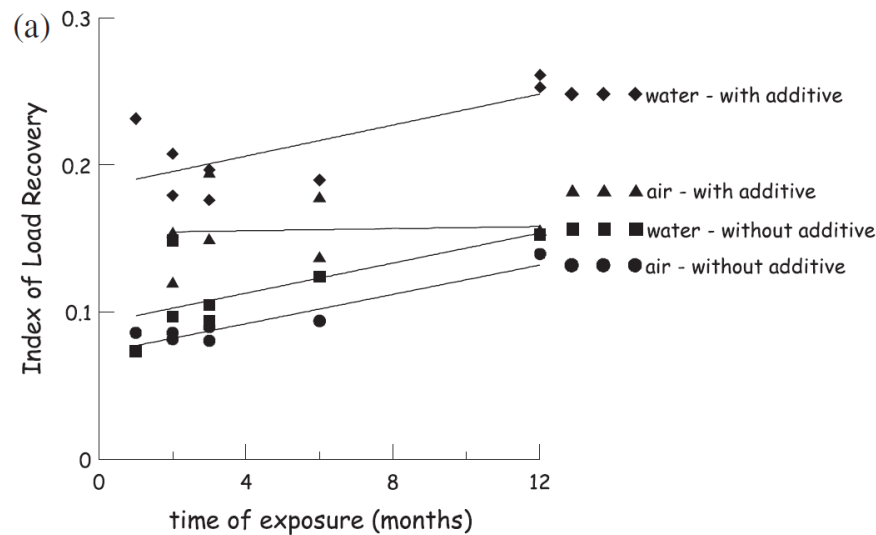
Figure 2.19. Evolution of flexural recovery (strength regain) for control and CA mixes in water and outdoor (air) exposures (Ferrara et al., 2014b)

While the previous studies worked with cracks created in mature concrete (≥ 28 days), Roig-Flores et al. (Roig-Flores et al., 2015; Roig-Flores et al., 2016) investigated self-healing of early age cracks created at 2 days and exposed in different conditions via crack closure and water permeability tests. While water immersion was found the most favourable condition for self-healing with CA, wet/dry cycles exposure resulted in low and high scattered self-healing

performance. Moreover, they did not find significant differences between the CA mix (4%-m_{cement} in addition) and the control mix.

Other studies also found no significant beneficial effect of CA, in terms of flexural recovery of beams, water permeability of concrete tie-specimens under tensile load (2%-m_{cement} in addition) (Escoffres et al., 2018) or under continuous water flow test (2%-m_{cement} in addition) (Azarsa et al., 2019).

Finally, Wang et al. (2018) and Park and Choi (2018) investigated mixes with a combination of several admixtures including CA. Wang et al. (2018) combined different mineral admixtures (CA, CSA, CHP = calcium hydrogen phosphate) in different dosages in cement replacement and the use of ceramsites (lightweight aggregates) as sodium carbonate carriers. They performed crack closure and gas permeability tests and found enhanced self-healing compared to the control mix. Park and Choi (2018) combined CA+CSA (1.5% and 10%-m_{cement} respectively in replacement) and found an accelerated self-healing compared to the control mix, measured via water permeability. Later, Park and Choi (2021) combined CSA with Na_2SO_3 or $Al_2(SO_4)_3$ considered as crystalline additives, and obtained a higher amount of healing products than the cement paste with CSA alone, via TGA analysis of scraped powder.

In conclusion, the use of CA seems to be efficient to heal small cracks (< 0.2 mm) under water immersion, but for larger crack widths and other expositions, the beneficial effect of CA for self-healing compared to the control mix is not unanimous. However, several studies reported less variation in the results when using CA. Finally, the combination of CA with CSA is interesting.

2.4.3 Expansive agents (CSA)

Expansive agents are shrinkage-reducing admixtures that can be distinguished by their composition:

- Type K: calcium sulfoaluminate-based (CSA);
- Type G: calcium oxide-based (CaO);
- Type MgO: magnesium oxide-based (MgO).

CSA-based expansive agents react with water and create expansion via ettringite formation. For CaO-based additives, expansion is generated via crystals growth resulting from the transformation

of CaO into portlandite $Ca(OH)_2$ in presence of water. Lastly, MgO-based agents are characterised by a delayed expansion, slowly forming brucite $Mg(OH)_2$ (Hamedanimojarrad et al., 2010).

The effect of CSA alone in self-healing concrete was determined by several researchers. Park and Choi (2021) obtained a higher amount of healing products with their CSA mix (10%-m_{cement} in replacement) compared to the control cement paste. Jiang et al. (2015) investigated several single admixtures (silica-based A, chemical expansive B, swelling material C and crystalline component D) (8%-m_{cement} in replacement) as well as combinations of 3 (ABC, ABD, BCD, ACD) and 4 additives (ABCD), with different dosages and compared their performance with a control mix (P). Via crack closure, water permeability and water absorption tests, they found that when considering one single admixture, the mortar containing the chemical expansive B performed the best, as illustrated in **Figure 2.20**, which shows water permeability results for specimens pre-cracked at 7 days (**Figure 2.20a**) and at 28 days (**Figure 2.20b**) exposed in still water exposure. When multiple minerals are considered, they found that the mix containing ACD showed the best performance and they pointed out that the swelling and crystalline components worked best together.

a)   b)
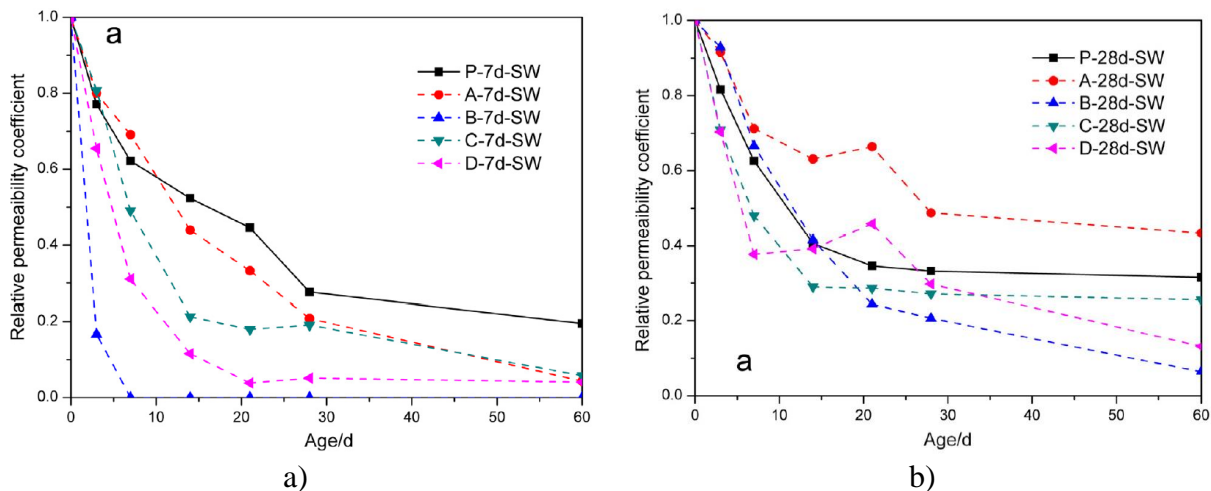
Figure 2.20. Water permeability results for mixes with a single admixture healed in still water and pre-cracked at a) 7 days and b) 28 days (Jiang et al., 2015)

Some studies have investigated CA with a CSA-based expansive agent, resulting in a synergy for the self-healing performance (Sisomphon et al., 2012, 2013). Other studies examined CSA in combinations with other additives and obtained an enhanced healing (Park & Choi, 2018; Park & Choi, 2021; Wang et al., 2018). Buller et al. (2019) compared mixes with SH1 = sodium carbonate

+ calcium stearate + zeolite (3%-mcement in addition) and SH2 = SH1 + CSA + bentonite (6%-mcement in addition) and found a better healing for SH2 in terms of water permeability and mechanical recovery.

The use of CaO-based expansive agent was studied by Fattahi (2015) via air permeability measures on pre-cracked mortars healed in humid chamber. She found enhanced healing with CaO expansive agent (10%-mcement in replacement), because it provided higher amount of portlandite in the matrix. When using cement pellets containing CaO in replacement of sand, the self-healing capacity was further increased with a high healing rate even after 6 months.

Finally, the use of MgO-based expansive additive as healing agent was more studied. Qureshi and Al-Tabbaa (2016) obtained a higher self-healing performance (crack closure, gas permeability, water absorption and mechanical recovery) in cement pastes containing MgO (4 to 12%-mcement in addition), with sealing of cracks up to 0.5 mm after 28 days under water. Sherir et al. (Sherir et al., 2016; Sherir et al., 2017a; Sherir et al., 2017b) studied recovery of mechanical properties (compressive and flexural strengths) of ECC containing 5%-m_{cement} of MgO and found higher self-healing with MgO than the control mix, whether in water immersion or in a real long-term outdoor exposure, even after repeated reloading. More recently, self-healing with MgO-based healing agents (blend of 5% of MgO, 5% of hydrated lime and 2.5% of bentonite by mass of cement in replacement) was studied in an interlaboratory study through water absorption, water permeability, chloride penetration and crack closure tests (Litina et al., 2021). The concretes containing the MgO-blend performed similarly as the reference mix but showed greater self-healing efficiency in the long-term because the additives remain longer unreacted.

In conclusion, CSA- and MgO-based expansive agents have been more studied as healing agents than the CaO-based one. Nevertheless, all these types of expansive agents brought enhanced healing at high dosage. CSA was often used in combination with other admixtures such as CA, providing a synergetic effect.

2.4.4 Superabsorbent polymers (SAP)

Superabsorbent polymers are natural or synthetic cross-linked polymers with a high capacity to absorb fluid, as illustrated in **Figure 2.21**. They are characterised by their absorption capacity and swelling time, which can be measured with the tea-bag method and the Vortex test (Zohuriaan & Kabiri, 2008). Their absorption capacity depends on the alkalinity and ions concentration of the solution. Hence, SAP will absorb less water in concrete than in demineralised water. It must be noted that SAP can also absorb the humidity in the ambient atmosphere (Snoeck et al., 2014b).
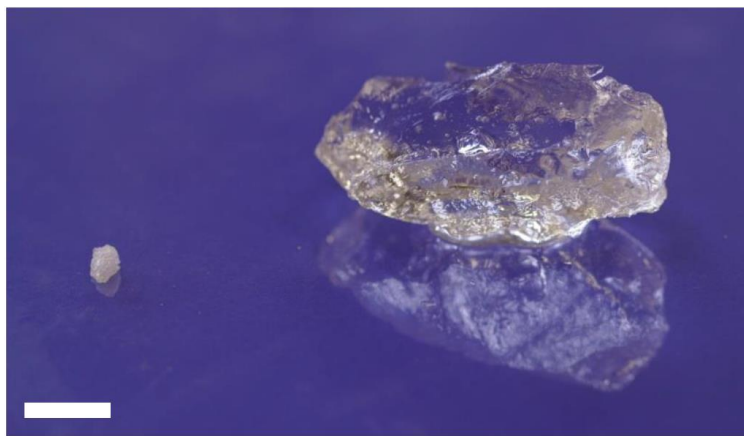
Figure 2.21. Unswollen (left) and swollen (right) SAP particles (scale bar = 10 mm) (Snoeck, 2015)

SAP greatly impacts the workability, microstructure and strength of concrete and this effect needs to be considered to develop adequate mixes. This has been specifically studied by Snoeck et al. (2014a), who compared mortars (w/c = 0.50) with SAP (0.5 and 1%-m_{cement} in addition) either with additional water or additional superplasticiser (SP) to reach the same flow of a reference mortar without SAP. Adding more water leads globally to the same microstructure as the reference (higher total w/c but same effective w/c) but the compressive strength is lower because of the macropores. On the other hand, adding more SP leads to a denser microstructure (same total w/c but lower effective w/c) and a lower decrease of the strength. While most studies used additional water in mixes containing SAP (Gruyaert et al., 2016; Hong & Choi, 2017; Lee et al., 2016; Snoeck & De Belie, 2016), Deng and Liao (2018) added more high range water reducer in their ECC mixes. Furthermore, because SAPs particles form macropores in the matrix when they release water and

shrink, they act as air voids, which increase freeze-thaw resistance of concrete (Jensen, 2008; Mönnig & Lura, 2007).

It must be noted that pH-sensitive SAPs have been developed (Mignon et al., 2015), to decrease swelling during mixing and hence reduce the size of formed macropores, overcoming the loss in mechanical properties. Another way is to add calcium ions to postpone its swelling (Lee et al., 2016; Li et al., 2020a). In that case, Li et al. (2020a) did not add additional water nor SP.

First used in concrete for internal curing to reduce autogenous shrinkage ($0.3 - 0.5\%$-m_{cement} in addition) (Assmann, 2013; Jensen & Hansen, 2001, 2002; Schröfl et al., 2012), SAPs have now been used for self-healing purpose. Self-healing with SAP has been largely studied in the last decade and it has been summarised that SAPs have a threefold action in concrete: crack mitigation, immediate self-healing and promotion of self-healing (De Belie et al., 2018). First, because they favour internal curing when relative humidity in the matrix decreases, they mitigate shrinkage cracking. Then, upon cracking and water ingress, SAPs swell and hence physically block the crack. Finally, in drier periods, they release the absorbed water and promote autogenous healing.

Many studies demonstrated the beneficial effect of SAP for self-healing in different laboratory expositions. Kim and Schlangen (2010) obtained higher flexural recovery for ECC specimens with SAP (0.5% and 1%-m_{cement} in addition) healed in wet/dry cycles (1h wet/3 days dry) than the control ECC specimens. But no healing could be observed in both mixes (with and without SAP) exposed in air condition (20°C and 50% RH). Snoeck et al. (2014b) also confirmed the positive effect of SAP for the flexural recovery of ECC specimens in wet/dry cycles (1 day wet/1 day dry) and in humid environments (RH > 90% and RH = 60%). This mechanical regain was confirmed even after repeated reloading (Snoeck & De Belie, 2016). Via water permeability and uniaxial tensile tests, Deng and Liao (2018) obtained faster self-healing in high/low RH cycle (24h 95% RH/24h 60% RH) than with a constant high RH. Finally, Hong et al. (2020) compared water immersion and wet/dry cycles (1h wet/47h dry) in terms of water permeability and compressive tests. The cement pastes and mortars containing SAP achieved rapid self-healing compared to the control specimens in both conditions, for cracks up to 0.3 mm. In addition, they found that the control specimens performed the best when healed under water, while the specimens containing SAP performed the best in wet/dry cycles (**Figure 2.22**).
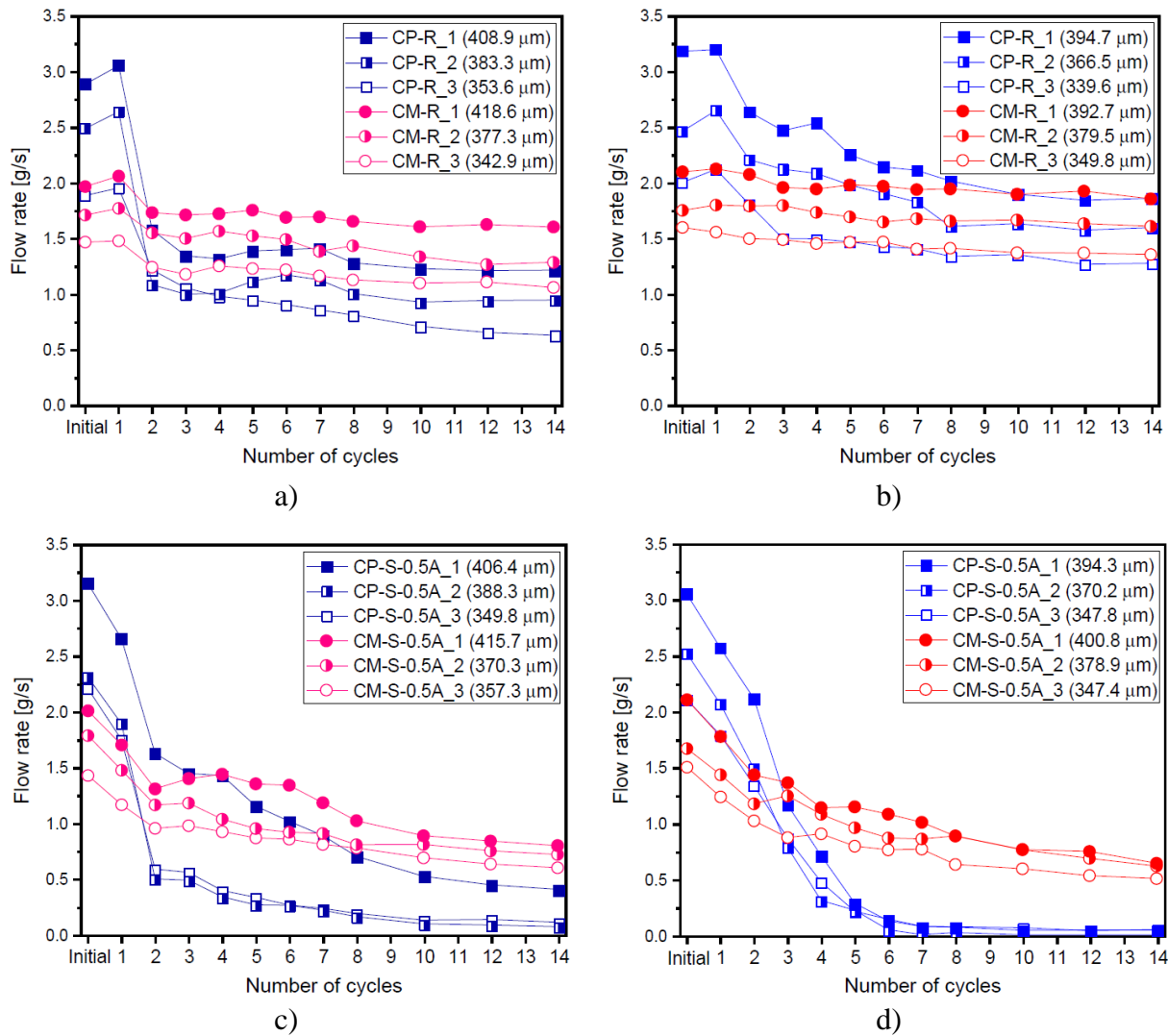
Figure 2.22. Flow rates results for control and SAP specimens in different expositions: a) control in water, b) control in wet/dry cycles, c) SAP in water and d) SAP in wet/dry cycles

The rapid self-sealing effect of SAP in continuous water flow test has also been investigated. Lee et al. (2016) observed faster self-sealing (1h against 5 days to reach negligible flow rate) in specimens with SAP ($4 - 5\%$-m_{cement} in addition), up to 0.3 mm cracks, compared to the control mix when subjected to a continuous water permeability test with a NaCl solution to simulate groundwater seepage in basements. They also tested higher dosages of SAP (8 and 13%-m_{cement}) with addition of calcium nitrate to depress the initial swelling of SAPs. The higher the dosage, the faster the sealing, but the compressive strength reduced drastically at high SAP dosage. Similar

results were also found by Li et al. (2020a). Hong and Choi (2017) reported a rapid crack sealing in mortars with continuous water flow test as well.

The size of the SAP particles is another important parameter for self-healing. The bigger the SAP particle size is, the higher the immediate self-sealing of the crack is upon water ingress (Deng & Liao, 2018; Gruyaert et al., 2016; Park & Choi, 2018; Snoeck et al., 2014b).

SAP was also combined with other admixtures to improve crack healing. Li et al. (2020a) have observed via their continuous water permeability test a faster complete self-healing for cracks up to 0.2 mm, when adding citric acid (crystalline additive) together with SAP in a mix. And Park and Choi (2018) observed a sharp decrease of water flow when adding SAP to a CA+CSA mix. They observed that the mineral additives (CA+CSA) produced more healing products around the SAP particles.

Furthermore, the beneficial effect of SAP has been demonstrated to improve the rebar-matrix bond behaviour in concrete (Mousavi et al., 2021; Mousavi et al., 2020).

In conclusion, the use of SAP is efficient to achieve rapid self-sealing under continuous water flow and to promote self-healing in humid environments (RH ≥ 60%). The dosage of SAP must be chosen to improve the self-healing capacity with a limited compressive strength decrease. Finally, combining SAP with other admixtures, such as CA, may further enhance healing.

2.5 Discussions and conclusions

Even if a few large- and full-scale applications of self-healing concrete have been implemented by different research groups (in the UK (Al-Tabbaa et al., 2019; Teall, 2016), Belgium (Tsangouri et al., 2019; Van Mullem et al., 2020b; Van Tittelboom et al., 2016), The Netherlands (Mors & Jonkers, 2019) and China (Wang et al., 2019)), this research area is still not mature yet. Self-healing concrete is clearly a multidisciplinary field of research involving biology, chemistry, materials science and civil engineering aspects.

As seen previously, a wide range of different specimens (type of crack, age), mix composition, healing conditions, testing methods and self-healing approaches were used in literature so that comparison between studies is not easy.

Concerning the first parameters, many studies worked with ECC that produce very narrow crack widths (< 60 µm), promoting autogenous healing. But in practice, larger crack widths are found in structures ($0.2 – 0.3$ mm). Moreover, most studies that carried out water permeability tests studied linear cracks, which are less encountered in structures. Lastly, several researchers worked with cement pastes or mortars, which can cause dilution problems of the self-healing agents when later upscaling to concrete scale (De Belie et al., 2018; Litina et al., 2021; Van Mullem et al., 2020a).

Different testing methods were used to assess self-healing. The choice of the type of test depends on the purpose of healing considered, whether durability, mechanical or even aesthetical aspects. The recovery of durability properties is important in concrete structures to stop the ingress of harmful agents and slow down further degradations. Water permeability test is easy to perform, non-destructive and less prone to application errors than sorptivity test. This test is thus ideal to measure the evolution of self-healing. The recovery of mechanical properties is also another important feature. The strength of the healing agent as well as the bond strength with the matrix should be higher than the original concrete strength to prevent the reopening of the healed cracks (Van Tittelboom & De Belie, 2013). Ferrara et al. (2018) even suggested the relevance of establishing the mechanical regain by self-healing to calibrate a "healing-modified" decaying mechanical law in a design perspective. Because mechanical tests are destructive, many different specimens are needed to determine an evolution of self-healing. For example, Ferrara et al. (2014b) performed 3-point bending tests on 1 or 2 prisms per condition at 1, 2, 3, 6 and 12 months exposition. Because of the well-known intrinsic heterogeneity in concrete, one can question the generalisation of these results. Finally, if the aesthetical aspect is the main issue, surface crack closure measurements are adequate to evaluate this aspect.

In addition, most studies assessed self-healing with visual observations to support either a durability or a mechanical test (**Table 2.2**). The studies that assessed both properties for self-healing (durability and mechanical) used different specimens and pre-cracking methods, which means different cracks and comparison of results less relevant. For example, cylinders are usually pre-cracked under splitting test for permeability measures, while prisms are pre-cracked by bending tests for the evaluation of mechanical recovery. Only Van Tittelboom et al. (2016) performed these three types of measures (visual crack closing, water permeability and 4-point bending tests, plus acoustic emissions) on the same large-scale concrete beams.

Different self-healing approaches have been developed and studied, from complex encapsulation methods (autonomous healing) to the use of mineral admixtures (stimulated autogenous healing). The latter approach, such as crystalline admixtures and expansive agents, is certainly cheaper and easier to implement in practice as they are already available and used in the concrete industry. Several studies reported beneficial effects of CA and CSA to promote self-healing in concrete, with a greater performance when combining both admixtures CA+CSA. In addition, SAPs are very interesting because of their capacity to promote self-healing even in dry environments. A few studies also combined CA and SAP and obtained accelerated healing, but they only investigated water immersion or continuous water flow tests. Besides, they worked with cement pastes or mortars and artificial cracks. Synergetic effects should be investigated under other more realistic exposure conditions.

In conclusion, from this literature review, some interesting research directions can first be pointed out:

- Exposing specimens outside for a long-term realistic condition;

- Performing multiple reloading to assess the repeatability of self-healing;

- Evaluating self-healing of specimens under sustained and cyclic loads;

- Combining different self-healing agents/approaches to maximise healing.

Secondly, other research aspects that are lacking and need more works can also be mentioned:

- Methodology to thoroughly assess self-healing via durability and mechanical recoveries on the same specimen;

- Better chemical and mineralogical characterisation of the healing products according to the exposure condition;

- Impact of self-healing on the fibre/rebar-matrix bond;

- Long-term durability of the healed concrete (resistance to corrosion, freeze-thaw resistance…);

- Long-term mechanical performance of the healed concrete (creep).

CHAPTER 3   METHODOLOGY

This chapter will present the general parameters and methodology chosen in this research project. Then, the experimental programs and their relevance with respect to the lacks in literature will be specified. Finally, the testing methods that are less detailed in the scientific articles will be explained.

3.1 Overview of the methodology

3.1.1 Parameters influencing self-healing

The cracking (width, age, type), mix composition, curing and healing conditions strongly influence the self-healing performance. The parameters chosen in this project are detailed in **Table 3.1**. The study of larger crack widths such as those found in common structures (0.2 – 0.3 mm) was selected in this project. Flexural cracks were also chosen for better representativeness of crack found in most structures. Then, it was decided to perform pre-cracking of specimens at 28 days (mature concrete) to better distinguish the effect of ongoing hydration from self-healing via carbonation. Finally, while some experimental works investigate the healing of a dormant crack, other experimental activities will evaluate healing of active cracks that will be reloaded several times (cracking/healing cycles).

A typical FRC mix previously tested at Polytechnique, with a w/b = 0.43, 0.75%-vol of macrofibres and compressive strength of 50 MPa, will be the reference material in this project. It was decided to evaluate self-healing directly at a concrete scale to avoid dilution problems with self-healing agents when working with cement pastes or mortars and later upscaling to concrete. Before pre-cracking, the specimens will be cured in lime-saturated water to prevent any leaching of matrix compounds and fibres corrosion.

Finally, the concrete specimens will be exposed in different healing conditions. The main laboratory conditions will be water immersion (without renewal) and wet/dry cycles (3.5 days wet/3.5 days dry) for 3 months. Additional specimens of the control mix will be exposed in air condition for 3 months as well, representing the reference condition with no/few healing. Continuous water flow test for around 1 week will be performed as well to see if it accelerates self-

healing as seen in previous studies in literature. Furthermore, because the evaluation of self-healing under realistic exposition is lacking, other specimens will be exposed outdoor for 1 year.

Table 3.1. Chosen parameters in this project

Parameter	Choice in this project
Cracking	- Crack width: 0.2 – 0.3 mm, corresponding to crack limits in standards - Flexural cracks - Age of pre-cracking: 28 days for mature concrete, in order to better distinguish the effect of ongoing hydration from self-healing via carbonation. - Dormant crack (Experimental Programs 1 and 2) - Cracks that will be reloaded several times (Experimental Program 3)
Mix composition	Typical composition previously used at Polytechnique: FRC with 0.75%-vol of fibres, cement containing 8% by mass of silica fume (GUb-SF), w/b = 0.43, compressive strength of 50 MPa.
Curing before pre-cracking	Lime-saturated water in order to prevent any leaching and corrosion of the fibres
Healing conditions	- Water immersion (20°C, without renewal) for 3 months - Continuous water flow for around 1 week - Wet/dry cycles (3.5 days wet/3.5 days dry) for 3 months - Air (20°C, 45% RH) for 3 months (only for the control mix) - Outdoor for 1 year

3.1.2 Testing methods to evaluate self-healing

As this project examines the self-healing capacity of different self-healing agents under different exposure conditions, the study of one single macrocrack has been chosen to facilitate the evaluation of self-healing and the comparison between the different mixes and expositions. For that purpose, a 3-point bending test was performed on notched prisms of small size (beams of 75 x 125 x 450 mm³) for easy handling.

The selection of the main method to evaluate self-healing was made considering that the most important aim of the healing process is the durability of concrete structures by slowing down their degradations and avoiding expensive repair and maintenance. Thus, a new water permeability set-up was developed in this project to measure water through prismatic specimens with a single flexural macrocrack (Experimental Program 1).

As several studies reported the non-correlations between surface crack closure measurements and water permeability results, it has been decided in this project to examine the evolution of the surface crack closure with macroscopic observations only for qualitative assessment.

Another aim of crack healing is to partly recover mechanical properties of structures. Because mechanical tests are destructive, the prisms in this project will be reloaded until failure only at the end of the healing period to assess the mechanical regain and compare it with the durability recovery (Experimental Program 2). In Experimental Program 3, the self-healing capacity will be evaluated after multiple reloading. In addition, the evaluation of water permeability and flexural recovery will be performed on the same prisms, which will enable to directly correlate a self-healing state with a mechanical regain. Only one study determined both durability and mechanical properties on the same specimen but the results were not conclusive.

Finally, according to Cuenca and Ferrara (2017), more research on the nature and properties of healing products and the chemical reactions depending on the exposition is needed. In this project, microscopic (SEM-EDS) analyses will be carried out to compare the mixes produced with various self-healing agents and exposed in different conditions.

Figure 3.1 summarises the sequence activities of the general methodology used in this project. After pre-cracking at the age of 28 days by means of a 3-point bending test, crack measurements (crack width w_i, length L_i, crack area A_i) and pictures were taken at four constant points with a digital microscope. The prisms were then exposed in different conditions for healing and, meanwhile, water permeability and optical observations were regularly evaluated. After the healing period, prisms were reloaded multiple times or until failure with the same 3-point bending test to assess mechanical recovery and finally, some prisms were cut at the cracks to analyse the healing products via microscopy (SEM-EDS).
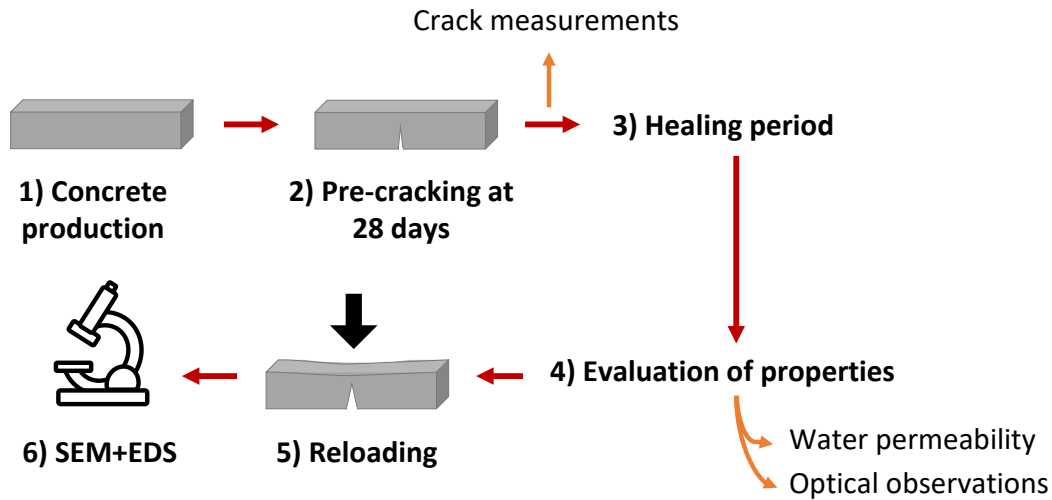
Figure 3.1. General methodology to assess self-healing

3.1.3 Self-healing approaches

The use of mineral admixtures, in particular crystalline admixtures and expansive agents, in this project has been preferred to other approaches, for lower costs and ease of implementation reasons (they are already available and used in the construction industry). These are considered great advantages even if the self-healing capacity of these mineral admixtures is lowered than encapsulated approaches, as they are partially consumed during the cement hydration before cracking.

As seen in the literature review, the use of crystalline admixture CA, CSA-based expansive agent and superabsorbent polymer SAP to enhance self-healing is promising and combining them can provide synergetic effects. In this project, the combinations CA+CSA and CA+SAP will be studied as well as the effect of the single admixtures (CSA, CA, SAP) at a concrete scale to confirm the potential synergy in several exposures including wet/dry cycles and real outdoor exposure.

3.2 Experimental programs

After presenting the materials used in this project, the three experimental programs carried out will be specified. **Table 3.3** summarises the experimental works as well as the parameters used in this research. Their distribution in the different chapters and the corresponding articles in this thesis is also indicated.

3.2.1 Materials

A reference composition of a fibre reinforced concrete (FRC) with a targeted compressive strength of 50 MPa, previously used in Polytechnique, was used in this research. It contains a blended General Use Portland cement with 8% by mass of silica fume (type GUb-SF), with a water to binder (w/b) ratio of 0.43. A low dosage (0.75%-vol) of hooked-end steel macrofibres (l_f = 35 mm and ϕ_f = 0.5 mm) was used to provide a stable post-cracking behaviour of prisms during the pre-cracking phase.

Six FRC mixes were produced and were identified according to the healing agent introduced in the mix: control, CSA, CA, SAP, CA+SAP and CA+CSA. The dosages of the admixtures were 3.33% of CSA (Denka Power CSA), 2% of CA (Penetron Admix) and 0.5% of SAP (BASF) by mass of cement, as recommended by the manufacturers. The SAP used is a cross-linked polyacrylamide with a nominal particle size of 100 μm. The characterisation of its absorption capacity and swelling time, as well as the adjustment of the amount of water or superplasticiser (SP) in the mix to reach the same flow of a control mix will be detailed in **Chapter 7** (**Section 7.1**). Based on these results at the fresh and hardened states, it has been decided to add more SP in order to keep similar mechanical performance between the mixes.

The compositions of the six FRC mixes are shown in **Table 3.2**. The dosages of SP and viscosity agent were adjusted to reach a flow around 500 mm. The mixes containing SAP and CA+SAP required three times more superplasticizer.

Table 3.2. Compositions of the FRC mixes

Material	Control	CSA	CA	SAP	CA+SAP	CA+CSA
Cement type GUb-SF (kg/m³)	550	550	550	550	550	550
CSA (kg/m³)	/	18.3	/	/	/	18.3
CA (kg/m³)	/	/	11	/	11	11
SAP (kg/m³)	/	/	/	2.75	2.75	/
Water (kg/m³)	237	237	237	237	237	237
Superplasticizer (l/m³)	10.0	10.0	10.5	30.0	30.0	10.5
Viscosity agent (l/m³)	0.70	0.85	0.71	0.70	0.70	0.85
Sand (kg/m³)	779	771	773	767	761	765
Coarse aggregates (kg/m³)	631	624	626	620	616	619
Steel fibre (kg/m³)	58.5	58.5	58.5	58.5	58.5	58.5

3.2.2 Experimental Program 1

The objective of the first experimental program was to adapt the water permeability device previously developed at Polytechnique Montreal for concrete tie-specimens (Desmettre & Charron, 2011). The device was adjusted for application on FRC prisms presenting a single flexural macrocrack, that can be reloaded after healing to assess mechanical recovery. Then, an experimental program was carried out to validate the set-up and understand the influencing factors for self-healing.

In this experimental program, only a reference FRC (control mix from **Table 3.2**) was produced. 10 prisms and 4 cylinders were made.

Detailed information on this experimental program is summarised in **Table 3.3**. After pre-cracking, the prisms were exposed in water immersion and permeability measures were taken at 0 (after pre-cracking), 7, 11 and 25 days of healing. The most sensitive indicator to cracking was determined between the flexural behaviour, the crack characteristics and the initial water permeability coefficient. The repeatability of the measurement as well as the influence of the pressure gradient (20, 30 and 40 kPa) on the water permeability coefficient were then assessed. In this experimental program, the crack width and area were determined at the end of the healing period as well. Correlations between the self-healing results (Healing Ratio and Closing Ratio) and crack parameters (initial crack area A_i, initial water permeability coefficient K_{wi}) were established. These prisms had not been reloaded for mechanical recovery.

3.2.3 Experimental Program 2

The objective of the second experimental program was to assess thoroughly self-healing of concrete containing various admixtures and subjected to several laboratory and outdoor expositions, via water permeability measures, mechanical recovery estimations, visual observations and microscopic analyses.

In this experimental program, the six FRC mixes were produced (**Table 3.2**). Two batches per mix were made for the outdoor (6 prims and 12 cylinders per mix) and indoor expositions (14 to 18 prisms and 12 cylinders per mix) respectively. A total of 124 prisms and 148 cylinders were investigated.

The experimental program exactly follows the general methodology in **Figure 3.1** and is summarised in **Table 3.3**. The laboratory expositions consisted in water immersion for 3 months, wet/dry cycles (3.5 days wet/3.5 days dry) for 3 months, ambient air (only for the control mix) for 3 months and continuous water flow for 1 week. The long-term outdoor exposure consisted in 1 year of exposition in the Northern climate of Montreal between March 2019 and March 2020. **Figure 3.2** shows pictures of the prisms exposed indoor, in water basins and dried in air. **Figure 3.3** illustrates the specimens exposed outside throughout the year. It must be noted that the prisms were always placed with face 1 (subjected to the inlet flow during the water permeability test) upward and face 2 downward, in all expositions.

Self-healing was assessed quantitatively by water permeability measures (pressure gradient $= 30$ kPa) and qualitatively via macroscopic observations, at 0, 11, 25, 53 and 91 days after pre-cracking for indoor specimens, and at 0, 3, 6, 9 and 12 months for outdoor specimens. For the water flow condition, the flow seeped through the pre-cracked specimen continuously for about 1 week. At the end of the healing period (age of 4 months for indoor and 14 months for outdoor specimens), all specimens were reloaded by the same 3-point bending test up to failure. Mechanical recovery indexes were calculated and microscopic analyses (SEM-EDS) were performed on fractured surfaces.

Additional analyses of fibres orientation and density were carried out to discriminate the effect of the mix composition on the initial flexural behaviour from the effect of fibres.

<center>a)   b)</center>

Figure 3.2. Specimens exposed indoor, a) water immersion in water containers (21 ± 3°C) and b) dried in air (21 ± 3°C and 45 ± 10% RH) for wet/dry cycles or air expositions

Figure 3.3. Specimens exposed outdoor throughout the year

3.2.4 Experimental Program 3

The third experimental program aims to evaluate the repeatability of self-healing of a crack under repeated reloading, for a constant maximal crack width or an increasing crack width. Repeated reloading with a constant crack width could simulate structures under a low traffic with a low magnitude, while reloading with increasing crack width could simulate structures under a high traffic with a higher magnitude or an exceptional load applied to the structure.

Two FRC mixes (control and CA+CSA from **Table 3.2**) were made. 12 prisms and 4 cylinders were produced per mix. It must be noted that due to COVID-19, only the CA+CSA mix was pre-cracked and tested. The control mix will be pre-cracked and tested in the future beyond the scope of this thesis.

Figure 3.4 and **Table 3.3** show an overview of the Experimental Program 3. The wet/dry cycles exposure was selected because it favoured more self-healing than water immersion and it was a representative accelerated condition of the outdoor exposure in Experimental Program 2. The FRC mix containing CA+CSA was chosen before completing the second experimental program. This mix presented the highest final Healing Ratio in wet/dry exposition (99%), while the Strength Regain reached 99% in Experimental Program 2. However, it was not the mix that performed the best in outdoor exposition in the end.

Initially, the prisms would have been pre-cracked at 28 days and then reloaded every 3 weeks (**Figure 3.4**). Due to COVID-19, pre-cracking was carried out at the age of 218 days. The prisms were healed for 2 weeks in wet/dry cycles (3.5 days wet/3.5 days dry) instead of 3 weeks. Some days were needed to measure water permeability after the elastomer sealing in the notch was dry, and to prepare the specimens for the 3-point bending test by removing the elastomer and installing several plates for the LVDTs and extensometer.

Water permeability and macroscopic observations were taken before and after each reloading phase. Hence, six measures of permeability coefficient (K_w) were obtained as seen in **Figure 3.4**.
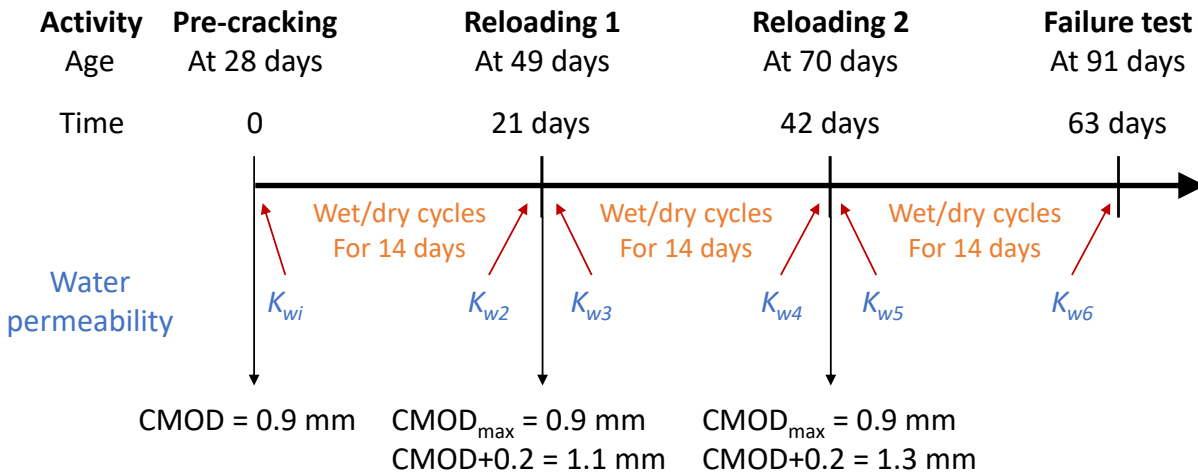
Figure 3.4. Overview of the experimental program of Experimental Program 3 (initial planning)

After the pre-cracking phase to a crack opening of 0.9 mm at the extensometer, the prisms were reloaded 2 times and then reloaded until failure the third time. Two types of repetitive reloading were performed: 1) reloading to the same maximal $CMOD_{max} = 0.9$ mm (constant crack width), and 2) reloading with an additional $\Delta CMOD = 0.2$ mm (increasing crack width).

For each type of reloading, 3 prisms and 2 companion reference cracked ones (placed in air exposition and reloaded) were used to see the impact of healing. In addition, 2 other reference cracked specimens were healed in wet/dry cycles without any reloading to see the impact of reloading. Finally, all prisms were reloaded up to failure after 63 days of exposure.

It must be noted that due to COVID-19, only the preliminary analyses of Experimental Program 3, namely the water permeability results, will be presented.

Table 3.3. Summary of the experimental programs of this research project

Exp. program	Objective	Exposi-tion	Mix	Macroscopic observations	Water permeability	Mechanical recovery	Microscopic analyses	Chapter in this thesis
N° 1	Development of a new water permeability set-up	Water	Control	Crack measurements before and after healing	- Repeatability - Influence of pressure gradient	-	-	**Chapter 4** Article 1
N° 2	Evaluation of the self-healing potential with various admixtures under laboratory and outdoor expositions	Water Wet/dry Outdoor Air Water flow	Control CSA CA SAP CA+SAP CA+CSA	- Crack measurements only before healing - Qualitative evolution of crack healing	Evolution of water permeability	-	Impact of the exposure condition on the microstructure	**Chapter 5** Article 2
					-	Strength and stiffness recoveries	Impact of the mix on the microstructure	**Chapter 6** Article 3
N° 3	Evaluation of the self-healing potential under repeated reloading	Wet/dry	(Control) CA+CSA	Crack measurements before and after repeated reloading	Evolution of water permeability	Evolution of mechanical properties	-	**Chapter 7** **Section 7.5**

3.2.5 Relevance of the experimental works of this project

As stated by (Cuenca & Ferrara, 2017; De Belie et al., 2018; Ferrara et al., 2018; Van Tittelboom & De Belie, 2013), further research should focus on the topics cited in **Table 3.4**, regarding the testing methods (for the laboratory and in situ), more realistic loading and healing conditions (under sustained load, after multiple damage events, real outdoor environment), potential synergy of different self-healing agents/approaches, more characterisation of healing products, and long-term performance of self-healing concrete and life cycle assessment (LCA).

The research activities carried out in the thesis are also shown in **Table 3.4**. It is clear that the experimental works will contribute to the lack of knowledge and understanding in several topics, and hopefully allow some recommendations to move forward to a better capacity of concrete to heal cracks and provide a longer durability to structures.

Table 3.4. Lacks of research in literature and the contributions of this thesis

More research is needed on	Contributions of this thesis
Development of standard testing methods	Development of a new water permeability set-up that will enable to evaluate self-healing thoroughly on the same specimen (durability property, mechanical recovery, visual observations) (**Experimental Program 1**)
Self-healing under sustained and cyclic loads	-
Repeatability of self-healing after multiple damage events	Evaluation of self-healing under repeated reloading (**Experimental Program 3**)
Self-healing in realistic exposition	Evaluation of self-healing of specimens exposed outside for 1 year (**Experimental Program 2**)
Synergy of self-healing agents/approaches	Study of various admixtures and combinations of two agents (CSA, CA, SAP, CA+CSA and CA+SAP) (**Experimental Program 2**)
Chemical and mineralogical characterisation of healing products	Microscopic analyses (SEM-EDS) of the healing products exposed in different conditions and from concretes containing various admixtures (**Experimental Program 2**)
Impact of self-healing on the fibre-matrix bond	-
Long-term performance of the healed concrete (creep, resistance to corrosion, freeze-thaw resistance…)	-
Life cycle assessment (LCA)	-

3.3 Testing methods

3.3.1 Loading procedures

For all the loading procedures, 3-point bending tests on notched prisms according to EN 14651 (European Committee for Standardization, 2005) were carried out. The loading was applied with a 240 kN hydraulic actuator, controlled with the average displacement of two linear variable displacement transducers (LVDTs) placed on each side of the specimen. An extensometer was also installed at 10 mm below the prism to measure the crack mouth opening displacement (CMOD) for pre-cracking and the repeated reloading. **Figure 3.5** shows the position of the crack width measured at the notch root (w) and the CMOD at the extensometer.
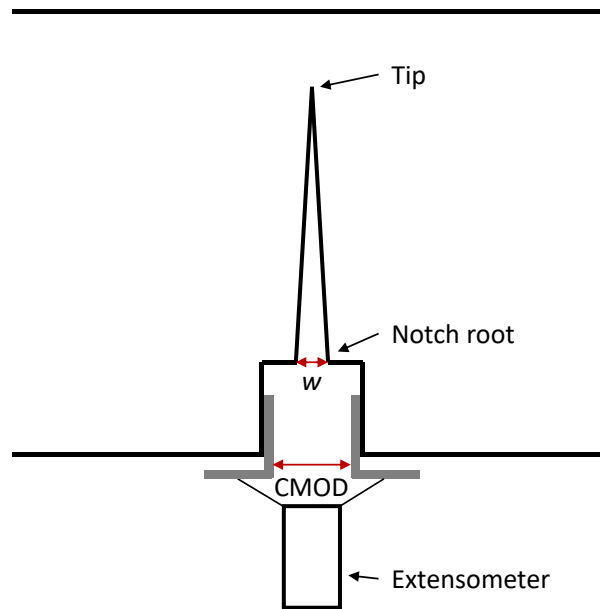
Figure 3.5. Schematic diagram of the crack width measured at the notch root (w) and the crack mouth opening displacement (CMOD) measured at the extensometer

3.3.1.1 Pre-cracking

The procedure consists in loading at a rate of 0.2 mm/min up to a CMOD of 0.9 mm and then unloading at a rate of 1 mm/min (**Figure 3.6**). This value enables to obtain the targeted residual crack width at the notch root w of the prism around 0.25 – 0.30 mm.
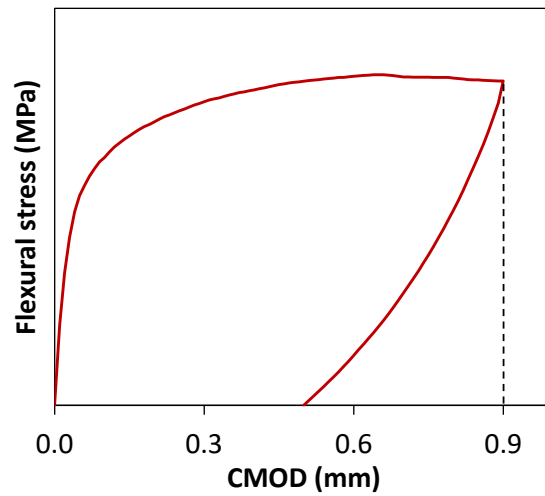
Figure 3.6. Example of a pre-cracking curve

3.3.1.2 Ultimate reloading

The ultimate reloading to failure consists in reloading the prisms with a rate of 0.2 mm/min until reaching 70% of the maximum load in the post-peak stage. Then the rate was increased to 0.5 mm/min until reaching 50% of the maximum load at post-peak and then to 1 mm/min until failure to perform the test in a reasonable duration. The reloading was stopped when a residual force of 4 kN was reached. **Figure 3.7** shows an example of the pre-cracking phase followed by the ultimate reloading. The graph is in displacement instead of CMOD as the extensometer will come off at one point during the reloading.
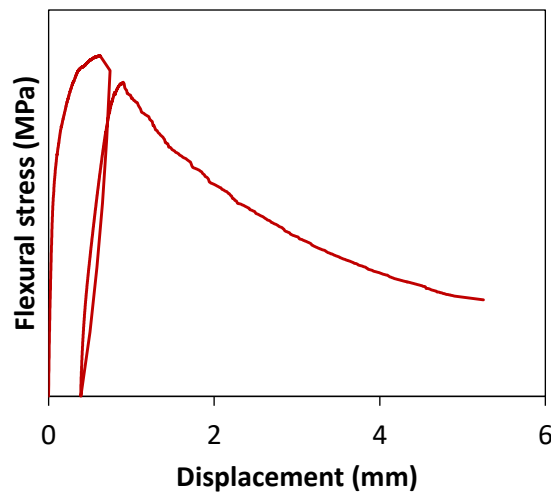
Figure 3.7. Example of a pre-cracking and ultimate reloading curve

3.3.1.3 Repeated reloading

Two types of repeated reloading were carried out after the pre-cracking phase in Experimental Program 3. The first one consisted in reloading up to the extensometer displacement $CMOD_{max} = 0.9$ mm (the same value at pre-cracking) in order to assess the repeatability of healing of the same crack with constant width and area. The second one consisted in reloading to an additional $\Delta CMOD = 0.2$ mm, which means up to 1.1 mm at reloading 1 and up to 1.3 mm at reloading 2, in order to evaluate the repeatability of healing of a crack that gets wider. These two types of reloading are illustrated in **Figure 3.8a** and **Figure 3.8b** respectively. After two reloading, the specimens were brought to failure as in the previous section.

a)   b)
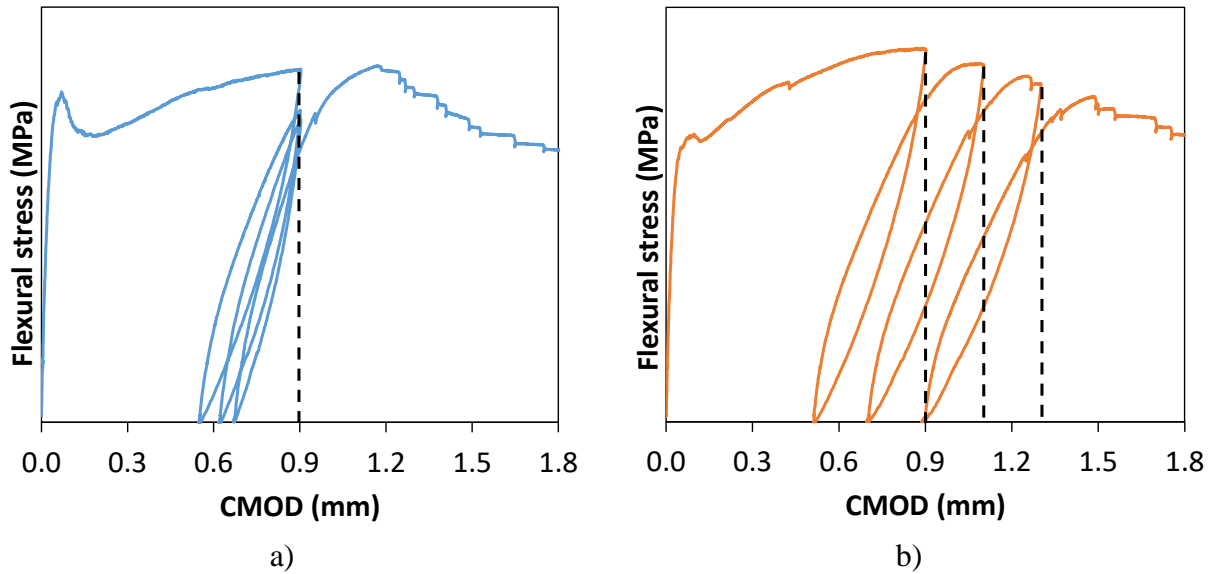
Figure 3.8. Two types of reloading, a) reloading at $CMOD_{max}$, b) reloading at CMOD+0.2

3.3.2 Water permeability measurement

Diagrams of the new water permeability set-up are shown in **Figure 3.9**. In **Figure 3.9a**, the set-up connected to water tanks from the previously developed permeability device (Desmettre & Charron, 2011) can be seen. It must be noted that three sets of inlet and outlet tanks (mini, small, large) exist but only one set is presented for sake of simplicity. **Figure 3.9b** shows an exploded view of the new set-up. Face 1 was defined as the face subjected to the inlet flow, while face 2 corresponded to the outlet flow.

Before obtaining this final set-up, different sealing materials (elastomer, expansive foam), configurations of sealing (permanent or reusable, at the boxes, in the notch), dimensions of prisms (75 x 100 x 400 mm³ and 150 x 150 x 600 mm³) and targeted CMOD before unloading (0.5 and 0.7 mm) had been tested. Two concrete batches had been produced and preliminary experimental programs had been carried out. A test to measure the permeability of prisms simultaneously under flexural loading was also experimented.
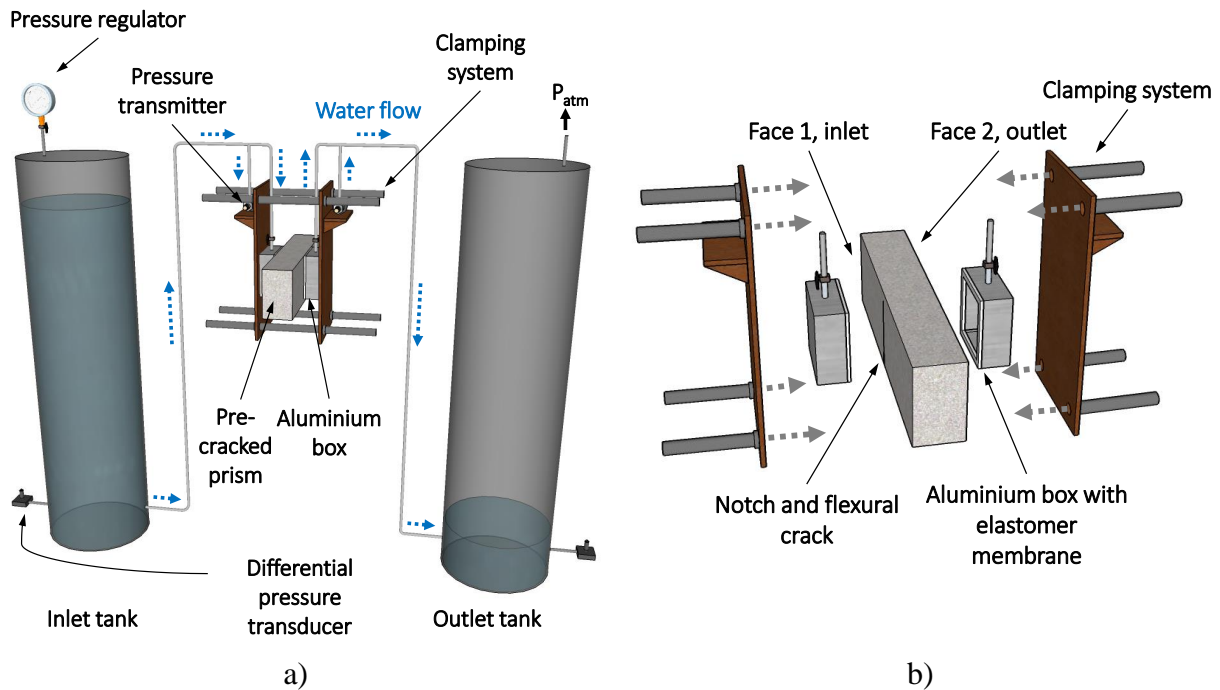
Figure 3.9. Water permeability device, a) whole system, b) zoom at the set-up

Figure 3.10 shows an example of raw permeability results obtained from the water permeability test. Inlet and outlet flows as well as the pressure gradient were recorded. As the pressure gradient varies with the volume of water in the tanks, it has to be adjusted manually to keep the targeted pressure gradient (30 kPa in that case). The test started with the mini tanks and then moved to the small tanks, as water seeped through the prisms (**Figure 3.10**). As the inlet and outlet flows are equal, the steady-state assumption can be verified and the water permeability coefficient $K_w = 1.2 \times 10^{-5}$ m/s, can be calculated from the slope (flow rate Q) at the end of the test, using Darcy's law. More information on the water permeability test and Darcy's law will be found in the first scientific article (**Chapter 4**).
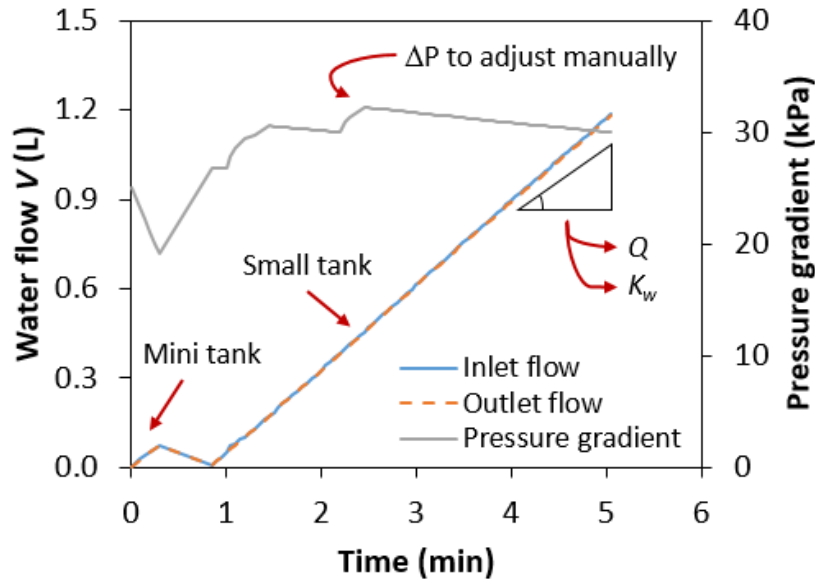
Figure 3.10. Example of raw water permeability results ($K_w = 1.2 \times 10^{-5}$ m/s)

3.3.3 Macroscopic observations

The macroscopic observations and crack width measurements were executed with the digital microscope PCE-MM200. After pre-cracking, equidistant lines (every 2.5 cm) were marked on the cracks of the prisms (on the two faces). Initial picture was taken and crack width w_i was measured at each of these points (4 points per face, 8 points per specimen). The length of the crack was also measured and the initial crack area A_i was calculated. Detailed procedure of the evaluation of the crack area A is presented in the first scientific article (**Chapter 4**). In Experimental Program 2, the crack characteristics were only measured before healing. Pictures of the cracks were taken though during healing each time before the water permeability test, to obtain a qualitative visual evolution of self-healing. **Figure 3.11** illustrates the use of the digital microscope to measure crack width and take pictures on the prism's faces.

Additional observations with binoculars (**Figure 3.12**) were also performed on some crack samples used for microscopic analyses (**Figure 3.13b**). These results are shown in the third scientific article (**Chapter 6**).
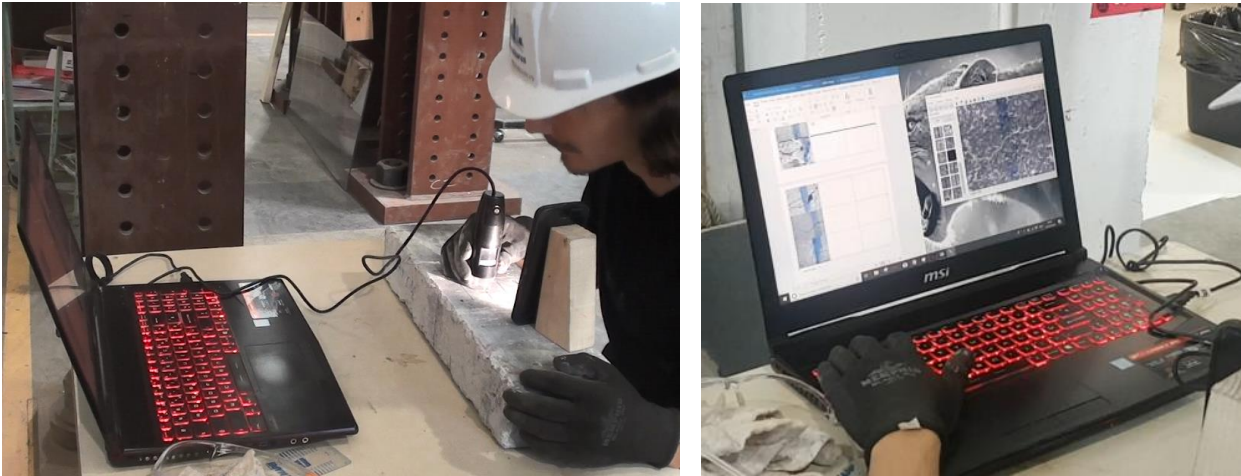
Figure 3.11. Observations and crack width measurements using a digital microscope at the prism's faces
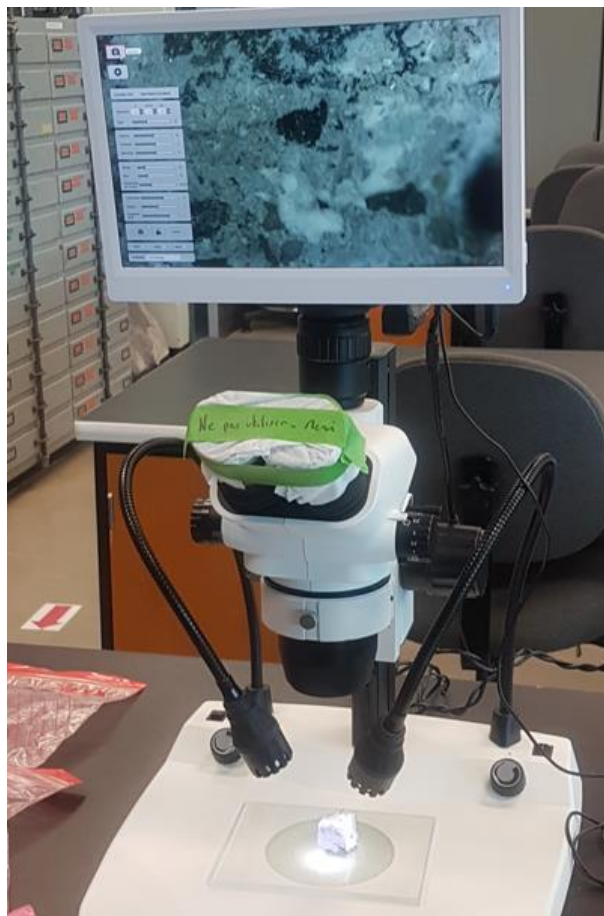
Figure 3.12. Observations with binoculars on fractured sample

3.3.4 Microscopic analyses

Microscopic analyses were performed at the Centre for Characterization and Microscopy of Materials of Polytechnique Montreal with JSM-7600F Schottky Field Emission Scanning Electron Microscope and at the Department of Civil Engineering and Building Engineering of Sherbrooke University with Hitachi S-3400 N Scanning Electron Microscope.

Two types of samples were analysed:

- Powders scratched with a scalpel at the prisms crack surface after healing and before reloading (**Figure 3.13a**). As very limited amount of powders could be collected, the powder of several prisms of the same testing condition was combined.

- Fractured surfaces of the crack cut at the notch root (**Figure 3.13b**). One prism of each testing condition was cut and provided 6 samples (2 samples at face 1, 2 samples in the middle and 2 samples at face 2). One sample (2 cm cube) was analysed (mostly from face 2 of the prism).

SEM pictures were taken at different magnifications (X 250 to X 2000) in several zones in the sample. EDS spectra were performed to identify the healing products.

a)   b)
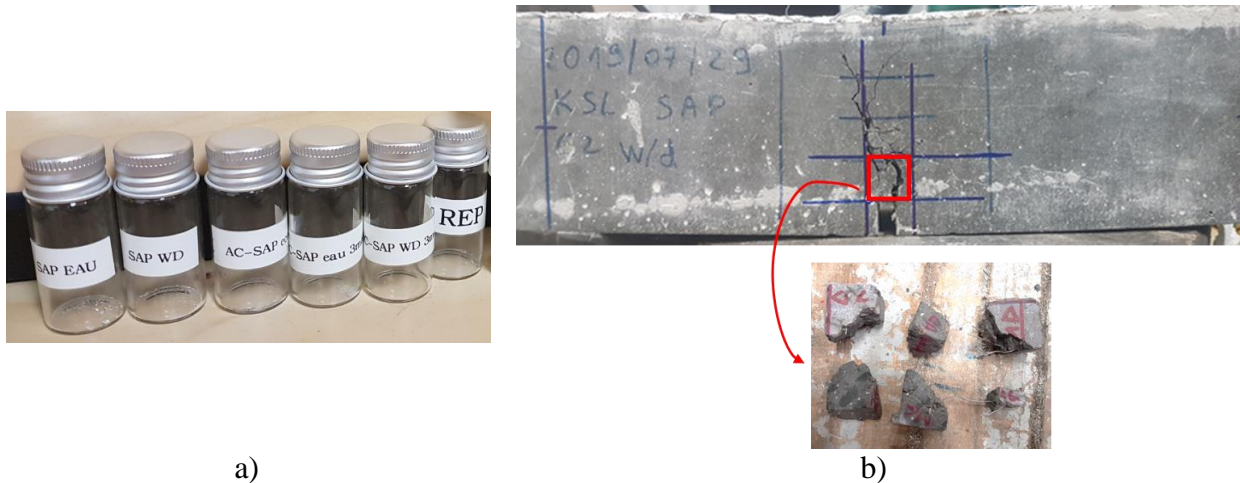
Figure 3.13. Samples taken from healed specimens to analyse the healing products using SEM-EDS, a) powder and b) fractured surfaces

3.3.5 Fibres orientation and density analyses

The procedure followed to analyse the fibres orientation and density was previously developed by Delsol (2012) at Polytechnique Montreal. First, slices were extracted from healed prisms after failure, very close to the crack (**Figure 3.14a**). One slice (75 x 125 x 20 mm³) per testing condition was taken. **Figure 3.14b** shows the 12 extracted slices.

a)   b)
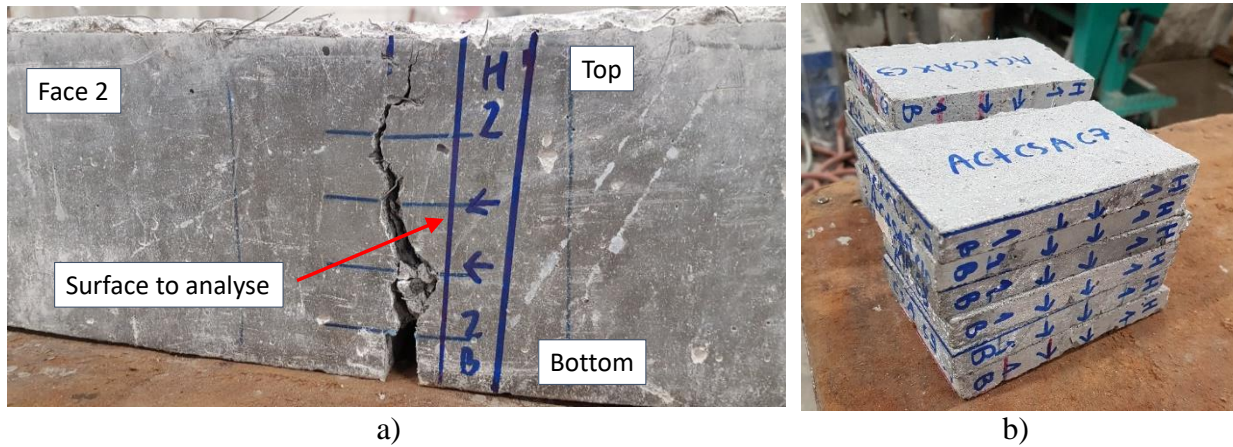
Figure 3.14. Example of the extraction of a slice from a prism, a) right next to the crack, b) all 12 slices

The slice surfaces to analyse were then polished and painted to increase the contrast between the steel fibres and the matrix. After digitalisation with a 2400 dpi resolution scanner, the image analysis consists in a binarisation of the image followed by fibre detection (**Figure 3.15**). The in-house program developed on MATLAB determines the number of fibres in each slice and the orientation angle of each fibre. These parameters are calculated knowing their geometrical characteristics and considering their elliptical cross-sections at the surface.
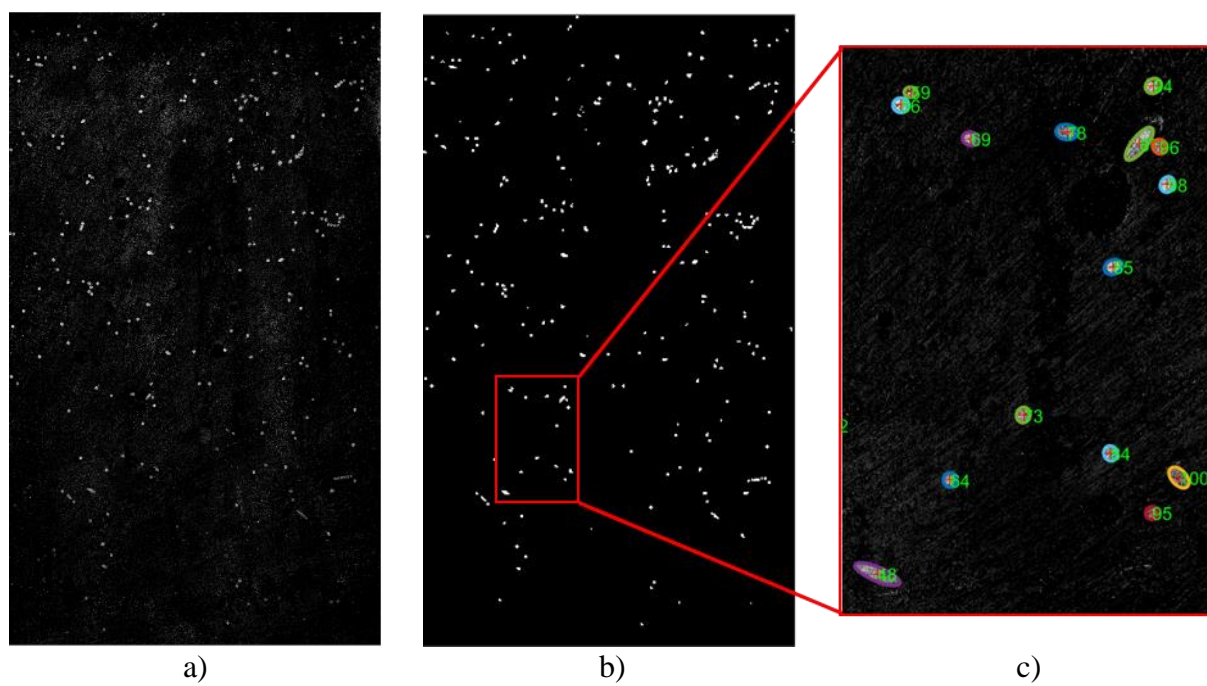
Figure 3.15. Process of image analysis: a) digitalisation, b) binarisation, and c) fibres detection

CHAPTER 4

ARTICLE 1: NEW WATER PERMEABILITY SET-UP AND FACTORS AFFECTING CONCRETE SELF-HEALING

Kim-Séang LAUCH, Clélia DESMETTRE, Jean-Philippe CHARRON

Department of Civil, Geological and Mining Engineering, Polytechnique Montreal

Corresponding Author:

Jean-Philippe CHARRON

Department of Civil, Geological and Mining Engineering

Polytechnique Montreal

B.O. Box 6079, Station Centre-Ville

Montreal, Qc, Canada H3C 3A7

Phone: 1-514-340-4711 ext 3433

Fax: 1-514-340-5881

Email: jean-philippe.charron@polymtl.ca

4.1 Abstract

This paper presents a new water permeability set-up developed to measure the water flow through a crack generated by means of 3-point bending test. After pre-cracking at 28 days, fibre reinforced concrete (FRC) prisms were kept under water and self-healing was measured over 25 days. First, sensitivity of damage measurements (flexural response, crack characteristics and permeability) was evaluated to establish the most representative indicator of cracking. Then, permeability coefficient being the best indicator, its repeatability and variation under various pressure gradients (20, 30 and 40 kPa) were evaluated. Finally, the most prominent factors for self-healing (Healing Ratio, Closing Ratio, permeability, crack area) were assessed by means of correlations.

Keywords: fibre reinforced concrete, bending behaviour, crack characteristics, water permeability, self-healing.

4.2 Introduction

In presence of water, cementitious materials have an intrinsic self-healing capacity, called autogenous healing, the main mechanisms being delayed hydration of anhydrous binder in the early age, while carbonation occurs at later ages [1]. To improve and better control the healing capacity, several approaches have been developed such as the use of bacteria, mineral admixtures, encapsulated chemicals or the use of fibres to increase crack control and obtain thinner cracks in concrete [2].

Reliable tests are needed to evaluate the self-healing potential of different concretes. There exists no standard to assess self-healing yet, but the methodology widely used is the following [3]: 1) production of specimens, 2) creation of damage, 3) study of initial properties (crack geometry, durability or mechanical parameters), 4) healing period, 5) study of variation of the considered properties and 6) microscopic analyses of the healing products. This paper focuses on the study of the self-healing capacity of concrete through durability tests as such tests give a straightforward measure of the whole crack volume.

Among durability tests, most researchers determined water [4-14], air or gas [4, 15-17] permeability, while others studied sorptivity [4, 14, 16-18]. As claimed by Picandet et al. [19], permeability is an intrinsic parameter and constitutes thus a great indicator to evaluate the effects

of cracks on concrete durability or performance. Moreover, Mengel et al. [20] underlined recently that permeability is the dominant mechanism in cracked concrete compared to capillary suction and diffusion. Finally, because durability issues in concrete structures are more related to the ingress of liquids and contaminants, water permeability has been selected in this project to assess self-healing in concrete.

Table 4.1 presents a comparison of different water permeability set-ups used in literature to evaluate self-healing and introduces the new set-up that will be detailed in this paper. Another review can be found in [21]. Different specimens and pre-cracking methods are used, which induces different types of cracks (linear, flexural, artificial) for healing. Besides, pressure gradients and measurement methods (inlet or outlet flow or both, periodically or continuously) vary as well.

It can be noted in **Table 4.1** that disks or cylinders specimens are mostly used for the water permeability tests. While Sisomphon et al. [5] and Van Tittelboom et al. [22] worked with linear macrocrack induced by splitting test, Palin et al. [23] completely split cylinders in halves and then reassembled the specimens. Other researchers also worked with such artificial cracks [8, 24]. During the permeability tests, Sisomphon et al. [5] and Palin et al. [23] recorded the outlet flow with a constant water head of 1 or 10 kPa respectively. The same methodology was also used by [9, 10], some with higher pressure gradient [6, 25]. On the other hand, Van Tittelboom et al. [22] and Snoeck et al. [26] measured the inlet flow and considered that a steady state flow has been reached when similar results were obtained during 5 consecutive days.

These configurations with cylinders are quite simple and many specimens can be tested at the same time. However, linear tensile cracks are less representative of flexural cracks found in structures and artificial cracks from reassembling two separate halves are not ideal [21]. In addition, such specimens cannot be reloaded to assess mechanical recovery.

The water flow test developed by Gruyaert et al. [27], implemented in a round robin test (RRT) [14], used in contrast prisms. In this test, water permeability is measured on prisms with a cast-in hole over their length, which are pre-cracked by means of a 3-point bending test so that one flexural macrocrack of variable width is created. The applied pressure gradient can be easily adjusted in this set-up and the outlet flow that leaked at the bottom of the specimen is measured. The set-up requires more specimen preparation and the permeability results depend on the position of the inner hole [14].

Besides, the crack width at the connection with the cast-in hole is not known accurately and small particles could block it [27].

Previous set-ups measured the inlet or outlet flow (not both) through the specimens and thus assumed a steady state when the flow is stabilized. This procedure does not allow to discriminate the effect of pore saturation from the self-healing as they both reduce the flow.

Desmettre & Charron [28] developed a water permeability set-up on reinforced concrete tie-specimens under tensile load to assess the autogenous healing of concrete under static, constant [7, 29] and cyclic loadings [30]. Both inlet and outlet flows are recorded and a steady-state flow is considered when both flows are equal. The pressure gradient can be easily adjusted. While this device enables to study healing of several cracks in reinforced concrete, the testing method requires a long implementation and test duration. The number of specimens and conditions that can be tested is thus limited.

The advantages and drawbacks of existing set-ups provide the basis of a new one. The first objective of this project aimed to develop a new water permeability set-up using the last permeability device [28] but adapted to fibre reinforced concrete (FRC) prisms pre-cracked by means of a 3-point bending test. This enables to study the self-healing capacity of one single flexural macrocrack (realistic crack) and to compare concretes with different self-healing agents. The second objective was to establish the most sensitive indicator of the initial state of damage of pre-cracked prism, between the flexural response, crack characteristics and permeability. Thirdly, the water permeability measurement repeatability and the influence of pressure gradient on this measure were evaluated. The fourth objective was to assess the self-healing of the specimens to identify, by means of correlations, which parameter (crack characteristics or permeability) gives more reliable information about the self-healing process.

Table 4.1. Comparison of different water permeability set-ups to evaluate self-healing

Refs	Specimens and pre-cracking	Crack	Pressure gradient	Measurement	Advantages	Disadvantages
Sisomphon et al. [5]	Disks Pre-cracked by splitting	Single tensile macrocrack (uniform width)	1 kPa (water head)	Mass of water passing during 10 min (outlet flow)	- Simple set-up - Many specimens can be tested at the same time	- Crack differs from structures - Specimens that cannot be reloaded
Palin et al. [23]	Cylinders with grooves Pre-cracked with a vise	Cylinder in halves and reassembled	10 kPa (water head)	Mass of water passing during 10 min (outlet flow)	- Simple set-up and quick specimen preparation - Many specimens can be tested at the same time	- Artificial crack - Specimens that cannot be reloaded
Van Tittelboom et al. [22]	Disks Pre-cracked by splitting	Single tensile macrocrack (uniform width)	Not mentioned	Drop in water level at regular time intervals (inlet flow)	- Simple set-up - Many specimens can be tested at the same time	- Crack differs from structures - Specimens that cannot be reloaded - Can take a very long time to achieve steady state flow
Gruyaert et al. [27]	Prisms with a cast-in hole over the length Pre-cracked by 3-pt bending	Single flexural macrocrack (variable width)	5, 100, 200 kPa (ΔP adjustable)	Outlet flow with time	- Realistic crack - Quick measurement - Specimens that could theoretically be reloaded (not performed)	- Requires more specimen preparation - Not robust, results depend on the position of the cast-in hole in the specimen
Desmettre & Charron [7, 28]	Tie-specimens under direct tensile load	Multiple tensile macrocracks (uniform width)	25, 50, 100 kPa (ΔP adjustable)	Inlet and outlet flows with time (+ tensile stress in reinforcement bar)	- Representative cracks found in reinforced concrete cover - Specimens under load (service condition) - Allows varying loading histories - Steady state flow verified when inlet and outlet flows are equal	- Long specimen preparation - Long test duration - Cannot perform multiple tests at the same time
This project	Prisms Pre-cracked by 3-pt bending	Single flexural macrocrack (variable width)	20, 30 and 40 kPa (ΔP adjustable)	Inlet and outlet flows with time	- Realistic crack - Quick measurement - Specimens that can be reloaded - Steady state flow verified when inlet and outlet flows are equal	- Cannot perform multiple tests at the same time

4.3 New water permeability set-up

4.3.1 Concept of the water permeability set-up

The new water permeability set-up was developed to reach multiple purposes. The first one was to characterise thoroughly the healing of a flexural crack mostly found in existing structures by water permeability and mechanical recovery on the same specimen to enable direct correlations between a self-healing state and mechanical regain. Visual observations (macro- and microscopic analyses) were also performed to bring additional information. Then, as there was only one available permeability device, multiple specimens could not be tested at the same time (**Table 4.1**). The second goal was hence to keep the set-up relatively simple to be able to perform numerous tests (at least 10) in one day. The last goal was to develop a multifunctional set-up that could be easily adapted to other testing opportunities if needed. For example, it could be used to measure the water permeability of a specimen under loading and/or on reinforced concrete beams.

4.3.2 Specimen and loading procedure

The testing specimen consists of a fibre reinforced concrete (FRC) prism of 75 mm wide x 125 mm high and 450 mm long. The specimen was notched by 20 mm deep and 5 mm wide using a circular saw at mid-span and then subjected to a 3-point bending test according to EN 14651 for pre-cracking and reloading. The goal was to produce one single flexural crack to evaluate and compare the self-healing potential of one crack in different healing conditions or for different concrete mixtures. The steel fibres control the crack width during the loading. The dimensions of the prism were chosen to reproduce a flexural crack representative of the service condition, while keeping the weight of the specimen relatively low for frequent handling. As crack width limits from Canadian standards are 0.3 mm for outdoor environment and 0.25 mm for concrete bridges, a crack width of 0.25 – 0.30 mm at the notch root was targeted at pre-cracking.

A 240 kN hydraulic cylinder was used to conduct the 3-point bending test. The loading was controlled with the average displacement of two linear variable displacement transducers (LVDT) placed on opposite sides of the specimen at the mid-span. An extensometer was installed at the bottom of the specimen, at 10 mm below the notch to measure the crack mouth opening displacement (CMOD). For pre-cracking, the specimens were loaded at a rate of 0.2 mm/min up

to a CMOD of 0.9 mm and were then unloaded at a rate of 1 mm/min. The residual crack width, at the bottom of the flexural crack (at the notch root), varied between 0.18 and 0.32 mm for the FRC presented in this paper, due to the inherent variability of concrete.

4.3.3 Permeability system

The permeability system is composed of new permeability cells linked to a testing device previously developed at Polytechnique Montreal to measure the water permeability of tie-specimens submitted to tensile loading [28]. The new set-up allows a unidirectional flow through the flexural crack of the testing prismatic specimens. It consists of two aluminium boxes clamped on the two opposite lateral faces of the prism. Each box is filled with water and linked by tubing to inlet and outlet tanks from the testing device for water circulation (**Figure 4.1**). Water in the inlet tank is put under pressure while the outlet tank remains at the atmospheric pressure, initiating the water flow from the inlet tank and box, through the cracked specimen and to the outlet box and tank. Two pressure transmitters, installed near the inlet and outlet aluminium boxes, record the real pressure gradient applied to the specimen. The ongoing and outgoing water flows are continuously measured by differential pressure transducers connected to the tanks. Although the steady-state flow was verified instantaneously on the cracked specimens, the measurement duration was fixed at 2 minutes in order to have a reliable flow rate result while minimizing its effect on the concrete self-healing. Although one set of tanks is depicted in **Figure 4.1** for sake of simplicity, the device includes 3 sets of tanks of different diameters that allow accurate measurement of flow for different damage states if needed. To ensure the watertightness of the set-up, the notch of the specimen is filled with an elastomer while elastomer membranes are fixed on the edges of the aluminium boxes. The interior dimensions of the boxes (96 x 96 mm²) constitute the flow area on each lateral face.
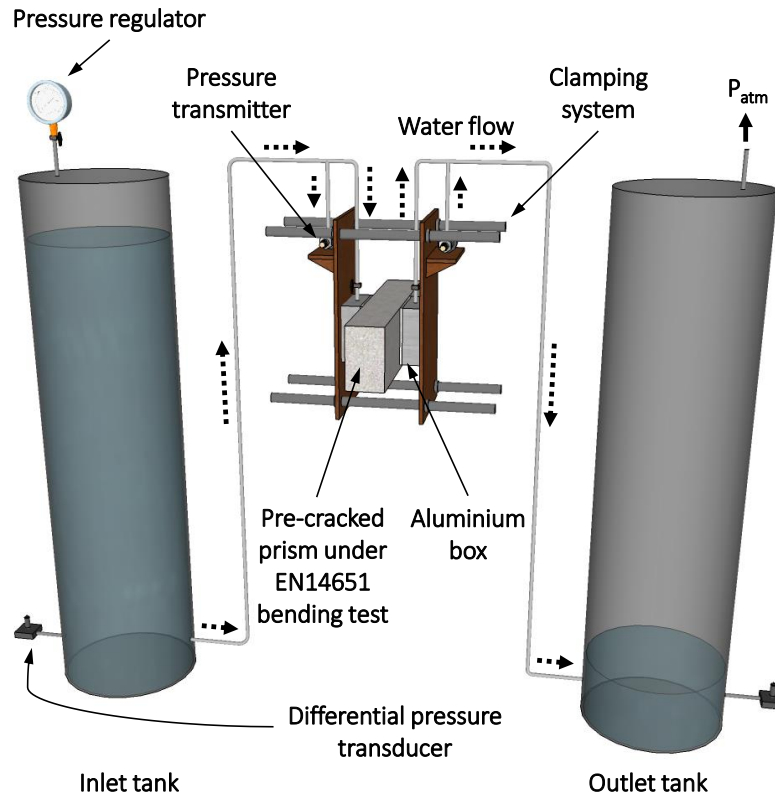
Figure 4.1. New water permeability set-up

4.3.4 Water permeability coefficient K_w

For an incompressible laminar flow through a homogeneous porous medium, the permeability coefficient K (m/s) can be determined using Darcy's law (**Eq. 4.1**). This law describes a proportional relationship between the applied pressure gradient $\Delta h/L$ and the flow rate Q (m³/s), while A (m²) represents the cross-section exposed to the unidirectional flow.

$$Q = K\, A\, \frac{\Delta h}{L} \tag{4.1}$$

The use of Darcy's law implies the validity of several assumptions. First, water is incompressible and the Reynolds number (Re) obtained in this study (much less than 1) confirms the laminar flow and validity of the equation. Second, the steady state equilibrium is verified experimentally when the inlet and outlet flows are equal. Third, the assumption on the homogeneity of the porous material is more questionable in the case of concrete. It is generally considered that a concrete

matrix uncracked [31] or uniformly cracked [7, 28, 31] is homogeneous at a macroscopic scale. But the homogeneous assumption is not well appropriate for one single crack, such as in a 3-point bending test. However, the permeability coefficient is the only available permeability index and is thus generally used also to characterise a flow through one single crack [19, 32-34] and compare quantitatively results from different studies and concrete mixtures. For these reasons, Darcy's law will also be used in this study. It is however important to verify the impact of the pressure gradient on the permeability coefficient to select the adequate experimental procedure.

Another equation, Poiseuille's law, is also used to describe the water flow through a crack into concrete. This law describes a flow through two parallel plates and is multiplied by a reduction factor ζ to take into account the roughness of the crack and the variation of its width (**Eq. 4.2**) [1]. In this equation, Δp (Pa) is the pressure gradient, b (m) the length of the crack, w (m) the crack width, μ (Pa s) the dynamic viscosity and d (m) the flow path length of the crack. Although this equation allows to study crack characteristics through the variation of factor ζ, it does not allow to determine a durability index. This equation shows that the flow rate is proportional to the cube of the crack width.

$$Q = \zeta \frac{\Delta p \, b \, w^3}{12 \, \mu \, d} \tag{4.2}$$

4.4 Experimental program

While the new water permeability set-up was developed to be able to evaluate self-healing thoroughly (visual observations, water permeability, mechanical recovery), this paper only focuses on the water permeability measurements. The main objectives of the research program presented in this paper were to identify the most sensitive indicator of the concrete damage prior to self-healing measurement, evaluate its repeatability and the impact of pressure gradient applied during the permeability test and, then, identify the most influencing factors on self-healing.

4.4.1 General methodology to assess self-healing

For this study, the FRC specimens were pre-cracked at 28 days by means of a 3-point bending test. After unloading, the geometrical characteristics of the cracks were recorded on both prism faces. The crack length was measured and the crack width w was determined at 4 points equidistant every 2.5 cm with a digital microscope (**Figure 4.2a**). The approximate crack area A on each face was then calculated considering the crack area as the sum of trapezoids and a triangle (**Figure 4.2b**). Once the crack was characterised, the initial water permeability coefficient K_{wi} was measured. The specimens were then immersed in lime-saturated water for healing and the permeability was determined at different times.
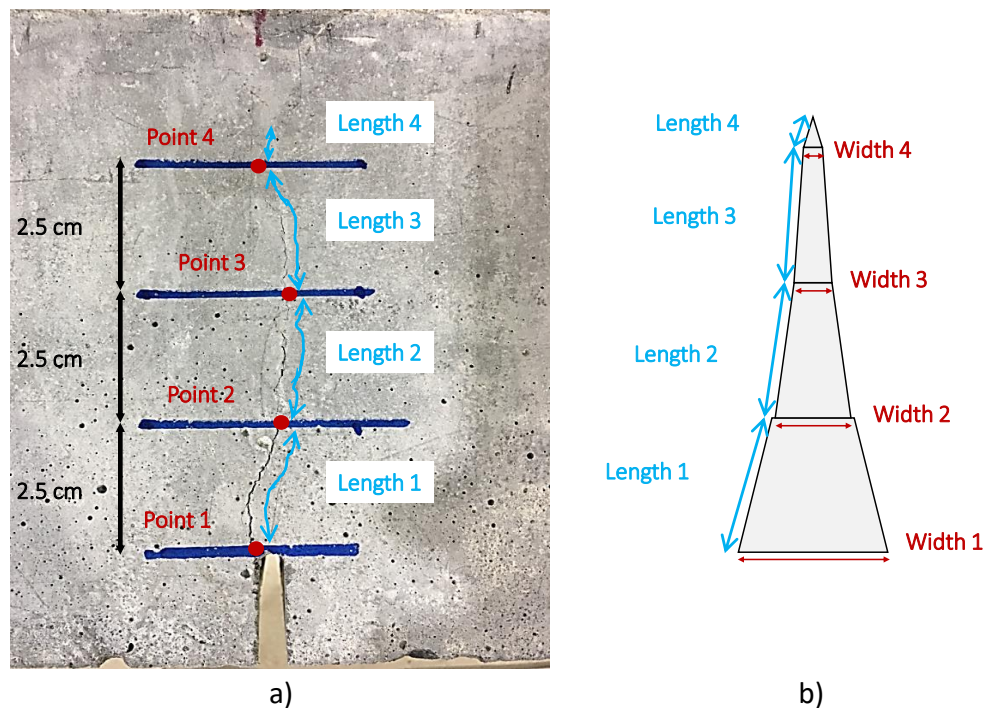
Figure 4.2. a) Lines and points to measure the characteristics of the cracks, b) approximate crack

4.4.2 Materials

This study was conducted on a FRC with a water to binder (w/b) ratio of 0.43 (**Table 4.2**). The mixture contains a blended General Use (GU) Portland cement, with 8% by mass of silica fume, and 0.75% in volume of hooked-end steel macrofibres of 35 mm length and 0.55 mm diameter.

Ten prisms (75 mm x 125 mm x 450 mm) for permeability measurements and four cylinders (100 mm diameter x 200 mm) for compressive strength characterisation were produced. 24h after casting, the specimens were demoulded and then cured under lime-saturated water for 28 days. The compressive strength (f_c) and the Young's modulus (E_c) were determined at 28 days in accordance with ASTM C39 and ASTM C469 respectively. The results were 63.9 MPa in average and 31.5 GPa respectively.

Table 4.2. Composition of the FRC mixture

Material	Control
Cement type GUb-SF (kg/m³)	550
Water (kg/m³)	229
Superplasticizer (l/m³)	10
Viscosity agent (l/m³)	0.7
Sand (kg/m³)	779
Coarse aggregates (kg/m³)	631
Steel fibres (kg/m³)	58.5

4.4.3 Water permeability measurements

The permeability of the 10 cracked prisms was measured after pre-cracking and after 7, 11 and 25 days of healing in water to investigate the self-healing kinetics. At each term, additional permeability measurements were made to investigate the repeatability and the influence of the pressure gradient.

The prisms were divided into two groups. The influence of the pressure gradient on the permeability coefficient was evaluated on 7 prisms to check the validity of Darcy's law. For this aim, three consecutive measures were taken at pressure gradients of 20, 40 and then 30 kPa (corresponding to a 2, 4 and 3-meter water depth). For each pressure gradient, the permeability measurement lasted 2 minutes, for a total duration of 6 minutes. The last measure at 30 kPa was considered for the evaluation of the self-healing at the corresponding term.

The repeatability of the water permeability measurements was evaluated on the 3 remaining prisms. The procedure consisted in measuring the water flow during 2 minutes at a pressure gradient of 30 kPa, which was repeated three times with disassembling and reassembling the whole

permeability set-up each time. The total duration was 6 minutes for the three measures. The average measure was kept for the evaluation of the self-healing at the corresponding term.

The selection of the specimens for the evaluation of the repeatability or the influence of the pressure gradient was made to cover a large permeability range in both cases. This allowed to also investigate the effect of the initial permeability coefficient K_{wi} on these results.

4.5 Results and discussion

4.5.1 Correlations between mechanical behaviour, crack characteristics and initial permeability (before healing)

The 10 prisms were submitted to the same pre-cracking phase with an expected crack width at unloading of around 0.25 mm at the notch root. Achieving reproducible cracking patterns is challenging, particularly for FRC where fibre orientation increases heterogeneity [3]. Discrepancies were thus observed between prisms. Correlations between parameters and their dispersion were analysed.

The maximum flexural stress σ_{max} reached during pre-cracking, the initial water permeability coefficient K_{wi} measured at 30 kPa after unloading and the characteristics of the residual crack (length, width and area) are summarised in **Table 4.3** for the 10 prisms. The crack length, width (at the notch root) and area are average values obtained from the prism's two lateral faces. Their average μ and coefficient of variation (COV) were calculated.

The best linear correlations between these parameters are illustrated in **Figure 4.3**. **Figure 4.3a** shows relationships between σ_{max} and the crack width ($R^2 = 0.56$) or K_{wi} ($R^2 = 0.56$), whereas the relationships between K_{wi} and the cube of crack width ($R^2 = 0.65$) or the cube of crack area ($R^2 = 0.80$) are presented in **Figure 4.3b**. It was chosen to represent the cube of the crack width and crack area in **Figure 4.3b** as the flow rate, and thus the permeability coefficient, is theoretically proportional to w^3 (according to Poiseuille's law, **Eq. 4.2**) and should evolve linearly as a function of this parameter.

Table 4.3. Results of the bending and initial permeability tests

	Bending test	Characteristics of the crack			Permeability
	σ_{max} (MPa)	Length (mm)	Width (mm)	Area (mm²)	K_{wi} (m/s)
C1	8.3	94	0.23	9.9	2.7×10^{-6}
C2	6.8	91	0.22	9.6	2.4×10^{-6}
C3	6.2	84	0.24	12.6	9.2×10^{-6}
C4	7.9	95	0.18	8.4	4.2×10^{-7}
C5	7.4	85	0.24	9.8	1.4×10^{-6}
C6	6.9	89	0.24	11.2	2.3×10^{-6}
C7	7.4	92	0.24	10.4	1.6×10^{-6}
C8	7.2	93	0.26	16.1	6.5×10^{-6}
C9	5.7	86	0.32	13.9	6.2×10^{-6}
C10	4.4	97	0.29	14.0	7.4×10^{-6}
μ	6.8	91	0.25	11.6	4.0×10^{-6}
COV	16%	5%	15%	20%	72%
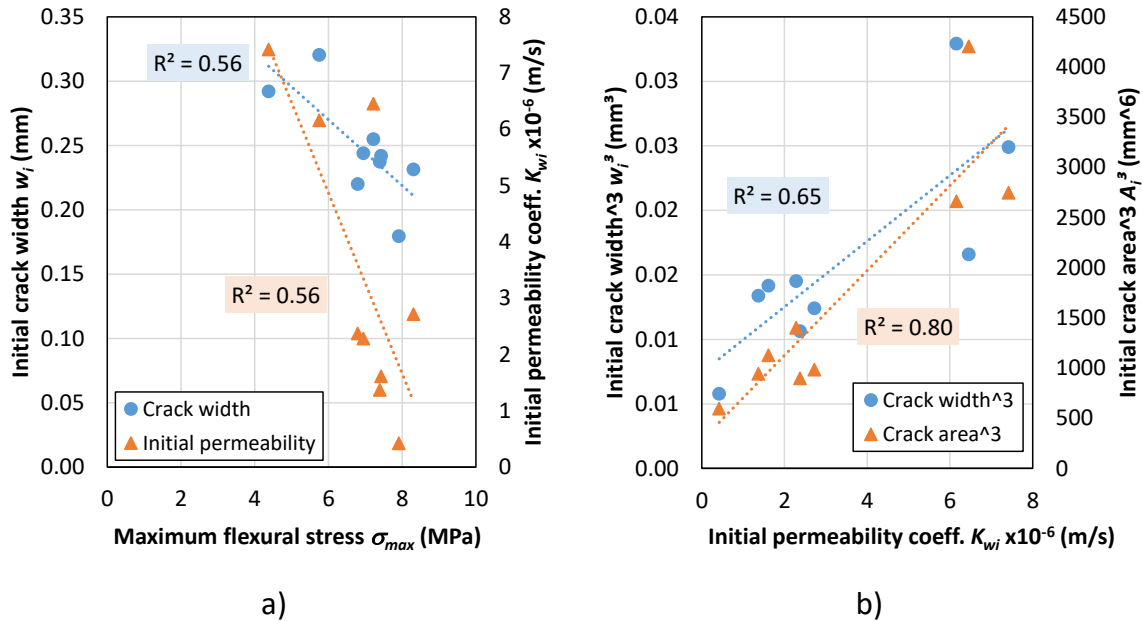
Figure 4.3. Correlations before healing between a) crack width and K_{wi} with σ_{max}, b) cube of crack width and cube of crack area with K_{wi}

Logically, higher σ_{max} reached in the pre-cracking bending test implied a better crack control of the fibres and narrower crack widths in prisms, and thus lower K_{wi} (**Figure 4.3a**). Following the same logic, K_{wi} increased with the crack width or crack area and thus with the cube of these parameters

in **Figure 4.3b**. The good correlations obtained in **Figure 4.3b** confirm the relationship from Poiseuille's law and the validity of the water permeability results. The correlation with the cube of the crack area ($R^2 = 0.80$) was stronger than with the cube of the crack width ($R^2 = 0.65$), as the crack area is more representative of the entire surface crack subjected to the water flow, rather than the crack width measured locally at the notch root. This was also observed by Roig-Flores et al. [6]. Variation between K_{wi} and crack area, measured at the specimen surface, may come from tortuosity and non-uniform opening inside the crack not considered by the crack area, while K_{wi} does. Overall, all correlations made between the parameters describing the initial state of damage (before self-healing) of the prisms are coherent and validates the methodology of pre-cracking and permeability measurements.

Besides, it is interesting to analyse the dispersion of the parameters measured before healing (**Table 4.3**). The 10 prisms showed a fair dispersion of σ_{max} reached in flexure during pre-cracking (COV = 16%), which led to COV of 5, 15 and 20% for the length, width and area of the crack respectively. Thus, the COV of mechanical parameters are within the same range (5-20%). In contrast, such dispersion of the crack characteristics induced a wide range of initial permeability coefficients, with a COV of 72%. As it will be shown further (**Section 4.5.2.1**), permeability coefficients were reliable and repetitive in this project. This wide range of permeabilities is obviously linked to the proportional relationship between the water flow and the cube of crack width that allows a higher sensitivity to damage [35], which means that permeability measure makes possible to account for small differences in the damage. This higher sensitivity of permeability to damage is also due to the consideration of the whole crack volume in permeability measures (width, length, tortuosity, and more particularly variations inside the crack) in comparison to crack characteristics measured at the crack surface, as also reported by [21]. This means that, even for identical crack width, different permeability results can be obtained. For example, specimens C3 and C5 have $w = 0.24$ mm, but C5 had a K_{wi} 85% lower than C3 (**Table 4.3**).

Therefore, among the mechanical and permeability parameters measured in this project to evaluate the prisms damage, water permeability is considered the most sensitive and should thus provide a good indicator of the self-healing capacity of prisms. For this reason, repeatability of measurement, the impact of pressure gradient and healing of prisms were assessed in the following sections mainly with permeability measurements.

4.5.2 Water permeability measurements

4.5.2.1 Repeatability

The three individual water permeability coefficients K_w, their average μ and coefficients of variation (COV), determined at 30 kPa during 2 minutes periods on the specimens subjected to repeatability measures(named C1, C2 and C3), are indicated in **Table 4.4**. First, one can observe that the average K_w values decreased with time (between 0, 7, 11 and 25 days). The healing effect observed will be discussed in more details in **Section 4.5.3**.

Analysis of the repeatability of measurements indicates no systematic evolution (increase or decrease) of K_w between the three consecutive measures performed on a specific specimen at a fixed term. This confirms that no significant effect of self-healing occurred between these measurements as the duration of the water permeability measurement (2 minutes) was very short.

In addition, except the two highest COV values of around 5% for K_{wi} of specimens C1 and C2, the rest of the COV were equal or below 2.5%. The COV globally did not seem to be linked to the permeability level. For example, the COV were 1.8% and 1.5% respectively for C2 and C3 at 25 days, while their K_w were different (respectively 1×10^{-6} and 6.1×10^{-6} m/s). These COV values are in the same range as those obtained by Van Mullem et al. [21] (0 – 5%), who also performed repetitive measurements to assess the inherent random error of their water flow test.

Therefore, the permeability disparities being not influenced by the short repetitive measures, nor the permeability level, they represent the inherent variability of the permeability test. It can be concluded that the measurements with this new permeability set-up are repeatable and reliable.

Table 4.4. Repeatability of permeability coefficients (m/s)

	K_w initial			K_w at 7 days			K_w at 11 days			K_w at 25 days		
	n°1	n°2	n°3	n°1	n°2	n°3	n°1	n°2	n°3	n°1	n°2	n°3
C1	2.9×10^{-6}	2.8×10^{-6}	2.5×10^{-6}	1.1×10^{-6}	1.1×10^{-6}	1.1×10^{-6}	9.3×10^{-7}	9.5×10^{-7}	NA	9.5×10^{-7}	9.6×10^{-7}	9.5×10^{-7}
C2	2.5×10^{-6}	2.4×10^{-6}	2.2×10^{-6}	9.7×10^{-7}	1.0×10^{-6}	1.0×10^{-6}	9.2×10^{-7}	9.7×10^{-7}	9.7×10^{-7}	9.7×10^{-7}	1.0×10^{-6}	1.0×10^{-6}
C3	9.1×10^{-6}	9.4×10^{-6}	9.2×10^{-6}	6.8×10^{-6}	6.8×10^{-6}	6.7×10^{-6}	6.5×10^{-6}	6.3×10^{-6}	6.4×10^{-6}	6.1×10^{-6}	6.1×10^{-6}	5.9×10^{-6}
C1 (μ/COV)	2.7×10^{-6} / 5.2%			1.1×10^{-6} / 0.3%			9.4×10^{-7} / 1.0%			9.5×10^{-7}/ 0.4%		
C2 (μ/COV)	2.4×10^{-6} / 4.8%			1.0×10^{-6} / 2.5%			9.6×10^{-7} / 2.3%			1.0×10^{-6}/ 1.8%		
C3 (μ/COV)	9.2×10^{-6} / 1.3%			6.8×10^{-6} / 0.6%			6.4×10^{-6} / 1.2%			6.1×10^{-6} / 1.5%		

μ : average, COV : coefficient of variation, NA : value non available

4.5.2.2 Influence of pressure gradient

The results of the initial permeability coefficients K_{wi} versus the applied pressure gradient (20-30-40 kPa) are illustrated in **Figure 4.4a**, while **Figure 4.4b** summarizes the differences of all K_w between 30 and 20 kPa and between 40 and 30 kPa, versus the K_w value at 20 kPa.
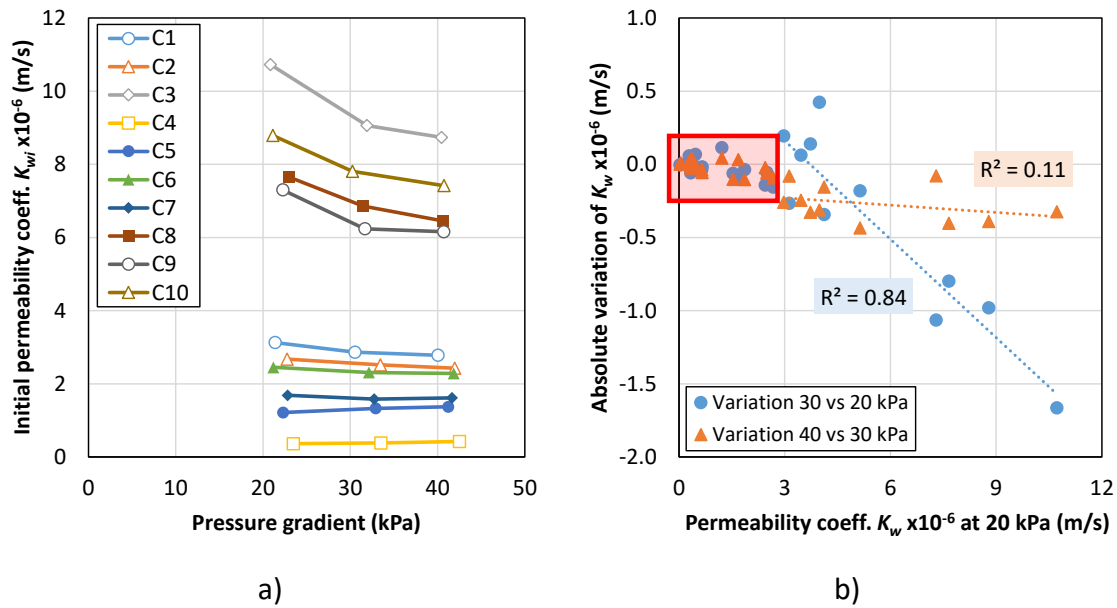
Figure 4.4. a) Initial permeability coefficients vs pressure gradient, b) variation of K_w depending on the pressure for all measures at all times

At 20 kPa, K_{wi} of the 10 prisms ranged from 3.6×10^{-7} to 1.1×10^{-5} m/s. In **Figure 4.4a**, it can be seen that K_w decreased with increasing pressure, with a more significant drop from 20 to 30 kPa compared to 30 to 40 kPa. The curves became flatter for the specimens with the lowest permeability coefficients, below 3×10^{-6} m/s, which means a lower effect of the pressure gradient for this range of K_w. This is also visible in the red area in **Figure 4.4b** where no important K_w variations were recorded and no clear trend could be deduced below 3×10^{-6} m/s.

Thus, the impact of pressure gradient on the permeability was not similar for all levels of K_w. In this study, for specimens with a K_w above around 3×10^{-6} m/s, the permeability coefficient decreased with increasing pressure gradient. Below this threshold, the variation of the pressure gradient did not really impact the permeability coefficient. This threshold could be explained by the validity of Darcy's law used to calculate the permeability coefficient and particularly the homogeneous

material assumption (**Section 4.3.4**). A high K_w means a wide crack is present in the prism, which clearly represents a non-uniform matrix. In such case, Darcy's law is less applicable. The flow rate Q is thus not proportional to the applied pressure gradient, which means that the permeability coefficient is not constant. When K_w is lower, the crack is thinner or notably healed, and even if the threshold $3\text{x}10^{-6}$ m/s still describes a permeable medium, this case represents more closely a homogeneous state.

Besides, above $3\text{x}10^{-6}$ m/s, increasing the pressure gradient from 20 to 30 kPa globally led to lower K_w values (directly visible in **Figure 4.4a** and through the negative absolute variations of K_w in **Figure 4.4b**). The absolute variation of K_w at 30 versus 20 kPa is quite well correlated to the value of K_w (linear correlation with $R^2 = 0.84$). Increasing the pressure gradient from 30 to 40 kPa in the same K_w range (above $3\text{x}10^{-6}$ m/s) also decreased the K_w values but much less significantly, especially for high values of K_w, and the absolute variation of K_w is much less dependent on K_w ($R^2 = 0.11$ for a linear trend). The lower impact of the pressure gradient on K_w between 30 and 40 kPa than between 20 and 30 kPa could be explained by the better flow and measurement when the applied pressure is higher. A pressure gradient of 20 kPa might be too low to induce a stable flow through the crack (inlet and outlet flows were not always exactly equal). On the other hand, it is assumed that a pressure gradient of 40 kPa could increase the risk of pulling away some healing products and/or bring more local flow turbulences [36]. More investigations are needed to confirm these assumptions but, as a precaution, a pressure gradient of 30 kPa was considered more appropriate for the water permeability measurements in this project. This pressure was chosen for the repeatability measures and to compare the evolution of self-healing.

The influence of pressure gradient on the water permeability coefficient was scarcely studied on cementitious materials. Kermani [37] observed a slight increase of the permeability coefficient with an increasing water pressure (3 500 to 10 500 kPa) for unstressed concrete. Desmettre & Charron [28] analysed the influence of pressure gradient (25, 50 and 100 kPa) on tie-specimens under a uniaxial tensile load and concluded that its impact on the permeability coefficient was negligible. Shin et al. [38] obtained lower permeability coefficients when increasing the water pressure (from 1.5 to 7 kPa) for cylinders pre-cracked by splitting tests with a crack width above 0.3 mm. Below this crack width, the permeability coefficients were less influenced by the pressure gradient, which is the same trend observed in this project. None of the previous studies provided

possible explanations of slight permeability variation under pressure gradient. Shin et al. [38] stated unknown parameters not considered in the calculation of permeability coefficient may affect the results. These parameters may come from 3D effects and localised turbulences caused by the applied pressure gradient in a flow through a crack, because of its internal crack pattern (width and tortuosity variation) [36]. In such case, the trickles of water tend to move away from the ideal parallel flow. It is assumed that when pressure gradient rises, the 3D and turbulent effects may increase, which would lead to lower permeability coefficient. These effects may be higher in larger cracks because there would be more space for these non-uniform tortuous effects to occur. In conclusion, there exists an impact of the pressure gradient on the permeability and it should be evaluated to make a wise choice of the pressure level in a test.

4.5.3 Self-healing

4.5.3.1 Self-healing kinetics and products

Previous results confirmed that water permeability coefficient was the most sensitive to cracking, that the permeability measurements were repeatable and reliable and that an adequate pressure gradient was selected for the test. The self-healing capacity of the FRC immersed in water was then evaluated. As the permeability measurement lasted 6 minutes (3 measures of 2 minutes) at each term for all the tested prisms, whether they were subjected to repeatability or pressure effect measurement, the ten prisms can be compared when regarding the effect of self-healing with the last measures made at 30 kPa for all specimens.

The evolution of the permeability coefficients K_w with time is illustrated in **Figure 4.5a**. As aforementioned, the initial permeability K_{wi} varies according to the initial damage (crack width, length, area, roughness) created by the same pre-cracking procedure. The permeability coefficients showed major drops in the first 7 days, then the self-healing slowed down (**Figure 4.5a**). This evolution of self-healing complies with the kinetics observed in literature [7, 15, 39]: a rapid healing at the beginning followed by a slower healing rate. This can be explained by a rapid precipitation of self-healing products on the crack surfaces of the mature concrete at the beginning of the process, as ions involved in the reaction are readily available at the surface. Once these ions are depleted, the ones inside the matrix diffuse slowly to the crack.
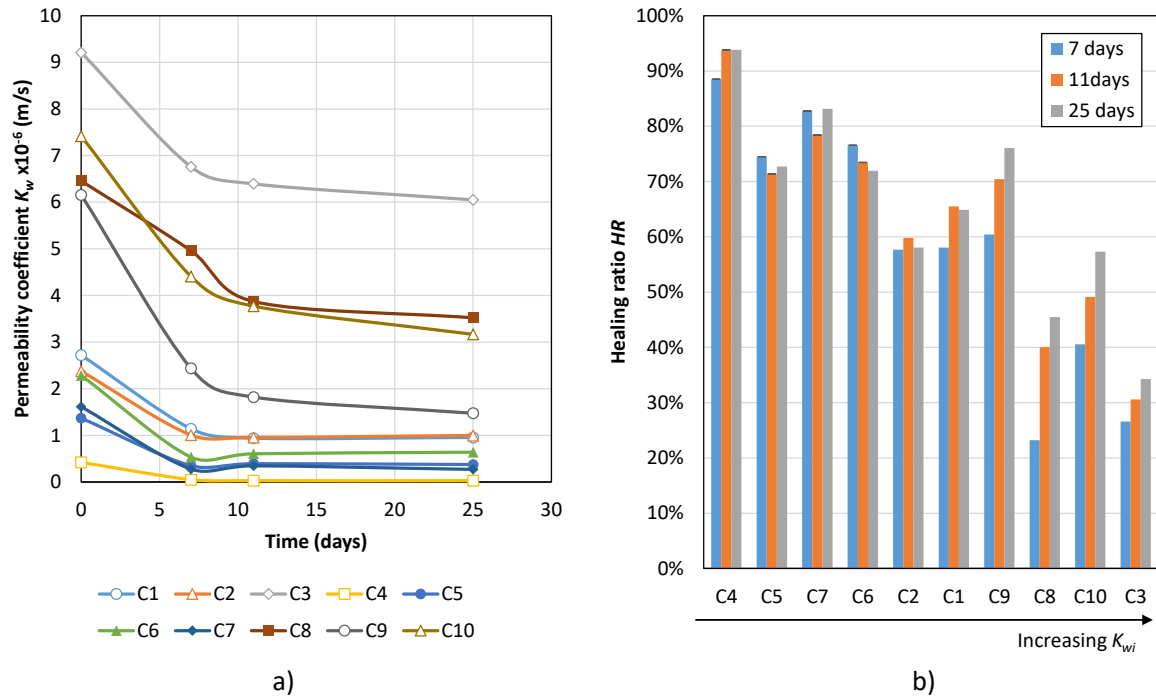
Figure 4.5. a) Evolution of the a) permeability coefficient with time and b) Healing Ratios with time

After permeability measurements, some specimens were cut to observe the internal crack surface (fractured surface) with an environmental scanning electron microscope (SEM). The presence of calcium carbonate crystals ($CaCO_3$), in a shape of small particles (calcite), and needles of ettringite were observed in the specimens immersed in water (**Figure 4.6a**). Energy-dispersive X-ray analysis (EDS) were also performed at crack surface and confirmed the composition of the calcite crystals (peaks of Ca in **Figure 4.6b**) and the composition of ettringite (peaks of Ca, S, Al in **Figure 4.6c**). As stated previously, calcium carbonate crystals are the main healing products observed in mature concrete. The ettringite may also be observed on crack surfaces kept under water since its formation requires a lot of water molecules. Ferrara et al. [40] also found ettringite at crack surface of a concrete specimen containing a crystalline additive and immersed in water.
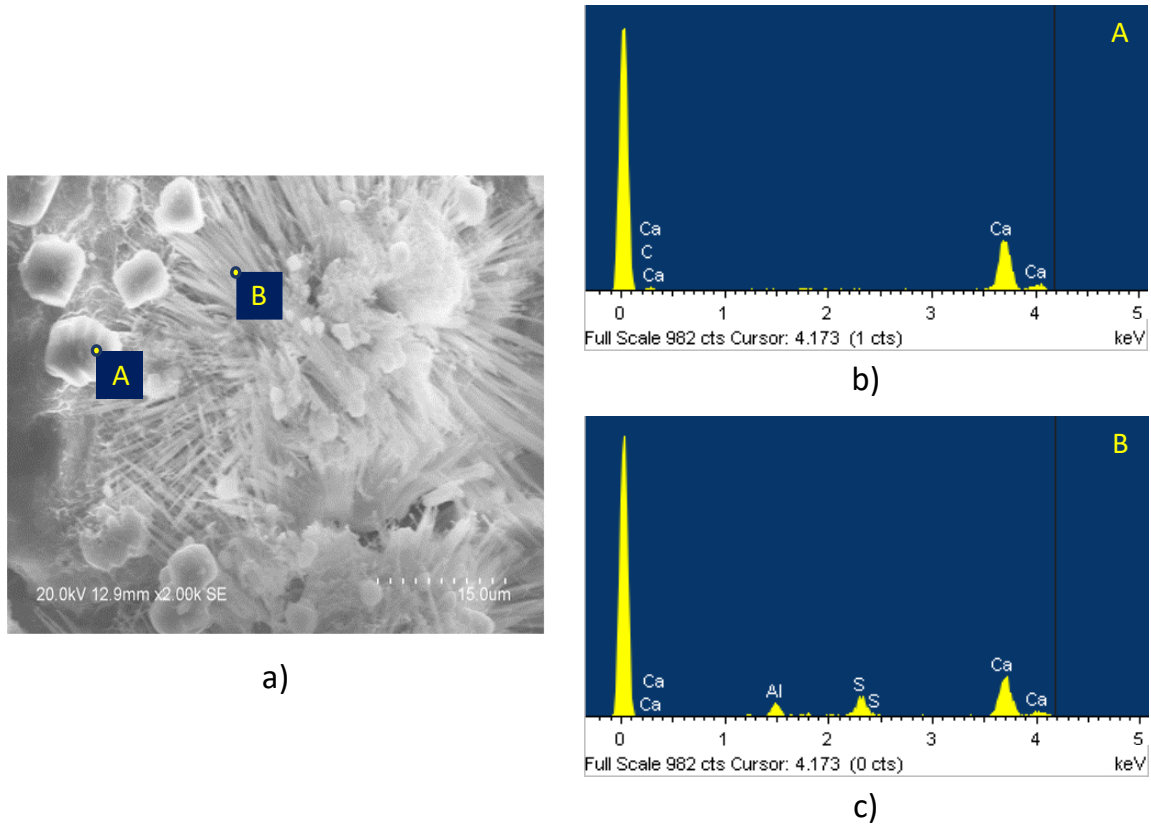
Figure 4.6. Healing products on a surface of a crack immersed in water shown by a) SEM picture, b) EDS analysis of calcite and c) EDS analysis of ettringite

Self-healing can be determined either with a Healing Ratio (*HR*) based on water permeability measurements or with a Closing Ratio (*CR*) based on surface crack measurements.

Healing Ratios *HR* can be expressed in terms of water flow [4, 6, 9, 10, 12, 25] or permeability coefficient [15], while other studies used relative permeabilities (K_t/K_i) [39]. In this project, the Healing Ratio was calculated by **Eq. 4.3.** *HR* represents the percentage of decrease of K_w due to self-healing at time *t* in comparison to the initial permeability (K_{wi}). A Healing Ratio of 0% means no healing occurred, while a value of 100% indicates a complete healing of the crack.

$$HR\ (\%) = \frac{K_{wi} - K_{wt}}{K_{wi}} \cdot 100 \tag{4.3}$$

The Closing Ratio *CR* has also been determined by **Eq. 4.4**, with A_i representing the initial crack area before healing and A_f being the final crack area after healing for 25 days. The crack area was

calculated via the approximate method explained in **Section 4.4.1**. The final crack widths measurements were taken at the same locations of the initial crack widths. These results will be discussed in the next section.

$$CR\ (\%) = \frac{A_i - A_f}{A_i} \cdot 100 \qquad \qquad \textbf{(4.4)}$$

The Healing Ratios *HR* corresponding to permeability measurements in **Figure 4.5a** are shown in **Figure 4.5b**. Prims submitted to the same procedure show large variation of their healing capacity (**Figure 4.5b**), which emphasises the fact that several specimens are needed to evaluate with confidence the self-healing capacity of a material. The Healing Ratios obtained in this study ranged from 23% to 89% at 7 days (with HR_{7d} superior to 75% for K_{wi} inferior to 2.3×10^{-6} m/s), 31% to 84% at 11 days and 34% to 94% at 25 days (**Figure 4.5b**). Comparison of permeability results with other studies is not easy as most of them show a ratio (Q_t/Q_i or K_{wt}/K_{wi}) without giving the initial flow/permeability, whereas K_{wi} is an important parameter influencing the Healing Ratios as it will be shown in the next analyses. Jiang et al. [39] found similar healing results (relative permeability coefficient converted in *HR*) for control mortars cracked at 28 days in still water: around 40% at 7 days, 60% at 14 days, 65% at 21 days and 67% at 28 days. The results from Sisomphon et al. [5] (relative flow rate converted in *HR*) are also in that range: around 30% at 7 days, 35% at 14 days and 40% at 28 days.

Figure 4.5 also reveals different self-healing kinetics depending on K_{wi} as *HR* globally decrease when K_{wi} of specimens increase. To underline this effect, the specimens were sorted by their initial permeability (increasing K_{wi} values) for the presentation in **Figure 4.5b** instead of their numbering.

4.5.3.2 Correlations with crack characteristics and initial permeability (after healing)

After the healing period, several correlations were studied. First, correlation between the initial and final permeability (K_{wi} *and* K_{wt}) were evaluated (**Figure 4.7**). Then, correlations between the Healing Ratio *HR* or Closing Ratio *CR* with the initial permeability K_{wi} (**Figure a** and **b**) or with the initial crack area A_i (**Figure c** and **d**) were examined. Whereas correlations were made between K_{wi} and the cube of the crack characteristics (w^3 and A^3) in **Section 4.5.1** (**Figure 4.3b**), the correlations between the Healing and Closing Ratios (*HR* and *CR*) were here evaluated in terms of

the crack area *A*. This choice was done as the goal of this analysis was to identify which initial parameter (K_{wi} or A_i) influences the most the self-healing capacity.

First, it can be seen from **Figure 4.7** that K_{wt} measured at various terms (7, 11 and 25 days) was strongly correlated with K_{wi} (linear correlation with $R^2 = 0.93$, 0.90 and 0.86 respectively). **Figure a** shows that *HR* was also largely correlated with K_{wi} (linear correlation with $R^2 = 0.78$, 0.73 and 0.62 respectively). Higher K_{wi} implied higher K_{wt} and lower *HR* at a specific time. This is logical as a higher K_{wi} indicates a higher crack volume that need more time to be completely healed, in comparison to thinner crack volumes with lower K_{wi}. Prisms with lower initial permeability (finer cracks) have thus the highest potential of self-healing, as previously observed by Gagné & Argouges [41]. The Closing Ratio *CR* was also dependent on the K_{wi} (**Figure b**), lower K_{wi} led to higher *CR*. However, the linear correlation was clearly lower ($R^2 = 0.33$). The relationships between *HR* and *CR* with the initial crack area A_i measured at the specimen surface (**Figure c** and **d**) are clearly less convincing than with K_{wi} (**Figure a** and **b**). The R^2 values were 0.60, 0.47 and 0.35 for *HR* at 7, 11 and 25 days respectively, while $R^2 = 0.19$ for *CR* at 25 days was obviously lower again.

The better correlation of the evolution of the permeability (K_{wt}) and Healing Ratio (*HR)* with the initial permeability (K_{wi}), rather than with the initial crack area (A_i), means that the self-healing comparison of two specimens of different testing conditions should be done on specimens presenting similar K_{wi} to be more relevant on the impact of the testing condition. Therefore, if the objective of a project is to evaluate the self-healing capabilities provided by various components added in a concrete or in different conditions, it may be preferable to compare specimens of different compositions having similar K_{wi} rather than ones with similar crack widths or areas to analyse the results. Moreover, even if the variability on the crack width could be reduced, the variability on the internal crack geometry in load-induced cracks is impossible to control, which will anyhow lead to different water flow results, as observed by Van Mullem et al. [21] when applying an active crack width control.

Besides, when comparing the self-healing process of cracks characterised by similar K_{wi}, one must keep in mind that some variations of the cracks self-healing can occur with time. This is illustrated by the R^2 correlation coefficients which systematically decreased with time (7, 11 and 25 days) in **Figure 4.7** and **Figure** , indicating a larger variation of parameters as self-healing proceeded. This

suggests that self-healing does not occur uniformly for all prisms, as cracking pattern in each prism is different.

Finally, **Figure 4.7** and **Figure** also illustrate that all the slopes of the linear trends decreased with time due to self-healing. This result was expected as with healing, the permeability of all prisms should stabilise toward the matrix permeability at a healed state, regardless of the K_{wi} or crack area.
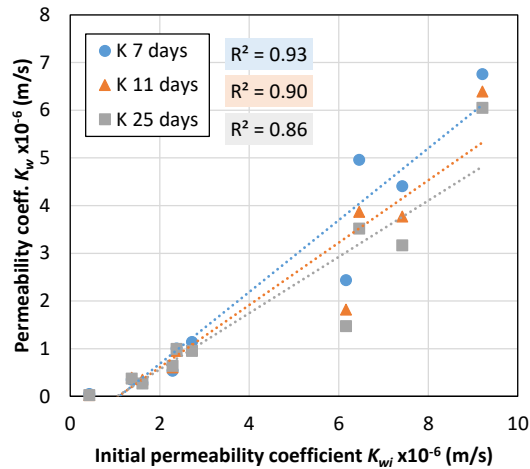
Figure 4.7. Correlations after healing between K_{wt} and K_{wi}
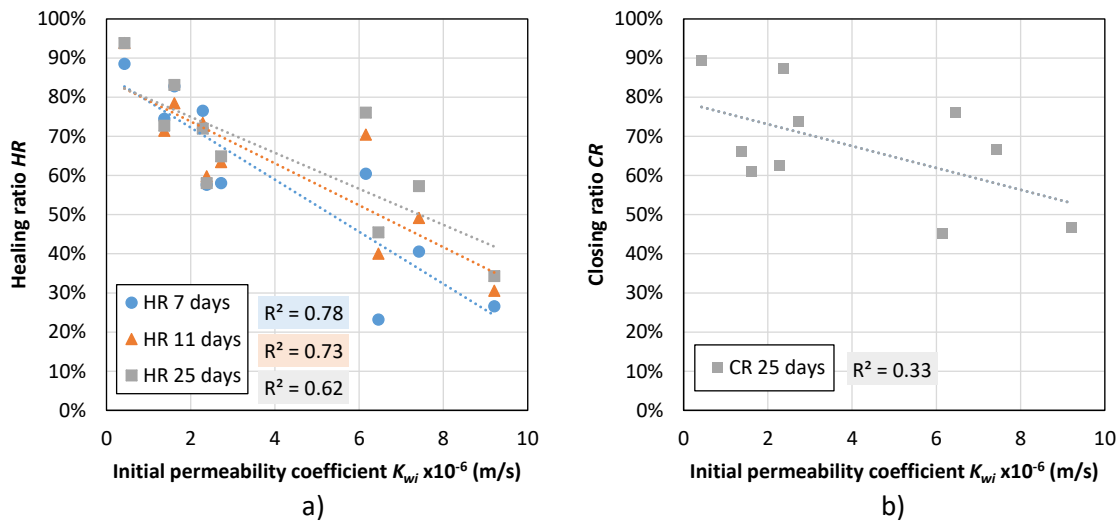
Figure 4.8. Correlations after healing between a) HR and K_{wi}, b) CR and K_{wi}, c) HR and A_i and d) CR and A_i
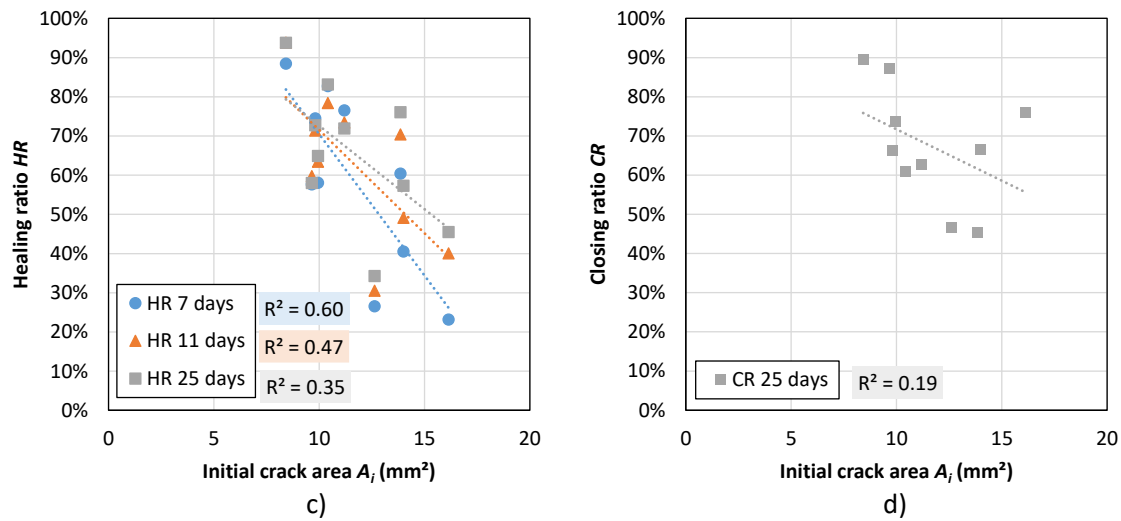
Figure 4.8. Correlations after healing between a) *HR* and K_{wi}, b) *CR* and K_{wi}, c) *HR* and A_i and d) *CR* and A_i (cont.)

4.5.3.3 Crack width uncertainties vs water permeability

From **Figure** , it clearly appears that assessing self-healing via Healing Ratio based on water permeability measurements is more accurate and adequate than using Closing Ratio based on crack width measurements at the surface. Measuring the crack width at constant points can be very approximate. **Figure 4.9** illustrates an example of a crack before and after 25 days of healing. In **Figure 4.9a**, the initial crack width measured at location 1 on the blue line was 0.102 mm. In **Figure 4.9b**, it can be seen that the crack was not homogenously healed after 25 days. The crack measurement taken at the same location 1 led to a complete sealing (w = 0 mm). However, right next at location 2, healing is less visible and the residual crack width measured 0.067 mm. The location 1 represented the best closure, while the location 2 at *w* = 0.067 mm represented the worst closure. The crack Closing Ratio can thus vary widely depending on the locations of the measurements. **Figure 4.10** presents the Healing Ratio vs the Closing Ratio when the crack measurements were taken in all prisms at the initial locations (**Figure 4.10a**), or right next to the initial location with the worst (**Figure 4.10b**) or the best closure (**Figure 4.10c**). While Roig-Flores et al. [42] concluded that *CR* may overestimate self-healing compared to *HR*, from **Figure 4.10b** and **Figure 4.10c**, it can be seen that *CR* may either underestimate (worst healing locations) or overestimate (best healing locations) the healing. Although **Figure 4.10a** represents an average

correlation between *HR* and *CR*, it can be noticed that similar *CR* values may lead to very different *HR* values and that a high *CR* can lead to a low *HR* and vice versa. **Figure 4.11** illustrates this last point through an example of two local sections of cracks of similar width (around 0.17 mm) of two different prisms before and after some healing. Although the healing products closing the crack were clearly visible in **Figure 4.11b** in comparison to **Figure 4.11a**, the Healing Ratio was lower for the specimen in **Figure 4.11b** (46% compared to 81%). This demonstration reveals that the crack measurement at the external surface is more limiting than measurements taking into account the whole cracking pattern, such as permeability or tomography. This was also reported by Roig-Flores et al. [42] and Park & Choi [8].

Although crack opening measurements could be more easily implemented in situ and cost-effective than permeability measurements, assessing self-healing only via crack width or area measurements at a limited number of points at the surface is thus not ideal and less precise. It must be noted however that there exist advanced image analysis techniques to accurately measure the whole surface crack using black pixels [43] or binarisation [44]. Such techniques would certainly reduce crack width uncertainties and improve the correlations between *HR* and *CR*. Regarding the different methodologies used in this project, the use of the water permeability coefficient K_{wt} and associated Healing Ratio *HR* is the most reliable to assess self-healing. It gives very accurate and repeatable measurement and takes into account the whole crack volume. Those characteristics were required for this research project as it allows better comparison between different specimens and testing conditions.
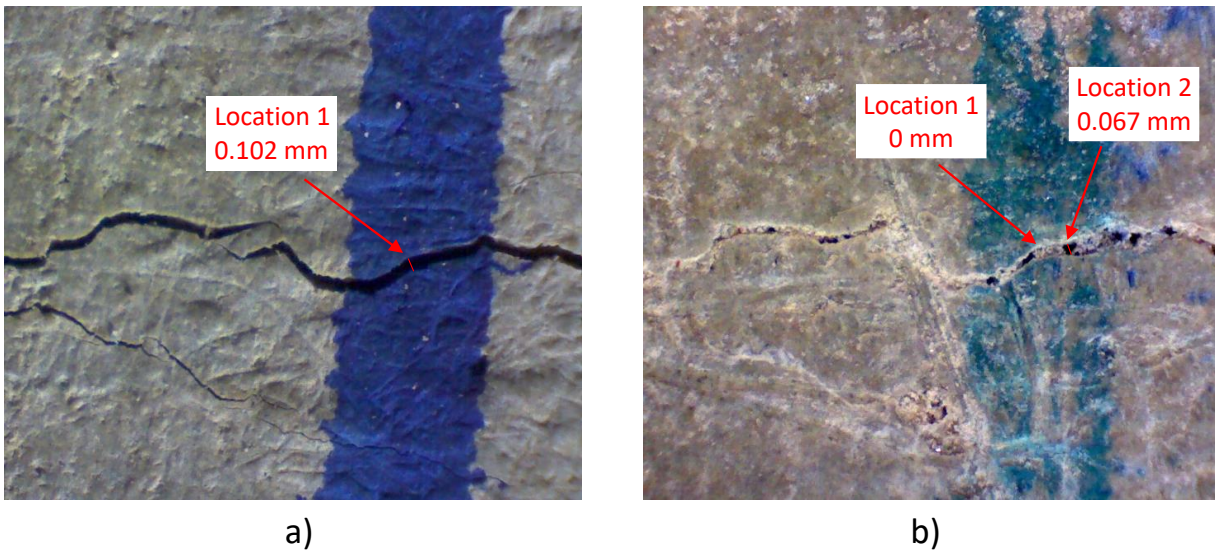
Figure 4.9. Pictures of a crack a) before healing, b) after healing for 25 days showing different crack width measurements depending on the locations
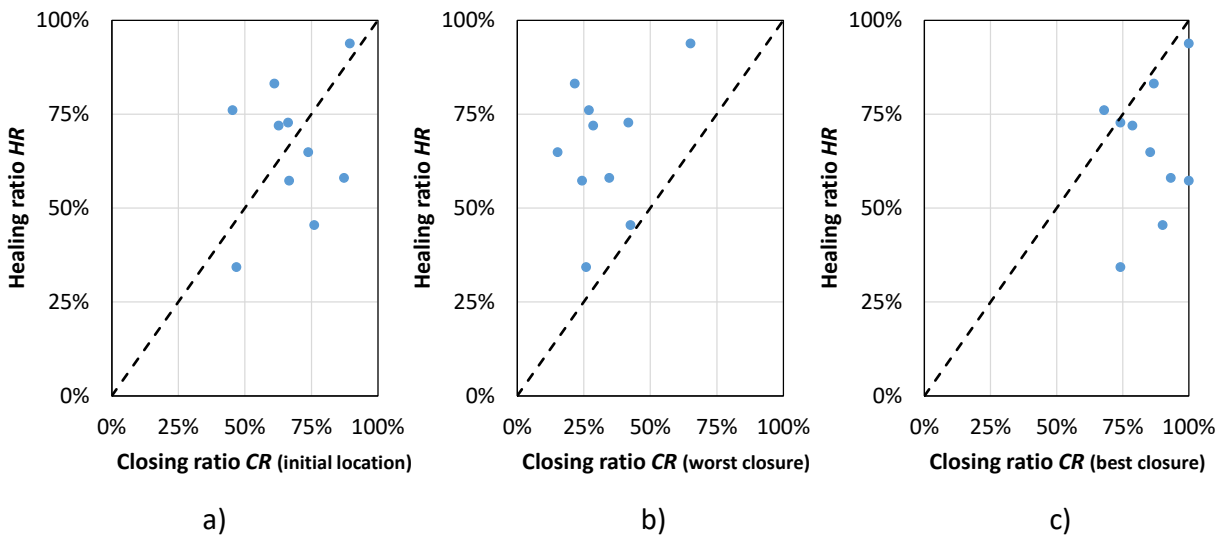
Figure 4.10. Healing Ratio (*HR*) vs Closing Ratio (*CR*) depending on the locations of the crack width measurements: a) at initial locations, b) locations presenting the worst healing and c) locations presenting the best healing

Before healing	After healing

a) Specimen with healing ratio (*HR*) of 81%

b) Specimen with healing ratio (*HR*) of 46%
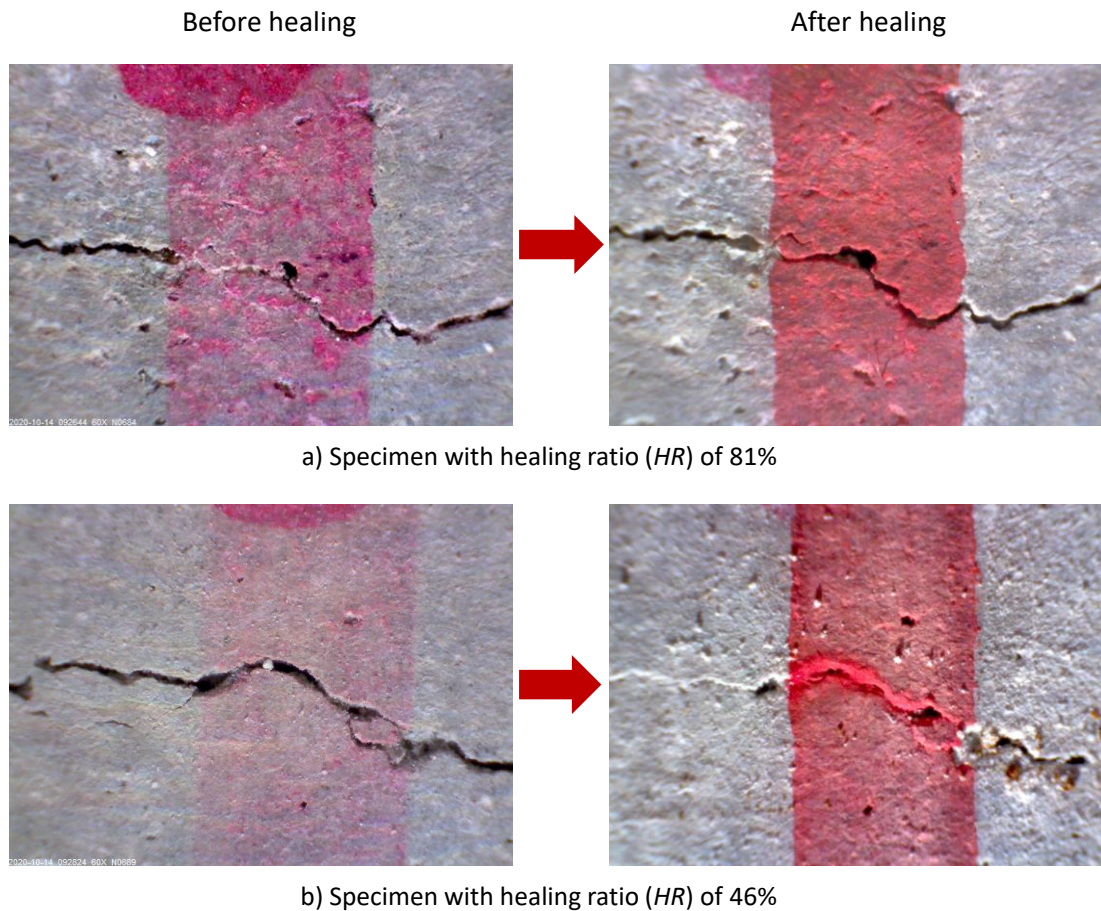
Figure 4.11. Pictures of local sections of cracks before and after healing for prisms with a) Healing Ratio = 81%, and (b) Healing Ratio = 46%, based on water permeability

4.6 Conclusions

A new water permeability set-up has been developed to evaluate the self-healing capacity of concrete prisms pre-cracked by means of a 3-point bending test. Visual, mechanical and permeability measurements were performed on pre-cracked fibre reinforced concrete (FRC) specimens to identify the most sensitive indicator of the concrete damage prior to self-healing measurement, to validate the good repeatability of the permeability measurement and to investigate the influence of the pressure gradient on this measurement. Once the procedure and permeability set-up were proved reliable, self-healing of the prisms was studied and the most influencing factors on self-healing were identified. Based on the results obtained in this experimental program, the main following conclusions can be drawn:

- Among the initial damage measurements (bending stress σ_{max}, crack length L_i, crack width w_i, crack area A_i and permeability K_{wi}) made on pre-cracked FRC prisms, water permeability coefficient was the most sensitive to cracking, because it takes into account the whole crack volume and internal crack geometry.

- The water permeability set-up allowed repeatable and reliable measurement of permeability, with coefficients of variations mostly below 2.5% between repeated measures. No significant effect of self-healing occurred between three repeated measures of 2 minutes.

- Increasing pressure gradient from 20 to 40 kPa did not impact permeability coefficient below 3×10^{-6} m/s. However, a slight decrease of permeability coefficient was observed above 3×10^{-6} m/s. A pressure gradient of 30 kPa was selected to minimize its impact on permeability coefficients.

- The kinetics of self-healing of the cracked FRC was rapid at the beginning and then significantly slower within a few days. The Healing Ratios ranged from 23% to 89% after 7 days, from 31% to 94% after 11 days and 34% to 94% after 25 days under lime-saturated water.

- The main healing products observed on crack surfaces of prisms were calcium carbonate and ettringite.

- Assessing self-healing via Healing Ratio, based on water permeability, is more accurate than via Closing Ratio, based on surface cracks area. Besides, Healing and Closing ratios showed higher correlations with the initial permeability than the crack area. Therefore, the initial permeability is the most prominent factor of self-healing.

- This suggests that self-healing capabilities provided by various additives added in concrete and in different conditions should be compared on specimens of similar initial permeability, rather than ones with similar crack widths or areas, to better interpret the results.

This paper presented the first phase of a project that aims to evaluate and compare the self-healing capacity of FRC containing several admixtures (crystalline admixture, expansive agent and

superabsorbent polymer) in different healing conditions (water, wet/dry cycles, ambient air and outdoor exposure). These results will be addressed in future papers based on the conclusions drawn here.

4.7 Acknowledgements

4.8 References

[1]   C. Edvardsen, "Water permeability and autogenous healing of cracks in concrete," *ACI Materials Journal*, vol. 96, no. 4, pp. 448-454, 1999.

[2]   N. De Belie et al., "A review of self-healing concrete for damage management of structures," *Advanced Materials Interfaces*, p. 28 pages, 2018.

[3]   L. Ferrara et al., "Experimental characterisation of the self-healing capacity of cement based materials and its effects on the material performance: A state of the art report by COST Action SARCOS WG2," *Construction and Building Materials*, Review vol. 167, pp. 115-142, 2018.

[4]   A. Beglarigale, D. Eyice, B. Tutkun, and H. Yazici, "Evaluation of enhanced autogenous self-healing ability of UHPC mixtures," *Construction and Building Materials*, vol. 280, 2021.

[5]   K. Sisomphon, O. Copuroglu, and E. A. B. Koenders, "Self-healing of surface cracks in mortars with expansive additive and crystalline additive," *Cement and Concrete Composites*, vol. 34, pp. 566-574, 2012.

[6]   M. Roig-Flores, S. Moscato, P. Serna, and L. Ferrara, "Self-healing capability of concrete with crystalline admixtures in different environments," *Construction and Building Materials*, vol. 86, pp. 1-11, 2015.

[7] P. Escoffres, C. Desmettre, and J.-P. Charron, "Effect of a crystalline admixture on the self-healing capability of high-performance fiber reinforced concretes in service conditions," *Construction and Building Materials*, vol. 173, pp. 763-774, 2018.

[8] B. Park and Y. C. Choi, "Self-healing capability of cementitious materials with crystalline admixtures and super absorbent polymers (SAPs)," *Construction and Building Materials*, vol. 189, pp. 1054-1066, 2018.

[9] A. S. Buller, F. U. R. Abro, K.-M. Lee, and S. Y. Jang, "Mechanical recovery of cracked fiber-reinforced mortar incorporating crystalline admixture, expansive agent, and geomaterial," *Advances in Materials Science and Engineering*, vol. 2019, 2019.

[10] G. Hong and S. Choi, "Rapid self-sealing of cracks in cementitious materials incorporating superabsorbent polymers," *Construction and Building Materials*, vol. 143, pp. 366-375, 2017.

[11] H. Deng and G. Liao, "Assessment of influence of self-healing behavior on water permeability and mechanical performance of ECC incorporating superabsorbent polymer (SAP) particles," *Construction and Building Materials*, vol. 170, pp. 455-465, 2018.

[12] D. Li, B. Chen, X. Chen, B. Fu, H. Wei, and X. Xiang, "Synergetic effect of superabsorbent polymer (SAP) and crystalline admixture (CA) on mortar macro-crack healing," *Construction and Building Materials*, vol. 247, 2020.

[13] G. Hong, C. Song, and S. Choi, "Autogenous healing of early-age cracks in cementitious materials by superabsorbent polymers," *Materials*, vol. 13, no. 3, 2020.

[14] T. Van Mullem et al., "Addressing the need for standardisation of test methods for self-healing concrete: an inter-laboratory study on concrete with macrocapsules," *Science and Technology of Advanced Materials*, vol. 21, no. 1, pp. 661-682, 2020/01/31 2020.

[15] X. Wang, C. Fang, D. Li, N. Han, and F. Xing, "A self-healing cementitious composite with mineral admixtures and built-in carbonate," *Cement and Concrete Composites*, vol. 92, pp. 216-229, 2018.

[16] T. S. Qureshi and A. Al-Tabbaa, "Self-healing of drying shrinkage cracks in cement-based materials incorporating reactive MgO," *Smart Material and Structures*, vol. 25, p. 16 pages, 2016.

[17] R. Alghamri and A. Al-Tabbaa, "Self-healing of cracks in mortars using novel PVA-coated pellets of different expansive agents," *Construction and Building Materials*, vol. 254, 2020.

[18] G. Li, S. Liu, M. Niu, Q. Liu, X. Yang, and M. Deng, "Effect of granulated blast furnace slag on the self-healing capability of mortar incorporating crystalline admixture," *Construction and Building Materials*, vol. 239, 2020.

[19] V. Picandet, A. Khelidj, and H. Bellegou, "Crack effects on gas and water permeability of concretes," *Cement and Concrete Research*, vol. 39, pp. 537-547, 2009.

[20] L. Mengel, H.-W. Krauss, and D. Lowke, "Water transport through cracks in plain and reinforced concrete – Influencing factors and open questions," *Construction and Building Materials*, vol. 254, 2020.

[21] T. Van Mullem, E. Gruyaert, B. Debbaut, R. Caspeele, and N. De Belie, "Novel active crack width control technique to reduce the variation on water permeability results for self-healing concrete," *Construction and Building Materials*, vol. 203, pp. 541-551, 2019.

[22] K. Van Tittelboom, N. De Belie, D. Van Loo, and P. Jacobs, "Self-healing efficiency of cementitious materials containing tubular capsules filled with healing agent," *Cement and Concrete Composites*, vol. 33, pp. 497-505, 2011.

[23] D. Palin, Y. Mo, V. Wiktor, and H. M. Jonkers, "An Improved Test for Generating Rapid, Accurate, and Reliable Crack Permeability Data for Cementitious Materials," *International Journal of Civil Engineering*, vol. 17, no. 5, pp. 645-652, 2019.

[24] H. X. D. Lee, H. S. Wong, and N. R. Buenfeld, "Self-sealing of cracks in concrete using superabsorbent polymers," *Cement and Concrete Research*, vol. 79, pp. 194-208, 2016.

[25] P. Azarsa, R. Gupta, and A. Biparva, "Assessment of self-healing and durability parameters of concretes incorporating crystalline admixtures and Portland Limestone Cement," *Cement and Concrete Composites*, vol. 99, pp. 17-31, 2019.

[26] D. Snoeck, K. Van Tittelboom, S. Steuperaert, P. Dubruel, and N. De Belie, "Self-healing cementitious materials by the combination of microfibres and superabsorbent polymers," *Journal of Intelligent Material Systems and Structures*, vol. 25, no. 1, pp. 13-24, 2014.

[27] E. Gruyaert et al., "Self-healing mortar with pH-sensitive superabsorbent polymers: testing of the sealing efficiency by water flow tests," *Smart Material and Structures*, vol. 25, p. 11 pages, 2016.

[28] C. Desmettre and J.-P. Charron, "Novel water permeability device for reinforced concrete under load," *Materials and Structures*, vol. 44, pp. 1713-1723, 2011.

[29] C. Desmettre and J.-P. Charron, "Water permeability of reinforced concrete with and without fiber subjected to static and constant tensile loading," *Cement and Concrete Research*, vol. 42, pp. 945-952, 2012.

[30] C. Desmettre and J.-P. Charron, "Water permeability of reinforced concrete subjected to cyclic tensile loading," *ACI Materials Journal*, vol. 110, no. 1, pp. 79-88, 2013.

[31] D. Breysse and B. Gérard, "Transport of fluids in cracked media," in "Report 16 - Penetration and permeability of concrete: barriers toorganic and contamining liquids," RILEM, Stuttgart1997, vol. 16.

[32] J.-P. Charron, E. Denarié, and E. Bühwiler, "Permeability of ultra high performance fiber reinforced concretes (UHPFRC) under high stresses," Materials and Structures, vol. 40, pp. 269-277, 2007.

[33] B. Gérard, D. Breysse, A. Ammouche, O. Houdusse, and O. Didry, "Cracking and permeability of concrete under tension," *Materials and Structures*, vol. 29, no. 187, pp. 141-151, 1996.

[34] J. Rapoport, C.-M. Aldea, S. P. Shah, B. Ankenman, and A. Karr, "Permeability of cracked steel fiber-reinforced concrete," *Journal of Materials in Civil Engineering*, vol. 14, no. 4, pp. 355-358, 2002.

[35] C.-M. Aldea, S. P. Shah, and A. Karr, "Effect of cracking on water and chloride permeability of concrete," *Journal of Materials in Civil Engineering*, vol. 11, no. 3, pp. 181-187, 1999.

[36] G. Rastiello, "Influence de la fissuration sur le transfert de fluides dans les structures en béton: stratégies de modélisation probabiliste et étude expérimentale," Université Paris-Est, 2013PEST1036, 2013.

[37] A. Kermani, "Permeability of stressed concrete," *Building Research and Information*, vol. 19, no. 6, pp. 360-366, 1991.

[38] K. J. Shin, W. Bae, S.-W. Choi, M. W. Son, and K. M. Lee, "Parameters influencing water permeability coefficient of cracked concrete specimens," *Construction and Building Materials*, vol. 151, pp. 907-915, 2017.

[39] Z. Jiang, W. Li, and Z. Yuan, "Influence of mineral additives and environmental conditions on the self-healing capabilities of cementitious materials," *Cement and Concrete Research*, vol. 57, pp. 116-127, 2015.

[40] L. Ferrara, V. Krelani, and M. Carsana, "A "fracture testing" based approach to assess crack healing of concrete with and without crystalline admixtures," *Construction and Building Materials*, vol. 68, pp. 535-551, 2014.

[41] R. Gagné and M. Argouges, "A study of the natural self-healing of mortars using air-flow measurements," *Materials and Structures*, vol. 45, pp. 1625-1638, 2012.

[42] M. Roig-Flores, F. Pirritano, P. Serna, and L. Ferrara, "Effect of crystalline admixtures on the self-healing capability of early-age concrete studied by means of permeability and crack closing tests," *Construction and Building Materials*, vol. 114, pp. 447-457, 2016.

[43] L. Ferrara, V. Krelani, and F. Moretti, "Autogenous healing on the recovery of mechanical performance of High Performance Fibre Reinforced Cementitious Composites (HPFRCCs): Part 2 - Correlation between healing of mechanical performance and crack sealing," *Cement and Concrete Composites*, vol. 73, pp. 299-315, 2016.

[44] E. Cuenca, A. Tejedor, and L. Ferrara, "A methodology to assess crack-sealing effectiveness of crystalline admixtures under repeated cracking-healing cycles*," Construction and Building Materials*, vol. 179, pp. 619-632, 2018.

CHAPTER 5

ARTICLE 2: SELF-HEALING OF CONCRETE CONTAINING DIFFERENT ADMIXTURES UNDER LABORATORY AND OUTDOOR EXPOSITIONS – PART 1: WATER PERMEABILITY

Kim-Séang LAUCH, Clélia DESMETTRE, Jean-Philippe CHARRON

Department of Civil, Geological and Mining Engineering, Polytechnique Montreal

Corresponding Author:

Jean-Philippe CHARRON

Department of Civil, Geological and Mining Engineering

Polytechnique Montreal

B.O. Box 6079, Station Centre-Ville

Montreal, Qc, Canada H3C 3A7

Phone: 1-514-340-4711 ext 3433

Fax: 1-514-340-5881

Email: jean-philippe.charron@polymtl.ca

5.1 Abstract

This project assessed the self-healing capacity of fibre reinforced concretes containing different admixtures (crystalline admixture CA, expansive agent CSA and superabsorbent polymer SAP) and submitted to different exposure conditions (water immersion, wet/dry cycles and ambient air in laboratory for 3 months, water flow for 1 week and outside for 1 year). Prisms were pre-cracked at 28 days by means of a 3-point bending test and self-healing was evaluated through water permeability test, mechanical recovery, macro- and microscopic analyses. This paper (part 1) focuses on the permeability measures. The results showed different self-healing kinetics, self-healing capacity and microstructure according to the mix, but especially to the exposition. The average final Healing Ratios reached 84% in water, 93% in wet/dry cycles and 71% in water flow and outside. These performances are explained via different densities and types of healing products found in each exposition (ettringite and calcite in water, calcite and vaterite in wet/dry, aragonite under water flow and larger calcite crystals outdoor). The best self-healing performance was obtained with CA and SAP mixes. No synergetic effect was found when combining CA+CSA and CA+SAP.

Keywords: self-healing, crystalline admixture, expansive agent, superabsorbent polymer, water permeability, outdoor, wet/dry

5.2 Introduction

Cracks found in reinforced concrete structures accelerate the penetration of aggressive agents (CO_2, chlorides, sulfates…) and hence reduce the durability of the structures. This led to an exponentially increase of research about self-healing of cracked concrete in the last decade. It is now generally agreed that autogenous healing, the intrinsic self-healing capacity of concrete is only efficient to completely heal small cracks (10 – 100 μm) and is not a reliable phenomenon [1]. That is why a wide range of self-healing approaches have been developed, either stimulated autogenous (such as the use fibres, mineral admixtures, superabsorbent polymer…) or autonomous (bacteria, encapsulated chemicals) self-healing processes, but none seems to prevail yet, as reviewed and discussed in previous state-of-the-art papers [1-3]. Even if few large- and full-scale projects

integrating self-healing concrete have been implemented by different research groups from the UK [4], Belgium [5-7], The Netherlands [8] and China [9], this research area is still not mature yet.

The use of admixtures such as crystalline admixture (CA), expansive agent (CSA) and superabsorbent polymer (SAP) for improving self-healing has been more investigated because of their ease of implementation (products available and used in the construction industry) and lower costs in comparison to other self-healing approaches.

Use of CA enhanced and accelerated self-healing in some studies [10-14], while others reported no significant beneficial effect of CA compared to a control mix [15-18]. And although studies agree that contact with water is required for an efficient self-healing of concrete containing CA [10, 11, 15, 19], as also observed for concrete without admixtures, the optimal exposure does not make consensus either. Some found higher self-healing under water immersion than under wet/dry cycles [15, 19], while others found the opposite [12]. Different reasons can explain this lack of consensus. First, a wide range of materials stand under the commercial label "crystalline admixtures" [1]. Secondly, the studied crack widths (generally between 10 μm to 400 μm), age of pre-cracking, mixture composition, healing conditions (exposure and duration) and techniques for healing measurement differ from one study to another.

Different types of expansive agents (CSA-based, CaO-based and MgO-based) to improve self-healing were also investigated. The use of CSA, besides enhancing the self-healing capacity of concrete [12, 13, 20, 21], also presented a synergy when combined with CA [12, 13]. Other studies examined CSA in combination with other additives (CA, sodium carbonate, $CaHPO_4 \cdot 2H_2O$, bentonite), but without studying the effect of CSA alone, and obtained improved healing in comparison to the control mix [22-24].

Besides, there has been growing interest for improving self-healing with superabsorbent polymer (SAP) [25-29]. SAPs are natural or synthetic cross-linked polymers with a high capacity to absorb fluid and have a threefold action in concrete: crack mitigation, immediate self-sealing and promotion of self-healing even in dry environments in playing the role of water reservoirs [1]. Many studies demonstrated the beneficial effect of SAP for self-healing in different laboratory expositions, such as water immersion [30], wet/dry cycles [26, 30] and humid chamber [25, 26] or its rapid self-sealing effect under continuous water flow [31-33]. Moreover, acceleration of self-healing was reported

when adding SAP to other admixtures (citric acid [32] or CA+CSA [22]) and Park & Choi [22] observed more healing products around the SAP particles. Usually, the bigger the size of SAP and the higher the dosage are, the better the self-healing capacity is. However, limited dosage of SAP is necessary to not drastically impact the mechanical strength.

Based on the potential synergetic effect of combining CA with CSA and also considering the effect of SAP to promote healing in dry environment, it was decided to study the impact of combining CA+CSA and CA+SAP, alongside the admixtures alone (CSA, CA and SAP).

In addition to the effect of the self-healing agents, the exposure condition has also a strong impact on the self-healing efficiency of concrete [12, 15, 19]. Most studies investigated laboratory healing conditions such as water immersion, water flow, wet/dry cycles, climate chamber, but few examined the self-healing capacity of concrete in realistic outdoor exposure. While self-healing approaches can be promising in controlled laboratory conditions, they may not be as efficient under long-term outdoor expositions, involving a wide and random range of temperatures and precipitations. Self-healing of specimens exposed in outdoor condition for 1 to 2 years, assessed by surface crack closure and mechanical recovery, was demonstrated by [10, 19, 34]. They found improved healing when incorporating CA in comparison to a control mix. However, no evaluation durability recovery has been determined in a long-term outdoor condition yet.

Hence, this project aims to evaluate the self-healing capacity of concretes containing crystalline admixture (CA), expansive agent (CSA), superabsorbent polymer (SAP) and the combinations CA+CSA and CA+SAP, exposed in several laboratory and long-term outdoor conditions. The self-healing performance was assessed with a new water permeability set-up [35] that enables to measure water permeability through a single flexural macrocrack on the same prisms that will be reloaded by 3-point bending test to evaluate the mechanical recovery. This paper (part 1) focuses on the water permeability results and examines the influence of the healing expositions and the self-healing agents. Comparisons between still water immersion and water flow, as well as accelerated wet/dry cycles and the outdoor exposure are discussed. Microscopic observations of the healed crack and the healing products bring further illustrations and explanations. The results of the mechanical tests as well as a global discussion between the water permeability, mechanical regain and microscopic analyses are the subject of the companion paper (part 2) [36].

5.3 Experimental program

5.3.1 Materials and characterisation tests

A fibre reinforced concrete (FRC) containing a blended General Use Portland cement with 8% by mass of silica fume (type GUb-SF), with a water to binder ratio of 0.43 and 0.75% in volume of hooked-end steel macrofibres (l_f = 35 mm and φ_f = 0.55 mm) was used in this project. Six FRC mixes were produced: a control mix, one with a calcium sulfoaluminate-based expansive agent (CSA), one with a crystalline admixture (CA), one with a superabsorbent polymer (SAP), one with the combination of CA+SAP, and one with the combination of CA+CSA. Compositions of mixes as well as the results of their characterisation tests at fresh and hardened states are shown in **Table 5.1**. The admixtures were added in proportion to the binder mass. Dosages of 3.33% for CSA (Power Denka CSA), 2% for CA (Penetron Admix) and 0.5% for SAP (from BASF) were recommended by the manufacturers. The SAP used is a cross-linked polyacrylamide with a nominal size particle of 100 μm. Its absorption capacity, measured with the tea-bag method [37], was 310 g of deionised water, 188 g of tap water and 38 g of cement filtrate by 1 g of SAP. These results are very similar to the SAP A used by Snoeck et al. [38]. Additional mortars containing 0.5% by mass of cement of SAP were also made in adjusting either the amount of water or superplasticiser (SP) to reach the same flow as a control mortar. Based on the compressive results, it was decided to adapt the SP amount instead of the water amount in the SAP concrete mix to compare mixes with similar mechanical performance.

The dosages of the superplasticizer and viscosity agent were adjusted in the FRC mixes to reach a similar flow around 500 mm (**Table 5.1**). The SAP and CA+SAP mixes required 3 times more superplasticizer than the others, as the SAP particles absorbed water. The slump flow of the CA+SAP was kept a little lower (330 mm) to avoid the addition of too much superplasticizer in comparison to the other mixes. The air content of the mixes containing SAP was also a little higher although in the expecting range (below 3%). The 28-days compressive strength and Young's modulus presented in **Table 5.1** were determined on cylinders (φ100 mm x 200 mm), in accordance with ASTM C39 and ASTM C469 respectively. They were quite similar for all mixes although slightly lower values were obtained for the mixes with SAP, probably due to weak zones introduced by SAP particles.

Table 5.1. Compositions and properties of the FRC mixes

Material	Control	CSA	CA	SAP	CA+SAP	CA+CSA
Cement type GUb-SF (kg/m³)	550	550	550	550	550	550
CSA (kg/m³)	-	18.3	-	-	-	18.3
CA (kg/m³)	-	-	11	-	11	11
SAP (kg/m³)	-	-	-	2.75	2.75	-
Water (kg/m³)	237	237	237	237	237	237
Superplasticizer (l/m³)	10.0	10.0	10.5	30.0	30.0	10.5
Viscosity agent (l/m³)	0.70	0.85	0.71	0.70	0.70	0.85
Sand (kg/m³)	779	771	773	767	761	765
Coarse aggregates (kg/m³)	631	624	626	620	616	619
Steel fibre (kg/m³)	58.5	58.5	58.5	58.5	58.5	58.5
Slump flow (mm)	530	583	503	443	330	595
Air content (%)	1.9	1.6	2.0	2.7	3.0	1.7
Density (kg/m³)	2326	2334	2316	2285	2268	2329
Comp strength (MPa)	61.3	64.9	60.3	58	54.2	59.6
Young's modulus (MPa)	33100	33200	31700	29000	27500	32500

Two batches of each concrete mix were produced. The first batch was made for the specimens intended for the long-term outdoor exposure, while the second one aimed to produce the specimens intended for the indoor exposure.

5.3.2 Methodology to assess self-healing

5.3.2.1 General methodology

The overview of the general methodology of this project is illustrated in **Figure 5.1**. The specimens consisted in prisms of 75 mm x 125 mm x 450 mm. They were demoulded 24h after casting and then cured under lime-saturated water for 28 days to prevent any leaching. The specimens from different mixes were kept in separated containers. Prisms were notched at mid-span (20 mm deep) and then pre-cracked by means of a 3-point bending test according to EN 14651 at the age of 28 days. The targeted residual crack width was 0.25 – 0.30 mm at the notch root, corresponding to the crack width limits from the Canadian standards CSA A23.3 and CSA S6.
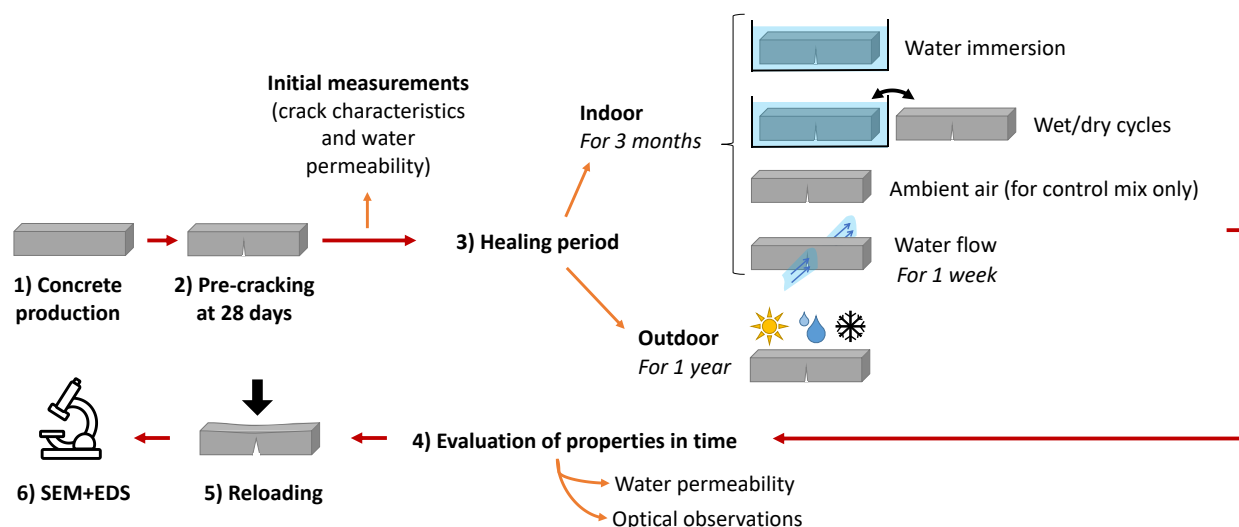
Figure 5.1. Overview of the general methodology of this project

After pre-cracking, initial measurements were made: crack length measured manually, crack widths evaluated with a digital microscope at four equidistant points along the crack length, approximate crack area calculated as the sum of trapezoids and a triangle [35] and initial water permeabiliy coefficient K_{wi} determined. The specimens were then submitted to different exposure conditions that will be described in **Section 5.3.2.2**.

The evolution of the healing process was evaluated through different properties and observations. The main parameter was the water permeability measured at different times. Besides, pictures of the cracks at the same four equidistant points were taken with a digital microscope at the same times for qualitative observations of the evolution of the surface self-healing. At the end of the healing period, all prisms were reloaded until failure via the same 3-point bending test to determine mechanical regain brought by the healing process. The mechanical response of the healed prisms and reference uncracked prisms is discussed in the companion paper (part 2) [36].

Finally, after failure, some prisms were cut to analyse the fractured surface of the crack with an environmental scanning electron microscope (SEM) and energy-dispersive X-ray analysis (EDS) to identify the healing products. The specimens were kept in a vacuum bell jar before the microscopic observations to prevent any carbonation. Crystals formed at the crack surface were also scratched with a scalpel, forming a powder that was also analysed by SEM-EDS.

5.3.2.2   Healing conditions

Several exposure conditions were studied to examine their influence on the self-healing performance of the six FRC mixes (**Figure 5.1**).

The indoor expositions were the following:

1) Water immersion for 3 months: in containers with lime-saturated tap water at 21 ± 3 °C without changing the water. This simulates submerged concrete elements and is often considered the most favourable exposition for self-healing.

2) Wet/dry cycles for 3 months: alternatively in containers in water immersion for 3.5 days and then in ambient air at 21 ± 3 °C and $45 \pm 10\%$ relative humidity for 3.5 days. This simulates concrete elements subjected to splash or water level variation. This also represents an accelerated condition of the long-term outdoor exposition.

3) Ambient air (only for the control mix) for 3 months: at 21 ± 3 °C and $45 \pm 10\%$ relative humidity. This simulates concrete elements protected from rain. As it is considered to be the least favourable condition for self-healing, this is the reference condition of no or low healing.

4) Water flow for 1 week: continuous water flow through the crack at a pressure gradient of 30 kPa. At the end of the testing week, the specimens were kept in ambient air until reloading at the same time of the other indoor specimens (after 3 months of exposure). This exposure condition simulates cracks in water-retaining structures (reservoirs, dams) and is considered to be an accelerated condition of water immersion.

For the outdoor condition, after their initial wet curing of 28 days, the specimens were kept indoor for an additional 28 days at ambient air. Then, the specimens were placed outside for 1 year, from March 2019 (**Figure 5.2**) to March 2020. During this period, the temperatures in Montreal ranged from -22.1 to 33.1 °C, the precipitations ranged from 43.7 to 261.2 mm/month and the snow on ground ranged between 0 and 90 cm.

Figure 5.2. Specimens placed outside in March 2019 in Montreal

In total, 124 prisms were produced and tested in this experimental program. **Table 5.2** summarises the number of specimens placed in each exposition. First, for the control mix only, prisms were exposed to ambient air exposure as reference cracked specimens with no or few healing. Second, for all expositions except the water flow, two additional reference uncracked specimens were subjected to the same exposure condition. They were then pre-cracked and reloaded at the end of the healing period. Ferrara et al. [39] highlighted the need to have companion undamaged specimens that are subjected to the same curing history to discriminate between healing and natural aging of concrete mechanical properties.

Table 5.2. Number of specimens for each healing condition

Exposure conditions	Control	CSA	CA	SAP	CA+SAP	CA+CSA
Water immersion	$5 + 2^{\#}$	$4 + 2^{\#}$	$5 + 2^{\#}$	$5 + 2^{\#}$	$4 + 2^{\#}$	$5 + 2^{\#}$
Wet/dry cycles	$4 + 2^{\#}$	$4 + 2^{\#}$	$4 + 2^{\#}$	$4 + 2^{\#}$	$4 + 2^{\#}$	$4 + 2^{\#}$
Ambient air	$2^{*} + 2^{\#}$	-	-	-	-	-
Water flow	1	1	1	1	1	1
Outdoor	$4 + 2^{\#}$	$4 + 2^{\#}$	$4 + 2^{\#}$	$4 + 2^{\#}$	$4 + 2^{\#}$	$4 + 2^{\#}$

*Reference cracked specimens kept in ambient air
#Reference uncracked specimens subjected to the same exposition

5.3.3 Water permeability measurements

The concept and advantages of the water permeability set-up used in this project (**Figure 5.3**) were previously detailed in [35]. It allows a unidirectional flow from the inlet tank under pressure, through the flexural cracked specimen and to the outlet tank. The ingoing and outgoing water flows as well as the real time pressure gradient are continuously recorded. These parameters (flow and pressure gradient) are then used to calculate the permeability coefficient K_w (m/s) according to Darcy's law (**Eq. 5.1**). In this equation, Q (m³/s) is the measured flow rate, A (m²) represents the cross-section exposed to the flow and $\Delta h/L$ is the applied pressure gradient.

$$Q = K_w \, A \, \frac{\Delta h}{L}$$

(5.1)

For the indoor prisms (except for the continuous water flow exposure), water permeability was measured at 0, 11, 25, 53 and 81 days after pre-cracking. For the outdoor prisms, the same number of measurements were performed but at 0, 3, 6, 9 and 12 months of exposure. Each measurement lasted for 5 minutes with an applied pressure gradient of 30 kPa, corresponding to a 3-meter water depth. This pressure level was selected after having studied the influence of different pressure gradients on the permeability results [35]. For the continuous water flow exposure, the flow through the pre-cracked specimen was continuously recorded during around 1 week in maintaining the same pressure gradient of 30 kPa.
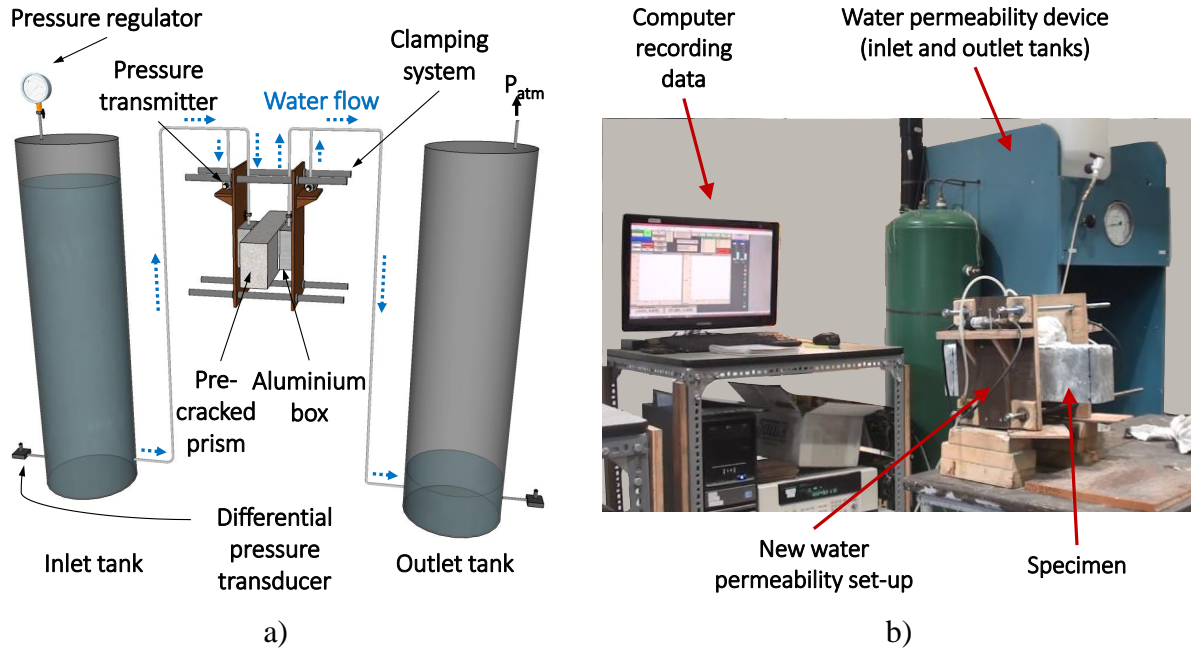
Figure 5.3. a) Illustration and b) picture of the new water permeability set-up

5.4 Results

5.4.1 Initial characterisation of the pre-cracked specimens (before healing)

After pre-cracking, the maximum flexural stress σ_{max}, the average crack width w_i at the notch root, the crack area A_i and the initial water permeability coefficient K_{wi} were determined for each prism. **Figure 5.4** presents the average results and standard deviations of the σ_{max} and w_i values (**Figure 5.4a**) and of the A_i and K_{wi} values (**Figure 5.4b**), for the indoor specimens. Specimens kept in outdoor conditions presented similar trends. Overall, lower flexural stresses led to larger crack width and area, and thus to a higher permeability coefficient. For example, CA mix had the lowest stress (7 MPa), the largest crack width (0.35 mm) and area (16.1 mm²) and the highest K_{wi} (1.0×10^{-5} m/s). These trends are logical because a lower flexural strength means a lower action of the fibres and thus a less efficient cracking control, resulting in a larger crack and higher K_{wi}. As the compressive strength of all mixes were quite similar (**Table 5.1**), their differences of flexural performance may mainly be explained by the variation of the orientation and/or density of fibres at the crack location in the mixes. This aspect is addressed in the companion paper [36].

The coefficients of variations (COV) of σ_{max} ranged from 13% to 20% depending on the mix. The COV of the surface crack characteristics (width and area) ranged from 13% to 30%, which induced COV variations from 40% to 105% for the initial permeability coefficient. This higher COV for K_{wi} is logical as the permeability is more sensitive to cracking for several reasons [35]. First, permeability is proportional to the cube of crack width [40]. Moreover, permeability takes into account the whole crack volume in comparison to surface cracking characterisation. For example, although the average crack areas of the control and CA+CSA mixes were similar (10.4 and 10.2 mm² respectively), their average permeability coefficients were greatly different. K_{wi} of CA+CSA mix was 30% higher than for the control mix (3.3×10^{-6} and 2.6×10^{-6} m/s respectively).

Due to the inherent variability of concrete and the fibres distribution, the residual crack widths obtained for all mixes varied between 0.15 and 0.45 mm, with an average crack width of 0.29 mm and the associated value of K_{wi} varied from 6.5×10^{-8} to 1.6×10^{-5} m/s with an average of 4.7×10^{-6} m/s. As reported by [39], variation of the residual crack width occurs in identical specimens loaded to the same crack width in a crack-width controlled test set-up, and this has been confirmed in a recent round robin test (RRT) concerning pre-cracking by means of a 3-point bending test [41].

a)   b)
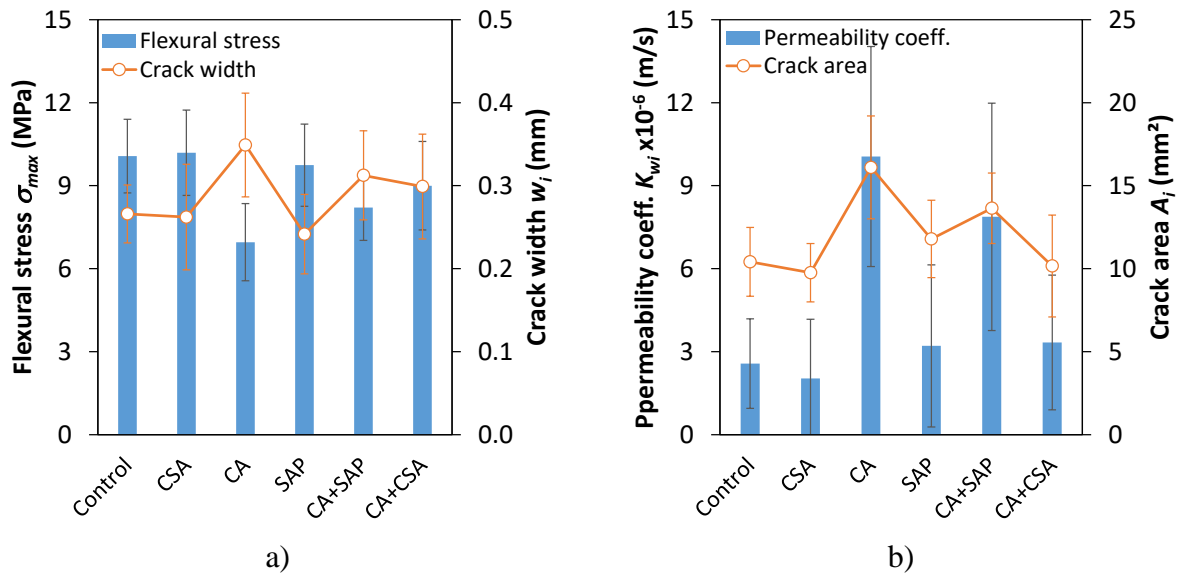
Figure 5.4. Initial results (indoor): a) flexural stress σ_{max} and initial crack width w_i, b) initial permeability coefficient K_{wi} and initial crack area A_i

5.4.2 Evaluation of self-healing through water permeability measurements

5.4.2.1 Introduction to the analysis of the results

As mentioned in **Section 5.3.3**, the water flow Q through the crack is recorded during the permeability test. This allows to calculate K_w according to Darcy's law (**Eq. 5.1**). **Figure 5.5** presents an example of the evolution of K_w for some control specimens under water immersion. Although these results represent the flow through the cracks, the large range of K_{wi} makes the comparison of the self-healing performance between mixes difficult. Hence, other methods can also be used to analyse the results.
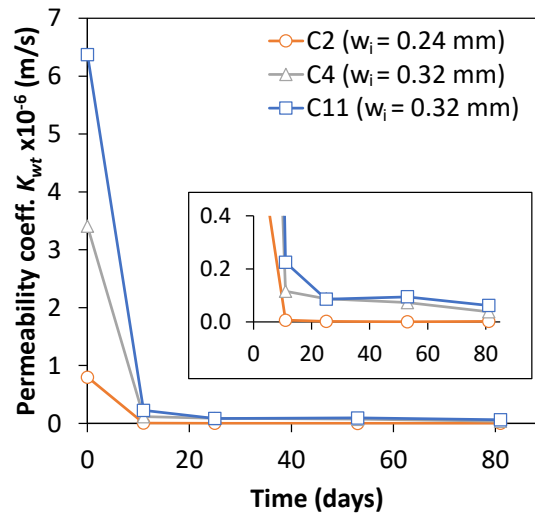
Figure 5.5. Example of evolution of Kw for some control specimens under water immersion

In many studies, analysis of results is done with relative flows or permeabilities (Q_t/Q_i or K_{wt}/K_{wi}), or with a Healing Ratio HR ($1–Q_t/Q_i$ or $1–K_{wt}/K_{wi}$). In this project, the Healing Ratio was calculated with **Eq. 5.2**, considering the permeability coefficient at a time t (K_{wt}) related to the initial permeability coefficient (K_{wi}).

$$HR_t \ (\%) = 1 - \frac{K_{wt}}{K_{wi}} \ . \ 100 \tag{5.2}$$

Figure 5.6a illustrates an example of the evolution of HR for the control specimens presented in **Figure 5.5**. This type of results has the advantage to point out the healing performance of each specimen, compared to their initial state (K_{wi}). Relative results or Healing Ratios are largely used

in literature [16, 18, 23, 32, 33, 42] and allow comparison with the results of this project. However, it may be more difficult to compare different specimens and conditions because of the dependence on the K_{wi}. A specimen with a low K_{wi} will obviously lead to high *HR* and vice versa. Based only on Healing Ratios, one might say that specimen C2 performed the best (*HR* = 99%). But this high *HR* may be partially explained by the low $K_{wi} = 8 \times 10^{-7}$ m/s of specimen C2 compared to the others.

Therefore, a second method consisting in determining equivalent crack widths (w_{eq}) was also used. This method is based on Poiseuille's law that describes the flow through a crack into concrete, multiplied by a reduction factor ζ (**Eq. 5.3**), which is an inherent parameter of each crack, taking into account its roughness and tortuosity [40]. In this equation, Δp (Pa) is the pressure gradient, b (m) is the length of the crack, w (m) is the crack width, μ (Pa s) is the dynamic viscosity and d (m) is the flow path length of the crack. From **Eq. 5.3**, the reduction factor ζ was calculated for each specimen based on the initial crack width measured at the notch root and the associated initial $Q_{measured}$. Then, the evolution of w_{eq} in time was determined from the evolution of $Q_{measured}$, assuming a constant value of ζ.

$$Q_{measured} = \zeta \ Q_{Poiseuille} = \zeta \frac{\Delta p \ b \ w^3}{12 \ \mu \ d} \tag{5.3}$$

Other studies also used this methodology to analyse water permeability measures to assess self-healing in concrete with linear cracks [22, 43]. It must be noted that Poiseuille's law describes a flow between two parallel plates, which is not the case of a triangular flexural crack in the prism. However, the measured initial flow was quite proportional to the cube of the initial crack width measured at the prism notch root as illustrated for the control mix in Figure 5.7. Van Mullem et al. [44], who also studied flexural cracks, determined equivalent crack width at the notch root as well. In this present study, ζ varied from 0.008 to 0.042, with an average value of 0.021. This average value is lower to the values of 0.25 and 0.27 found by Edvardsen [40] and Gupta & Biparva [43] respectively on parallel cracks, but is quite in the same order of magnitude than the value of 0.043 obtained by Van Mullem et al. [44] on flexural cracks.

An example of the evolution of w_{eq} with time is illustrated in **Figure 5.6b** for the same control specimens as in **Figure 5.6a**. While K_{wi} ranged from 8×10^{-7} to 6.4×10^{-6} m/s (coefficient of variation COV = 65%), w_{eq} varied from 0.24 to 0.32 mm (COV = 13%). Specimen C2 did not have a similar

w_{eq} to the others, but it can be observed that the healing performance is very similar (curves almost parallel) to the other two specimens. This type of results allows to better compare specimens with different initial permeabilities because of the narrower range of the results compared to K_w and because of the additional information of the initial state ($w_{eq,i}$) compared to *HR*. However, such results are less prevalent in literature and limit comparison with this project.

a)   b)
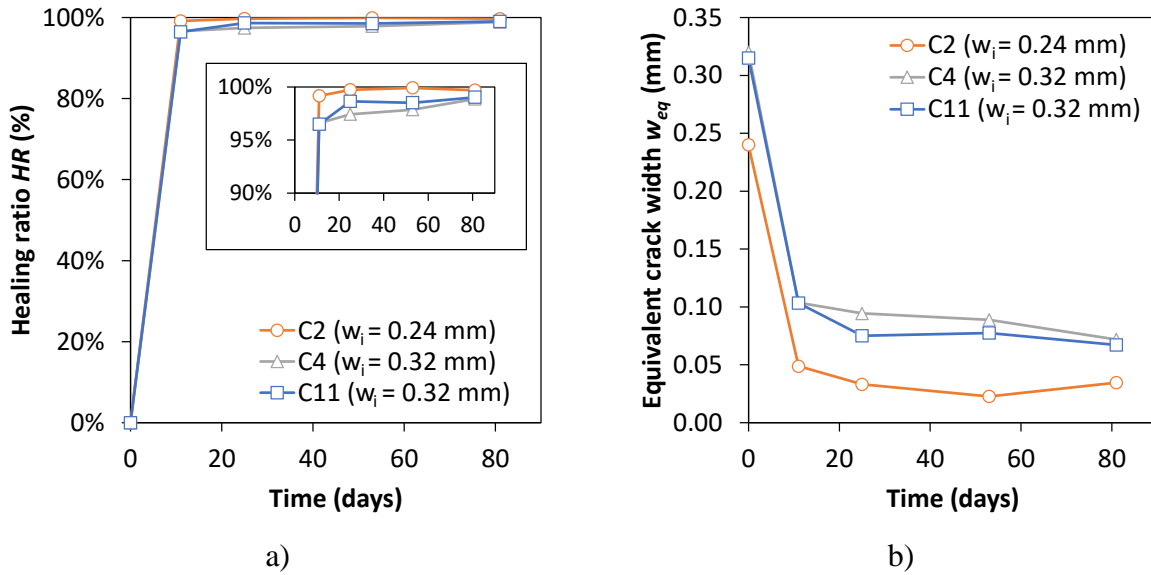
Figure 5.6. Example of evolutions of a) Healing Ratios HR and b) equivalent crack width weq for the same control specimens as **Figure 5.5**
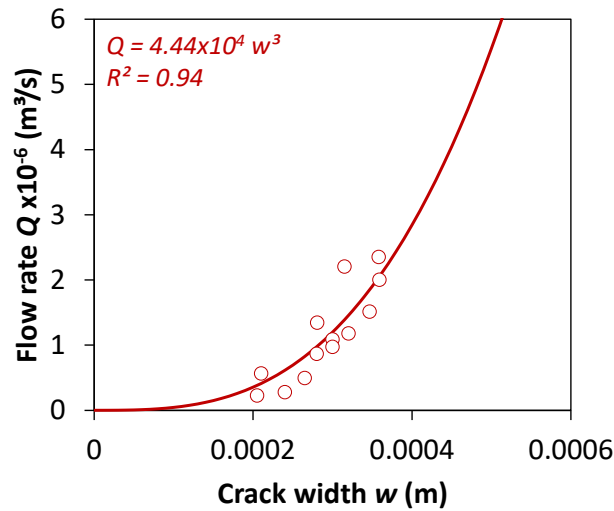
Figure 5.7. Flow rate Q in function of average crack width wi with cubic regression for the control mix

In this paper, the water permeability results will be presented in *HR* for the influence of the exposure condition (**Section 5.4.2.2**), for easier comparison with the literature. Then, the results will be presented in w_{eq} for the influence of the mix composition (**Section 5.4.2.3**), to compare the different mixes in this study. Despite little variation in the results between the different specimens of a same testing condition (**Figure 5.6**), a global trend shown by the average curve is representative of the condition for all mixes. As a consequence, only the average result of each condition will be presented in the next sections.

5.4.2.2   Influence of the exposure condition

Figure 5.8 presents the evolution of the average Healing Ratios (*HR*) of all FRC mixes per exposure condition: water immersion in **Figure 5.8a**, continuous water flow (only one specimen) in **Figure 5.8b**, wet/dry cycles in **Figure 5.8c** and outdoor exposure in **Figure 5.8d**. The cursors in **Figure 5.8b** represent the average *HR* obtained after 11 days of water immersion for sake of comparison and the dotted part of the curves is an extrapolation of the continuous flow measured. Also, as the outdoor self-healing occurred on a longer period, the time scale is in months for this condition instead of days for the indoor expositions.

It must be noted that some curves in **Figure 5.8** sometimes showed a small decrease of *HR* (due to an increase of water permeability) compared to previous measures. This phenomenon was already observed by [21, 22, 30] and could be explained by the fact that the water flow under pressure during the permeability test may pull out some healing products that were not tightly attached or may slightly dissolve some of them [13]. Another possibility is that detached loose particles may have temporary blocked the flow pathway in the previous measurement and overestimate a little the associated healing state at this time.

Table 5.3 summarises the initial HR_i and final HR_f for all mixes and expositions, as well as the ratios HR_i/HR_f and the average of all mixes.
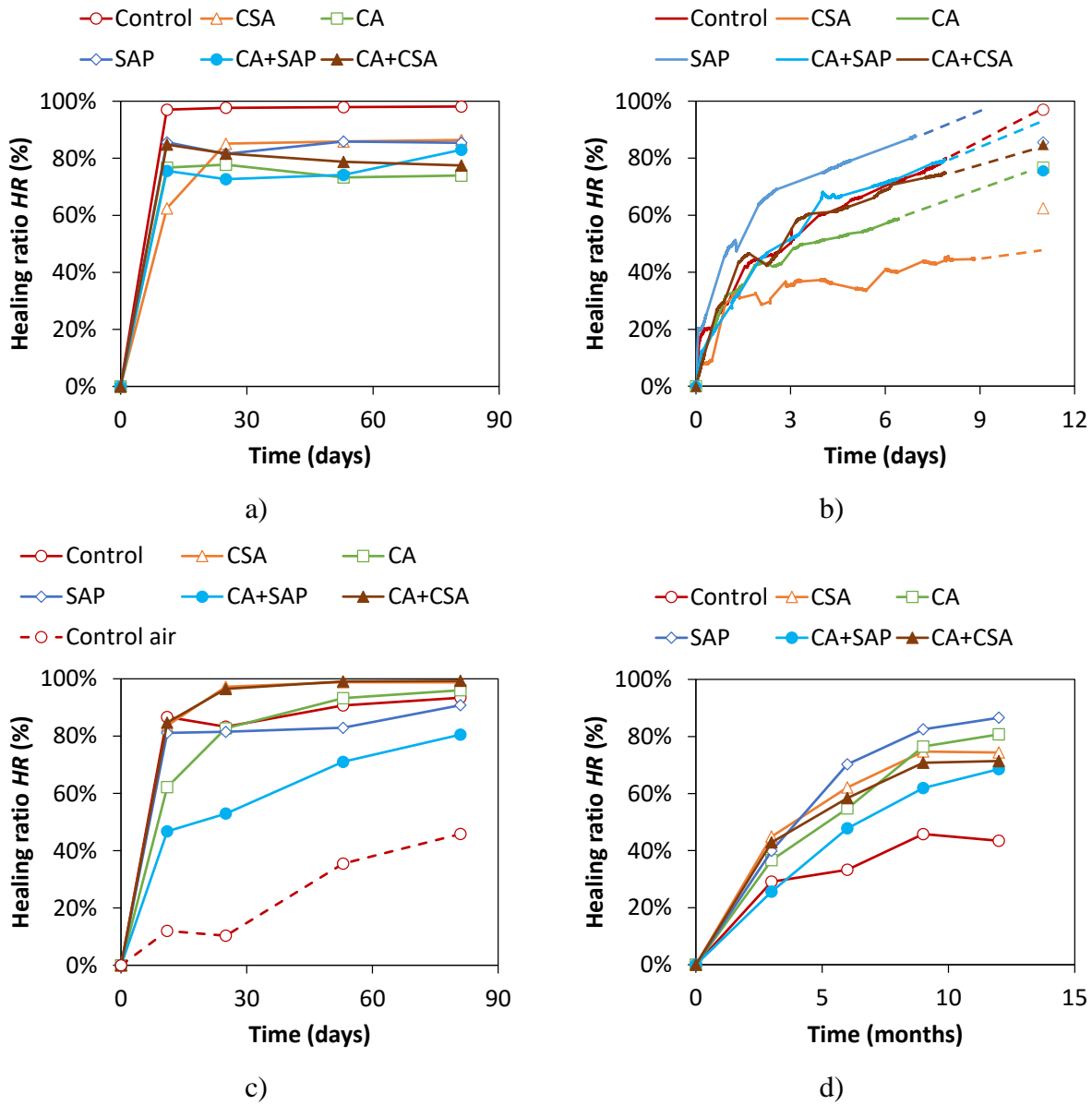
Figure 5.8. Evolution of average Healing Ratios for all the mixes in a) water immersion, b) continuous water flow, c) wet/dry cycles and ambient air for control mix and d) outdoor

Table 5.3. Initial and final average Healing Ratios, ratios HR_i/HR_f for all mixes and expositions and average of all mixes per exposition

Average Healing Ratios	Control	CSA	CA	SAP	CA+SAP	CA+CSA	Avg
Water immersion							
Initial HR_i (11 days)	97%	62%	77%	86%	76%	85%	80%
Final HR_f (81 days)	98%	86%	74%	85%	83%	77%	84%
HR_i/HR_f	99%	72%	104%	100%	91%	109%	96%
Wet/dry cycles							
Initial HR_i (11 days)	87%	84%	62%	81%	47%	85%	74%
Final HR_f (81 days)	93%	99%	96%	91%	80%	99%	93%
HR_i/HR_f	93%	85%	65%	89%	58%	85%	79%
Air							
Initial HR_i (11 days)	12%	-	-	-	-	-	-
Final HR_f (81 days)	46%	-	-	-	-	-	-
HR_i/HR_f	26%	-	-	-	-	-	-
Continuous water flow							
Final HR_f (7-8 days)	80%	45%	60%	88%	79%	75%	71%
Outdoor							
Initial HR_i (3 months)	29%	45%	37%	40%	26%	43%	37%
Final HR_f (12 months)	43%	74%	81%	87%	69%	71%	71%
HR_i/HR_f	67%	60%	45%	46%	37%	60%	53%

From **Figure 5.8**, it can be seen that the exposure condition definitely impacts the self-healing performance of the FRC mixes. The final Healing Ratios were in average 84% after 3 months in water immersion, 93% after 3 months of wet/dry cycles, 71% after 7 days of continuous water flow and 71% after 1 year outdoor (**Table 5.3**).

The evolution of the Healing Ratios for the specimens in water immersion stabilized quickly after the first measurement (**Figure 5.8a**), while the evolution of HR for the specimens in wet/dry cycles was more gradual (**Figure 5.8c**). The initial HR (at 11 days) attained 72% to 109% of their final HR in water immersion (**Table 5.3**), demonstrating an already high healing at the beginning followed by a lower evolution of HR in time. In contrast, the initial HR (at 11 days) in wet/dry cycles reached 58% to 93% of their final HR. This gradual evolution of HR was also observed for the continuous water flow (**Figure 5.8b**) and outdoor conditions (**Figure 5.8d**).

Under continuous water flow exposure, the final *HR* obtained after 1 week were in general lower than after 11 days in water immersion (**Table 5.3**). However, from the extrapolated dashed lines in **Figure 5.8b**, the water flow condition would have reached similar values at 11 days. Exception can be mentioned for SAP and CA+SAP mixes that presented a little improvement of self-healing under continuous water flow and the CSA mix that shows the opposite. As there was only 1 specimen tested under continuous water flow, definite conclusions cannot be drawn between the mixes. Exposing the concrete crack to a continuous water flow under pressure did not seem to accelerate self-healing, in contrast to what was expected. Nevertheless, the continuous water flow test has the advantage to provide the detailed self-healing kinetics at early age (between 0 and 11 days).

The self-healing in outdoor exposure proceeded slower (**Figure 5.8d**). After the first measurement (3 months), the *HR* reached 37% to 67% of their final *HR* (**Table 5.3**). While the control mix performed well in the other expositions, it showed the worst behaviour in real outdoor exposition. Its final *HR* was 43%, while the other mixes reached higher final *HR* (69 to 87%) according to **Table 5.3**. The performance of the control mix outside was very similar to its performance in ambient air for 3 months (final *HR* = 46%) (**Figure 5.8c** and **Table 5.3**). It could be deduced that ambient air condition (21°C and 45% RH) during 3 months may simulate healing of about 1 year in external condition in Montreal for the control mix.

It must be noted that the reason for the better self-healing observed in water for the control mix against all the other mixes is not clear and needs more investigation. On the other hand, the worst self-healing for the control mix in outdoor condition compared to the other mixes could be explained by the lower total amount of cementitious materials as there are no added self-healing agent, which means a lower potential of healing capacity.

As wet/dry cycles could simulate the realistic outdoor exposition in an accelerated way, time equivalence to reach similar self-healing was done between both exposure conditions. **Figure 5.9** illustrates this time equivalence for the CA mix. For this mix, the final Healing Ratio after 25 days in wet/dry cycles corresponds to around 12 months outside. The same analysis was done for all mixes and results are summarised in **Table 5.4**. Although these values are approximate, they provide an estimate of the time equivalence of 25 days of wet/dry cycles and the corresponding time in outdoor condition. These results will be further analysed in the following **Section 5.4.2.3**.
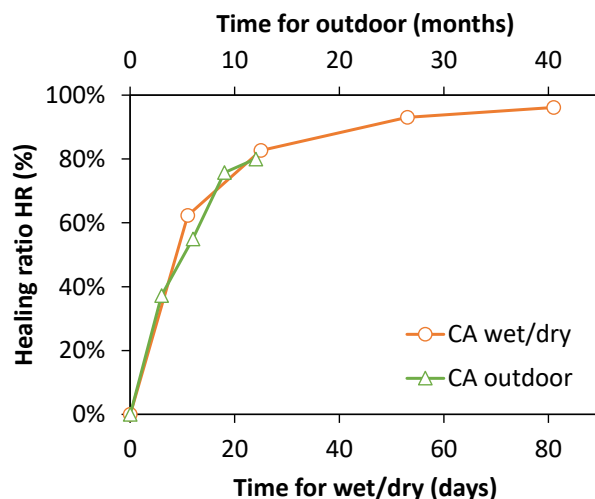
Figure 5.9. Time equivalence between wet/dry and outdoor exposures for CA mix

Table 5.4. Time equivalence between wet/dry and outdoor exposures

Mix	25 days in wet/dry is equivalent to
CA+SAP	5 months outside
CA	12 months outside
SAP	20 months outside
CA+CSA	30 months outside
CSA	40 months outside
Control	50 months outside

5.4.2.3 Influence of the concrete mix composition

Figure 5.10 presents the evolution of the average equivalent crack widths (w_{eq}) of all mixes for water immersion (**Figure 5.10a**), wet/dry (**Figure 5.10b**) and outdoor (**Figure 5.10c**) exposures. The initial w_{eq} at notch root ranged between 0.2 to 0.4 mm for all conditions. One can observe again the self-healing kinetics difference between expositions: a rapid drop and then an almost stagnant phase in water, a more gradual reduction in wet/dry and an lower gradual decrease outside.
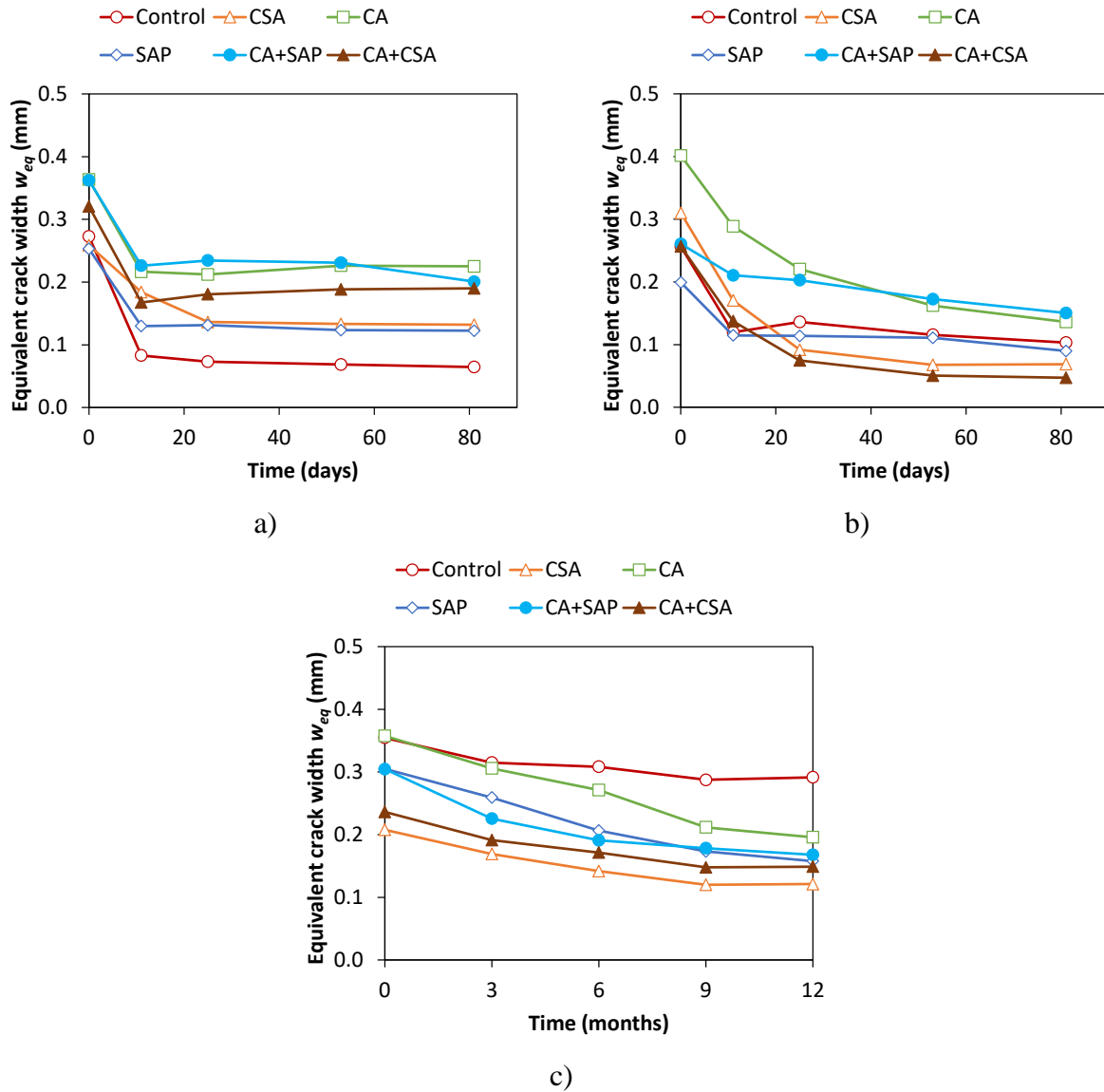
Figure 5.10. Evolution of equivalent crack width for all mixes in a) water immersion, b) wet/dry cycles and c) outdoor exposition

The initial and last slopes of these curves, representing equivalent crack closure rates, were then determined in **Figure 5.11a** and **Figure 5.11b** respectively to compare the self-healing performance of the different mixes. Although the time scale for the outdoor condition is in months in **Figure 5.10c**, all rates were expressed in mm/days in **Figure 5.11** for a better comparison between the indoor and outdoor conditions. It must be noticed that the final closure rates were about 10 times lower than the initial closure rates.

As seen in the previous **Section 5.4.2.2**, the self-healing performances of the mixes varied according to the exposition as well. Under water immersion, the control mix had the highest initial crack closure rate (0.017 mm/days), whereas the CSA mix had the lowest one (0.007 mm/days) (**Figure 5.11a**). Regarding the final slope (between 2 and 3 months exposure), the healing process stabilized for all mixes, except CA+SAP (**Figure 5.11b**). Overall, the control mix showed the highest healing in water immersion with a final equivalent crack closure of 0.21 mm.

Under wet/dry cycles, the CSA and control mixes presented the highest initial crack closure rate (0.013 and 0.012 mm/days respectively), whereas the CA+SAP had the lowest one (0.005 mm/days) (**Figure 5.11a**). Regarding the final slope (**Figure 5.11b**), the crack closure rate was zero or negligible for CSA, CA+CSA and control mixes (≤ 0.0004 mm/days), while the healing process for CA, SAP and CA+SAP mixes increases slightly (0.001 mm/days). Overall, the CA and CSA mixes showed the highest healing in wet/dry cycles with a final equivalent crack closure of 0.27 and 0.24 mm respectively.

Under a real long-term outside exposure, the initial crack closure rate (**Figure 5.11a**) was quite similar for most mixes (around 0.0005 mm/days), except for the CA+SAP mix that presented a much higher closure rate (0.0009 mm/days). Regarding the final slope (between 9 and 12 months of outdoor exposure, **Figure 5.11b**), the equivalent crack closure rates were almost zero for the control, CSA and CA+CSA mixes, whereas the healing process for CA, SAP and CA+SAP mixes slightly continues (0.0002 mm/days), as already observed under wet/dry condition. Overall, the CA, SAP and CA+SAP mixes showed the highest healing in outdoor exposure with a final equivalent crack closure of 0.16, 0.15 and 0.14 mm respectively. **Table 5.4** also illustrates that the real outdoor condition favors the healing of the CA, SAP and CA+SAP mixes in comparison with the other mixes, as it took less months for these mixes to reach the same healing as under 25 days of wet/dry cycles.
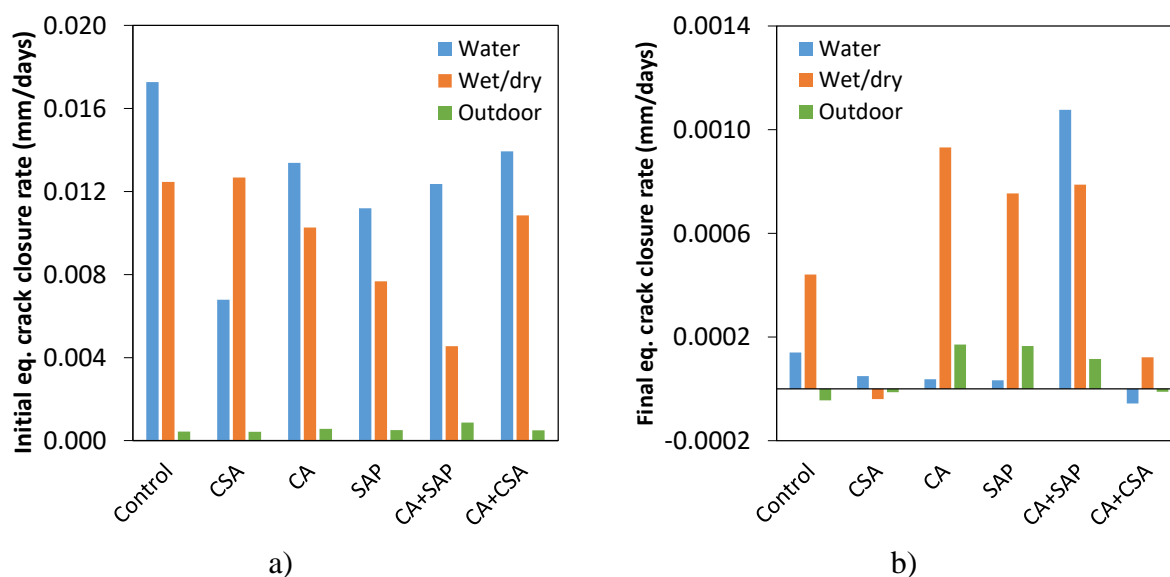
Figure 5.11. a) Initial and b) final equivalent crack closure from the first and last slopes of **Figure 5.10** for all mixes and expositions

5.4.3 Microscopic analyses (SEM-EDS)

The formation of white products was visible through macroscopic pictures as seen in **Figure 5.12** for a crack section of a CSA prism in water immersion. Similar white products were observed for all mixes in all exposure conditions. These macroscopic pictures on healed specimens were only used for qualitative observations, since estimating self-healing based on surface cracks may lead to over- or underestimations of the healing process [35]. This paper focuses on the SEM-EDS analyses that give more detailed information about the nature of the self-healing products.

| Before healing | After 11 days in water | After 3 months in water |
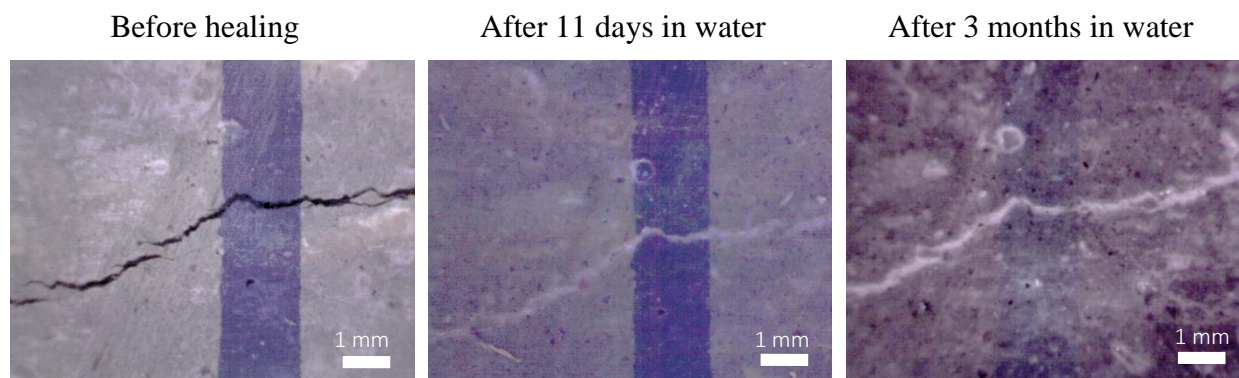
Figure 5.12. Macroscopic pictures of the healing of a crack section for a CSA specimen in water

Figure 5.13 compares SEM pictures of the control mix of a fresh fractured surface before healing (**Figure 5.13a**) and a fractured surface of a crack after healing in water (**Figure 5.13b**). In the first picture, only the concrete matrix was visible, while in the second picture many healing products deposits were observed on the matrix, which clearly demonstrates the healing process.

a)   b)
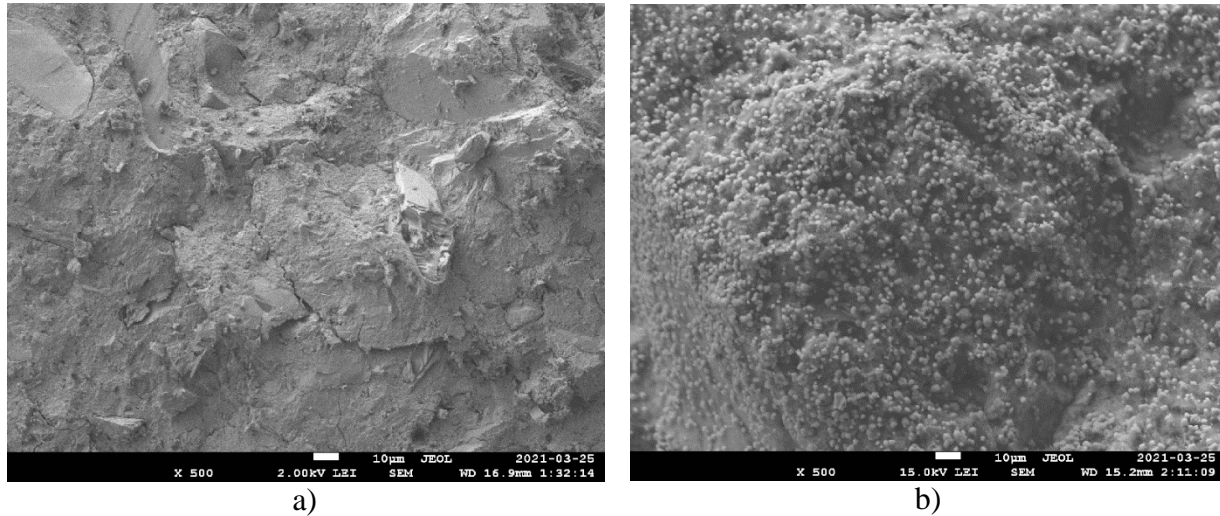
Figure 5.13. SEM pictures of cracks for the control mix a) before healing and b) after healing in water

Microscopic analyses (SEM-EDS) of the healed internal cracks are shown in **Figure** for the control mix in different exposure conditions. The influence of the exposition was clearly visible and the trend was similar for all mixes. In water immersion, most healing products found were calcite (peak of Ca in the first spectrum) and ettringite (peaks of Ca, Si and Al in the second spectrum) as shown in **Figurea**. In the second spectrum, the peak of Si may come from the matrix below the ettringite needles. In wet/dry (**Figureb**), some healing particles were smaller and had less defined shape than in water. As the EDS analysis indicated mainly the presence of calcium, these particles may be calcium carbonate in the form of vaterite, alongside calcite. Overall, the distribution of healing products was denser in wet/dry cycles compared to water immersion.

In outdoor exposure (**Figurec**), large well defined crystals of calcite (according to high peak of Ca) were observed in some zones, whereas other zones were free of healing products. The distribution of the healing products was dense and sometimes less homogeneous than in water or wet/dry exposures. It must be noted that at a macroscopic scale, white products were covering the whole crack surface for water and wet/dry conditions (like in **Figure 5.12**) in contrast to outdoor exposure,

where fewer products were seen at the surface. However, more products could be present in depth in the crack.

Crystals formed at the crack surface of the specimen subjected to the water flow test were scratched and analysed. Acicular crystals can be observed in **Figured**, which may be another calcium carbonate polymorph, aragonite, according to the high peak of Ca in the corresponding EDS analysis. More investigations (thermogravimetry or X-ray powder diffraction) would be needed to confirm the presence of vaterite and aragonite.

Finally, it must be noted that the specimen kept in ambient air condition showed mostly calcite crystals, but fewer and most dispersed deposits (many zones with no healing products) than for other conditions. Also, new C-S-H crystals were also found in all conditions. These observations and their correlations with the permeability results obtained from the different exposure conditions will be discussed in the next **Section 5.5**. More microscopic analyses are presented in the companion paper (part 2) [36] to discuss the influence of the concrete composition regarding the permeability and the mechanical results.
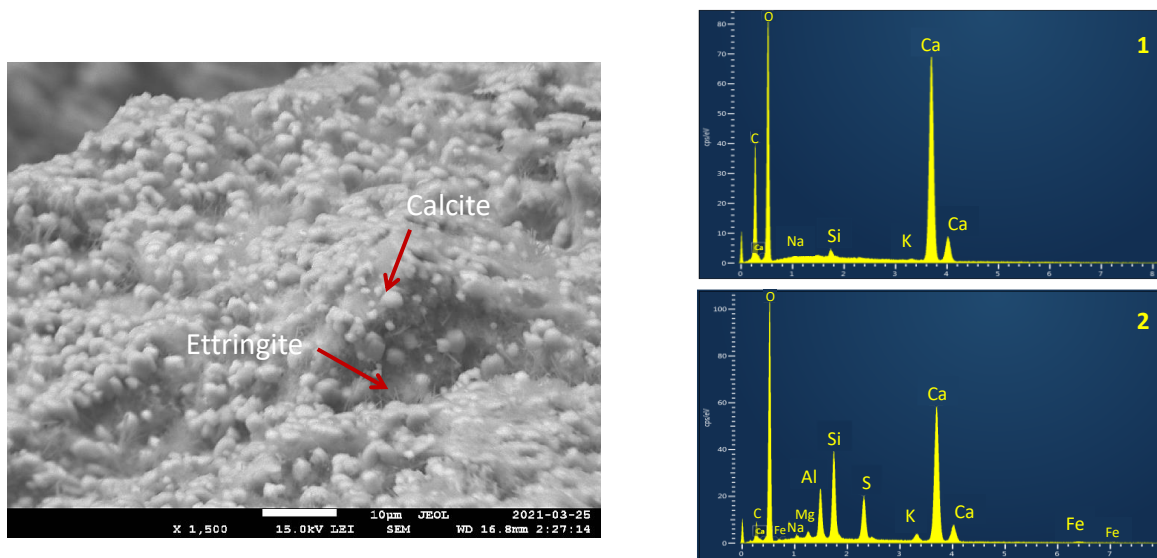
a) After healing in water for 3 months (X 1500)

Figure 5.14. SEM pictures and EDS analysis of healing products found in different exposure conditions for the control mix: a) water immersion, b) wet/dry cycles, c) outdoor and d) water flow
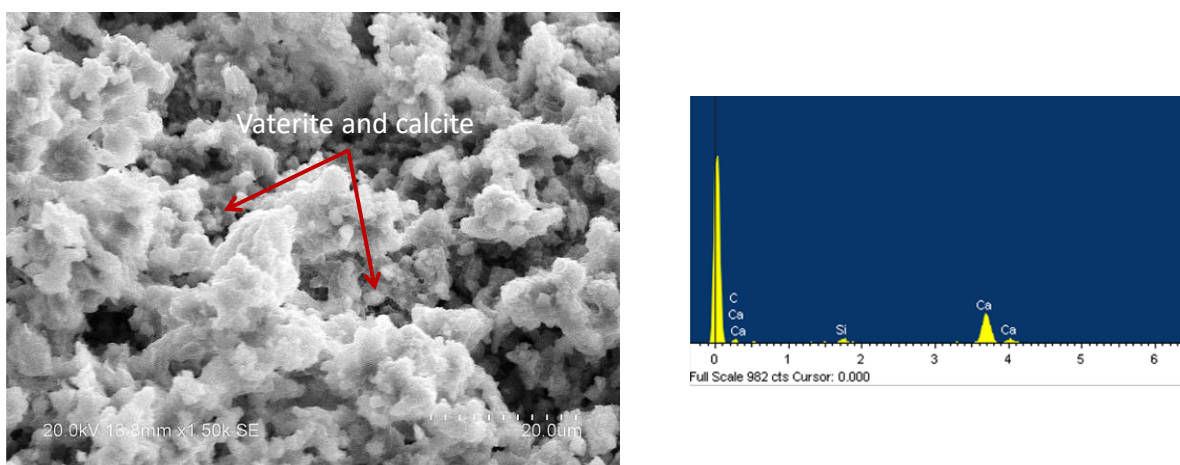
b) After healing in wet/dry for 3 months (X 1500)
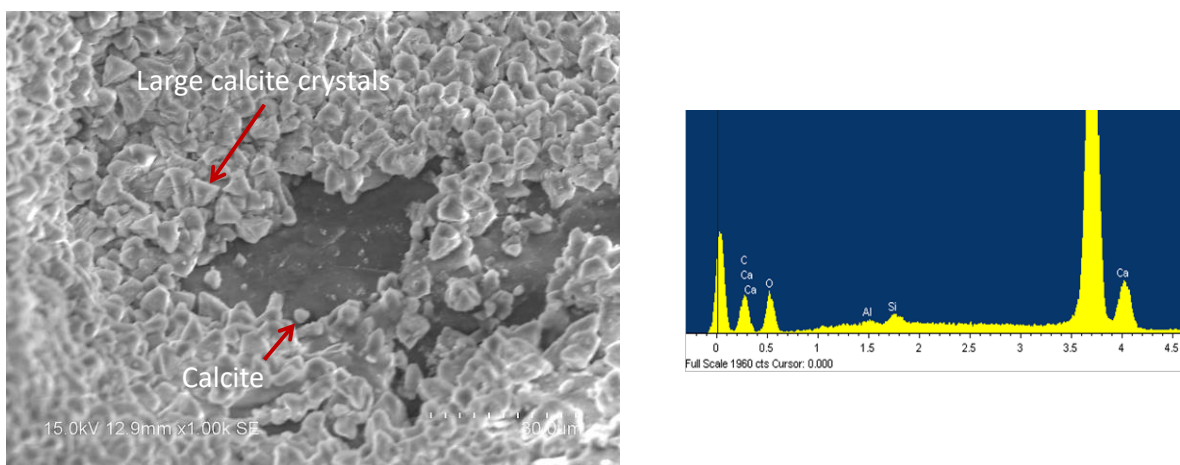
c) After healing in outdoor for 1 year (X 1000)
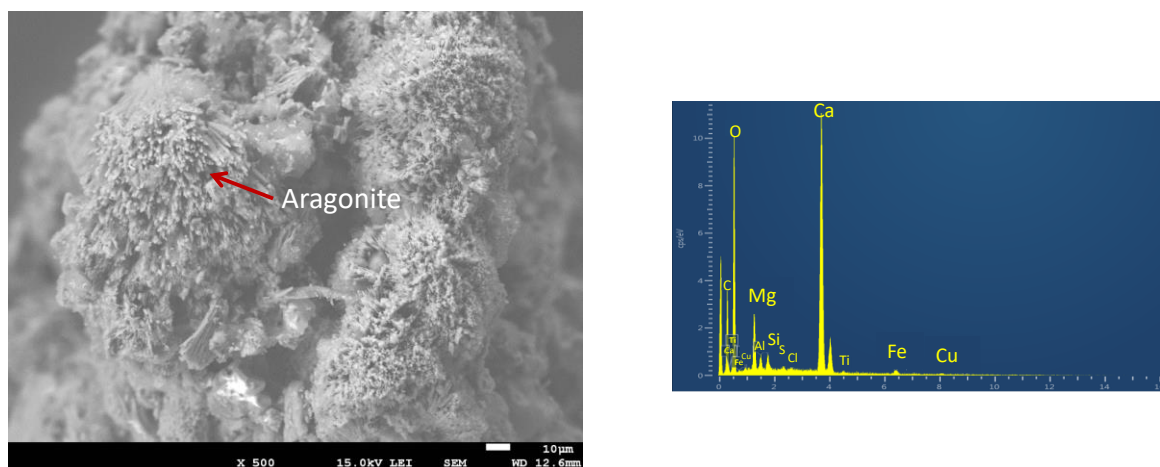
d) After healing in water flow for 1 week (X 500)

Figure 5.14. SEM pictures and EDS analysis of healing products found in different exposure conditions for the control mix: a) water immersion, b) wet/dry cycles, c) outdoor and d) water flow (cont.)

5.5 Discussion

5.5.1 Influence of the exposure condition

5.5.1.1 Water exposure (still water immersion vs continuous water flow)

Under water immersion, water permeability dropped rapidly (in the first 11 days) and then stabilized (**Figure 5.8a** and **Figure 5.10a**). The main healing product was calcium carbonate ($CaCO_3$) in the form of calcite (**Figurea**) as also found in literature for such exposure condition [14, 17, 23]. The healing kinetics observed under water immersion can be explained by the formation of $CaCO_3$ in concrete cracks that is characterised by a first rapid surface-controlled phase, followed by a slower diffusion-controlled second phase [40]. The first phase occurs as calcium ions (Ca^{++}), readily available at the crack surfaces, quickly react with CO_2 present in the water. In the second phase, $CaCO_3$ formation becomes slower as the Ca^{++} ions must diffuse through the matrix and the $CaCO_3$ layer up to the crack to be available for the reaction. A lack of CO_2 in the water can also prevent the reaction [13]. In this project, both effects could explain the healing stabilization. As the initial Healing Ratio was high (**Table 5.3**), a thick layer of $CaCO_3$ was rapidly formed, which significantly slowed down the diffusion of calcium ions for further reaction, as well as the penetration of water and CO_2. Moreover, as the water in the containers was not renewed, the amount of carbon dioxide in the water may have been depleted. Besides, ettringite needles were found in all mixes under water immersion (**Figurea**) and very rarely in other exposure conditions. This is probably due to the large amount of water required for the ettringite formation. Other studies [10, 12, 17, 19, 23] also found ettringite in cracked specimens under water.

Regarding the continuous water flow exposure, it did not accelerate the self-healing kinetics compared to still water immersion. The final Healing Ratios after around 1 week (average *HR* = 71%) were in general not superior to the *HR* achieved at 11 days in water immersion (average *HR* = 80%) (**Figure 5.8b** and **Table 5.3**). However, a difference in the healing products was observed. Acicular crystals similar to aragonite [45], another calcium carbonate polymorph, were found in most mixes under water flow (peaks of Ca and Mg [17] in **Figured**). Other researchers found aragonite as healing products [17, 23, 46]. Several reasons may explain the formation of aragonite in water flow contrary to still water immersion. First, as water is kept under pressure

(pressure gradient of 30 kPa), it may modify the self-healing process. Secondly, aragonite formation may be favoured by low pH of the pore solution caused by the dilution of ions in water [46], which was probable in this project as the permeability system operates in a closed loop (water in the tanks is not changed regularly). Finally, Auroy et al. [47] reported that the carbonation of ettringite generates aragonite, which may explain why no ettringite was found in the specimens subjected to water flow.

5.5.1.2   Wet/dry cycles and air exposures

During wet/dry cycles, the healing kinetics was more progressive than under water immersion (**Figure 5.8c** and **Figure 5.10b**), as found in [30]. The slowest initial evolution of healing under wet/dry cycles could be explained by a shorter time spend in water (3.5 days wet/3.5 days dry). However, after longer exposition, the healing potential became higher than under water (average final *HR* of 93% versus 84% respectively, **Table 5.3**). This could be explained by the fact that the periods in air provided additional CO_2, whereas the amount of CO_2 was probably depleted in non renewed water. Wet/dry exposition was also reported to favour the interaction of water, CO_2 and unhydrated cementitious materials, compared to water immersion [12, 48].

The healing products were also different between the wet/dry cycles and water immersion. Under wet/dry cycles, alongside calcite, smaller and less defined particles were observed (**Figureb**), which may look like vaterite spherules observed by [45]. While calcite is the most common healing product found, vaterite is another form of calcium carbonate that was observed by Yildirim et al. [46]. They systematically found less vaterite in ECC specimens healed under water compared to those exposed to air condition (50°C and 50% RH). According to Black et al. [49] who studied carbonated phases in synthesized C-S-H samples via Raman spectroscopy, vaterite can be formed following exposure of C-S-H gels to CO_2 and upon carbonation of pastes with high lime contents. These conditions were encountered in this study for the specimens in wet/dry cycles. During the wet period, typical hydration products like C-S-H were formed and the matrix had probably high lime content as the water in the containers were lime-saturated. Then, during the dry period, the paste was subjected to carbonation (more CO_2 in the air compared to water immersion), which may have favoured vaterite formation.

Besides, large amounts of small particles tightly packed were observed in wet/dry compared to water immersion (**Figure**). The higher density in wet/dry cycles could explain the higher final *HR* obtained in that condition. This is in accordance with the correlations between the self-healing performance (in terms of water flow reduction) and the quantitative amounts of healing products found by Park & Choi [20].

It can be noticed that the presence of liquid water is essential to achieve large self-healing when comparing the control mix in ambient air (21°C and 45% RH) and in wet/dry cycles (**Figure 5.8c**). Nonetheless, the control mix reached a *HR* = 46% after 3 months (**Table 5.3**), which was higher than expected. In this case, calcium ions were limited to the amount in the matrix and CO_2 was available in the air. 45% of relative humidity is enough for carbonation to occur slowly and partially heal the cracks. Roig-Flores et al. [16] also found similar Healing Ratios for specimens after 42 days in ambient air exposure (17°C and 40% RH).

5.5.1.3   Outdoor exposure

In outdoor exposure, with wide range of temperatures and precipitations, the healing process was slower (**Figure 5.8d** and **Figure 5.10c**) than under the other exposure conditions. The impact of the temperature on the evolution of Healing Ratios is hardly visible in **Figure 5.15a**. But the influence of the precipitations on the *HR* in **Figure 5.15b** is more noticeable. Between 6 and 9 months of exposure, a peak of precipitations occurred (261.2 mm in October 2019), which may explain the self-healing regain for the control and CA mixes as the slopes between 6 and 9 months were higher than between 3 and 6 months. However, a period of 2 or 3 years would have provided a better understanding of the effect of the weather on the self-healing process.
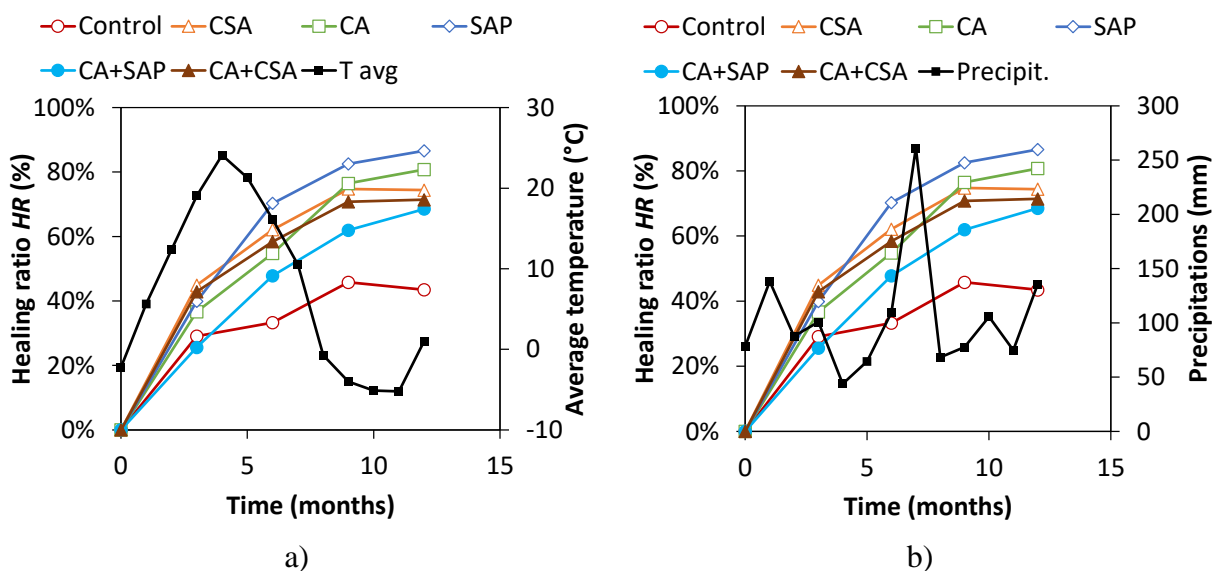
Figure 5.15. Comparison of the Healing Ratios for the outdoor specimens with a) the average temperature and b) the precipitations (from March 2019 to March 2020)

For the outdoor specimens, calcium ions were limited to the amount in the matrix and CO_2 was abundantly available in the air. The presence of water is necessary for carbon dioxide dissolution and reaction with calcium ions, and abundant precipitations may have boosted the self-healing capacity at some periods. In **Figurec**, large calcite crystals can be observed. As calcite is the most thermodynamically stable form of calcium carbonate [45, 49], it is logical to only find this $CaCO_3$ polymorph in specimens exposed outside for 1 year. The extended exposition provided more time to calcite to grow and probably explains the larger crystals found. This study is the first to present permeability measurements on specimens kept in outdoor conditions, thus the average *HR* of 71% after 1 year (**Table 5.3**) for the mixes cannot be compared. Moreover, in outdoor exposure, zones with no healing products could be seen on the crack surface (**Figurec**). Besides, at a macroscopic scale, the healing products were not covering the whole surface. These reasons may explain the lower *HR* found in that condition.

Finally, wet/dry cycles (3.5 days wet/3.5 days dry) could represent an accelerated condition of the outdoor exposition. A period of 25 days in wet/dry would be equivalent to a period of 5 to 50 months outside, depending on the concrete mix (**Table 5.4**).

5.5.2 Influence of the self-healing agents

The healing performance of the concrete mixes varies upon the exposition condition considered (**Table 5.3**, **Figure 5.8** and **Figure 5.11**). This impact of the exposition may be explained by differences of healing products as well as their growth rates according to the exposure condition. The impact of each mix is discussed below and compared with literature results.

5.5.2.1 Effect of expansive agent CSA

In comparison to other mixes, the FRC containing CSA achieved the second highest Healing Ratio (after the control mix) after 3 months in water immersion (86%), the highest one after 3 months in wet/dry cycles (99%) and the third one after 1 year outdoor (74%) (**Table 5.3**). However, at the end of these healing periods, the self-healing process was stabilized for this mix (**Figure 5.11b**).

Whereas the concrete mix with CSA performed better in wet/dry cycles than under water immersion in this study, Jiang et al. [21] found the opposite with lower Healing Ratios after 60 days in wet/dry (around 60%, 1 day wet/1 day dry) in comparison to water immersion (around 90%) on a mortar containing an expansive agent. Difference of duration of each wet and dry phases, environment during the dry cycles and expansive agent could explain the divergence with the results of this study. Other studies that investigated CSA only considered water immersion condition and found in general high self-healing performance compared to the control mix [13, 20]. Park & Choi [20] found a *HR* of around 75% after 21 days in water for a cement paste containing CSA, which is quite similar to the $HR = 85\%$ reached by the CSA mix in this study after 25 days in water (**Figure 5.8a**).

In conclusion, although discrepancies exist in experimental programs of existing studies and this present project (CSA product and dosage, pre-cracking age and exposure length), mixes with CSA generally present a good self-healing performance.

5.5.2.2 Effect of crystalline admixture CA

In comparison to other mixes, the FRC containing CA achieved the lowest Healing Ratio after 3 months in water immersion (74%), the third highest one after 3 months in wet/dry cycles (96%) and the second one after 1 year outdoor (81%) (**Table 5.3**). At the end of these healing periods, the self-healing process continued for the CA mix (**Figure 5.11b**).

The performance of CA and its optimal exposure condition does not make consensus in literature. The Healing Ratio of 74% after 3 months in water immersion in this study is lower than in several studies (almost 100% after 56 days for [13] and around 90% after 42 days for [15]).

Concerning the higher self-healing found in wet/dry cycles than in water immersion in this project, it is consistent with the results of Sisomphon et al. [12], based on mechanical considerations. However, Roig-Flores et al. [15] found that CA mix performed better in water immersion compared to wet/dry cycles (average *HR* of around 90% versus around 45%). As their wet/dry cycles were similar to the ones applied in this project (3.5 days in water at 15°C and 3.5 days in air at 17°C and 40% RH), the difference can come from the early cracking age (2 days) in their study. In such case, ongoing hydration is the dominant self-healing mechanism, which is definitely favoured in contact with water. When comparing the CA mix to the control mix performances, other studies did not find any significant improvement in wet/dry, water expositions [15] or in water flow test [18], which was also the case in this project. Lastly, in contrast to what has been reported in previous studies [10, 16, 17], the effect of CA in reducing the healing variation was not observed in this study.

In conclusion, a larger variety of performances is observed for mixes with CA. In addition to the usual discrepancies of experimental procedures in studies, a wide range of compositions stand under the name "crystalline admixtures". This situation makes comparison between studies difficult. In this project, the FRC with CA showed a good self-healing performance.

5.5.2.3 Effect of superabsorbent polymer SAP

In comparison to other mixes, the FRC containing SAP achieved the third highest Healing Ratio after 3 months in water immersion (85%), the fifth highest one after 3 months in wet/dry cycles (91%) and the highest one after 1 year outdoor (87%) (**Table 5.3**). At the end of these healing periods, the self-healing process continued for this mix (**Figure 5.11b**). With respect to these high final Healing Ratios in all expositions, it appeared that the SAP mix was less influenced by the exposure condition compared to the other mixes. This is explained by the fact that SAP can absorb liquid and moisture during wet periods and release it for crack healing in dry periods.

In general, the use of SAP led to high healing in water immersion after 30 days [26], with sometimes a complete healing after 42 days [22]. Regarding the influence of the exposure condition, the control mix of Hong et al. [30] performed better in water than their mixes containing

SAP, whereas it was the opposite under wet/dry cycles (1h wet/48h dry at 20°C and 50% RH), as observed in this study. They observed that the main healing products formed by SAP mixes were calcium carbonate, whose formation was enhanced by wet/dry cycles, which is in agreement with the results found in this study as well. Several studies [32, 33] performed water flow tests and usually found similar *HR* as in this project. For example, Li et al. [32] found a *HR* of about 95% after 7 days of water flow for a SAP mortar (size 200 μm, dosage 1%) pre-cracked at 14 days. This result is in the same range as the SAP mix in this project with *HR* = 88% after 7 days. The slightly lower *HR* found in this study may be due to the lower size particle (100 μm vs 200 μm) and dosage (0.5% vs 1%), but also the later pre-cracking age (28 days vs 14 days). Li et al. [32] found lower *HR* when increasing the pre-cracking age (from 3 to 28 days).

In conclusion, the size and dosage of the SAP in the mix are important influencing factors for its self-healing performance. Bigger particles and higher dosage improve healing performance, but decrease compressive strength in return. Despite the variability of the experimental conditions in literature, in general a very good self-healing performance was reported, as observed in this project.

5.5.2.4   Effect of combining CA+CSA and CA+SAP

The combinations of admixtures tested in this project (CA+CSA and CA+SAP) provided generally lower *HR* in comparison to the single admixtures in all exposure conditions (**Figure 5.8**, **Figure 5.11** and **Table 5.3**), thus the combinations did not provide synergetic effect.

While Sisomphon et al. [12] observed a synergy with CA+CSA in terms of mechanical recovery, Li et al. [32] obtained a faster complete healing with a combination of CA+SAP (3% of SAP and 0.2% of citric acid) compared to the mixes with SAP alone. Other studies examined combinations of CA+CSA [22, 23] and CA+CSA+SAP [22], but without studying the single admixtures alongside. For example, Park & Choi [22] found a complete equivalent crack closure (100%) after 28 days in water for cement pastes containing 10% CSA + 1.5% CA pre-cracked at 7 days, which is higher than the performance of CA+CSA in this study (81% of equivalent crack closure). Their earlier age of pre-cracking and larger admixtures amounts (cement paste versus concrete) probably promoted more healing.

5.5.2.5 Concrete mix with the best self-healing performance

The FRC mix with the best global self-healing performance in terms of water tightness should heal quickly (high initial *HR* in **Figure 5.8** and **Table 5.3** or equivalent initial crack closure rate in **Figure 5.11a**) and reach a great healing capacity (high final *HR* in **Figure 5.8** and **Table 5.3**). Moreover, the potential for further healing after the exposition period is also an asset (high final equivalent crack closure rate in **Figure 5.11b**). Finally, a good self-healing performance in real outdoor exposition is obviously essential. Considering all these criteria, the CA and SAP mixes are the best candidates, since they were in the first positions in outdoor exposure. The companion paper (part 2) will validate if these mixes still stand out when regarding their mechanical recovery [36].

5.6 Conclusions

This project evaluated the self-healing capacity of six fibre reinforced concretes (FRC) with no admixture (control), a single admixture (expansive agent CSA, crystalline admixture CA, superabsorbent polymer SAP) and combination of admixtures (CA+SAP and CA+CSA). After pre-cracking at 28 days by means of a 3-point bending test, concrete specimens were exposed in indoor conditions (water immersion, wet/dry cycles and ambient air for 3 months and water flow for 1 week) and outside for 1 year. This paper presented the water permeability results and some microscopic observations.

Based on the results of this experimental program, the following conclusions can be drawn:

- The influence of the exposition was clearly visible with water permeability measures and microscopic observations. The self-healing kinetics in water immersion consisted in a rapid initial healing and then a drastic slowdown. For the other expositions, the evolution of healing was more progressive after the first measure. Wet/dry cycles (*HR* = 93% in average) was the most favourable exposition for healing in comparison to water immersion (*HR* = 84% in average) and ambient air (*HR* = 46% in average). After 1 year outside in Montreal climate, a *HR* = 71% in average was reached.

- Specimens subjected to a continuous water flow for 1 week did not accelerate the self-healing process compared to still water immersion. Besides, wet/dry cycles can be

considered as an accelerated condition of the long-term outdoor exposure. 25 days in wet/dry could represent 5 to 50 months outside, depending on the mix.

- The SEM-EDS analyses showed different types and densities of healing products according to the exposition, which could explain the different healing performances. Calcium carbonate was found in all conditions but in different polymorphs. In water immersion, calcite crystals and ettringite were observed. Calcite was found in outdoor as well, but larger crystals were observed. In wet/dry cycles, a large amount of small particles, probably vaterite, was noticed. In water flow, acicular products, probably aragonite, were found.

- The influence of the self-healing agents was not straightforward as the performance of each concrete mix varied according to the exposure condition. However, the mix containing SAP was less influenced by the exposition, which may demonstrate the beneficial effect of SAP to absorb and release water for healing.

- Overall, CA and SAP mixes showed the best self-healing performance regarding water permeability measurements, in terms of initial and final Healing Ratio and equivalent crack closure, especially in realistic outdoor exposure. In contrast to what was reported in literature, no synergetic effect was found with CA+SAP and CA+CSA mixes.

- Except the lower crack healing for the control mix kept in ambient air, moderate to high self-healing of cracks were observed for all the tested mixes, through permeability measurements and macro- and microscopic observations.

5.7 Acknowledgements

5.8 References

[1]   N. De Belie *et al.*, "A review of self-healing concrete for damage management of structures," *Advanced Materials Interfaces,* p. 28 pages, 2018.

[2]   K. Van Tittelboom and N. De Belie, "Self-healing in cementitious materials - A review," *Materials,* vol. 6, no. 6, pp. 2182-2217, 2013.

[3]   V. Li and E. Herbert, "Robust self-healing concrete for sustainable infrastructure," *Journal of Advanced Concrete Technology,* vol. 10, pp. 207-218, 2012.

[4]   A. Al-Tabbaa, C. Litina, P. Giannaros, A. Kanellopoulos, and L. Souza, "First UK field application and performance of microcapsule-based self-healing concrete," *Construction and Building Materials,* vol. 208, pp. 669-685, 2019.

[5]   K. Van Tittelboom *et al.*, "Comparison of different approaches for self-healing concrete in a large-scale lab test," *Construction and Building Materials,* vol. 107, pp. 125-137, 2016.

[6]   T. Van Mullem, E. Gruyaert, R. Caspeele, and N. D. Belie, "First large scale application with self-healing concrete in Belgium: Analysis of the laboratory control tests," *Materials,* vol. 13, no. 4, 2020.

[7]   E. Tsangouri *et al.*, "Feasibility study on real-scale, self-healing concrete slab by developing a smart capsules network and assessed by a plethora of advanced monitoring techniques," *Construction and Building Materials,* vol. 228, 2019.

[8]   R. M. Mors and H. M. Jonkers, "Bacteria-based self-healing concrete: evaluation of full scale demonstrator projects," *RILEM Technical Letters,* vol. 4, pp. 138-144, 2019.

[9]   X. Wang *et al.*, "Laboratory and field study on the performance of microcapsule-based self-healing concrete in tunnel engineering," *Construction and Building Materials,* vol. 220, pp. 90-101, 2019.

[10]   L. Ferrara, V. Krelani, and M. Carsana, "A "fracture testing" based approach to assess crack healing of concrete with and without crystalline admixtures," *Construction and Building Materials,* vol. 68, pp. 535-551, 2014.

[11] L. Ferrara, V. Krelani, and F. Moretti, "On the use of crystalline admixtures in cement based construction materials: from porosity reducers to promoters of self healing," *Smart Material and Structures,* vol. 25, p. 17p, 2016.

[12] K. Sisomphon, O. Copuroglu, and E. A. B. Koenders, "Effect of exposure conditions on self healing behavior of strain hardening cementitious composites incorporating various cementitious materials," *Construction and Building Materials,* vol. 42, pp. 217-224, 2013.

[13] K. Sisomphon, O. Copuroglu, and E. A. B. Koenders, "Self-healing of surface cracks in mortars with expansive additive and crystalline additive," *Cement and Concrete Composites,* vol. 34, pp. 566-574, 2012.

[14] G. Li, S. Liu, M. Niu, Q. Liu, X. Yang, and M. Deng, "Effect of granulated blast furnace slag on the self-healing capability of mortar incorporating crystalline admixture," *Construction and Building Materials,* vol. 239, 2020.

[15] M. Roig-Flores, F. Pirritano, P. Serna, and L. Ferrara, "Effect of crystalline admixtures on the self-healing capability of early-age concrete studied by means of permeability and crack closing tests," *Construction and Building Materials,* vol. 114, pp. 447-457, 2016.

[16] M. Roig-Flores, S. Moscato, P. Serna, and L. Ferrara, "Self-healing capability of concrete with crystalline admixtures in different environments," *Construction and Building Materials,* vol. 86, pp. 1-11, 2015.

[17] P. Escoffres, C. Desmettre, and J.-P. Charron, "Effect of a crystalline admixture on the self-healing capability of high-performance fiber reinforced concretes in service conditions," *Construction and Building Materials,* vol. 173, pp. 763-774, 2018.

[18] P. Azarsa, R. Gupta, and A. Biparva, "Assessment of self-healing and durability parameters of concretes incorporating crystalline admixtures and Portland Limestone Cement," *Cement and Concrete Composites,* vol. 99, pp. 17-31, 2019.

[19] E. Cuenca, A. Tejedor, and L. Ferrara, "A methodology to assess crack-sealing effectiveness of crystalline admixtures under repeated cracking-healing cycles," *Construction and Building Materials,* vol. 179, pp. 619-632, 2018.

[20] B. Park and Y. C. Choi, "Effect of healing products on the self-healing performance of cementitious materials with crystalline admixtures," *Construction and Building Materials,* vol. 270, 2021.

[21] Z. Jiang, W. Li, and Z. Yuan, "Influence of mineral additives and environmental conditions on the self-healing capabilities of cementitious materials," *Cement and Concrete Research,* vol. 57, pp. 116-127, 2015.

[22] B. Park and Y. C. Choi, "Self-healing capability of cementitious materials with crystalline admixtures and super absorbent polymers (SAPs)," *Construction and Building Materials,* vol. 189, pp. 1054-1066, 2018.

[23] X. Wang, C. Fang, D. Li, N. Han, and F. Xing, "A self-healing cementitious composite with mineral admixtures and built-in carbonate," *Cement and Concrete Composites,* vol. 92, pp. 216-229, 2018.

[24] A. S. Buller, F. U. Abro, K. M. Lee, and S. Y. Jang, "Mechanical recovery of cracked fiber-reinforced mortar incorporating crystalline admixture, expansive agent, and geomaterial," *Advances in Materials Science and Engineering,* vol. 2019, 2019.

[25] H. Deng and G. Liao, "Assessment of influence of self-healing behavior on water permeability and mechanical performance of ECC incorporating superabsorbent polymer (SAP) particles," *Construction and Building Materials,* vol. 170, pp. 455-465, 2018.

[26] D. Snoeck, K. Van Tittelboom, S. Steuperaert, P. Dubruel, and N. De Belie, "Self-healing cementitious materials by the combination of microfibres and superabsorbent polymers," *Journal of Intelligent Material Systems and Structures,* vol. 25, no. 1, pp. 13-24, 2014.

[27] E. Gruyaert *et al.*, "Self-healing mortar with pH-sensitive superabsorbent polymers: testing of the sealing efficiency by water flow tests," *Smart Material and Structures,* vol. 25, p. 11 pages, 2016.

[28] J. Pelto, M. Leivo, E. Gruyaert, B. Debbaut, D. Snoeck, and N. De Belie, "Application of encapsulated superabsorbent polymers in cementitious materials for stimulated autogenous healing," *Smart Material and Structures,* vol. 26, no. 10, p. 14 pages, 2017.

[29] D. Snoeck and N. De Belie, "Repeated autogenous healing in strain-hardening cementitious composites by using superabsorbent polymers," *Journal of Materials in Civil Engineering,* vol. 28, no. 1, p. 11 pages, 2016.

[30] G. Hong, C. Song, and S. Choi, "Autogenous healing of early-age cracks in cementitious materials by superabsorbent polymers," *Materials,* vol. 13, no. 3, 2020.

[31] H. X. D. Lee, H. S. Wong, and N. R. Buenfeld, "Self-sealing of cracks in concrete using superabsorbent polymers," *Cement and Concrete Research,* vol. 79, pp. 194-208, 2016.

[32] D. Li, B. Chen, X. Chen, B. Fu, H. Wei, and X. Xiang, "Synergetic effect of superabsorbent polymer (SAP) and crystalline admixture (CA) on mortar macro-crack healing," *Construction and Building Materials,* vol. 247, 2020.

[33] G. Hong and S. Choi, "Rapid self-sealing of cracks in cementitious materials incorporating superabsorbent polymers," *Construction and Building Materials,* vol. 143, pp. 366-375, 2017.

[34] R. P. Borg, E. Cuenca, E. Maria Gastaldo Brac, and L. Ferrara, "Crack sealing capacity in chloride-rich environments of mortars containing different cement substitutes and crystalline admixtures," *Journal of Sustainable Cement-based Materials,* vol. 7, no. 3, pp. 141-159, 2018.

[35] K.-S. Lauch, C. Desmettre, and J.-P. Charron, "New water permeability set-up and factors affecting concrete self-healing," *Construction and Building Materials,* vol. 294, 2021.

[36] K.-S. Lauch, J.-P. Charron, and C. Desmettre, "Self-healing of concrete containing different admixtures under laboratory and outdoor expositions - Part 2: mechanical behaviour," *Submitted for publication in Cement and Concrete Composites,* 2021.

[37] D. Snoeck, C. Schrofl, and V. Mechtcherine, "Recommendation of RILEM TC 260-RSC: testing sorption by superabsorbent polymers (SAP) prior to implementation in cement-based materials," *Materials and Structures/Materiaux et Constructions,* vol. 51, no. 5, 2018.

[38] D. Snoeck, D. Schaubroeck, P. Dubruel, and N. De Belie, "Effect of high amounts of superabsorbent polymers and additional water on the workability, microstructure and

strength of mortars with a water-to-cement ratio of 0.50," *Construction and Building Materials,* vol. 72, pp. 148 - 157, 2014.

[39] L. Ferrara *et al.*, "Experimental characterisation of the self-healing capacity of cement based materials and its effects on the material performance: A state of the art report by COST Action SARCOS WG2," *Construction and Building Materials,* Review vol. 167, pp. 115-142, 2018.

[40] C. Edvardsen, "Water permeability and autogenous healing of cracks in concrete," *ACI Materials Journal,* vol. 96, no. 4, pp. 448-454, 1999.

[41] T. Van Mullem *et al.*, "Addressing the need for standardisation of test methods for self-healing concrete: an inter-laboratory study on concrete with macrocapsules," *Science and Technology of Advanced Materials,* vol. 21, no. 1, pp. 661-682, 2020/01/31 2020.

[42] A. Beglarigale, D. Eyice, B. Tutkun, and H. Yazici, "Evaluation of enhanced autogenous self-healing ability of UHPC mixtures," *Construction and Building Materials,* vol. 280, 2021.

[43] R. Gupta and A. Biparva, "Innovative test technique to evaluate "self-sealing" of concrete," *Journal of Testing and Evaluation,* vol. 43, no. 5, pp. 1091-1098, 2015.

[44] T. Van Mullem, E. Gruyaert, B. Debbaut, R. Caspeele, and N. De Belie, "Novel active crack width control technique to reduce the variation on water permeability results for self-healing concrete," *Construction and Building Materials,* vol. 203, pp. 541-551, 2019.

[45] R. Sevcik, P. Sasek, and A. Viani, "Physical and nanomechanical properties of the synthetic anhydrous crystalline $CaCO_3$ polymorphs: vaterite, aragonite and calcite," *Journal of Materials Science,* vol. 53, no. 6, pp. 4022-4033, 2018.

[46] G. Yildirim, A. H. Khiavi, S. Yeilmen, and M. Sahmaran, "Self-healing performance of aged cementitious composites," *Cement and Concrete Composites,* vol. 87, pp. 172-186, 2018.

[47] M. Auroy *et al.*, "Comparison between natural and accelerated carbonation (3% CO_2): Impact on mineralogy, microstructure, water retention and cracking," *Cement and Concrete Research,* vol. 109, pp. 64-80, 2018/07/01/ 2018.

[48] S. Z. Qian, J. Zhou, and E. Schlangen, "Influence of curing condition and precracking time on the self-healing behavior of Engineered Cementitious Composites," *Cement and Concrete Composites,* vol. 32, no. 9, pp. 686-693, 2010.

[49] L. Black, C. Breen, J. Yarwood, K. Garbev, P. Stemmermann, and B. Gasharova, "Structural Features of C–S–H(I) and Its Carbonation in Air—A Raman Spectroscopic Study. Part II: Carbonated Phases," *Journal of the American Ceramic Society,* vol. 90, no. 3, pp. 908-917, 2007.

CHAPTER 6

ARTICLE 3: SELF-HEALING OF CONCRETE CONTAINING DIFFERENT ADMIXTURES UNDER LABORATORY AND OUTDOOR EXPOSITIONS – PART 2: MECHANICAL BEHAVIOUR

Kim-Séang LAUCH, Jean-Philippe CHARRON, Clélia DESMETTRE

Department of Civil, Geological and Mining Engineering, Polytechnique Montreal

Paper submitted to *Cement and Concrete Composites* on the 5th of July 2021

Corresponding Author:

Jean-Philippe CHARRON

Department of Civil, Geological and Mining Engineering

Polytechnique Montreal

B.O. Box 6079, Station Centre-Ville

Montreal, Qc, Canada H3C 3A7

Phone: 1-514-340-4711 ext 3433

Fax: 1-514-340-5881

Email: jean-philippe.charron@polymtl.ca

6.1 Abstract

This project presents the evaluation of the self-healing of fibre reinforced concretes containing various admixtures (crystalline admixture, expansive agent, superabsorbent polymer), subjected to several laboratory conditions (water immersion, wet/dry cycles ambient air for 3 months, water flow for 1 week) and a long-term outdoor exposure (1 year). Self-healing capacity was assessed by water permeability measurements, mechanical recovery, visual observations and microscopic analyses. This part 2 presents the mechanical behaviour and the correlations with the water permeability measures presented in part 1. At the end of the healing period, the prisms were reloaded until failure with the same 3-point bending test as pre-cracking. The results showed that a high healing of cracks based on water permeability (Healing Ratio) did not necessarily lead to a high mechanical recovery. The highest Strength Regains (109% in average) were obtained for the specimens exposed outside that presented the lowest Healing Ratios (71% in average). The local density of the healing products may govern the Healing Ratio, while the type of healing products and their extent in the crack depth may control the Strength Regain. Finally, the SAP mix showed overall the best self-healing performance, regarding both durability and mechanical properties.

Keywords: self-healing concrete, crystalline admixture, expansive agent, superabsorbent polymer, mechanical recovery, healing products

6.2 Introduction

First discovered by the French Academy of Sciences in 1836 in water-retaining structures [1], the self-healing process in concrete has been largely and more thoroughly studied in the last decade. Interest in this topic has increased exponentially, as the number of published papers has been multiplied almost tenfold between 2010 and 2020 (from 25 to 233 papers)[2]. The change of mentalities towards more sustainable solutions combined with the enormous costs of maintenance and repair of concrete structures [2] motivate research about materials with self-healing capabilities. In this project, concretes with different admixtures (crystalline admixture CA,

---

[2] Data from Web of Science with the words "self healing concrete" as topic, accessed date: 02/02/2021

expansive agent CSA, superabsorbent polymer SAP and combinations of CA+SAP and CA+CSA) were studied, as previously discussed in [3].

Nowadays, there is no standardized testing method to evaluate self-healing in concrete yet. Comprehensive reviews on the experimental characterisation of self-healing (crack closing, durability, mechanical, microstructure) has been published [4, 5]. Experimental methods based on transport or durability properties enable the characterisation of the whole crack volumes and constitute thus adequate methods to evaluate self-healing. Experimental methods based on the recovery of the mechanical properties of concrete, such as stiffness and strength, are also important to identify a robust self-healing allowing later consideration in the structural capacity. While most studies investigated the self-healing capacity via the recovery of a durability property [6-12], fewer determined the recovery of mechanical properties [13-15].

Mechanical tests do not give a straightforward evaluation of the cracks, as further analysis and interpretation of the results are needed to establish a healing contribution on the mechanical behaviour of concrete. Recovery of peak or first-cracking strength (in load P or stress σ values) and stiffness (from stress-strain or σ-COD or P-COD curves) are determined with different indexes (**Table 6.1**), when performing bending tests.

Strength recoveries are evaluated with several equations. **Eq. 6.1** (direct ratio) was used either considering σ for first-cracking [15], $\sigma_{pre-load}$ and σ_{reload} at the same crack opening displacement (COD) [16] or $\sigma_{pre-load}$ for first-cracking and σ_{reload} at peak [17]. Then, **Eq. 6.2** (ratio with subtraction of unloaded value) was mostly used by Ferrara et al. [13, 18] and others considering the peak values with σ results [19] or with P results [20-22], or the first-cracking values in σ [19]. Lastly, Namnoum et al. [23] used **Eq. 6.3** considering a reference unhealed specimen undergoing the same curing condition. With respect to the studies that used the same admixtures (CA, CSA, SAP) as this present project, maximum strength regains of around 30% [13] and 90% [16] were reported when using CA, 27% [22] when using a combination of several agents with CSA, and 70% [15] to 250% [19] were obtained when using SAP.

The stiffness recovery is also calculated from several equations. Direct ratios (**Eq. 6.4**) were used from stress-strain curve considering the slopes of loading curves at peak or at 40% of the peak [21]. **Eq. 6.5** was used by Ferrara et al. [13] from σ-COD curve, by Buller et al. [22] from P-COD curves

and by Snoeck & De Belie [15] from σ-ε curves. Finally, Namnoum et al. [23] used **Eq. 6.6** considering a reference unhealed specimen again. Stiffness recoveries of 75% [13], 63% and 70% [15] were reported when using CA, CSA and SAP respectively.

In addition to all these different ratios considered, a wide range of different loading procedures (and hence cracking states), specimens (mix composition, form and dimensions of specimens) as well as loading and healing conditions (age of pre-cracking, type of crack, crack width, healing condition) are used, which makes comparison of mechanical recovery indexes between studies difficult. In this project, **Eq. 6.7** (with σ values) and **Eq. 6.8** (from σ-displacement curve) will be used (**Table 6.1**). These choices were made because of the bending test carried out and crack width selected in this project, as it will be explained in the methodology section.

Table 6.1. Expressions of mechanical recovery index used when performing bending test

Mechanical recovery index	References	Equation
$Strength\ recovery = \dfrac{\sigma_{reload}}{\sigma_{pre-load}}$	[15-17]	**(6.1)**
$Strength\ recovery = \dfrac{P\ or\ \sigma_{reload} - P\ or\ \sigma_{unload}}{P\ or\ \sigma_{pre-load} - P\ or\ \sigma_{unload}}$	[13, 18-22]	**(6.2)**
$Strength\ recovery = \dfrac{P_{reload} - P_{reload,ref}}{P_{pre-load,ref} - P_{reload,ref}}$	[23]	**(6.3)**
$Stiffness\ recovery = \dfrac{K_{reload}}{K_{pre-load}}$	[17, 21]	**(6.4)**
$Stiffness\ recovery = \dfrac{K_{reload} - K_{unload}}{K_{pre-load} - K_{unload}}$	[13, 15, 22]	**(6.5)**
$Stiffness\ recovery = \dfrac{K_{reload} - K_{reload,ref}}{K_{pre-load,ref} - K_{reload,ref}}$	[23]	**(6.6)**
$Strength\ recovery = \dfrac{\sigma_{reload}}{\sigma_{unload}}$	This study	**(6.7)**
$Stiffness\ recovery = \dfrac{K_{reload}}{K_{pre-load}}$	This study	**(6.8)**

pre-load = from pre-cracking curve, *unload* = from pre-cracking curve, *reload* = from reloading curve, ref = from a reference unhealed specimen

Some researchers determined both durability and mechanical properties of healed concrete. They used in that case different specimens and pre-loading procedures for the two types of tests [14, 17, 19, 22, 24-27], which means different crack patterns that can impact results comparisons. For example, cylinders are cracked in tension for permeability tests and prisms are cracked in bending

to assess the recovery of mechanical properties [17, 19, 22]. Hence, durability and mechanical recoveries could not be correlated. Only, Van Tittelboom et al. [28] undertook one of the most complete evaluation of self-healing via four types of measurements (visual, durability, mechanical and microscopic) on the same specimen. Unfortunately, no conclusions could be drawn from the water permeability and mechanical tests.

In this project, four types of measurements have been performed to assess the self-healing capacity of fibre reinforced concrete (FRC) on the same specimen. FRC containing different admixtures (crystalline admixture CA, expansive agent CSA, superabsorbent polymer SAP and combinations of CA+SAP and CA+CSA) were studied. 3-point bending tests have been carried out on prisms for pre-cracking and reloading, water permeability tests and crack width observations were conducted on the same prisms. Microscopic analyses were then carried out to identify the healing products observed in the cracks. This procedure allows the establishment of relationships between a healing state from durability and mechanical recovery perspectives with the nature of the healing products. While the companion paper (part 1) presented the water permeability results [3], this paper focuses on the mechanical aspects (part 2).

6.3 Experimental program

6.3.1 Materials and characterisation tests

Six fibre reinforced concretes (FRC), with a water to binder ratio of 0.43 and 0.75% in volume of steel macrofibres ($l_f = 35$ mm and $\varphi_f = 0.55$ mm), were made: one with no admixture (control), one with 3.33% of calcium sulfoaluminated-based expansive agent (CSA), one with 2% of crystalline admixture (CA), one with 0.5% of superabsorbent polymer (SAP), one with the combination of crystalline admixture and superabsorbent polymer (CA+SAP) and the last one with crystalline admixture and expansive agent combined (CA+CSA). The dosages of the admixtures by mass of cement followed the recommendations of the manufacturers. The absorption capacity of the SAP used (100 μm size particle), measured with the tea-bag method, was 310 g/g SAP of deionised water, 188 g/g SAP of tap water and 38 g/g SAP of cement filtrate. To take this absorption into account and based on additional tests, more superplasticiser SP has been added in the mixes containing SAP to keep similar mechanical performance to the others mixes.

The compositions and characterisation results of the mixes are shown in **Table 6.2**. The fresh and hardened properties were overall quite similar for all mixes and in the expected range, except for the SAP mixes showing slightly reduced workability and strength.

Table 6.2. Compositions of the FRC mixtures and characterisation results from [3]

Material	Control	CSA	CA	SAP	CA+SAP	CA+CSA
Cement type GUb-SF (kg/m³)	550	550	550	550	550	550
CSA (kg/m³)	-	18.3	-	-	-	18.3
CA (kg/m³)	-	-	11	-	11	11
SAP (kg/m³)	-	-	-	2.75	2.75	-
Water (kg/m³)	237	237	237	237	237	237
Superplasticizer (l/m³)	10.0	10.0	10.5	30.0	30.0	10.5
Viscosity agent (l/m³)	0.70	0.85	0.71	0.70	0.70	0.85
Sand (kg/m³)	779	771	773	767	761	765
Coarse aggregates (kg/m³)	631	624	626	620	616	619
Steel fibre (kg/m³)	58.5	58.5	58.5	58.5	58.5	58.5
Slump flow (mm)	530	583	503	443	330	595
Air content (%)	1.9	1.6	2.0	2.7	3.0	1.7
Density (kg/m³)	2326	2334	2316	2285	2268	2329
f_c 28 days (MPa)	61.3	64.9	60.3	58	54.2	59.6
E_c 28 days (MPa)	33100	33200	31700	29000	27500	32500

A first batch of each FRC was made for the preparation of the specimens intended for the outdoor exposition, while a second batch was produced for the specimens intended for the indoor conditions. The specimens were immersed in lime-saturated water (to prevent any leaching) for curing during 28 days.

6.3.2 Methodology to assess self-healing

The general methodology used in this project was thoroughly presented in the companion paper (part 1) [3]. It consists of : (1) producing the specimens, (2) pre-cracking at 28 days by means of a 3-point bending test, (3) subjecting the specimens in several healing conditions, (4) assessing self-healing via optical observations and water permeability tests, (5) reloading the specimens at the end of the healing period until failure to evaluate a potential mechanical recovery and (6) analysing and identifying healing products via microscopic observations (scanning electron microscopy SEM

and energy-dispersive X-ray analysis EDS). The water permeability measurements were presented in the part 1. The mechanical tests are described in the next sections.

The healing conditions studied in this project as well as the number of prisms concerned for each mix are described in **Table 6.3**. A total of 124 prisms were produced for this experimental program. Pre-cracked prisms and 2 reference uncracked ones were placed either in water immersion or wet/dry cycles for 3 months (in laboratory), or outside for 1 year in Montreal climate from March 2019 to March 2020. Outdoor specimens were first partially dried in ambient air condition for 28 days after pre-cracking prior to exposing them outside as it was freezing at that time. The ambient air condition was considered only for the control mix. The continuous water flow was studied with only 1 specimen per mix because of the duration of the durability test (1 week). The role of the reference uncracked specimens will be explained in **Section 6.3.3**.

Table 6.3. Description of the healing conditions and the number of prisms per mix

Exposure conditions	Description	Duration	Number of prisms
Water immersion	Immersion in lime-saturated water at 21 ± 3 °C, no water renewal	3 months	4 or 5 + 2[#]
Wet/dry cycles	3.5 days immersion in lime-saturated water at 21 ± 3 °C, followed by 3.5 days drying in ambient air at 21 ± 3 °C and $45 \pm 10\%$ relative humidity	3 months	4 + 2[#]
Ambient air (control mix only)	Storage in a climatic chamber at 21 ± 3 °C and $45 \pm 10\%$ relative humidity	3 months	2* + 2[#]
Water flow	Continuous water flow at 30 kPa (3-meter water depth)	1 week	1
Outdoor	Outside in Montreal climate, temperatures ranged from -22.1 to 33.1 °C, the precipitations ranged from 43.7 to 261.2 mm/month and the snow on ground ranged between 0 and 90 cm	1 year	4 + 2[#]

* Reference cracked specimens kept in ambient air
[#] Reference uncracked specimens subjected to the same exposition

6.3.3 Pre-cracking and reloading procedures

The pre-cracking phase consisted in a 3-point bending test on 75 mm x 125 mm x 450 mm prism according to EN 14651 [29], as illustrated in **Figure 6.1**. The prism was notched (20 mm deep and 5 mm wide) at mid-span with a circular saw. The loading, applied with a 240 kN hydraulic actuator, was controlled with the average displacement of two linear variable displacement transducers (LVDTs) placed on each side of the prism. The crack mouth opening displacement (CMOD) was measured with an extensometer installed at 10 mm below the prism. The procedure consisted in loading at a rate of 0.2 mm/min up to an extensometer displacement of 0.9 mm and then unloading at a rate of 1 mm/min. The average residual crack width at the notch root (at the bottom of the flexural crack) for this experimental program was 0.29 mm (standard deviation of 0.07 mm), measured by digital microscope.
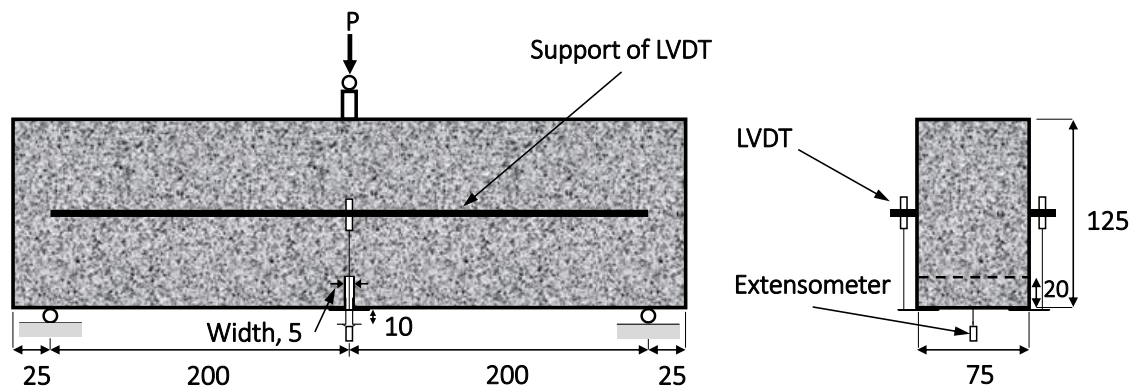
Figure 6.1. 3-point bending test on notched prisms

At the end of the healing period, all specimens were reloaded until failure, via the same 3-point bending test used for the pre-cracking phase. The reloading rate was 0.2 mm/min until reaching 70% of the maximum load in the post-peak stage. Then it was increased at 0.5 mm/min until reaching 50% of the maximum load at post-peak and then at 1 mm/min until failure to perform the test in a reasonable duration. The loading was stopped when reaching a residual force of 4 kN.

Figure 6.2 presents an overview of the different phases of loading and of the test timelines of the different types of specimens. First, the cracked specimens, the majority of the tested prisms, were pre-cracked at 28 days, followed by a healing period and then reloaded at either an age of 4 months (120 days) for indoor specimens or 14 months for outdoor specimens. Secondly, the reference

uncracked specimens (2 prisms per healing condition per mix) were placed in the different healing conditions uncracked since a previous study [4] highlighted the need to have such companion undamaged specimens. They were then pre-cracked and reloaded the same day as the final reloading of the cracked specimens (4 and 14 months for the indoor and outdoor prisms respectively). An example of typical curves for the cracked and reference uncracked specimens is shown in **Figure 6.3**. The cracked and healed specimen (blue line) is expected to reach a higher stress at reloading because of a potential mechanical regain. The reference uncracked prism (orange dashed line) is assumed to have slightly higher flexural strength during pre-cracking because of concrete maturity, and also a lower stress at reloading because there is no healing.

Finally, the last type of specimens was the reference cracked ones (2 prisms and only for the control mix). These prisms had the same loading history as the indoor cracked specimens (pre-cracking at 28 days and reloading at 4 months), but they were kept in ambient air condition. It is expected that these reference cracked prisms present almost no healing and thus a lower stress at reloading such as the orange dashed line in **Figure 6.3**.
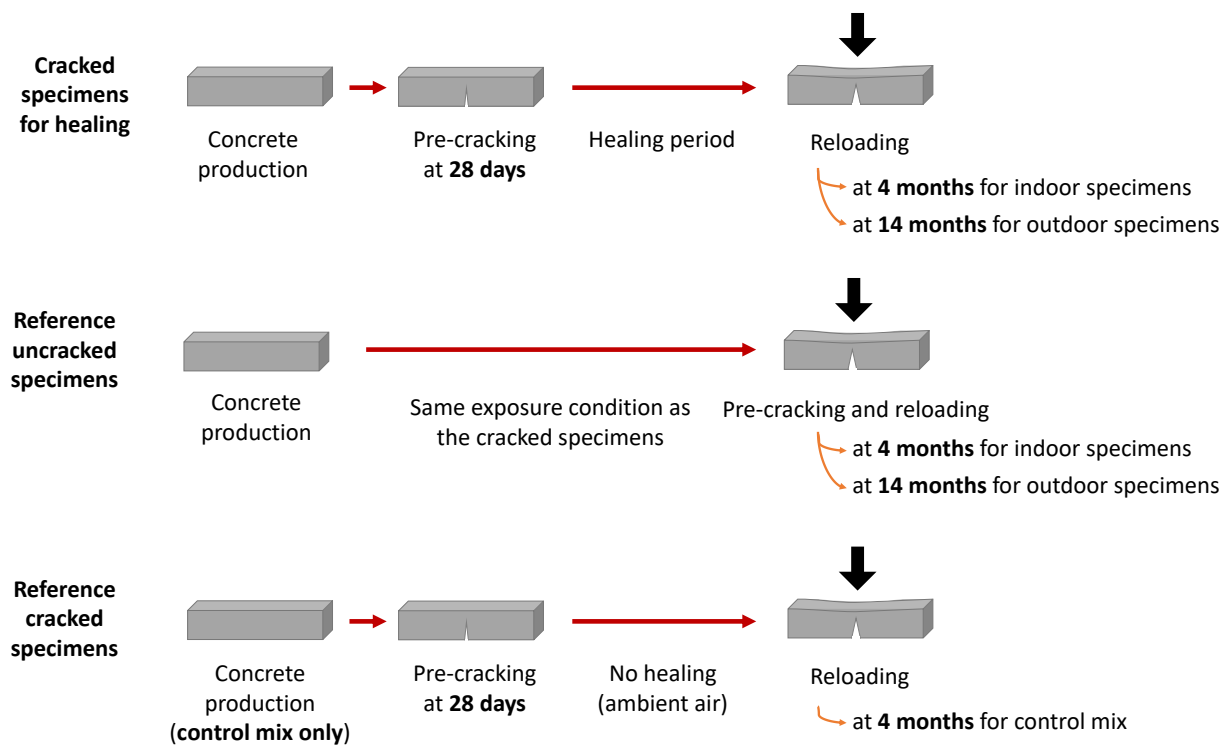
Figure 6.2. Overview of the cracked and uncracked specimens for pre-cracking and reloading phases
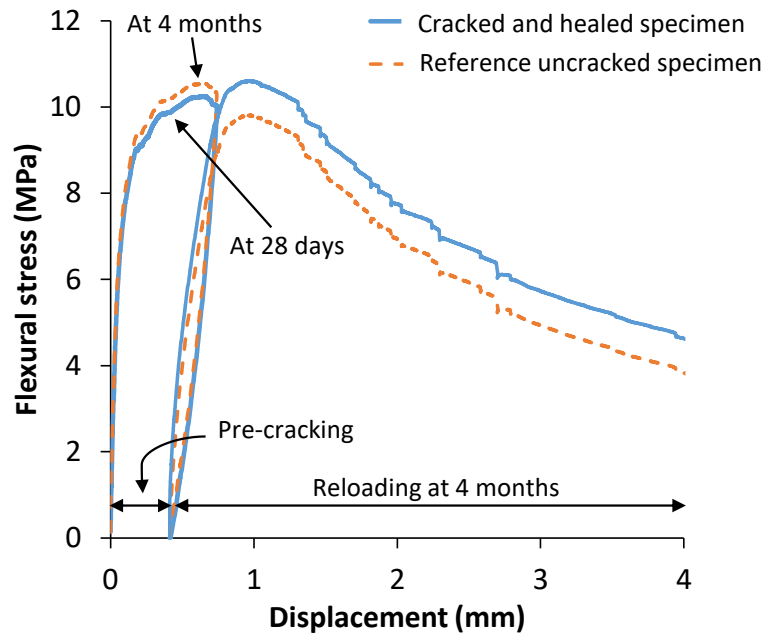
Figure 6.3. Typical flexural curve for pre-cracking and reloading for a cracked and healed specimen (blue line) and the corresponding reference uncracked specimen (orange dashed line)

Figure 6.4 illustrates the individual and average flexural curves obtained for the control prisms immersed in water, with the whole curves (pre-cracking + reloading) in **Figure 6.4a** and a zoom in **Figure 6.4b** to better visualize the pre-cracking phase. In the next sections, only the average curves of each condition will be presented for better visibility. However, the variability of the strength and stiffness regain ratios will be analysed.
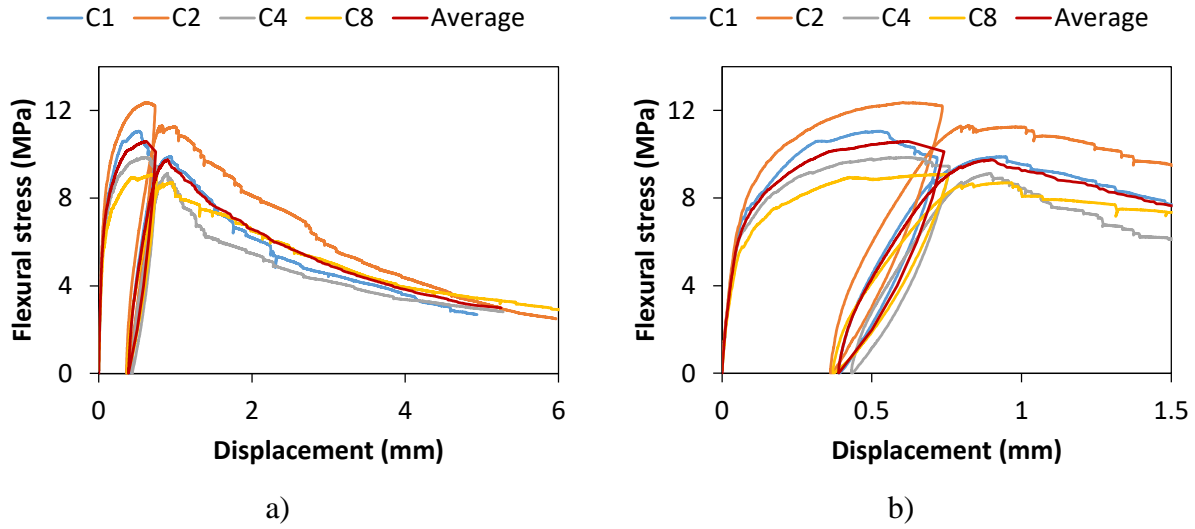
Figure 6.4. Example of an average curve for the control prisms under water immersion, a) the whole pre-cracking and reloading curve and b) zoom at pre-cracking (see web version for the colours)

6.3.4 Mechanical recovery evaluation

Figure 6.5 illustrates the parameters considered to analyse the mechanical behaviour of the different FRC mixes under the various healing conditions and between the healed and companion reference prisms. In the pre-cracking curve, the maximal flexural strength $\sigma_{pre\text{-}load,max}$, the stress before unloading σ_{unload}, as well as the stiffness $K_{pre\text{-}load}$ were determined. In the reloading curve, the maximal flexural stress $\sigma_{reload,max}$, the stiffness K_{reload} and the final displacement at 3 MPa were analysed.
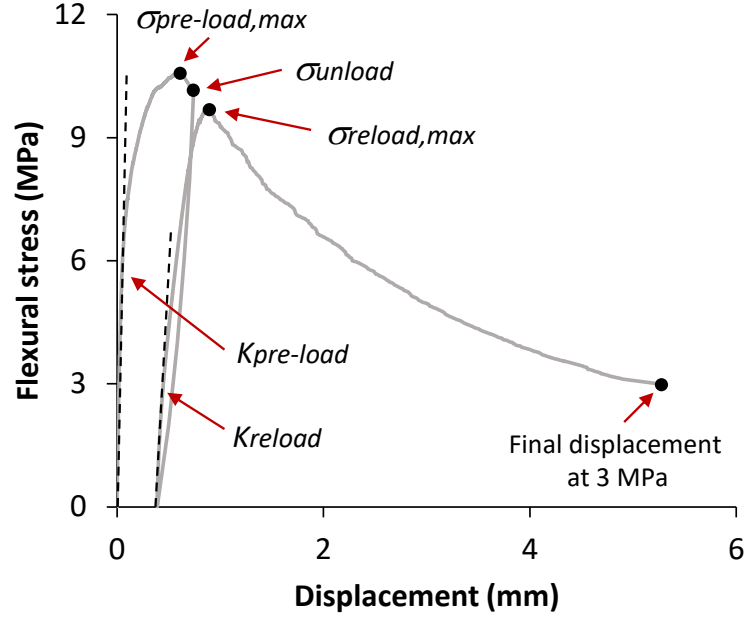
Figure 6.5. Parameters considered to analyse and compare mechanical behaviour of prisms

The stiffness $K_{pre\text{-}load}$ and K_{reload} were calculated with **Eq. 6.9** and **Eq. 6.10** respectively, based on the formula used to calculate the Young's modulus in ASTM C469 [30], with d_1 and d_2 the displacements corresponding to 40% of $\sigma_{pre\text{-}load,max}$ and 40% of $\sigma_{reload,max}$ respectively. The same procedure was used by [21].

$$K_{pre-load} = \frac{0.4\,\sigma_{pre-load,max}}{d_1} \tag{6.9}$$

$$K_{reload} = \frac{0.4\,\sigma_{reload,max}}{d_2} \tag{6.10}$$

To reach the targeted crack width of 0.25 – 0.30 mm, the pre-cracking phase ended near the peak strength or quickly after (**Figure 6.5**). The final pre-cracking stress σ_{unload} was thus high and subtracting this value to $\sigma_{pre\text{-}load,\,max}$ and $\sigma_{reload,\,max}$ to calculate the strength regain like in **Eq. 6.2** (**Table 6.1**) was not optimal. Moreover, as two reference uncracked specimens were used in this project instead of one as [23], the use of **Eq. 6.3** led to high variation in the results depending on the reference uncracked prisms chosen.

Hence, the strength and the stiffness regains were defined by **Eq. 6.7** and **Eq. 6.8** (**Table 6.1**) respectively. They are direct ratios between strength and stiffness values measured at reloading and pre-loading. These regains will be compared to those of the reference uncracked specimens of the same testing condition. Higher recovery indexes than those of the reference specimens will demonstrate the self-healing effect.

6.3.5 Fibres orientation and density analyses

Fibres orientation and density analyses were performed on prisms, following a procedure detailed in [31], to discriminate the effect of the self-healing agents on the mechanical performance of the mixes. Thin vertical slices were extracted from prisms near the crack location and were painted and polished. After digitalisation, the in-house image analysis program automatically counts the number of fibres and detects their orientation angle (via their geometrical characteristics). One specimen per mix and condition (indoor and outdoor), which pre-cracking curve was the closest to the average flexural behaviour of the mix, was analysed.

Eq. 6.11 proposed by [32, 33] was used to evaluate a weighting coefficient (γ_i) for each mix i to adjust the strength values measured in flexural test, with $\theta(°)$ = orientation angle and ρ (fibres/cm²) = density, with respect to the values of the control mix. The orientation angle is defined as the angle formed between the prism vertical plane and the longitudinal axis of the fibre.

$$\gamma_i = \sqrt{\frac{\theta_i}{\theta_{control}} \times \frac{\rho_{control}}{\rho_i}} \qquad (6.11)$$

6.4 Results

6.4.1 Mechanical properties

6.4.1.1 Pre-cracking

The average pre-cracking curves for the indoor mixes are shown in **Figure 6.6a**. From **Figure 6.6a**, it may seem that the concrete mix composition has an impact on the bending behaviour. However, it is known that the fibres orientation affects the flexural performance [33, 34]. Due to the inherent

variation of the fibres distribution in each prism at casting, fibres well oriented to control crack in the prism will lead to higher flexural performance.

Table 6.4 shows the density ρ, the average orientation angle θ and the weighting coefficient γ (**Eq. 11**) for the analysed specimen of each mix exposed indoor. The stress values of each average flexural curve of **Figure 6.6a** were multiplied by their corresponding γ. The resulting weighted curves are presented in **Figure 6.6b**. The associated initial and weighted average maximal stresses $\sigma_{pre\text{-}load,max}$ obtained for each mix are presented in **Figure 6.7a** and **Figure 6.7b** respectively.

Table 6.4. Results from the fibres orientation and density analyses for the indoor mixes

Mix	Density ρ (fibres/cm²)	Orientation angle θ (°)	Weighting coefficient γ (-)
Control	2.47	45.3	1.00
CSA	2.54	40.1	0.93
CA	2.32	43.1	1.01
SAP	1.78	37.5	1.07
CA+SAP	1.32	38.1	1.25
CA+CSA	2.20	38.3	0.98

From **Figure 6.6** and **Figure 6.7**, the effect of the fibres orientation and density on the flexural stress is obvious. For example, the CA+SAP mix had an initial maximal stress of 8.2 MPa and this value increased by 25% (10.3 MPa) after the fibres analyses. This is mainly due to its lowest fibres density (1.32 fibres/cm²).

Overall, when considering the fibres efficiency (**Figure 6.6b** and **Figure 6.7b**), there are no significant differences between the tested FRC mixes, except the CA mix that stood out with the lowest and less hardening flexural performance. This mix already stood out before the fibres analyses. The standard deviations of $\sigma_{pre\text{-}load,max}$ before the fibres analyses (error bars in **Figure 6.7a**) were in the same order for each mix. The coefficients of variation (COV) ranged from 13% (control mix) to 20% (CA mix). In conclusion, except the CA mix that presented a lower flexural performance, all the other mixes performed similarly. These trends were similar for the outdoor mixes.
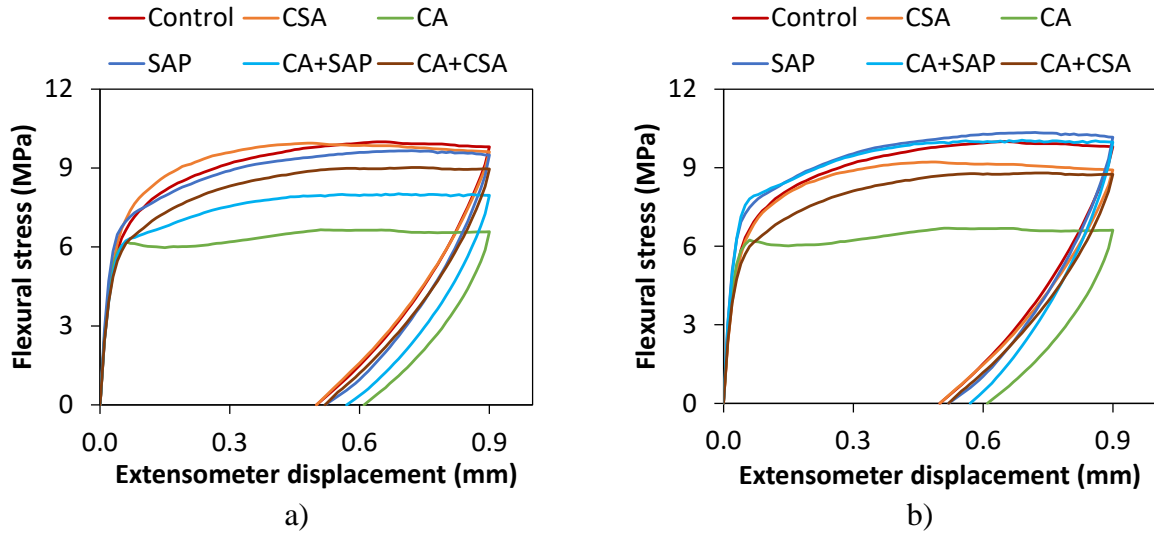
Figure 6.6. Average pre-cracking curves for indoor mixes a) before and b) after consideration of fibres orientation and density analyses (see web version for the colours)
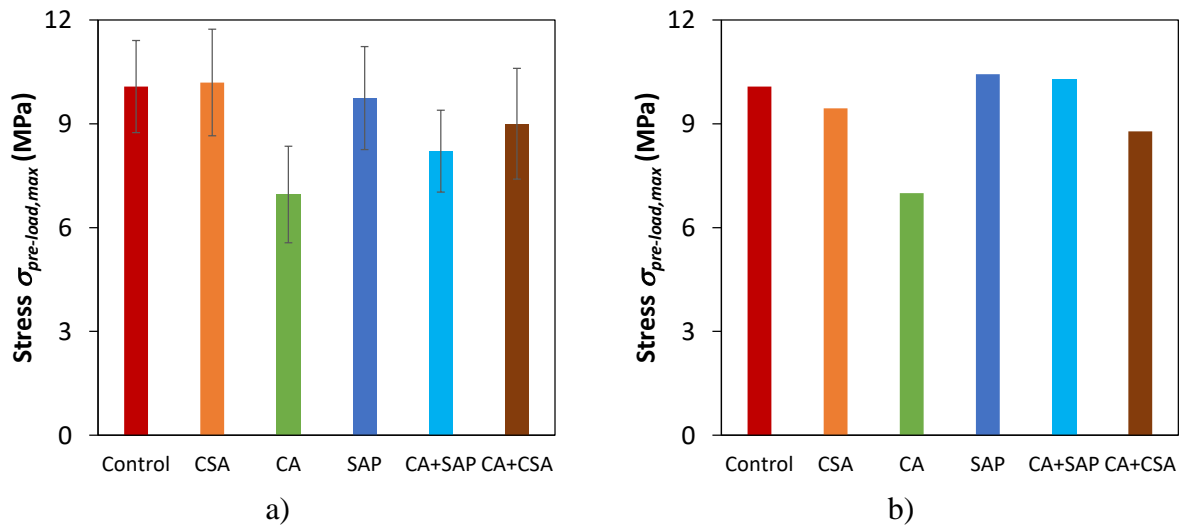
Figure 6.7. Average maximal pre-cracking stress for indoor mixes a) before and b) after fibres orientation and density analyses

Weighting coefficients were only used to analyse the global mechanical performance of the different mixes before healing. In the following sections, where the mechanical behaviour of prisms after healing is analysed, unweighted results are considered.

6.4.1.2 Strength recovery

The average flexural results for the control mix in all expositions are shown in **Figure 6.8**. **Figure 6.8a** presents the average flexural curves of the healed cracked specimens in all expositions, while **Figure 6.8b** shows an example of the same healed specimens in air and wet/dry exposures only in comparison to their reference uncracked specimens. Then, the Strength Regains (*SR*) calculated with **Eq. 6.7** for all the healed prisms and their associated uncracked reference prisms of the control mix are illustrated in **Figure 6.8c**.

A Strength Regain equals to 100% means that a prism after healing ($\sigma_{reload,max}$) has the same strength as at unloading (σ_{unload}) (**Figure 6.5**). The reference uncracked specimens never reached a Strength Regain above 100% (*SR* = 89% in water, 96% in wet/dry and outdoor and 87% in air) because of the post-peak phase. In contrast, the Strength Regains of the healed cracked specimens were higher (*SR* = 92% in water, 98% in wet/dry, 110% outdoor and 90% in air) than the reference prisms, hence demonstrating the impact of self-healing. This was the case for all mixes as well.

The influence of the exposition is shown in **Figure 6.8a** and **Figure 6.8c**. The outdoor exposure stood out with the highest Strength Regain (*SR* = 110%), while the results in various indoor conditions were lower and not significantly different.

The greater performance of the outdoor specimens may be explained by the combination of the higher maturity of the prisms, as they were reloaded at the age of 14 months, and the self-healing. However, several reasons demonstrate that the greater performance is mainly related to the healing process. First, in pre-cracked prisms, the crack mainly controls the flexural performance at reloading and not the concrete matrix. In such case, the effect of the higher maturity of the matrix is negligible. Secondly, the comparison between the flexural behaviour of the reference uncracked and reference cracked prisms of the control mix exposed in ambient air (**Figure 6.2**) also indicated a negligible impact of the concrete maturity. In fact, both specimens performed very similarly (from the flexural curves in **Figure 6.8b** and the Strength Regain in **Figure 6.8c**) despite the older age (4 months versus 28 days) of the uncracked prisms at pre-cracking. As no maturity effect was visible after 4 months, one could assume that the maturity effect was also negligible after 14 months considering that the hydration process evolves more slowly than between 28 days and 4 months.

In addition, the maturation of the outdoor prisms was negligible when they were exposed to average temperatures below 0°C during 5 months.

a)

b)

c)
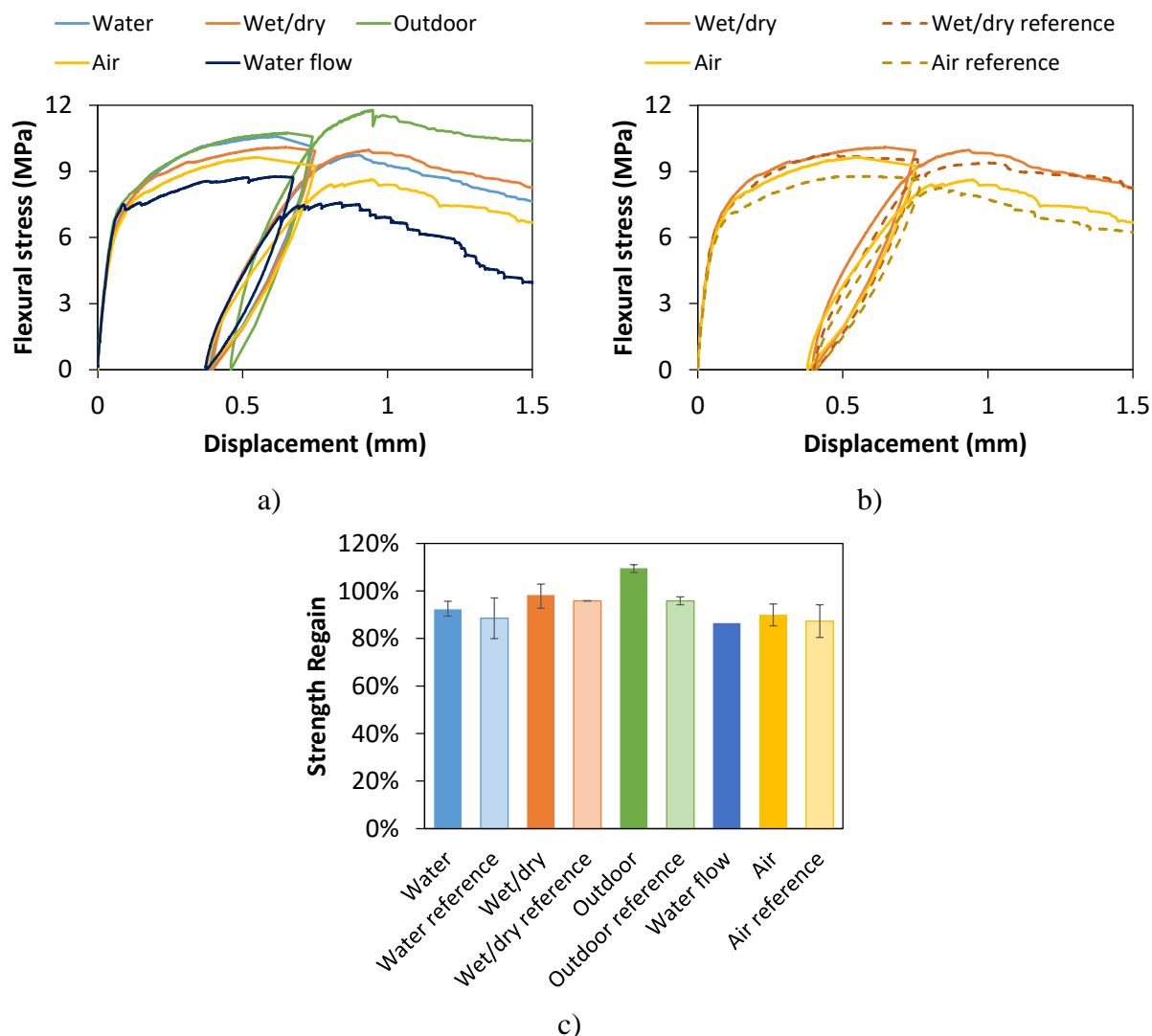
Figure 6.8. Average results for the control mix in all expositions a) flexural curves, b) comparison with uncracked references and c) Strength Regain (see web version for the colours)

Finally, the Strength Regains obtained for the healed cracked specimens of all mixes are compared in **Figure 6.9**. As previously observed for the control mix, the outdoor specimens of all mixes stood out from the other exposure conditions ($SR = 106\%$ in average). In average for all mixes, the Strength Regains of prisms in wet/dry cycles ($SR = 99\%$) were always higher than those for the prisms in water immersion ($SR = 95\%$). However, with the variation of the error bars (min and max of the results), the difference is not very significant. The prisms subjected to a continuous water

flow reached a Strength Regain between 83% and 101%. However, as there was only 1 specimen per mix in this exposure condition, no clear conclusion can be drawn. This exposure condition was not specifically tested to evaluate its impact on the mechanical regains, but for verifying if it could accelerate self-healing compared to still water immersion. It was not the case, as found in the companion paper (part 1) [3].

As found in the water permeability results, the impact of the exposition was greater than the effect of the mix compositions. The influence of the self-healing agents will be thoroughly discussed in **Section 6.5.2**.
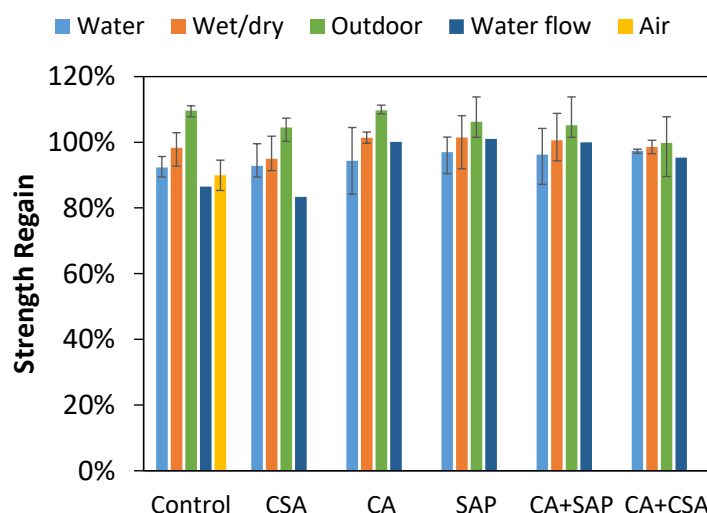
Figure 6.9. Strength Regain for all mixes and expositions

6.4.1.3 Stiffness recovery

The stiffness recovery ratios of the control mix, illustrated in **Figure 6.10**, ranged from 23% to 41% for the healed specimens. These values are significantly lower than the strength recovery ratios. This was expected as the Stiffness Regain (**Eq. 6.8**) compares a cracked state (during reloading) with the elastic state at pre-cracking, while the Strength Regain (**Eq. 6.7**) compares two cracked states (at reloading versus at pre-cracking). For the control mix, the healed cracked prisms showed higher Stiffness Regains than the corresponding reference uncracked prisms. However, this was not the case for all mixes. Moreover, it can be observed that the Stiffness Regain inside a same exposure condition was mainly proportional to the mechanical performance at pre-cracking, as demonstrated in **Figure 6.11**. This is logical since a higher efficiency of the fibres (linked to a

higher value of $\sigma_{pre\text{-}load,max}$) implies a higher cracked stiffness even during reloading (K_{reload}), whereas the elastic stiffness ($K_{pre\text{-}load}$) stays the same for all prisms regardless of the fibres efficiency. In consequence, the effect of self-healing is probably hidden by the impact of the fibres efficiency and no conclusion can be drawn regarding the impact of self-healing on the stiffness recovery. However, some differences can be observed in **Figure 6.11**, when comparing the Stiffness Regains of the outdoor and the indoor mixes. Despite similar pre-cracking behaviours and thus a same range of $\sigma_{pre\ load,max}$ values (6 to 12 MPa) obtained, the Stiffness Regain of the outdoor mixes was in average 44% higher than the one of the indoor mixes. This shows an impact of the self-healing in outdoor exposure and it is coherent with the higher mechanical regain observed through the Strength Regain for that condition in **Section 6.4.1.2**
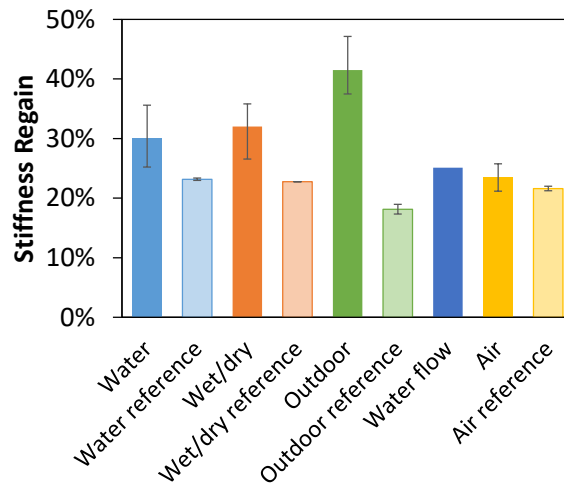
Figure 6.10. Average Stiffness Regains for the control mix in all expositions
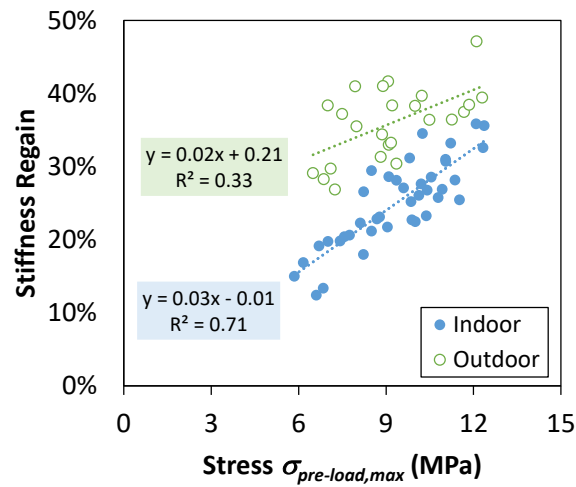
Figure 6.11. Stiffness Regains vs maximal pre-load maximal strengths for all indoor and outdoor mixes

6.4.1.4   Deflection capacity and failure

The global average pre-cracking and reloading curves of prisms are shown for water immersion (**Figure 6.12a**), wet/dry cycles (**Figure 6.12b**) and outdoor exposure (**Figure 6.12c**). In average, the deflection capacity (fixed as the final displacement at 3 MPa) ranged from 4.5 to 6 mm for all mixes and expositions, with a few exceptions reaching above 8 mm and the CSA mix outdoor reaching below 4 mm. The goal of this analysis was to evaluate the impacts of the exposure condition and the self-healing agents on the ductility of the concrete prisms. However, from **Figure 6.12**, no clear trends can be found except the reduced ductility of the control prisms kept in air ambient with limited healing. Additional correlation analyses showed no particular relationships between the deflection capacity and the mechanical (pre-cracking behaviour and mechanical regain), nor the self-healing (Healing Ratio) performances.
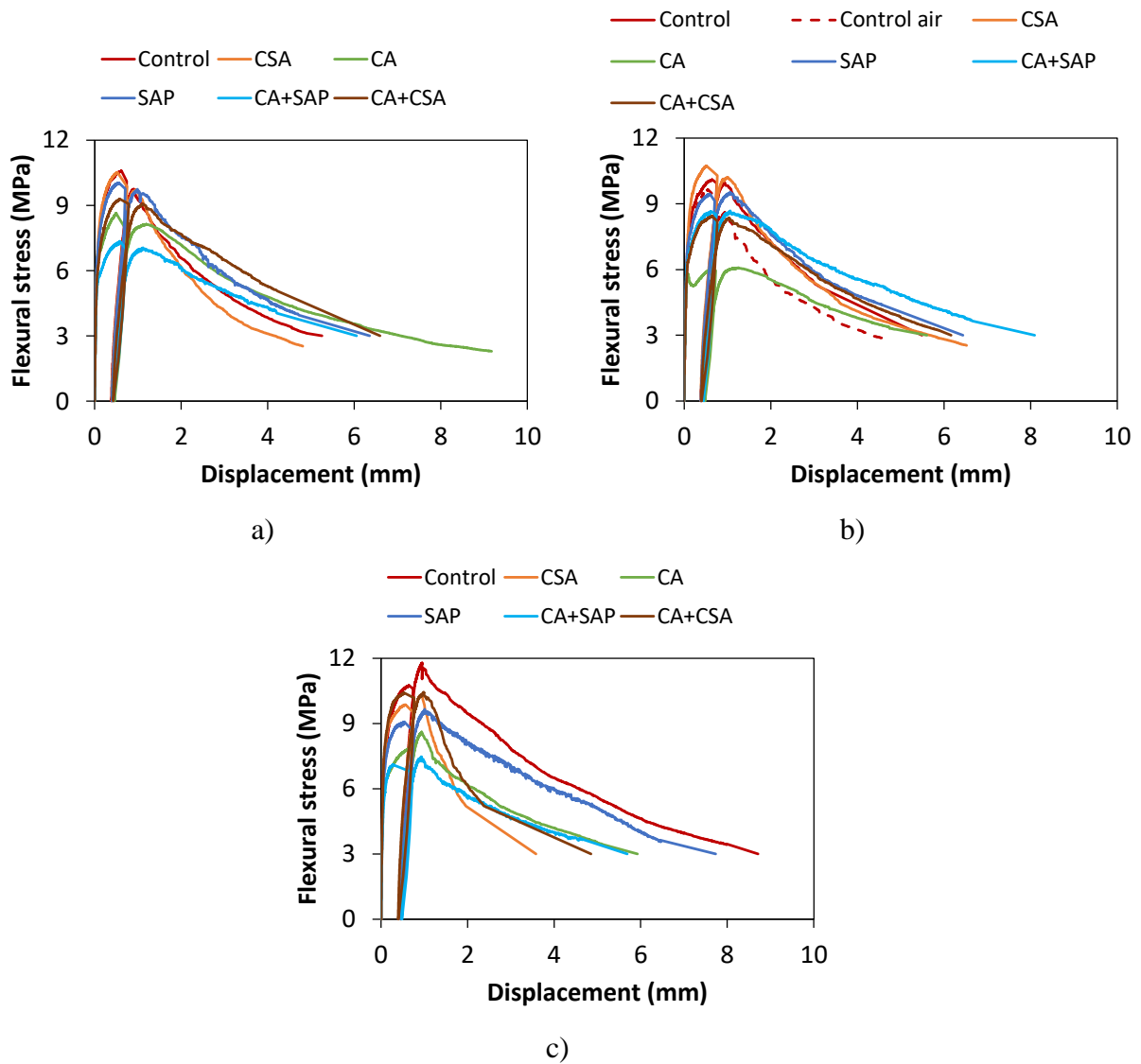
Figure 6.12. Whole pre-cracking and reloading curves in a) water, b) wet/dry cycles and c) outdoor expositions

6.4.2 Mechanical (Strength Regain) vs durability (Healing Ratio) recoveries

A summary of the Strength Regains and final Healing Ratios retrieved from water permeability measurement in the companion paper [3] is shown in **Figure 6.13** for all mixes and expositions. **Figure 6.13a** shows the results per exposition, while **Figure 6.13b** presents the results per mix in wet/dry and outdoor exposures. In both cases, the Strength Regains were not correlated to the final Healing Ratios.

Results presented according to the healing exposition (**Figure 6.13a**) highlight that the outdoor condition differentiated again with the highest Strength Regains ($SR = 106\%$ in average), while the HR ranged from 30% to 97% with an average value of 71%. In wet/dry cycles, despite the best healing performance ($HR = 93\%$ in average), the Strength Regain was lower ($SR = 99\%$ in average). In water immersion, the average HR and SR reached 85% and 95% respectively.

Results presented according to the mix (**Figure 6.13b**) show that the Strength Regain was not correlated to the final Healing Ratio regardless of the mix. For example, the CSA and CA+CSA mixes presented the highest average $HR = 99\%$ in wet/dry, but achieved $SR = 95\%$ and 99% respectively. In contrast, the CA+SAP mix had the lowest $HR = 80\%$ in wet/dry, but reached $SR = 101\%$.

These results mean that a prism that did not heal efficiently from permeability measurements can have a high Strength Regain, and vice versa. The macroscopic observations (distribution of healing products in the crack) and microscopic analyses (density and types of healing products) will bring explanations for this observation (**Section 6.5.4**).
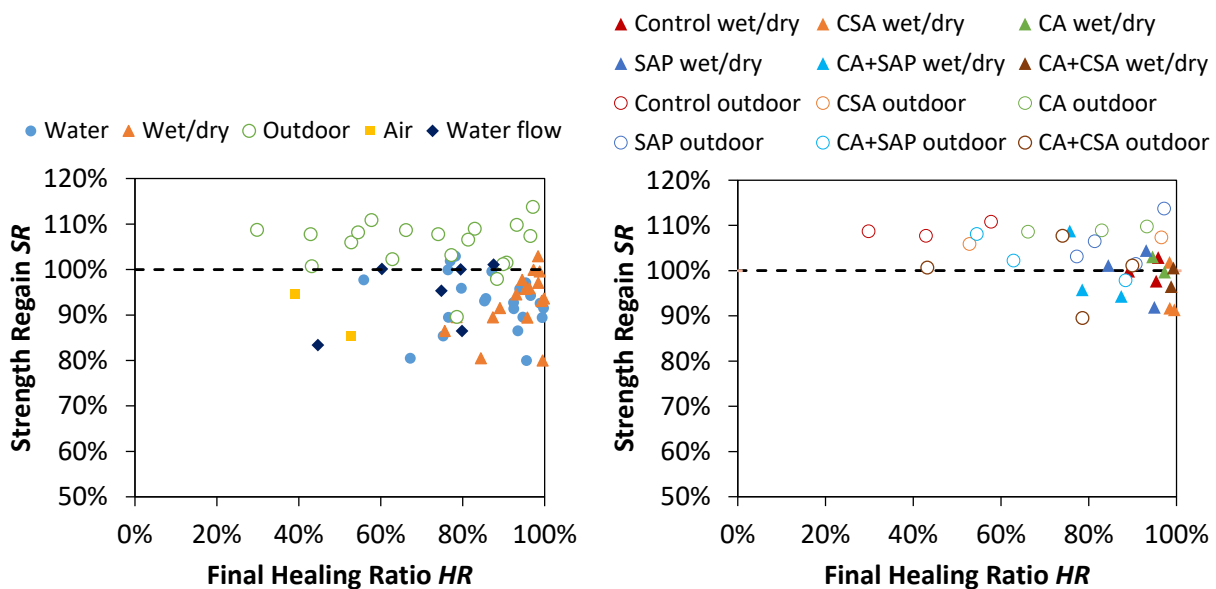
Figure 6.13. Strength Regains vs final Healing Ratios for all mixes a) per exposition and b) per mix in wet/dry and outdoor exposures

6.4.3 Macro- and microscopic observations

6.4.3.1 Macroscopic observations

Pictures of local sections of cracks of similar widths are shown in **Figure 6.14** to illustrate the non-concordance between visual observations, Healing Ratio and Strength Regain for two different prisms of the control mix exposed in several conditions. The upper and lower photos illustrated the cracks before and after healing, respectively. Under water, white products filling completely the crack section can be seen (**Figure 6.14a**), in contrast to the crack in **Figure 6.14b** that was not completely sealed in outdoor exposure. Specimen C2 reached $HR = 100\%$ and $SR = 91\%$ after 3 months under water immersion. Specimen C1 attained a lower HR of 43% (after 12 months outside), but a higher SR of 108%. This demonstration reveals that criteria to obtain healing from mechanical and durability properties are different.

$w_i = 0.20$ mm, $HR = 100\%$, $SR = 91\%$
a) Specimen C2 after 3 months in water

$w_i = 0.20$ mm, $HR = 43\%$, $SR = 108\%$
b) Specimen C1 after 12 months outside
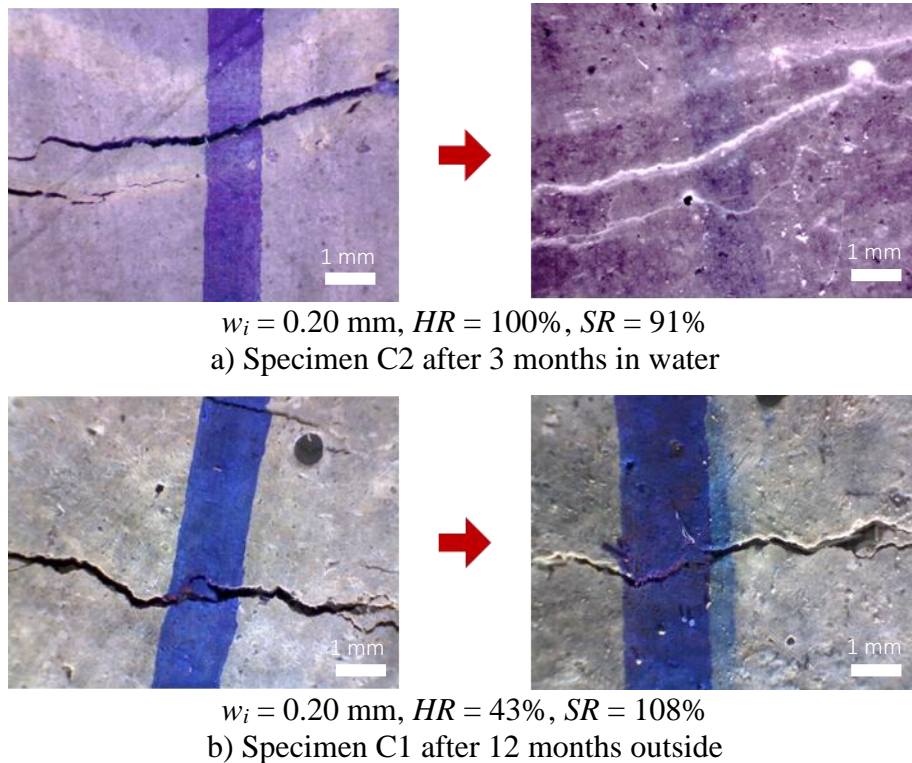
Figure 6.14. Macroscopic pictures of the healing of local sections of cracks for control mix a) after 3 months in water and b) after 12 months outside

After reloading, some prisms were cut to analyse the fractured crack surfaces. Complementary macroscopic observations with binoculars were performed on some of these fractured crack samples. **Figure 6.15** shows pictures of samples for the SAP mix at the crack surface (**Figure 6.15a** and **Figure 6.15c**) and inside the crack (**Figure 6.15b** and **Figure 6.15d**). Under water immersion, a lot of white products can be seen at the crack surface (**Figure 6.15a**) compared to inside the crack (**Figure 6.15b**). Outdoor, less white products are visible as the self-healing was lower, but healing products can be observed at the surface (**Figure 6.15c**) and also inside the crack (**Figure 6.15d**). This trend was similar for all mixes. **Figure 6.14**, also confirmed the presence of more healing products at the crack surfaces for indoor conditions compared to the outdoor exposure. Furthermore, more white products can be seen around a SAP void in **Figure 6.15d**.
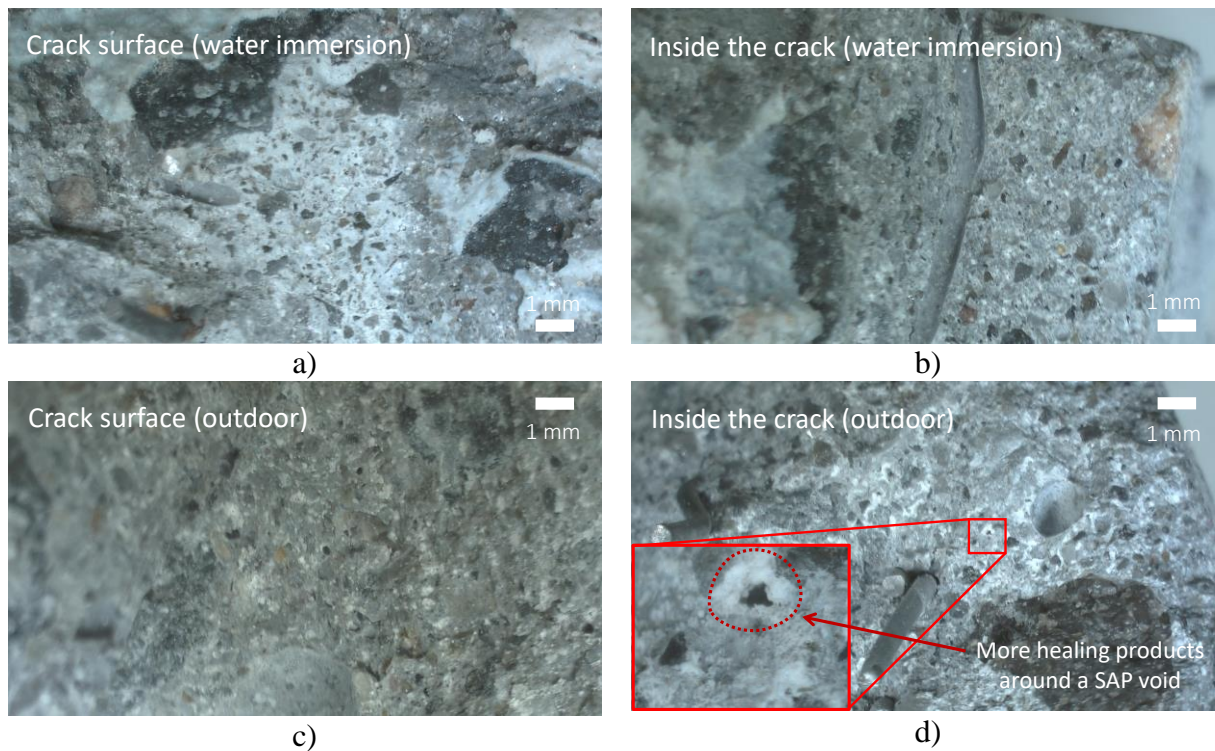
Figure 6.15. Macroscopic observations with binoculars of SAP mix a) under water near the surface, b) under water inside the crack, c) outdoor near the surface and d) outdoor inside the crack

6.4.3.2 Microscopic analyses (SEM-EDS)

The fractured crack samples (at cracks surfaces) were also analysed with SEM-EDS. In the companion paper [3], the microscopic analyses helped to identify different types and densities of healing products according to the exposure condition. In this study, the microscopic analyses focused on the difference between the mix compositions.

Figure 6.16a shows the microstructure and an EDS spectrum of the control mix before healing. The other pictures present the healing products after healing in water on prisms of the control (**Figure 6.16b**), CSA (**Figure 6.16c**), CA (**Figure 6.16d**) and SAP (**Figure 6.16e**) mixes. The presence of healing products is obvious when comparing the microstructure before and after healing (**Figure 6.16a**-**b**). The matrix of the control mix before healing showed typical hydration products (C-S-H, portlandite, aluminate phases) revealed by major peaks of Ca, O, Si and minor peaks of Al, Mg and K as seen in the EDS spectrum.

After healing in water, all mixes showed presence of calcium carbonates ($CaCO_3$) and ettringite at crack surfaces (**Figure 6.16b-e**), as confirmed by major peaks of Ca, S and Al in EDS spectra (not shown). C-S-H was also found in all mixes. $CaCO_3$ was mainly in the form of calcite for all mixes. Polymorphs of $CaCO_3$ as well as the densities were more influenced by the exposition [3] rather than the mixes. Concerning the ettringite, one characteristic varied according to the mix composition. Longer needles were observed for CSA, CA and SAP mixes (**Figure 6.16c-e**) in comparison to the control mix that showed very small and short needles (**Figure 6.16b**). Another characteristic of the microscopic observation of the SAP mix is the presence of voids left by shrunk SAP particles (**Figure 6.16e**). The microscopic analyses on CA+SAP and CA+CSA mixes were not different from the ones of CA, SAP and CSA mixes presented here.

In conclusion, although some differences of microstructure could be observed between the different FRC mixes, there were no major distinctions (same types of healing products and similar densities) between them.
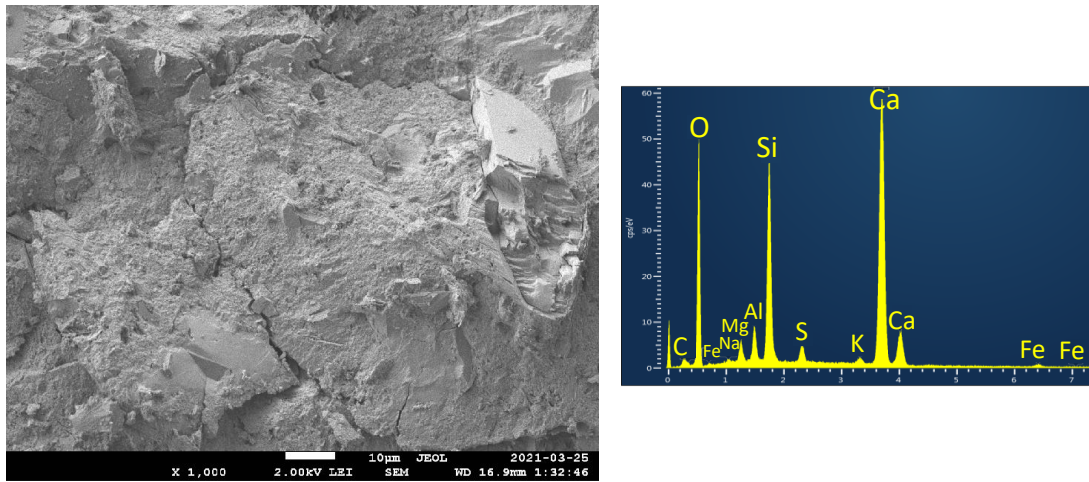
a) Control before healing (X 1000)
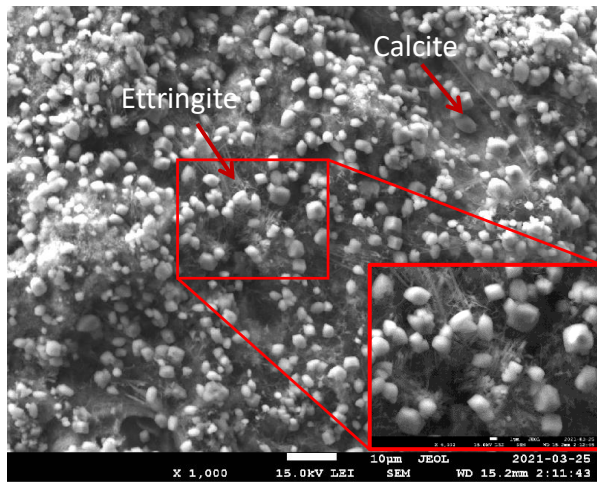
b) Control after healing (X 1000)
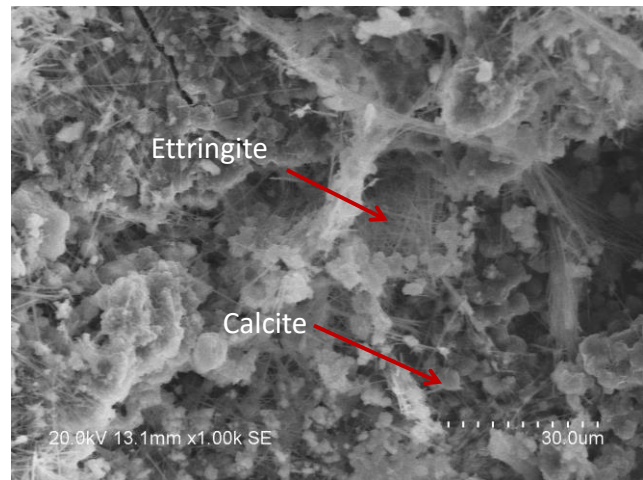
c) CSA after healing (X 1000)
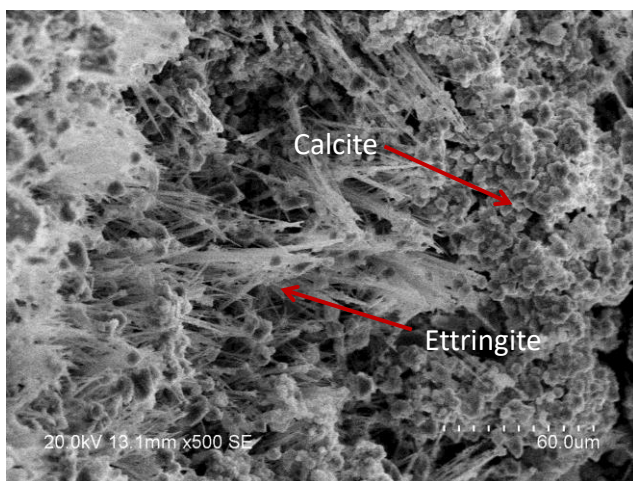
d) CA after healing (X 500)
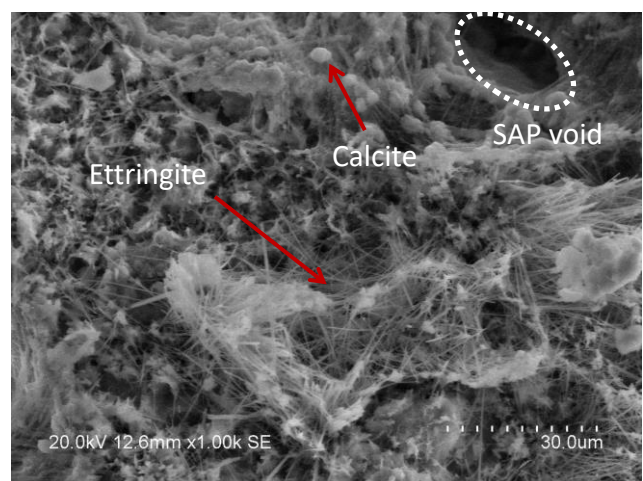
e) SAP after healing (X 1000)

Figure 6.16. Microstructure for different mixes: a) control before healing, b) control, c) CSA, d) CA and e) SAP after healing under water

6.5 Discussion

6.5.1 Influence of the exposure condition on the Strength Regain

The influence of the exposure condition can be examined in **Figure 6.8a** (flexural curves for the control mix), **Figure 6.8c** (Strength Regain for the control mix) and **Figure 6.9** (Strength Regain for all mixes). The highest Strength Regains were obtained in outdoor ($SR = 106\%$ in average for all mixes), followed by wet/dry ($SR = 99\%$ in average) and water expositions ($SR = 95\%$ in average).

Considering the errors bars in **Figure 6.9**, the Strength Regains were not significantly different for the wet/dry cycles and water immersion, but they were in average superior to 100% for all mixes in outdoor exposure. In contrast, Ferrara et al. [13] did not find enhanced strength recovery for specimens exposed outside for 1 year compared to water immersion for 3 months.

The control specimens in air exposure representing poorly healed specimens showed lower Strength Regain ($SR = 90\%$ in average), but with no major difference with the regains obtained under water and wet/dry expositions. Sisomphon et al. [35] also found flexural strength of the specimens in air condition close to water and wet/dry (12h wet/12h dry) expositions. They also observed overall the best performance in wet/dry cycles, followed by water and air exposure conditions as found in this study. Escoffres et al. [16] also did not observe significant difference between the strength regains of cracked flexural prisms in water and in air expositions. Finally, Snoeck et al. [15, 19] observed lower strength regains for the specimens in humid chamber (60% and 90% relative humidity) than for the ones subjected to wet/dry cycles (1 day wet/1 day dry).

The various specimens, dimensions, concrete composition but especially, the loading procedures could explain some differences observed between studies. It must be noted that most studies pre-loaded their specimens clearly beyond the peak load, resulting in a longer post-peak phase in contrast to this present project. The strength recoveries were also determined with various indexes that impede strict comparisons. Nevertheless, the trends observed were overall in agreement with the literature.

It must be noted that the impact of the exposition on the strength recovery was less important than on the durability recovery (average Healing Ratios of 93%, 84% and 71% in wet/dry, water immersion and outdoor exposures respectively) [3].

6.5.2 Influence of the self-healing agents on the mechanical properties

The impact of the self-healing agents on the mechanical properties, compressive strength (**Table 6.2**), flexural pre-cracking (**Figure 6.6** and **Figure 6.7**) and Strength Regains (**Figure 6.9**), was limited. During pre-loading of prisms, only the CA mix showed lower flexural stresses even after consideration of the orientation and density of the fibres. In opposite, other studies obtained similar flexural strengths for CA mix compared to the control mix [16, 35]. More investigation is needed to explain such results.

The Strength Regains ranged from 92% to 97% in water immersion, from 95% to 101% in wet/dry cycles and from 100% to 110% in outdoor exposure for all mixes (**Figure 6.9**), with a global average of 100% and a coefficient of variation (COV) of 5%. Variations between FRC mixes are slightly greater that this COV value, which limits clear distinction of the effect of the different mixes. However, CA and SAP mixes presented high Strength Regains both in wet/dry ($SR = 101\%$ for both mixes) and outdoor exposures ($SR = 110\%$ and 106% respectively), while CSA mix presented lower Strength Regains $SR = 95\%$ in wet/dry and 105% outdoor) than CA and SAP mixes. Furthermore, the combinations CA+SAP and CA+CSA generally did not show better Strength Regains than the admixtures alone.

Comparison with literature will here focus on studies with similar crack widths as those studied in this research. Consistently with this study, Buller et al. [22] observed similar strength recoveries for a control mix and a combination of products with CSA (sodium carbonate, calcium stearate + CSA + bentonite) on specimens with crack widths superior to 100 µm. Escoffres et al. [16] did not find any significant difference between the control and CA mixes either (crack width around 0.2 mm), in terms of flexural strength recovery of cracked specimens kept in water immersion (strength recoveries of 85% and 90% for the control and CA mixes respectively) or at ambient laboratory air (77 and 76% respectively). In contrast, Ferrara et al. [13] reported a major beneficial effect of their CA mix compared to the control mix (crack width of 0.1 – 0.2 mm), whether exposed outside for 1 year or in water for 3 months. Concerning the SAP performance, Van Tittelboom et al. [28] did not find differences of mechanical recovery between the control and SAP mixes either (crack width around 0.2 mm). Finally, the synergetic effect of self-healing agents on the strength recovery was not often studied. Sisomphon et al. [35] found a synergy for their CA+CSA mix in comparison to

the mixes with the admixtures alone. However, this synergetic effect was more visible in terms of deflection capacity than of flexural strength for their strain-hardening cementitious composites (crack width of 0.01 – 0.05 mm). In conclusion, the trends observed in this study are generally in agreement with results in literature.

It must be noted that the low impact of the concrete mix composition on the strength recoveries of the healed prisms was also observed in the durability recovery results showed in part 1 [3].

6.5.3 Influence of the self-healing agents on the healing products

The healing products found in this project were generally in line with the ones found in literature. For the CSA mix, calcium carbonate and long ettringite needles were seen under water immersion (**Figure 6.16c**), which is in agreement with Sisomphon et al. [36] in the same condition. This is logical as ettringite is a reaction product of CSA [8, 35]. This is also consistent with the needle-type hydrates found by Park & Choi [8] in their mixture containing CSA and CA.

The CA mix led to formation of calcium carbonate and long ettringite needles under water as well (**Figure 6.16d**). Wang et al. [7] and Ferrara et al. [13] also observed ettringite in their mix with CA. They found typical hydration products of cement, with an additional peak of sulphur compared to their control mix. It must be noted that in this project, a peak of S was present in the matrix before healing (**Figure 6.16a**). Cuenca et al. [37] found calcium carbonate in cubic and acicular forms in specimens with CA compared to the control mix, where only cubic $CaCO_3$ was observed. On the other hand, Escoffres et al. [16] found aragonite in their mix with CA instead of ettringite and calcite in their control mix. The formation of aragonite was explained by their crystalline admixture containing a high amount of magnesium.

The SAP mix showed calcium carbonate and long ettringite needles under water immersion (**Figure 6.16e**). Acting as water reservoirs, the SAP particles may have provided additional water to form more ettringite compared to the control mix. This was also reported by Park & Choi [8], who observed more ettringite in their mixes with SAP. In addition, more healing products could be seen around SAP voids (**Figure 6.15d**), as observed by Park & Choi [8].

6.5.4 Interpretation of water permeability, mechanical and macro- and microscopic results

Table 6.5 presents a summary of the relevant permeability, mechanical and SEM-EDS results for all FRC mixes and the main expositions investigated (water, wet/dry and outdoor). The final Healing Ratios (*HR*) and Strength Regains (*SR*) are presented in descending order, which also represents decreasing performances (from very high to low). For the microscopic analyses, the same order as for *HR* was kept and the density of the healing products (very dense to less dense) as well as the type of the main observed healing products are reported as well. C-S-H was found in all exposure conditions in this project, but it was not listed in **Table 6.5**, since no differences could be observed between the expositions or mix compositions. Finally, the last column summarizes complementary qualitative observations performed with a digital microscope (**Figure 6.14**) and with binoculars on fractured samples at the crack surfaces or inside the cracks (**Figure 6.15**).

The micro- and macroscopic analyses of the type and distribution of the healed products may explain the non-correlation between the durability and mechanical recoveries. As explained in **Section 6.4.3.1**, the healing products in outdoor exposure were more distributed in the crack depth in comparison to the water or wet/dry exposure conditions, where the products were mainly at the crack external surfaces. This could be explained by the slower healing process in outdoor exposure compared to indoor conditions. For the prisms subjected to water immersion or wet/dry cycles, the cracks healed faster and rapidly covered the external surfaces that were directly exposed. This fast healing at external surface then blocks other reactants to penetrate inside the crack so that the crack is less healed in depth. For the prisms exposed outdoor, more reactants could penetrate inside the crack, forming healing products inside. The better distribution of these products inside the crack but with less occurrences at the crack external surfaces could explain a greater effect on the Strength Regain despite a lower effect on the Healing Ratio.

In addition, the density and nature of the healing products in the self-healed zones can also explain the results obtained in durability and mechanical tests. First, high Healing Ratios were obtained when the densities of products were high. As an example, the highest *HR* were obtained for the wet/dry cycles, which provided the highest densities of healing products. The denser the products, the better they fill up and seal the crack against water penetration. This is in agreement with the

results found by Park & Choi [38], who correlated the greater water flow reductions with higher amounts of healing products measured by thermogravimetric analysis (TGA). The healing products observed in water and outdoor expositions were less dense. But at a macroscopic scale, the healing products were covering the whole external crack surfaces in water immersion in contrast to outdoor exposure where less products were found, which probably explains the lowest *HR* obtained in outside condition.

Secondly, the type of healing products impacted the Strength Regain, regardless of the Healing Ratio. Higher Strength Regain could be related to healing products' stiffness, as ettringite, calcite and vaterite have an average Young modulus of 26 GPa [39], 68 GPa and 44 GPa [40] respectively. For example, the Strength Regains were lower in water immersion than in wet/dry cycles, the latter having only the stiffer products (calcite and vaterite). Concerning the outdoor condition, in addition to more products inside the crack as explained before, the presence of large calcite crystals may have also contributed to the highest Strength Regain.

In conclusion, the density of the healing products covering the crack surface may control the Healing Ratios, while the type of the healing products and their presence inside the crack may govern the mechanical recovery. More investigation with 3D scan or other techniques is needed to confirm these assumptions.

Table 6.5. Summary of the water permeability, mechanical and SEM-EDS results (see web version for colours)

	Permeability recovery		Mechanical recovery		Microscopic analyses			Macroscopic observations
	Final Healing Ratio		Strength Regain		Density		Type	
Water	Control	0.98	CA+CSA	0.97	Control	+	Ettringite and calcite	Healing products covering the whole external crack surfaces, few inside the cracks
	CSA	0.86	SAP	0.97	CSA	+		
	SAP	0.85	CA+SAP	0.96	SAP	+		
	CA+SAP	0.83	CA	0.94	CA+SAP	+		
	CA+CSA	0.77	CSA	0.93	CA+CSA	-		
	CA	0.74	Control	0.92	CA	+		
Wet/dry	CA+CSA	0.99	SAP	1.01	CA+CSA	++	Calcite and vaterite	Healing products covering the whole external crack surfaces, few inside the cracks
	CSA	0.99	CA	1.01	CSA	++		
	CA	0.96	CA+SAP	1.01	CA	+		
	Control	0.93	CA+CSA	0.99	Control	++		
	SAP	0.91	Control	0.98	SAP	++		
	CA+SAP	0.80	CSA	0.95	CA+SAP	+		
Outdoor	SAP	0.87	CA	1.10	SAP	+	Calcite (larger crystals observed)	Healing products covering less the external surfaces, but more present inside the cracks
	CA	0.81	Control	1.10	CA	+		
	CSA	0.74	SAP	1.06	CSA	-		
	CA+CSA	0.71	CA+SAP	1.05	CA+CSA	+		
	CA+SAP	0.69	CSA	1.05	CA+SAP	+		
	Control	0.43	CA+CSA	1.00	Control	+		

Permeability	Mechanical	Density
Very high	Very high	++ Very dense
High	High	+ Dense
Moderate	Moderate	- Less dense
Low		

6.5.5 Concrete mix with the best self-healing performance

From the companion paper [3] detailing the permeability measures, the concrete mixes containing CA and SAP presented the best self-healing performances in terms of initial *HR* (quickly healing), final *HR* (healing intensity), final equivalent crack closure (potential for further healing) and considering essentially the performance in realistic outdoor condition.

Considering the mechanical performance, a mix with a good initial flexural behaviour ($\sigma_{pre-load,max}$ in **Figure 6.7**) is expected before any healing. Then, the self-healing performance in terms of Strength Regain (**Figure 6.9** and **Table 6.5**) and performance in outdoor condition are essential.

Finally, a high deflection capacity (**Figure 6.12**) provides more ductility before failure. In regard to these criteria, the SAP concrete mix is the best candidate, while the CA mix ranked second because of its lower initial flexural behaviour.

6.6 Conclusions

This paper is the second part of a research project about self-healing of fibre reinforced concrete containing different admixtures, pre-cracked at 28 days by means of a 3-point bending test, submitted to several healing conditions (water flow for 1 week, water immersion, wet/dry cycles and ambient air for 3 months, and outside for 1 year) and reloaded at failure at the end of the healing period. Self-healing was assessed via water permeability measures, mechanical results and macro- and microscopic observations. Six concrete mixes were studied: control with no admixture and mixes with expansive agent (CSA), crystalline admixture (CA), superabsorbent polymer (SAP), combination of (CA+SAP) and combination of (CA+CSA). Based on the experimental results detailed in this paper (part 2), the main following conclusions can be made:

- The impact of the exposure condition on the Strength Regain was mainly visible between the indoor and outdoor prisms, while less significant between the different indoor expositions (water and wet/dry). The average Strength Regains for all mixes were equal to 109%, 99% and 95% for the outdoor, wet/dry and water immersion expositions respectively.

- The impact of the self-healing agents on the Strength Regain was less apparent than the impact of the exposure condition and no clear conclusion could be drawn. On the whole, the CA and SAP mixes showed high Strength Regains (among the top 3) in wet/dry and outdoor exposures, while CSA mix had lower results (among the bottom 2). Also, no synergetic effect was found with combinations of admixtures (CA+SAP and CA+CSA) in comparison to the healing agents alone.

- The stiffness regain was proportional to the pre-loading flexural behaviour and more dependent on the fibres distribution than on the mixes and exposure conditions. However, for the same range of pre-cracking stresses, the stiffness regains were 44% higher for the outdoor exposure, sign of some healing effect.

- The Strength Regains were not correlated to the durability regains (Healing Ratios), as a high Healing Ratio did not necessarily lead to a high Strength Regain. The non-correlation between both regains can be explained by the micro- and macroscopic analyses. Higher local density of the healing products at crack surfaces implied higher Healing Ratios, while the Strength Regains were mainly impacted by the type of healing products and the presence of more products inside the cracks than at the external crack surfaces.

- Overall, the SAP mix showed the best mechanical performance in terms of initial flexural stress, Strength Regain after healing and deflection capacity, especially in realistic outdoor exposure. From part 1, the CA and SAP mixes performed the best regarding water permeability measures. In conclusion, SAP mix was judged to have the greatest self-healing potential considering both durability and mechanical perspectives.

While this project evaluated the self-healing capacity of a dormant crack (constant width), studying the self-healing under repeated reloading (active crack) is also of great interest. To assess the repeatability of the self-healing process, an experimental program has been carried out with the results will be addressed in a future publication.

6.7 Acknowledgements

6.8 References

[1]   N. Hearn, "Self-sealing, autogenous healing and continued hydration : what is the difference ?," *Materials and Structures,* vol. 31, pp. 563-567, 1998.

[2]   M. Lachemi, K. M. A. Hossain, M. Ramcharitar, and M. H. Shehata, "Bridge deck rehabilitation practices in North America," *Journal of Infrastructure Systems,* vol. 13, pp. 225-234, 2007.

[3]   K.-S. Lauch, C. Desmettre, and J.-P. Charron, "Self-healing of concrete containing different admixtures under laboratory and outdoor expositions - Water permeability measurements," *Submitted for publication in Cement and Concrete Composites,* 2021.

[4]   L. Ferrara *et al.*, "Experimental characterization of the self-healing capacity of cement based materials and its effects on the material performance: A state of the art report by COST Action SARCOS WG2," *Construction and Building Materials,* Review vol. 167, pp. 115-142, 2018.

[5]   W. Tang, O. Kardani, and H. Cui, "Robust evaluation of self-healing efficiency in cementitious materials - A review," *Construction and Building Materials,* vol. 81, pp. 233-247, 2015.

[6]   M. Roig-Flores, S. Moscato, P. Serna, and L. Ferrara, "Self-healing capability of concrete with crystalline admixtures in different environments," *Construction and Building Materials,* vol. 86, pp. 1-11, 2015.

[7]   X. Wang, C. Fang, D. Li, N. Han, and F. Xing, "A self-healing cementitious composite with mineral admixtures and built-in carbonate," *Cement and Concrete Composites,* vol. 92, pp. 216-229, 2018.

[8]   B. Park and Y. C. Choi, "Self-healing capability of cementitious materials with crystalline admixtures and super absorbent polymers (SAPs)," *Construction and Building Materials,* vol. 189, pp. 1054-1066, 2018.

[9]   D. Li, B. Chen, X. Chen, B. Fu, H. Wei, and X. Xiang, "Synergetic effect of superabsorbent polymer (SAP) and crystalline admixture (CA) on mortar macro-crack healing," *Construction and Building Materials,* vol. 247, 2020.

[10]   Z. Jiang, W. Li, and Z. Yuan, "Influence of mineral additives and environmental conditions on the self-healing capabilities of cementitious materials," *Cement and Concrete Research,* vol. 57, pp. 116-127, 2015.

[11]   H. X. D. Lee, H. S. Wong, and N. R. Buenfeld, "Self-sealing of cracks in concrete using superabsorbent polymers," *Cement and Concrete Research,* vol. 79, pp. 194-208, 2016.

[12] G. Hong and S. Choi, "Rapid self-sealing of cracks in cementitious materials incorporating superabsorbent polymers," *Construction and Building Materials,* vol. 143, pp. 366-375, 2017.

[13] L. Ferrara, V. Krelani, and M. Carsana, "A "fracture testing" based approach to assess crack healing of concrete with and without crystalline admixtures," *Construction and Building Materials,* vol. 68, pp. 535-551, 2014.

[14] G. Li, S. Liu, M. Niu, Q. Liu, X. Yang, and M. Deng, "Effect of granulated blast furnace slag on the self-healing capability of mortar incorporating crystalline admixture," *Construction and Building Materials,* vol. 239, 2020.

[15] D. Snoeck and N. De Belie, "Repeated autogenous healing in strain-hardening cementitious composites by using superabsorbent polymers," *Journal of Materials in Civil Engineering,* vol. 28, no. 1, p. 11 pages, 2016.

[16] P. Escoffres, C. Desmettre, and J.-P. Charron, "Effect of a crystalline admixture on the self-healing capability of high-performance fiber reinforced concretes in service conditions," *Construction and Building Materials,* vol. 173, pp. 763-774, 2018.

[17] R. Alghamri and A. Al-Tabbaa, "Self-healing of cracks in mortars using novel PVA-coated pellets of different expansive agents," *Construction and Building Materials,* vol. 254, 2020.

[18] L. Ferrara, V. Krelani, and F. Moretti, "On the use of crystalline admixtures in cement based construction materials: from porosity reducers to promoters of self healing," *Smart Material and Structures,* vol. 25, p. 17p, 2016.

[19] D. Snoeck, K. Van Tittelboom, S. Steuperaert, P. Dubruel, and N. De Belie, "Self-healing cementitious materials by the combination of microfibres and superabsorbent polymers," *Journal of Intelligent Material Systems and Structures,* vol. 25, no. 1, pp. 13-24, 2014.

[20] G. Anglani, J.-M. Tulliani, and P. Antonaci, "Behaviour of pre-cracked self-healing cementitious materials under static and cyclic loading," *Materials,* vol. 13, no. 5, 2020.

[21] K. Van Tittelboom, N. De Belie, F. Lehmann, and C. U. Grosse, "Acoustic emission analysis for the quantification of autonomous crack healing in concrete," *Construction and Building Materials,* vol. 28, no. 1, pp. 333-341, 2012.

[22] A. S. Buller, F. U. Abro, K. M. Lee, and S. Y. Jang, "Mechanical recovery of cracked fiber-reinforced mortar incorporating crystalline admixture, expansive agent, and geomaterial," *Advances in Materials Science and Engineering,* 2019.

[23] C. Y. Namnoum, B. Hilloulin, F. Grondin, and A. Loukili, "Determination of the origin of the strength regain after self-healing of binary and ternary cementitious materials including slag and metakaolin," *Journal of Building Engineering,* p. 102739, 2021/05/26/ 2021.

[24] T. S. Qureshi and A. Al-Tabbaa, "Self-healing of drying shrinkage cracks in cement-based materials incorporating reactive MgO," *Smart Material and Structures,* vol. 25, p. 16 pages, 2016.

[25] A. Beglarigale, D. Eyice, B. Tutkun, and H. Yazici, "Evaluation of enhanced autogenous self-healing ability of UHPC mixtures," *Construction and Building Materials,* vol. 280, 2021.

[26] H. Deng and G. Liao, "Assessment of influence of self-healing behavior on water permeability and mechanical performance of ECC incorporating superabsorbent polymer (SAP) particles," *Construction and Building Materials,* vol. 170, pp. 455-465, 2018.

[27] G. Hong, C. Song, and S. Choi, "Autogenous healing of early-age cracks in cementitious materials by superabsorbent polymers," *Materials,* vol. 13, no. 3, 2020.

[28] K. Van Tittelboom *et al.*, "Comparison of different approaches for self-healing concrete in a large-scale lab test," *Construction and Building Materials,* vol. 107, pp. 125-137, 2016.

[29] *EN 14651 : Test method for metallic fibered concrete - Measuring the flexural tensile strength*, 2005.

[30] *ASTM C469 : Standard Test Method for Static Modulus of Elasticity and Poisson's Ratio of Concrete in Compression*, 2014.

[31] S. Delsol and J.-P. Charron, "Numerical modeling of UHPFRC mechanical behavior based on fibre orientation," presented at the International Symposium on Ultra-High Performance Fibre-Reinforced Concrete UHPFRC, Marseille, France, 2013.

[32] A. Abrishambaf, M. Pimentel, and S. Nunes, "Influence of fibre orientation on the tensile behaviour of ultra-high performance fibre reinforced cementitious composites," *Cement and Concrete Research,* vol. 97, pp. 28-40, 2017/07/01/ 2017.

[33] C. Androuët, O. Deaux, and J. P. Charron, "Impact of mixing and curing temperatures on fresh and hardened states properties of UHPC," *Canadian Journal of Civil Engineering,* 2021.

[34] J. Doyon-Barbant and J.-P. Charron, "Impact of fibre orientation on tensile, bending and shear behaviors of a steel fibre reinforced concrete," *Materials and Structures,* vol. 51, no. 157, 2018.

[35] K. Sisomphon, O. Copuroglu, and E. A. B. Koenders, "Effect of exposure conditions on self healing behavior of strain hardening cementitious composites incorporating various cementitious materials," *Construction and Building Materials,* vol. 42, pp. 217-224, 2013.

[36] K. Sisomphon, O. Copuroglu, and E. A. B. Koenders, "Self-healing of surface cracks in mortars with expansive additive and crystalline additive," *Cement and Concrete Composites,* vol. 34, pp. 566-574, 2012.

[37] E. Cuenca, A. Tejedor, and L. Ferrara, "A methodology to assess crack-sealing effectiveness of crystalline admixtures under repeated cracking-healing cycles," *Construction and Building Materials,* vol. 179, pp. 619-632, 2018.

[38] B. Park and Y. C. Choi, "Effect of healing products on the self-healing performance of cementitious materials with crystalline admixtures," *Construction and Building Materials,* vol. 270, 2021.

[39] E. Scholtzová, D. Tunega, and S. Speziale, "Mechanical properties of ettringite and thaumasite—DFT and experimental study," *Cement and Concrete Research,* vol. 77, pp. 9-15, 2015/11/01/ 2015.

[40] R. Sevcik, P. Sasek, and A. Viani, "Physical and nanomechanical properties of the synthetic anhydrous crystalline $CaCO_3$ polymorphs: vaterite, aragonite and calcite," *Journal of Materials Science,* vol. 53, no. 6, pp. 4022-4033, 2018.

CHAPTER 7   COMPLEMENTARY STUDIES

This chapter will present complementary studies about Experimental Program 2, as well as the preliminary results of Experimental Program 3.

The complementary results of Experimental Program 2 are presented in **Sections 7.1-7.4**. First, the additional tests carried out on mortars to optimise the mix containing SAP will be described in **Section 7.1**. Then, the evolution of concrete's compressive strength will be presented in **Section 7.2**. Further details about the analyses of the fibres orientation and density will be given in **Section 7.3**. The evaluation of mechanical recovery of prisms with other indexes will be discussed thereafter in **Section 7.4**.

The preliminary results of Experimental Program 3 are detailed in   **Section 7.5**. This program focused on the impact of repeated reloading on self-healing.

7.1 Optimisation of the mix containing SAP (Exp. Program 2)

The SAP used is a cross-linked polyacrylamide with a nominal size particle of 100 µm. SAPs are initially dry when they get in contact with water in the mixer. If the absorption capacity of SAP is not considered, part of the water of the mix initially planned for the workability is lost and can generate problems for casting the material. Moreover, the water content of the mix is of prime importance to cement hydration that controls the mechanical strength of the material.

The absorption capacity of SAP was determined in deionised water, tap water and cement filtrate (150 g of cement mixed in 1.5 kg of water) according to the tea-bag method (Snoeck et al., 2018), while the swelling time was determined by the vortex method (Zohuriaan & Kabiri, 2008). The results are shown in **Table 7.1**.

Mortars containing 0.5%-m_{cement} of SAP in addition were produced in order to evaluate the real absorption of SAP in a mortar. Additional water or superplasticiser (SP) was introduced in the mortar mixes until reaching the same workability of the control mortar (slump and flow). An increase of 35 kg/m³ and 20 L/m³ of water and SP respectively were needed to adjust the workability. From these tests on mortar, it was found that SAP absorbed 13 g water/g SAP. Such result is lower than the one found by Snoeck et al. (2014a) for an equivalent SAP and may be explained by the different mortar composition used. The average fresh and hardened results of the

control mortar, the one with SAP and additional water (+35 kg/m³ compared to control) and the one with SAP and additional SP (+20 L/m³ or +4%) are presented in **Table 7.2.** The compressive strengths of the mixes were determined on cylinders (ɸ75 mm x 150 mm), cured in humid chamber for 28 days and then left in ambient air in the laboratory for another month. Compared to the control mortar without SAP, the SAP+water and SAP+SP mixes showed strength decreases of 29% and 9% respectively. This in agreement with (Snoeck et al., 2014a), because the effective w/c ratio is lower for the SAP+SP option.

As the project aims to test several materials of equivalent strength, it was preferable to choose the SAP+SP option to prepare the FRC mixes.

Table 7.1. Properties of the SAP used (average and standard deviation σ)

Absorption capacity (g/g SAP)				Swelling time (s)
Deionised water	**Tap water**	**Cement filtrate**	**Mortar**	
310 ± 11.83	118 ± 9.58	38 ± 0.83	13	11 ± 4.37

Table 7.2. Results of the mortars: control, SAP and additional water and SAP and additional superplasticiser

	Control	**SAP+water**	**SAP+SP**
Slump (mm)	110	112	115
Slump flow (mm)	162.5	166.5	172.5
Comp. strength $\mu \pm \sigma$ (MPa)	73.7 ± 4.67	52.5 ± 0.85	67.1 ± 5.09

It must be noticed that even if the dosage of SP has been adjusted in the FRC mixes containing SAP and CA+SAP (**Table 5.1**), their slump flows were lower than the targeted 500 mm. For the SAP mix, it reached 443 mm, which can be considered in the target range of ± 50 mm. However, the CA+SAP mix had a slump flow of 330 mm, which is considerably lower. In this latter mix, the addition of CA with SAP has modified the consumption of water in the mixer, either for the SAP absorption or for the early hydration of cement or CA. This aspect has not been considered in the short study on SAP absorption.

7.2 Evolution of the compressive strength (Exp. Program 2)

For each mix tested in the main program experimental of this project (Experimental Program 2, see **Section 3.2.3**), the compression strength was evaluated at different times: at 28 days and then after 3 months of exposure for the indoor mixes, and at 28 days and then after 6 months and 12 months of exposure for the outdoor mixes. Three cylinders (ϕ100 mm x 200 mm) were tested at each time.

The evolution of compressive strength is shown in **Figure 7.1a** and **Figure 7.1b** for the mixes exposed indoor and outdoor respectively.

In laboratory conditions (**Figure 7.1a**), the compressive strengths increased by 7 to 22% depending on the mix, after 3 months of exposure in water and wet/dry cycles with respect to the results at 28 days. In contrast, the strength only increased by 3% for the cylinders kept in air condition for 3 months. The increase of strength is related to the maturity effect, hydration of cement continuing with time, particularly in exposure conditions with high humidity.

In outdoor exposure (**Figure 7.1b**), the compressive strengths increased by 3 to 30% depending on the mix after 6 months outside. Then, between 6 and 12 months of exposure, the strength evolution was limited, except for the SAP and CA+SAP mixes, with an increase of 10 and 26% respectively, and the CA+CSA mix with a decrease of 13%. The presence of SAP promoted internal curing even in drier periods, which is the main utility of this product in concrete. Strength reduction observed at later ages for CA+CSA mix was not expected but is consistent with the small decreases measured on the CA and CSA mixes at the same period. This may be attributed to the dissolution of hydration products formed by CA and CSA in the matrix in outdoor condition. More investigation is needed to verify this assumption.

For most mixes, there is no significant difference between the compressive strength gains between 28 days and after 3 months in indoor condition or between 28 days and after 12 months in outdoor exposure. This means that the impact of concrete maturity on the Strength Regains of the indoor versus outdoor healed prisms (presented in **Chapter 6**) should be negligible. Furthermore, this impact of the concrete maturity during the reloading to failure should be negligible as the mechanical response of the already cracked prisms should be mainly controlled by the crack rather than the matrix. The crack is not influenced by the hydration in the matrix.
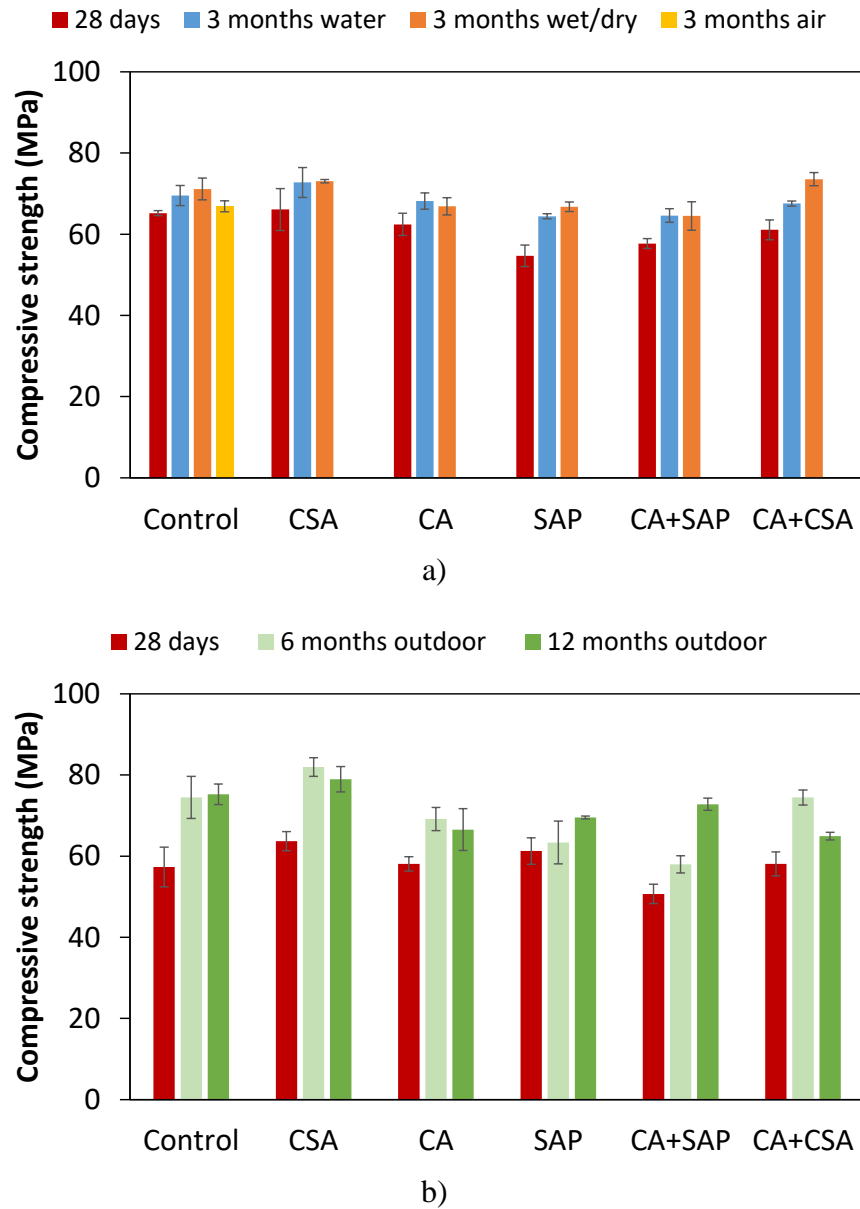
Figure 7.1. Evolution of compressive strength for all mixes exposed a) indoor and b) outdoor

7.3 Analyses of fibres orientation and density in prisms (Exp. Program 2)

As mentioned in **Section 3.3.5**, fibres orientation and density analyses were performed on slices of prisms tested in Experimental Program 2 to discriminate the effect of the self-healing agents from the impact of fibres on the flexural pre-cracking behaviour.

After detection of the fibres (**Figure 7.2a**), the fibres analysis program gives the orientation angle of each fibre. The spatial configuration of the fibres on the plane of the slice can be classified in different ranges of orientation angles, from well-oriented fibres [0-30°] to poorly oriented ones [60-90°], as illustrated in **Figure 7.2b**. The fibre is perfectly oriented when the longitudinal axis of the fibre is perpendicular to prism vertical plane.

The program also gives the average orientation angle of the fibres as well as the fibres density. These results are summarised in **Table 7.3** for all the specimens analysed. The total fibres surface (sum of the areas of ellipses/total surface area) is quite close to the fibres volumetric dosage used in concrete (0.75%) for most specimens, while there were larger discrepancies in SAP and CA+SAP mixes indoor and CA+SAP mix outdoor. These mixes had lower workability (**Table 5.1**). This may have led to a less homogeneous distribution of the fibres into the concrete volume and in some prisms and affects the fibres densities found at a specific location near the crack of these prisms. Moreover, the percentages of the distribution of the orientation angle of the fibres in each category, are quite similar for all mixes. This confirms that a similar and repetitive casting procedure was applied to all mixes in the project.
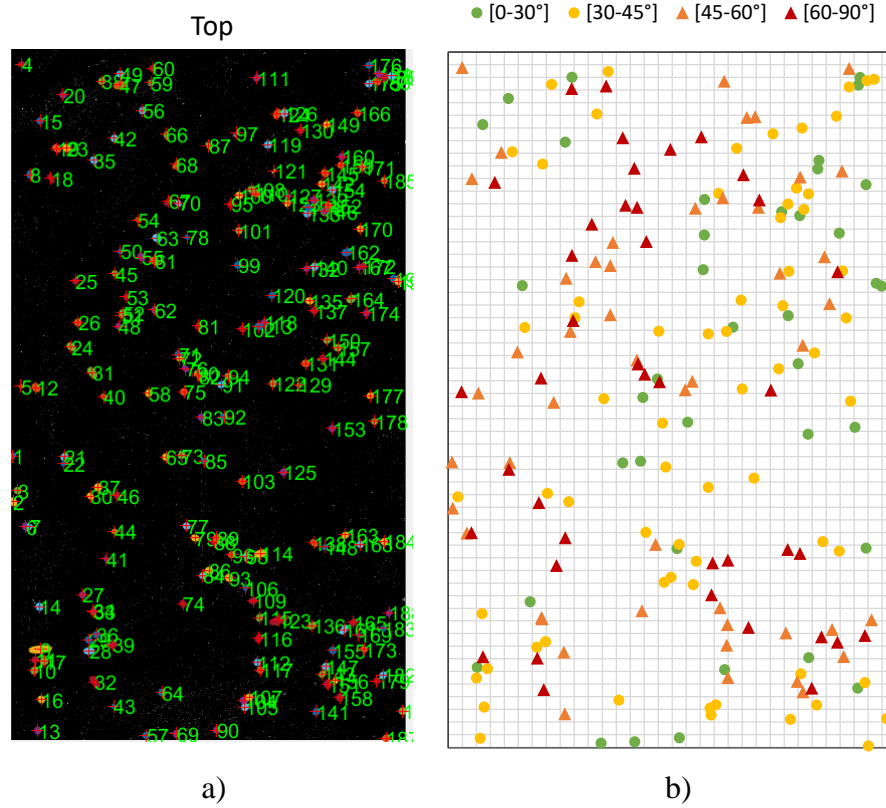
Figure 7.2. Example of fibres orientation analyses for the control prism, a) raw output of the program, b) results of different ranges of fibre orientation angle (each cursor represents a fibre)

Table 7.3. Results of the analyses of the fibres orientation and density

	Specimen	Density (nb/cm²) ρ	Fibres surface (%)	Orientation angle θ		Distribution of orientation angles (%)			
				μ	σ	[0-30°]	[30-45°]	[45-60°]	[60-90°]
INDOOR	Control	2.47	0.72%	45.3	17.4	20%	34%	25%	21%
	CSA	2.54	0.67%	40.1	16.2	30%	41%	14%	16%
	CA	2.32	0.62%	43.1	16.7	26%	38%	17%	20%
	SAP	1.78	0.47%	37.5	16.0	40%	36%	11%	13%
	CA+SAP	1.32	0.35%	38.1	17.4	36%	43%	9%	13%
	CA+CSA	2.20	0.63%	38.3	14.9	30%	43%	17%	10%
OUTDOOR	Control	3.02	0.90%	41.0	17.9	33%	33%	15%	19%
	CSA	2.71	0.78%	39.3	16.4	33%	39%	16%	13%
	CA	2.40	0.72%	42.2	17.2	30%	30%	23%	17%
	SAP	2.14	0.66%	44.9	17.4	21%	36%	21%	22%
	CA+SAP	1.42	0.42%	43.3	16.8	21%	42%	19%	18%
	CA+CSA	2.10	0.58%	41.1	18.7	34%	32%	16%	17%

Figure shows the relationships between the maximal flexural stress at pre-cracking and the fibres density (**Figurea**) and the average orientation angle (**Figureb**). It can be noticed that the flexural stress of prisms at pre-cracking is quite proportional to the fibres density: the higher the density, the greater the flexural stress. This is logical as more fibres are present to prevent the crack opening. Despite the lower fibres densities for SAP and CA+SAP mixes indoor, the higher flexural stresses could be explained by the higher proportion of well-oriented fibres [0-30°] (40% and 36% respectively) compared to the other mixes.

The relationship of the flexural strength with the average orientation angle alone is less apparent, however. It is expected that the better the fibres orientation is (the lower the angle), the better the flexural performance is. But the average orientation angles were not very different between the mixes (from 37.5 to 45.3° in **Table 7.3**) and given the high standard deviation σ (from 14.9 to 18.7° in **Table 7.3**), no trend can be drawn.

a)

Figure 7.3. Relationship between the maximal flexural stress at pre-cracking with the a) fibres density and b) average fibres orientation angle

b)
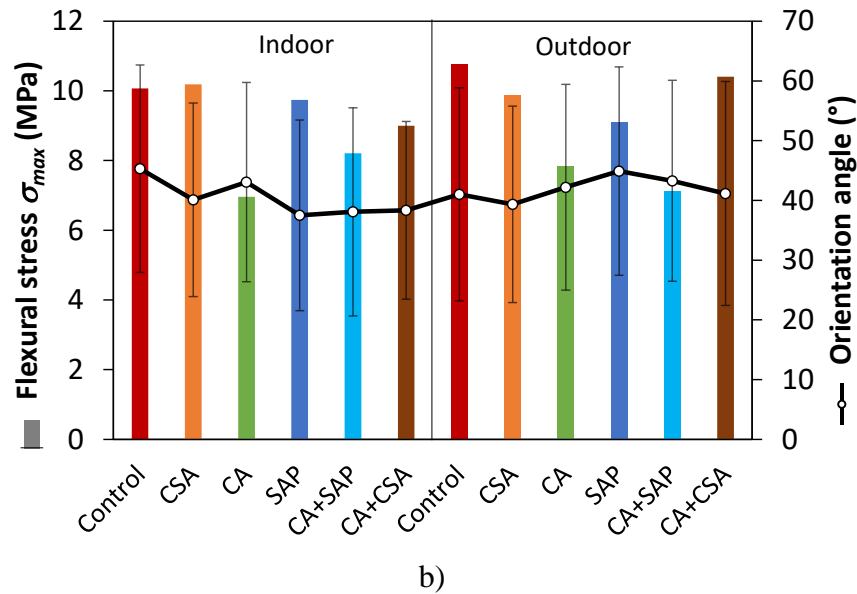
Figure7.3. Relationship between the maximal flexural stress at pre-cracking with the a) fibres density and b) average fibres orientation angle (cont.)

Both fibres density and orientation angle should be considered to adequately assess the impact of the fibres. That is why weighting coefficients γ considering the two parameters were calculated to adjust the strength values of flexural tests. In this study, **Eq. 7.1** has been used for each mix i, with θ the average orientation angle and ρ the density of fibres, with respect to the values of the control mix. The calculated weighting factors are shown in **Table 7.4** and **Figure 7.4** presents the initial (**Figure 7.4a**) and weighted (**Figure 7.4b**) flexural curves for the outdoor mixes. It appeared that the CA mix also showed the lowest flexural performance as for indoor mixes (**Figure 6.6**).

$$\gamma_i = \sqrt{\frac{\theta_i}{\theta_{control}} \times \frac{\rho_{control}}{\rho_i}}$$ (7.1)

Table 7.4. Calculated weighting factors for each mix

	Specimen	Weighting factor γ		Specimen	Weighting factor γ
INDOOR	Control	1.00	**OUTDOOR**	Control	1.00
	CSA	0.93		CSA	1.03
	CA	1.01		CA	1.14
	SAP	1.07		SAP	1.24
	CA+SAP	1.25		CA+SAP	1.50
	CA+CSA	0.98		CA+CSA	1.20

a)   b)
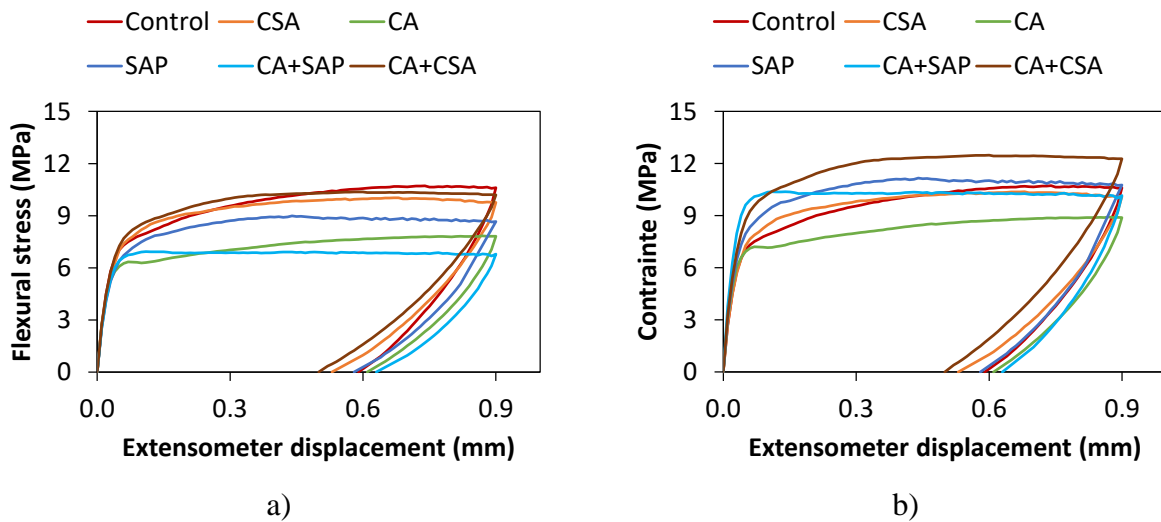
Figure 7.4. Average pre-cracking curves for outdoor mixes a) before and b) after consideration of fibres orientation and density analyses

7.4 Evaluation of the mechanical recovery of prisms after healing (Exp. Program 2)

On this project, self-healing was quantitatively investigated through permeability and mechanical recovery evaluation on prisms. As seen in the literature review in **Chapter 2** (**Section 2.3.5**), different indexes can be used for mechanical recovery. In this project, **Eq. 7.2** was used for the Strength Regain, while most studies used **Eq. 7.3** when performing flexural tests (3- or 4-point bending). More recently Namnoum et al. (2021), who also had companion uncracked specimens exposed in the same condition as in this project, used **Eq. 7.4** with reference to the companion

uncracked (but with load values). The choice of **Eq. 7.2** in this project was made after evaluating the relevance of other equations (**Eq. 7.3** and **Eq. 7.4**) for this particular study.

Figure 7.5 illustrates typical pre-cracking and reloading curves in literature (**Figure 7.5a**) and from this project (**Figure 7.5b**), with a shorter post-peak phase. **Figure 7.6** shows the values of the strength regains for the control mix calculated via **Eq. 7.3** (**Figure 7.6a**) and **Eq. 7.4** (**Figure 7.6b**) respectively. Because of the shorter post-peak phase in this project in comparison to most studies that use **Eq. 7.3**, $\sigma_{reload,max}$ was not always higher than σ_{unload}. This fact resulted in negative results in **Figure 7.6a**. On the other hand, when $\sigma_{reload,max}$ was higher than σ_{unload}, because $\sigma_{pre-load,max}$ was very close to σ_{unload}, this led to very high strength regains as obtained for the outdoor specimens (value of 8.31 in **Figure 7.6a**). Furthermore, two companion uncracked prisms were made in this project, compared to only one uncracked specimen in (Namnoum et al., 2021). As there was variation between the two reference uncracked prisms, this led to different strength regains when using **Eq. 7.4** as seen in **Figure 7.6b**. In conclusion, **Eq. 7.3** and **Eq. 7.4** did not allow to obtain reliable criteria in this project to analyse the impact of self-healing on the mechanical recovery. Consequently, **Eq. 7.2** was proposed to analyse the Strength Regain.

$$Strength\ regain = \frac{\sigma_{reload,max}}{\sigma_{unload}} \tag{7.2}$$

$$Strength\ regain = \frac{\sigma_{reload,max} - \sigma_{unload}}{\sigma_{pre-load,max} - \sigma_{unload}} \tag{7.3}$$

$$Strength\ regain = \frac{\sigma_{reload,max} - \sigma_{reload,max,ref}}{\sigma_{pre-load,max,ref} - \sigma_{reload,max,ref}} \tag{7.4}$$

a)   b)
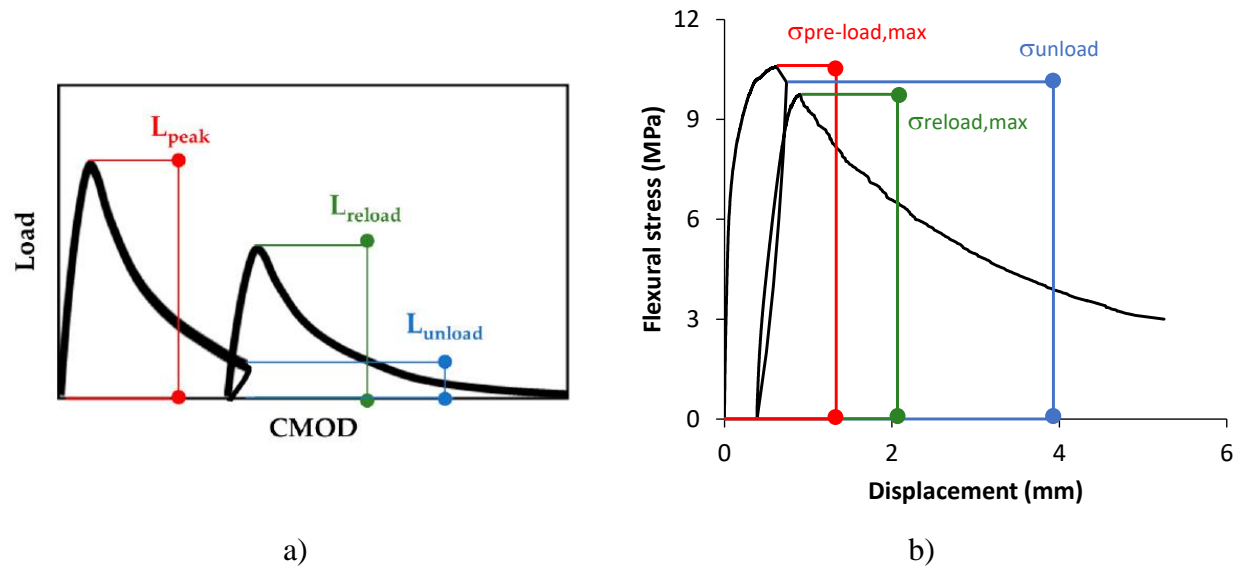
Figure 7.5. Typical pre-cracking and reloading curves with a) longer post-peak phase from (Anglani et al., 2020) and b) shorter post-peak phase in this project

a)   b)
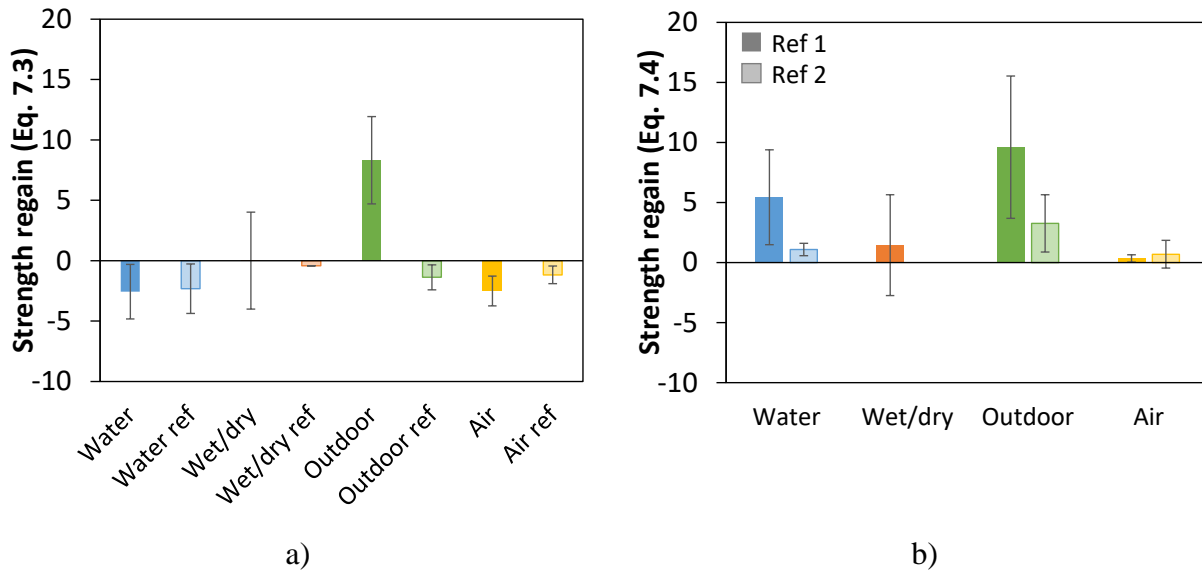
Figure 7.6. Strength regains for the control mix calculated with a) **Eq. 7.3** and b) **Eq. 7.4**

Finally, although the stiffness recovery was found to be proportional to the pre-cracking flexural stress (**Figure 6.11**, **Chapter 6**), no correlation was found between the Strength Regain and the pre-cracking flexural behaviour as demonstrated in **Figure 7.7**. This means that the Strength Regain is more dependent on the healing state of prisms and is thus adequate to evaluate the impact of the self-healing. From **Figure 7.7**, it can be noticed again that the outdoor mixes presented higher Strength Regains than the indoor mixes for the same range of flexural stresses.
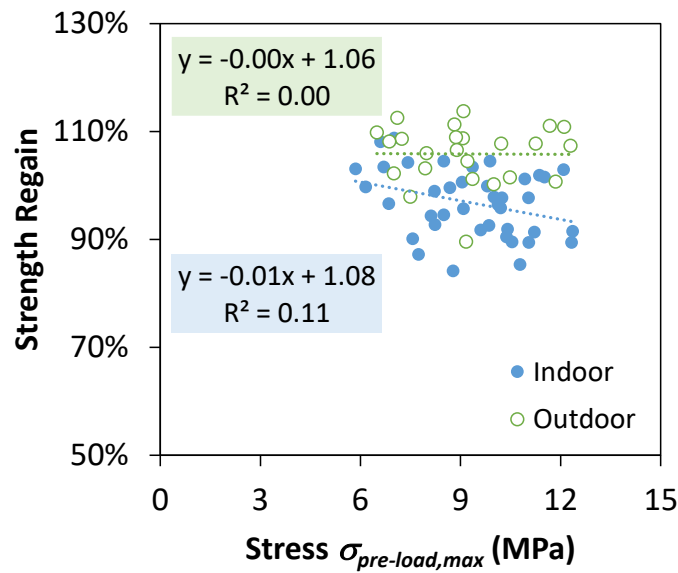
Figure 7.7. Strength Regain vs maximal pre-load stress for indoor and outdoor mixes

In addition to the flexural reloading performed at the end of the healing period, some ultrasonic pulse velocity (UPV) tests were also carried out in this project to evaluate the evolution of self-healing in time. Such non-destructive tests have the advantage to be quick and easy. However, because of the presence of fibres in prisms and disruptive effects because of the coupling between the UPV sensors and the concrete surface, the results were not reliable and were thus not exploited.

7.5 Evaluation of self-healing under repeated reloading (Exp. Program 3)

The objective of the third experimental program was to evaluate the repeatability of self-healing of a crack under repeated reloading. Two FRC mixes (control and CA+CSA) were produced but only the CA+CSA mix was tested due to COVID-19. The testing methodology followed in this experimental program was detailed in **Section 3.2.4** and the loading procedures described in **Section 3.3.1.3**. A summary is described hereafter.

After pre-cracking, the CA+CSA prisms were reloaded 2 times and then reloaded until failure the third time. The prisms were healed in wet/dry cycles between the reloads. Two types of reloading were applied to the prisms. One type of reloading aimed to reopen the crack to its initial crack opening reached at pre-cracking, which means to $CMOD_{max} = 0.9$ mm, simulating a structure under low traffic at low magnitude. The second type of reloading had the objective to reopen the crack to a superior value, which was CMOD+0.2 mm, simulating a structure under high traffic at high magnitude.

Experimental Program 3 was shortened (study of one mix versus two initially planned) and the available results of this program were thus not introduced in a full chapter nor a scientific article yet because of delays due to COVID-19. This program will be completed beyond the scope of this thesis. However, this section will present a preliminary analysis of the water permeability results.

7.5.1 Properties of the CA+CSA mix

The fresh state and hardened properties of the CA+CSA mix are shown in **Table 7.5**. The slump flow was lower than the batch produced during the Experimental Program 2 (325 vs 595 mm). This difference may be explained by the fact that a different concrete mixer was used for the indoor batch of the Experimental Program 2.

Regarding the hardened properties, because of the COVID-19, the specimens could not be tested at 28 days as in the other experimental programs. At the end of their period of 28 days in water, they were let in laboratory air condition until being pre-cracked at 218 days. This delay explains the higher compressive strength obtained in this program for the tested mix (74.1 vs 59.6 MPa).

Table 7.5. Characterisation of the CA+CSA mix

Fresh properties		Hardened properties at 218 days	
Slump flow (mm)	325	Compressive strength (MPa)	74.1 ± 0.77
Air (%)	2.2	E-modulus (MPa)	30 000
Density (kg/m³)	2310		

7.5.2 Pre-cracking and initial water permeability coefficient

The pre-cracking flexural curves of the 12 prisms of CA+CSA are shown in **Figure 7.8**. The average σ_{max} of 9.64 MPa was very similar to the values obtained for the indoor and outdoor batches of the Experimental Program 2 (9.18 and 10.41 MPa respectively). After unloading, the residual crack widths at the notch root ranged between 0.18 and 0.29 mm, with an average value of 0.22 mm, which was slightly lower than the average values of 0.30 and 0.24 mm for the indoor and outdoor batches of the Experimental Program 2.
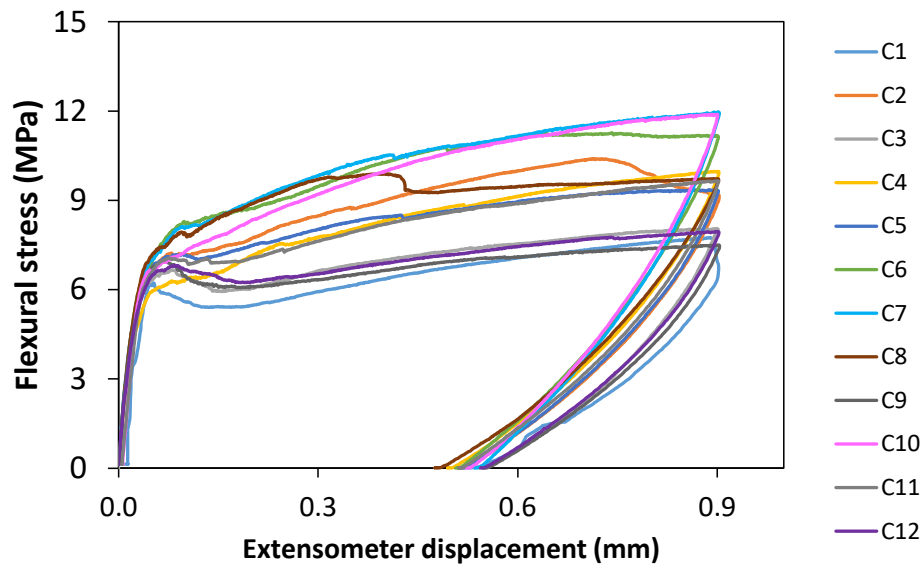
Figure 7.8. Pre-cracking curves of Experimental Program 3

After pre-cracking, the initial water permeability coefficient K_{wi} was measured on each specimen. The results, presented in **Figure 7.9**, ranged from 3.9×10^{-7} to 6.8×10^{-6} m/s, with a coefficient of variation (COV) of 53%, which is in the same order as the previous COV obtained in the Experimental Program 2. Based on these K_{wi} values, the prisms were distributed into the different types of reloading applied, as indicated by the colour code in **Figure 7.9**.

Prisms with different ranges of K_{wi} were allocated to the following testing conditions:

- Prisms reloaded to $CMOD_{max}$:

    o C1, C4 and C9 to be healed in wet/dry cycles;

    o C3 and C10 as companion reference specimens to be exposed in ambient air condition;

- Prisms reloaded to CMOD+0.2 mm:

    o C5, C6 and C8 to be healed in wet/dry cycles;

    o C2 and C11 as companion reference specimens to be exposed in ambient air condition;

- Prisms with no repeated reloading:

    o C7 and C12 as companion reference specimens healed in wet/dry cycles.
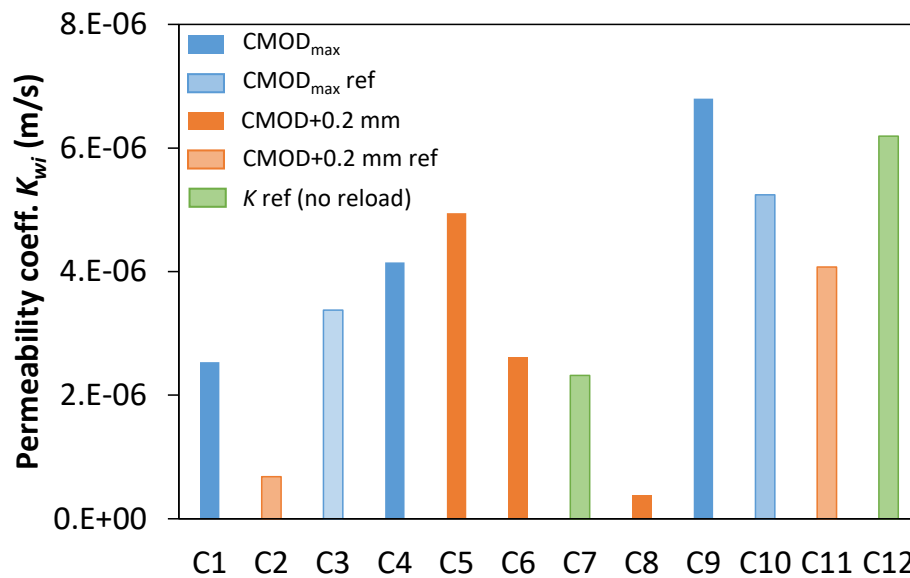
Figure 7.9. Initial water permeability coefficient and selection for the types of reloading

7.5.3 Evolution of crack with macroscopic observations

Figure 7.10 and **Figure 7.11** show examples of the evolution of cracks surfaces of prisms subjected to a reloading up to $CMOD_{max}$ and to CMOD+0.2 respectively. In **Figure 7.10**, except a small concrete particle that broke off after the initial pre-cracking, the residual crack width stayed the same during all the reloading. This was expected as the loading was controlled to always reach the same crack width. It can also be seen in **Figure 7.10** that, before failure, a portion of crack was almost completely sealed compared to the initial picture. On the other hand, the reloading of prisms to CMOD+0.2 widened more and more the crack (**Figure 7.11**). Despite the crack width increase, some white healing products can be seen inside the crack, especially before failure. This confirms that self-healing products can form even in case of active crack growth.

Complete observation of the cracks will be carried out after this thesis to accurately quantify the crack width variation (decrease or increase) and to correlate these results with the water permeability and mechanical results.
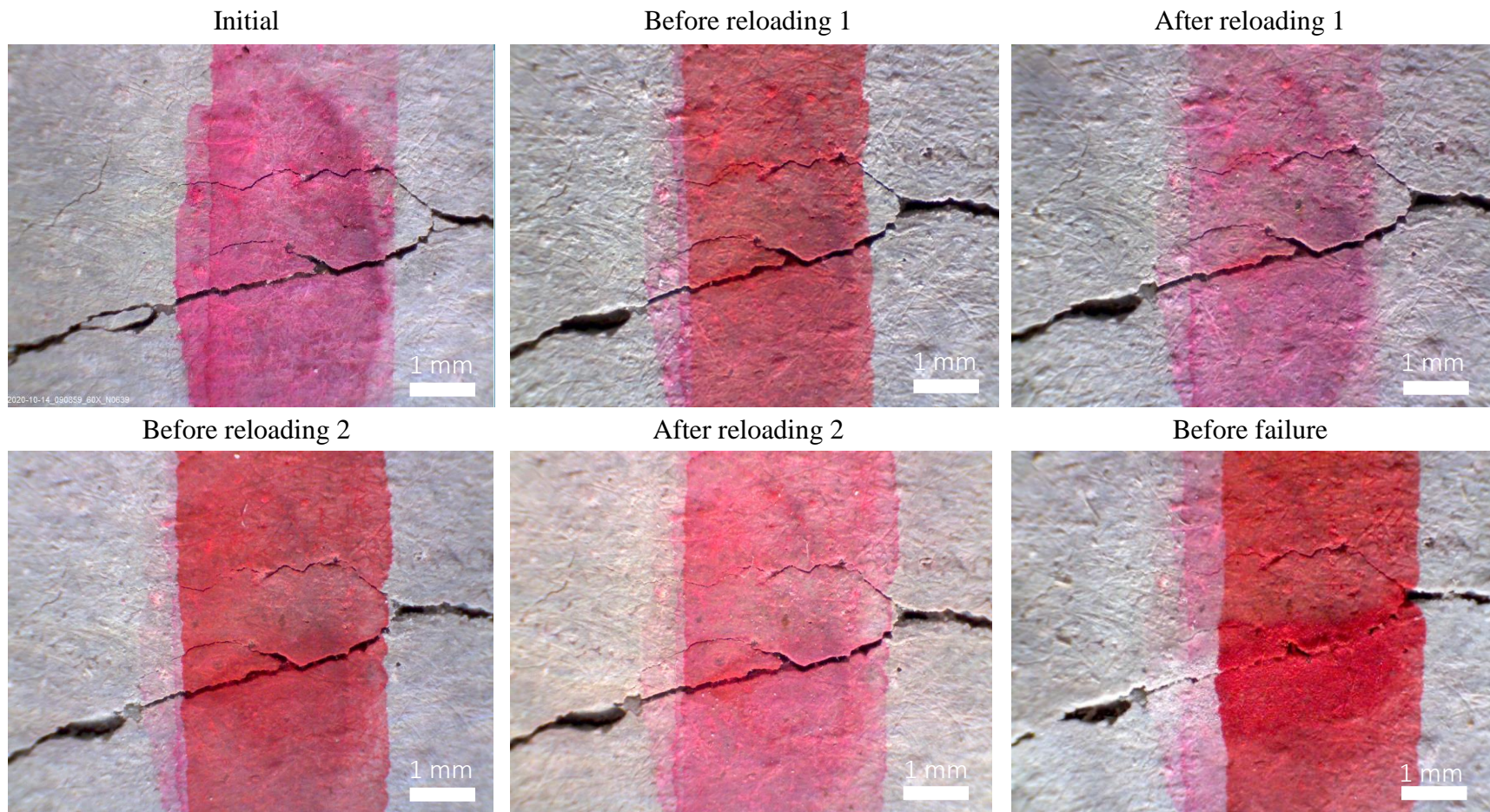
Figure 7.10. Evolution of a section of a crack for a prism reloaded up to $CMOD_{max}$ (specimen C1, $w_i = 0.10$ mm)

Initial	Before reloading 1	After reloading 1

Before reloading 2	After reloading 2	Before failure
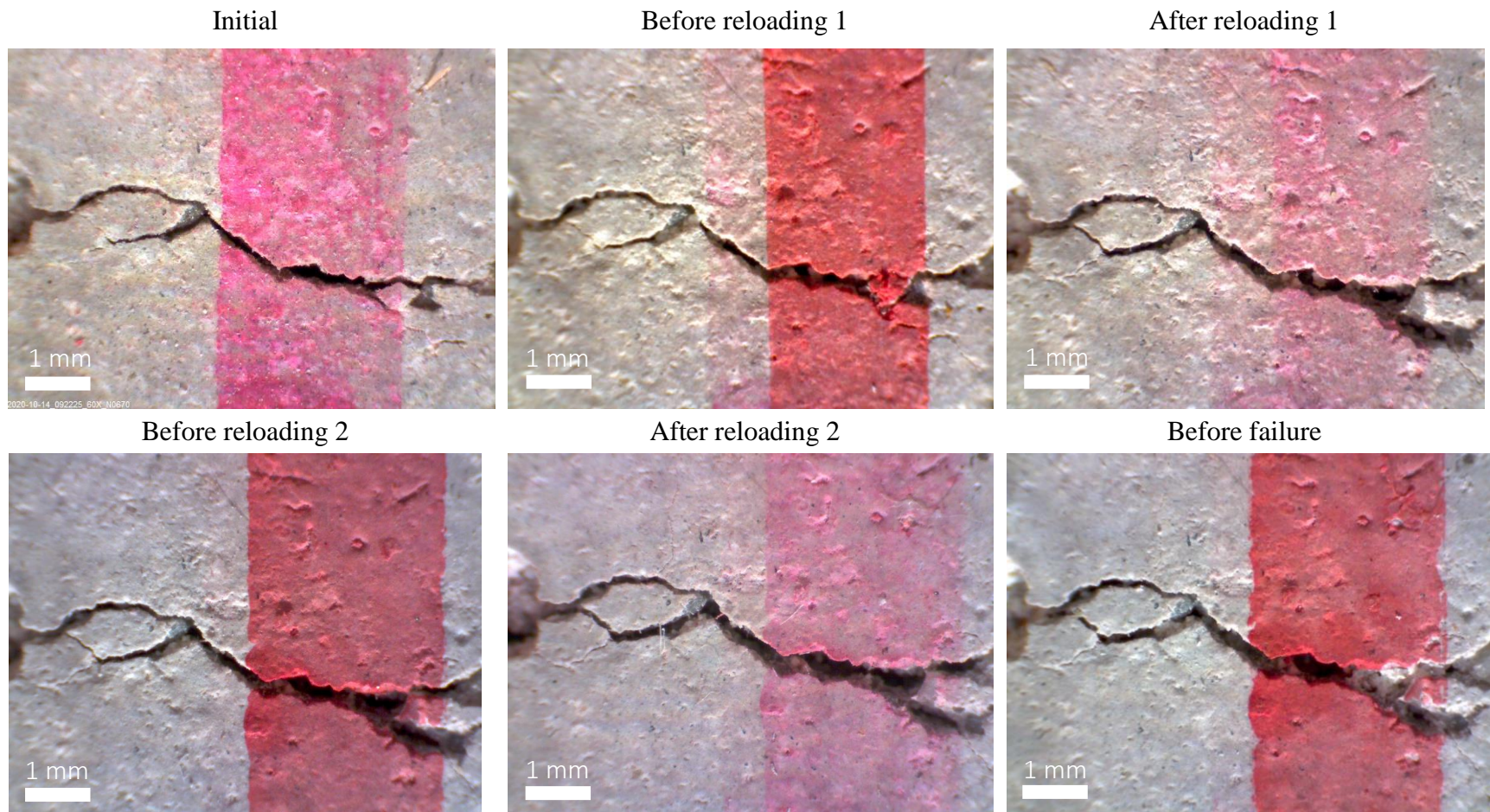
Figure 7.11. Evolution of a section of a crack for a prism reloaded to CMOD+0.2 mm (specimen C5, $w_i = 0.15$ mm)

7.5.4 Evolution of water permeability

The evolution of water permeability coefficient K_{wt} is shown in **Figure 7.12a** and **Figure 7.12b** for the reloading up to $CMOD_{max}$ and to CMOD+0.2 respectively. The healed companion reference specimens C7 and C12 are also shown in both figures. The healing, represented by the decrease of K_w and reloading, revealed by the increase of K_w, can clearly be seen in both figures. After repeated reloading to the same $CMOD_{max}$ (**Figure 7.12a**), it can be seen that the permeability never increased above the initial permeability K_{wi}, which means that the healing products stayed partially efficient after the reloading. The permeability results of companion reference prisms C3 and C10 were not greatly influenced by the healing periods (slight decrease of K_w) nor the reloading, because they were exposed in air. This may be explained by the fact that reloading damages healing products of healed specimens more than widens the crack.

On the other hand, the permeability coefficient increased greatly after each reloading to CMOD+0.2 as the crack got wider (**Figure 7.12b**), particularly at reloading 2, exceeding largely K_{wi}. This greater impact of reloading 2 was also visible for the companion reference specimens C2 and C11. Reloading with increasing crack width led to an increase of permeability, loading damage affecting more than healing. Impact of damage vs healing would have been different according to another loading procedure.

It must be noted that companion reference prisms C7 and C12 were kept in ambient air condition during the preparation and reloading of the other prisms, so that they had exactly the same exposition as the healed prisms. As they were not reloaded, the healing process continued with the expected kinetics described in **Section 2.1.3**: fast healing in the first days when Ca^{++} ions are readily available and then more and more slowly as calcium ions are depleted.

Figure 7.12. Evolution of permeability coefficient Kwt for a) reloading up to CMODmax and b) reloading to CMOD+0.2 mm, C7 and C12 are reference specimens not reloaded

The results presented in **Figure 7.12** were converted in Healing Ratios (*HR*) (**Section 4.5.3.1** for equation) and are shown in **Figure 7.13**.

In **Figure 7.13a**, the healed specimens in wet/dry condition, C1, C4 and C9, reloaded at CMOD$_{max}$, reached an average *HR* = 28% after 56 days, while companion reference specimens C3 and C10, kept in air, reached an average *HR* = 12%. Wet/dry condition was favourable to healing as noted in Experimental Program 2.

In **Figure 7.13b**, the healed specimens in wet/dry condition, C5, C6 and C8, reloaded at CMOD+0.2, reached an average *HR* = -74%, while companion reference specimens C2 and C11, kept in air, reached an average *HR* = -39%. These negative Healing Ratios mean that K_w increased above K_{wi}. Surprisingly, with increasing crack opening, prisms kept in ambient air were less impacted by the reloading, having a smaller negative *HR*.

Although reloading up to CMOD+0.2 mm increases K_{wi}, it also raised the healing potential as the last slopes in **Figure 7.13b** are more than 6 times higher in average than the ones in **Figure 7.13a**. This is probably due to new surfaces available for healing created by the increase of crack length.

The new surface with high content of Ca^{++} promoted healing. This observation and explanation are consistent with those of Desmettre and Charron (2013) observed on FRC tie-specimens under a cyclic loading.

Finally, one can observe that reference prisms C7 and C12 kept in wet/dry condition with no reloading showed the best healing ($HR = 52$ and 70% respectively). This observation was expected since no reloading could break healing products already formed. Therefore, partial results of this Experimental Program 3 demonstrate that application of reloading or reopening of cracks in structures should lead to a deceleration of self-healing. The evolution of healing in active cracks will obviously vary according to the loading conditions or crack reopening. These preliminary observations will be verified by testing the remaining FRC control mix.
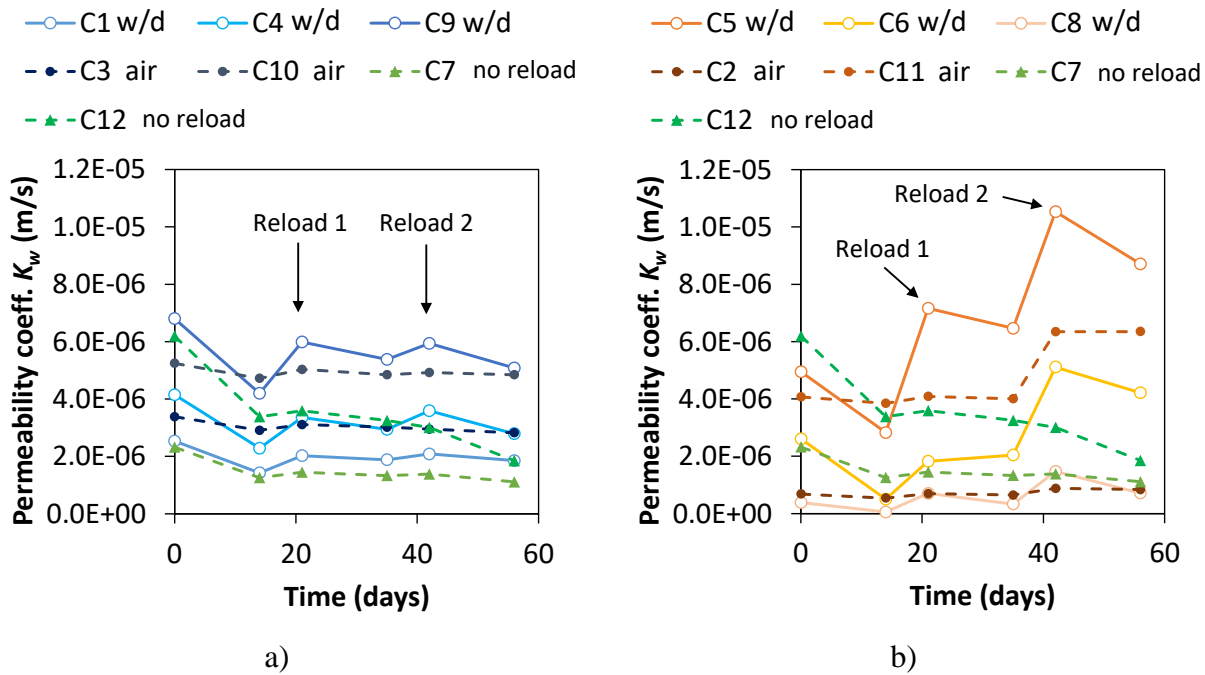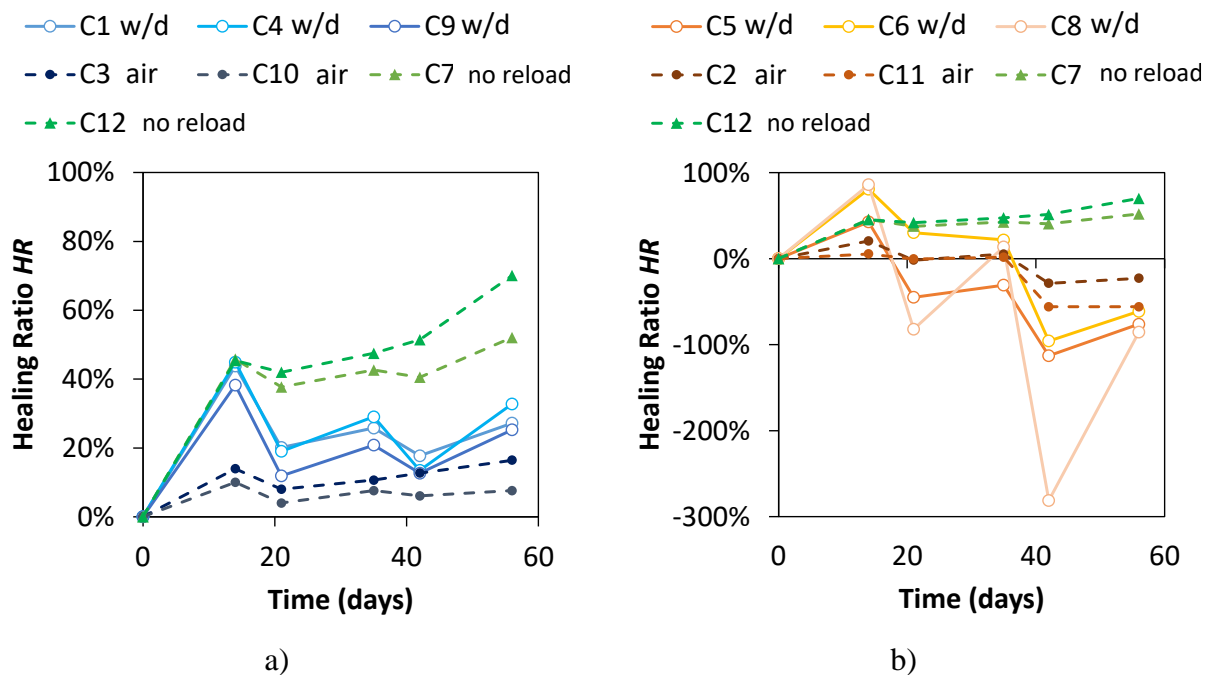

Figure 7.13. Evolution of Healing Ratio *HR* for a) reloading up to $CMOD_{max}$ and b) reloading to CMOD+0.2 mm, C7 and C12 are reference specimens not reloaded

7.5.5 Discussions and conclusions

The impact of reloading when increasing the crack widths (CMOD+0.2 mm) (**Figure 7.12b** and **Figure 7.13b**) was greater than reloading with constant crack widths (CMOD$_{max}$) on the self-healing process. Two phenomena occur at the same time with opposite effects. The first one is the damage effect of reloading, which either widens the crack opening or breaks the healing products. The second one is the healing process, where old healed surface stays at a low speed of healing or new surface has a high speed of healing.

Moreover, when increasing the crack width (CMOD+0.2 mm), the impact of reloading 2 was greater than reloading 1. This is certainly due to the fact that the water flow Q, and hence K_w, is proportional to the cube of crack width as previously mentioned (Poiseuille's law).

Based on the water permeability results presented previously, it can be concluded that self-healing still occurred under repeated reloading. When reloading to the same maximal crack width CMOD$_{max}$, the self-healing process enabled to keep a certain portion of the initial healing and reach final *HR* higher than the companion reference specimens in air exposure (unhealed specimens). In that case, the damage effect is lower than the healing effect.

On the other hand, when reloading to widen the cracks (CMOD+0.2 mm), the initial self-healing effect disappeared with the impact of the reloading, reaching permeabilities higher than K_{wi}. In that case, the damage effect is superior to the healing one. However, the self-healing potential was higher (slope of healing curve) for this type of reloading (CMOD+0.2 mm), because new crack surfaces are created that will heal fast and a same thickness of healing products will lead to a greater permeability reduction compared to the first type of reloading (CMOD$_{max}$) due to Poiseuille's law.

Further analyses of the results of this experimental program will be performed beyond the scope of this thesis, such as measuring the crack widths, transforming the water permeability results in the form of equivalent crack width to better compare the different prisms performance and choosing adequate mechanical recovery indexes to highlight the self-healing and reloading effects.

CHAPTER 8   GENERAL DISCUSSION

This chapter will first present a general discussion regarding self-healing from a scientific point of view, based on all the results found in this research project. Then practical considerations of self-healing, such as robustness criteria, real applications and costs will be addressed.

8.1 Scientific discussions

8.1.1 What is the most influencing self-healing parameter?

The healing condition! As seen in **Figure 5.8** (**Chapter 5**), the exposition impacted greatly the self-healing kinetics, regardless of the mix. In water immersion, the self-healing rate in terms of Healing Ratio started in average with 7.3%/day (permeability reduction at 11 days) and then decreased to 0.2%/day after the second measurement at 25 days, 0%/day after 2 months and 0.1%/day after 3 months (**Figure 8.1a**). In wet/dry cycles, the self-healing occurred more progressively. The average self-healing rate started with 6.7%/day, followed by 0.6%/day after 25 days, 0.2%/day after 2 months and 0.1%/day after 3 months (**Figure 8.1a**). In outdoor exposure, the self-healing kinetics were also progressive and obviously slower. The self-healing rate started with 0.4%/day, followed by 0.2%/day after 3 months, 0.2%/day after 9 months and 0.01%/day after 12 months (**Figure 8.1b**).
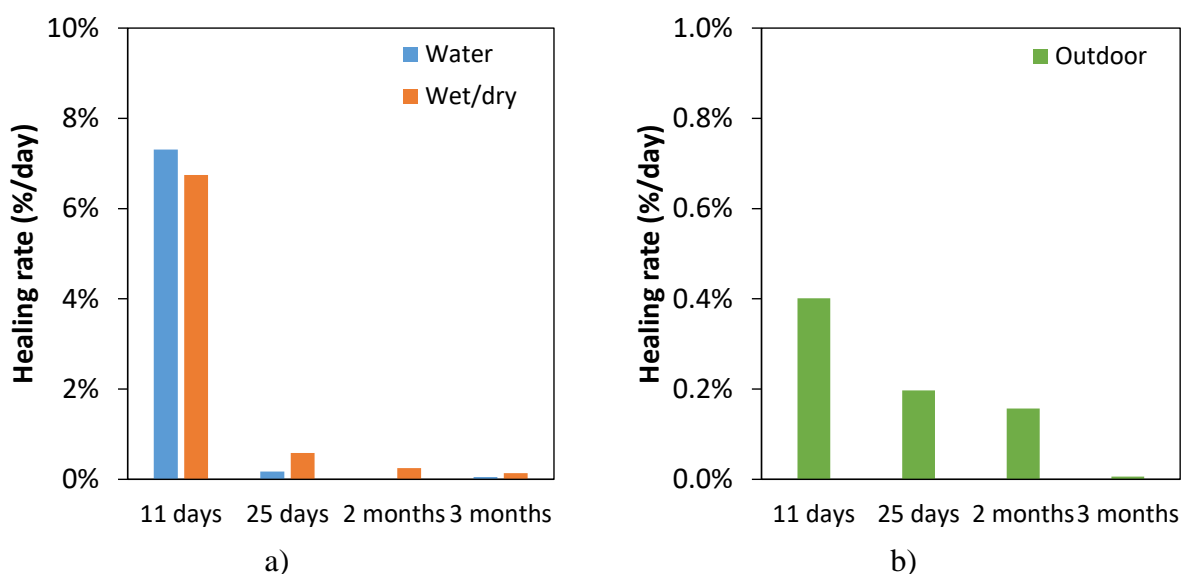
Figure 8.1. Average healing rate per day of all mixes for a) water and wet/dry and b) outdoor exposures

The healing condition also strongly impacted the final healing capacity, the Strength Regain and the type of healing products observed in cracks. Information is summarised in **Table 6.5** (**Chapter 6**). The final *HR* were in average higher in wet/dry (93%), followed by water (84%) and outdoor (71%) exposures. The Strength Regains were in average higher in outdoor (106%), followed by wet/dry (99%) and water (95%) exposures. The healing products were also different according to the exposition: ettringite and calcite in water, calcite and vaterite in wet/dry and larger calcite crystals in outdoor exposures.

8.1.2 Does self-healing occur in outdoor condition in northern climate?

Yes, but at a slower rate, as described in the previous section. As seen in **Figure 5.15** (**Chapter 5**), the precipitations in Montreal between March 2019 and March 2020 were mostly between 50 to 150 mm/month, with a peak of 261 mm in October. According to Gouvernement du Québec (2021), the climate in Montreal is cold and humid. This high humidity and frequent precipitations probably favoured self-healing. On the other hand, the cold temperature has a negative effect on the healing process as all chemical reactions are hindered close to 0°C. During the long-term exposition, the temperature reached a minimum of -22°C (February 2020) and the average temperatures were below 0°C for 5 months. In warmer climates with sufficient humidity, the self-healing capacity would probably be greater.

The use of self-healing agents, which will be discussed further (**Section 8.1.5**), can enhance the self-healing capacity outdoor.

8.1.3 Do partially or completely healed cracks have a mechanical recovery?

Yes, partially healed cracks presented high Strength Regains, particularly for the outdoor exposition, regardless of the mix. However, as seen in **Figure 6.13** (**Chapter 6**), the Strength Regains (*SR*) were not correlated to the final Healing Ratio (*HR*). Macroscopic observations taken with the digital microscope on prisms exposed indoor and outdoor, demonstrate again, in **Appendix B,** the non-correlation between the surface crack closure, Healing Ratio and Strength Regain. The readers are also invited to look at **Appendix C** for more microscopic observations. As presented in **Chapter 6**, the absence of correlations between these parameters can be explained by

the difference in the type of healing products as well as their distribution and densities at micro- and macroscopic scales in the whole crack (inside and at crack surfaces).

As a reminder, the prisms were placed with face 1 upward and face 2 downward (**Figure 3.2b**) in all expositions. In **Figure 8.2**, white products were visible along the whole crack length on face 1 and face 2 of a prism after healing under water immersion for 25 days. This was also the case for the prisms in wet/dry cycles (**Figures B.1-B.4** in **Appendix B**).
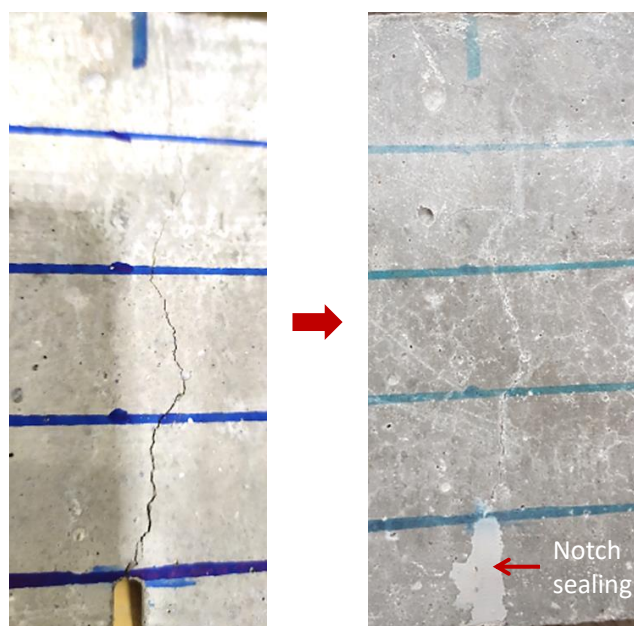
Figure 8.2. Pictures of the crack before and after healing under 25 days in water immersion

However, the prisms exposed outdoor had more white crystals in the cracks on face 2 than on face 1 (**Figure B.5** in **Appendix B**), which is due to water droplets penetrating in the crack via face 1 and went down to face 2 due to gravity. Moreover, observations through binoculars performed on the interior of the cracks also showed that more healing products were located near faces 1 and 2 on the indoor specimens, whereas they were more distributed inside the cracks for the outdoor specimens (**Figure 6.15** in **Chapter 6**).

Figure 8.3 presents a simplified sketch of the healing products and densities found in the cracks of prisms exposed to water, wet/dry and outdoor conditions (**Table 6.5** in **Chapter 6**). In water immersion, ettringite and calcite were more present on both external faces of the prism with fewer products inside the crack, which could explain the high Healing Ratio and lowest Strength Regain

compared to the other expositions. In wet/dry cycles, very dense vaterite and calcite crystals were mainly present in both external faces of the prism too. The denser and the more robust healing products could explain the highest *HR* and higher *SR* than under water immersion. Finally, for the outdoor exposure, calcite under the shape of small and larger crystals were observed. In comparison to the indoor healed specimens, there was less products along the crack length at the external surfaces (**Figure 6.14** and **Figure**), but more products were found inside the crack (**Figure 6.15**). This could explain the lowest *HR*, as crack remained partially filled, but the highest *SR*, with more healing products distributed inside the crack.
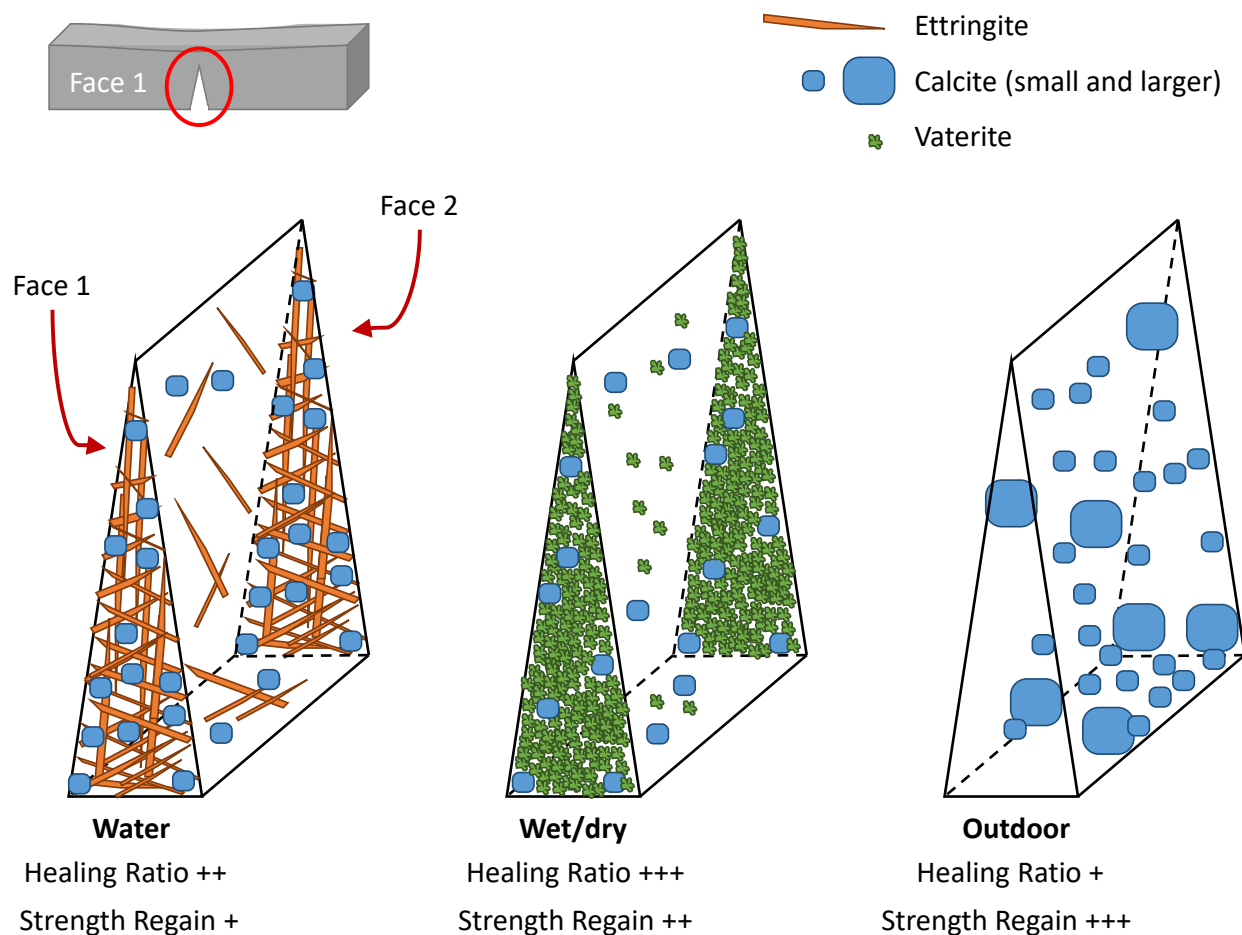
Figure 8.3. Simplified sketch of the microstructure of the healing products in the cracks explaining the performances observed in water, wet/dry and outdoor conditions

8.1.4 Which aspect of healing, durability or mechanical, is the most important?

In the author's opinion, self-healing that resists against penetration of water and hence ingress of potential harmful agents, is of utmost importance to reduce degradation of concrete structures, increase their durability and avoid expensive repair and maintenance, which is the main purpose of self-healing. Therefore, the healing performance measured by water permeability is preferable to the performance evaluated by mechanical recovery measurement. It must be noted however that Litina et al. (2021) observed that water tightness obtained after healing does not necessarily prevent the ingress of chloride, as they found chloride ingress in specimens that presented a complete healing in water permeability tests.

The mechanical regain brought by self-healing is here considered as a bonus. Van Tittelboom and De Belie (2013) also declared that the mechanical recovery is less important, but they insisted that the strength of the healing products as well as the bond strength between them and the matrix should be higher than the concrete strength to prevent the reopening of the healed cracks. Ferrara et al. (2018) suggested, on the other hand, to consider the mechanical regain in a design perspective to calibrate a "healing-modified" decaying law. Finally, Buller et al. (2019) recommended to evaluate both durability and mechanical properties of healed concrete to ensure the sustainability of concrete structures.

Besides, the choice of the self-healing approach and the selection of the healing objective (recovery of a durability and/or a mechanical property) would depend on the structure. These practical considerations will be discussed further in **Section 8.2**.

8.1.5 Do crystalline admixtures, expansive agents and superabsorbent polymers enhance self-healing?

Yes, the addition of CA, CSA and SAP enhanced self-healing compared to the control mix, regarding water permeability measures and mechanical recovery evaluations. The beneficial effect of these self-healing agents was particularly noticeable regarding Healing Ratio in outdoor exposure (**Figure 5.8d** in **Chapter 5**).

The concrete mix composition that showed the best performance is not straightforward because of the greater dependency on the healing condition and because there were slight differences between

the FRC mixes in each condition. A complete revision of the results is required to establish the best self-healing agents. **Table 8.1** lists the criteria considered for the self-healing performance and the classification of the FRC mixes (best and worst performances). In terms of water permeability, the ideal FRC mix should heal quickly (high initial *HR* and initial equivalent crack closure rate), have a high healing capacity (high final *HR*) and have potential for further healing (final equivalent crack closure rate). In addition, a good self-healing performance in outdoor exposition is considered essential. The SAP and CA mixes performed the best in outdoor exposure, while the control mix performed the worst. Overall, the SAP and CA mixes performed the best regarding water permeability.

In terms of mechanical recovery, the ideal FRC mix should have a good initial flexural behaviour before any healing, a high Strength Regain, a high deflection capacity for ductility and a good performance in outdoor exposition. The SAP, CA and control mixes performed the best in outdoor exposure, while the CA+CSA mix performed the worst. Overall, the SAP mix performed the best regarding mechanical recovery, because the CA mix presented the lowest initial flexural behaviour and because the control mix ranked among the worst in other expositions.

In conclusion, regarding both durability and mechanical properties, the SAP mix is considered the best candidate.

In addition, the combinations of CA+SAP and CA+CSA did not present any synergetic effect. The effect of the SAP was noticeable as SAP and CA+SAP mixes were less impacted by the exposure condition (high *HR* in **Table 5.3** for all expositions in **Chapter 5**), because SAP particles released water during drier periods.

In any case, the choice of the self-healing approach must be taken considering the application, as it will be discussed in **Section 8.2**.

Table 8.1. Criteria for the self-healing performance and classification of the FRC mixes

Criteria		Best FRC mixes	Worst FRC mixes
Water permeability (**Figure 5.8,** **Table 5.3**, **Table 6.5**, **Figure 5.11**)	Quick initial healing (high initial *HR* and high initial crack closure rate)	Water: control > **SAP** ≥ CA+CSA Wet/dry: control > CA+CSA ≥ CSA > **SAP** Outdoor: CSA > CA+CSA > **SAP**	Water: CSA > CA+SAP ≥ **CA** Wet/dry: CA+SAP > **CA** Outdoor: CA+SAP > **control** > CA
	Great healing capacity (high final *HR*)	Water: control > CSA ≥ **SAP** > CA+SAP Wet/dry: CA+CSA ≥ CSA > **CA** > control > **SAP** Outdoor: **SAP** > **CA** > CSA > CA+CSA > CA+SAP	Water: **CA** > CA+CSA Wet/dry: CA+SAP Outdoor: **control**
	Potential for further healing (high final equivalent crack closure rate)	Water: CA+SAP > control > CSA Wet/dry: **CA** > CA+SAP > **SAP** Outdoor: **CA** ≥ **SAP** > CA+SAP	Water: CA+CSA > **SAP** > **CA** Wet/dry: CSA > CA+CSA > **control** Outdoor: **control** > CA+CSA > CSA
	Good performance in real outdoor exposition	**SAP** and **CA**	**Control**
	→ Best mix overall	**SAP** and **CA**	
Mechanical recovery (**Figure 6.7,** **Figure 6.9,** **Table 6.5**, **Figure 6.12**)	Good initial flexural behaviour (fibres orientation and density considered)	Indoor batch: **SAP** ≥ CA+SAP ≥ **control** Outdoor batch: CA+CSA > **SAP** ≥ **control** ≥ CA+SAP ≥ CSA	Indoor batch: **CA** > **CA+CSA** > CSA Outdoor batch: **CA**
	Great strength recovery (high *SR*)	Water: CA+CSA ≥ **SAP** > CA+SAP Wet/dry: **SAP** ≥ **CA** ≥ CA+SAP Outdoor: **CA** ≥ **control** > **SAP** ≥ CA+SAP ≥ CSA	Water: **control** > CSA > **CA** Wet/dry: CSA > **control** ≥ **CA+CSA** Outdoor: **CA+CSA**
	High deflection capacity	Water: **CA** ≥ CA+CSA ≥ **SAP** Wet/dry: CA+SAP > CA+CSA ≥ **SAP** Outdoor: **control** > **SAP** > **CA** ≥ CA+SAP	Water: CSA > **control** > CA+SAP Wet/dry: **control** > **CA** > CSA Outdoor: CSA > **CA+CSA**
	Good performance in real outdoor exposition	**SAP**, **CA** and **control**	**CA+CSA**
	→ Best mix overall	**SAP**	

8.1.6 Is self-healing robust under repeated reloading?

Yes, the self-healing capacity measured by water permeability tests showed robustness under repeated damage but it depends on the type of reloading. Two phenomena occur at the same time with opposite effects: healing (in wet/dry cycles) and damage (during reload) (**Figure 7.13**). According to the type of reloading, one effect dominates over the other.

When the reloading is limited to the same $CMOD_{max}$, the effect of the self-healing process is superior to the one of damage (permeability coefficient stayed below the initial K_{wi}). One can imagine that after more healing/cracking cycles, the crack would gradually heal completely.

When the reloading gets further (CMOD+0.2 mm), the effect of healing became inferior to the one of damage in this project (water permeability coefficient exceeded the initial K_{wi}, leading to negative *HR*). This observation is surely related to the increase of cracks at each reload. $\Delta CMOD = 0.2$ mm was selected to observe healing in a critical context, but it is probably too high a variation of crack opening in comparison with the variations expected in structures. Despite this high variation, self-healing occurred after each reload.

In conclusion, repeated reloading slows down healing but self-healing always occurs!

8.2 Practical considerations

8.2.1 Robustness of the testing methods to evaluate self-healing

Tang et al. (2015) proposed the following criteria to establish the robustness of the self-healing evaluation method: reliability, quality of the results, operational considerations and in-situ applicability. These criteria were verified for the methods used in this project (water permeability and mechanical recovery of the same specimen) as shown in **Table 8.2**.

From this table, it can be concluded that the methodology used in this project meets most of the robustness criteria, except the in-situ applicability, which was not considered a priority in this research project. The water permeability measurements provided clearer trends though between the mix compositions and exposure conditions compared to the mechanical tests.

In any case, future standard tests to evaluate self-healing could be inspired by the methodology used in this project to assess water permeability and mechanical recovery of the same specimen.

Table 8.2. Review of the self-healing evaluation methods used in this project regarding robustness criteria proposed by (Tang et al., 2015)

Criteria	Methods used in this project to evaluate self-healing
Reliability (repeatability and reproducibility, existing standard test)	- Water permeability test does not come from an existing standard test, but the 3-point bending test does (EN 14651). - The repeatability and reproducibility of the water permeability test were confirmed. - Although the 3-point bending test is standardised, variation between the prisms of a same mix was observed.
Quality of the results (qualitative or quantitative results, straightforward results or further interpretation required)	- Both water permeability and mechanical tests give quantitative results. - Water permeability test gives straightforward results. Flow rate Q, and then K_w, HR and w_{eq} can be calculated. - Flexural test gives results that require further interpretation. Many different recovery indexes are used that depend on the loading procedure and the materials used.
Operational considerations (simplicity and safety concerns)	- Both water permeability and mechanical tests are simple to perform and do not require highly specialised trained operators. - Water permeability measure requires more equipment and operations, though. - Both tests are safe and present minimal hazards.
In-situ applicability (destructiveness of the method and field application	- Water permeability test is a non-destructive test, while the flexural test is destructive. - Both water permeability and mechanical tests are limited to the laboratory application. They cannot be applied on a structure.

8.2.2 Robustness of the self-healing approaches

Li and Herbert (2012) proposed the following criteria to evaluate the robustness of the self-healing approaches: shelf life, pervasiveness, quality, reliability, versatility and repeatability. The quality of the self-healing represents the recovery of mechanical and of durability properties. The duration and complexity of implementation of the approach as well as the costs are additional criteria considered. A review of the results obtained in this project was combined with an evaluation of other self-healing approaches (chemical encapsulation, bacteria, glass tubing, ECC) by Li and Herbert (2012) and is presented in **Table 8.3**.

Table 8.3. Review of self-healing approaches from (Li & Herbert, 2012) including the healing agents used in this project regarding robustness criteria

Criteria	Chemical encapsula-tion	Glass tubing	Bacteria	ECC/ UHPC	Admixtures in this project
					CA, CSA, SAP
Shelf life	±	±	−	+	+
Pervasiveness	+	−	+	+	+
Quality (recovery of durability and mechanical properties)	+	+	+	+	+
Reliability (low coefficient of variation)	?	?	?	?	+
Versatility (in wide range of environments)	+	+	±	±	±
Repeatability	±	−	?	+	+
Implementation	−	−	−	+	+
Costs	−	−	−	−	+

+ positive, ± intermediate, − negative effects, ? not enough data

The shelf life ranges from about 1 year to 3 years for chemicals like epoxy and polyurethane (PUR), and 5 years for SAP particles (De Belie et al., 2018), before they start to degrade. Bacteria have long-term viability issues in concrete. Mineral admixtures (CA and CSA) have a long shelf life, they remain active as they are unhydrated.

Most self-healing approaches are pervasive except glass tubing, where capsules are placed at some locations. Concerning the quality of the self-healing approach, in particular the recovery of mechanical properties, it has been indicated that different loading procedures and recovery indexes are used and comparison regarding this criterion is difficult. Besides, as seen in this project, the healing condition impacts the Strength Regain. In general, most self-healing approaches present a mechanical regain to a certain extent compared to the control mix. However, only when using polymeric agents (epoxy resin, PUR, cyanoacrylate), the healed specimens can recover their initial mechanical properties.

Furthermore, low coefficient of variations (COV) are needed to have reliable self-healing approaches. In this project, the variation between the specimens of the same condition depended on the self-healing process. When self-healing was favoured, low variation was obtained. For example,

COV ranged from 0.4% (CA+CSA mix) to 6% (CA+SAP mix) for the final Healing Ratio in wet/dry exposure. CA+CSA and CA+SAP mixes showed the highest and lowest final *HR* respectively. In outdoor exposure, as healing was slower, the COV ranged from 9% (SAP mix) to 26% (control mix). Finally, regarding the Strength Regain, COV ranged from 1 to 11% in all conditions. Not enough data are available for proper assessment of the reliability of the other approaches.

Only chemical encapsulation techniques are completely versatile as they are truly autonomic approaches. Their mechanism is triggered with cracking and contact with air, and do not need water to react. Bacteria need water, as well as approaches that stimulate autogenous healing (mineral admixtures, SAP and ECC/UHPC).

The self-healing repeatability has not been largely examined yet. Glass tubing is not repeatable as the tubes run out upon cracking. Depending on the amount of microcapsules, they could be repeatable. The stimulated autogenous healing approaches including mineral admixtures and ECC/UHPC are repeatable as long as there remain unhydrated particles. Most approaches may be repeatable, but the self-healing capacity may be limited depending on the reloading condition. In any case, infinite repeatability is surely not possible.

The last criteria concern the implementation and costs of the healing approaches. The use of CA, CSA and SAP admixtures are easier to implement and cheaper than the other approaches, as it will be detailed in **Section 8.2.4**. CA and CSA are admixtures already established in the market and they do not modify the concrete production procedure.

In conclusion, self-healing approaches with admixtures like CA, CSA and SAP meet most of the criteria required for their implementation in concrete structures, making them relevant and interesting.

8.2.3 Applications of self-healing approaches in concrete structures

As mentioned previously, the choice of the self-healing approach depends on the application, and especially the exposition of the concrete structure. The importance of the structural element must also be considered.

Table 8.4 presents some examples of potential applications for each self-healing approach. Encapsulated chemical agents (such as epoxy and PUR) allow to heal very fast because they harden upon contact with air upon cracking. Such approaches would be necessary for structures that need quick healing and that need a high mechanical regain, such as nuclear power plants. Because glass tubes need to be placed manually in the moulds, they can only be installed in precast concrete. As bacteria need water to react, they will be efficient in water-retaining structures. For strain-hardening materials that are characterised by very narrow cracks (ECC and UHPFRC), they would be interesting for concrete structures under severe exposition such as marine structures, bridges decks and piles.

Finally, the use of mineral admixtures, such as CA and CSA, would be efficient in structures exposed to water immersion and more particularly in wet/dry periods, as seen in this project. For example, applications in bridges decks and piles as well as roads would be useful. The use of SAP would be adequate in wet/dry environment as well as in humid condition with no contact with liquid water as SAPs can absorb water from humidity. Thus application in tunnels would be possible, in addition to applications on bridges and roads.

Besides, self-healing concrete could also be used as a repair material. For example, Wiktor and Jonkers (2012) developed a liquid bio-based repair system that can be sprayed onto a concrete surface to heal the cracks (Sangadji et al., 2017). (U)HPFRC is also employed for repairing existing concrete beams, columns and joints (Sánchez et al., 2018), and such material enhance self-healing (Ferrara et al., 2016b). Vascular systems, where healing agents can be supplied anytime with human intervention, are very similar to the concept of injecting repair agents (De Belie et al., 2018).

As Mors and Jonkers (2019) stated, the use of self-healing approaches would enable to do crack management instead of crack prevention. That means reducing the cost and amount of steel reinforcement to limit the crack width at 0.3 or 0.4 mm for bridges in Canada instead of 0.25 mm.

Table 8.4. Examples of potential applications for each self-healing approach

	Chemical encapsulation	Glass tubing	Bacteria	ECC UHPFRC	Admixtures in this project	
					CA, CSA	SAP
Best favourable condition	Any exposition	Any exposition	Water	Water	Water and wet/dry periods	Wet/dry and humid environment
Application	For structures that need quick healing and/or high mechanical recovery		For structures that are permanently in contact with water	For structures that need very limited crack widths for example in severe condition	For structures that are sometimes wet, sometimes dry	For structures that could not be in contact with liquid water
Examples	Nuclear power plants	Precast concrete	Water-retaining structures	Marine structures, bridges decks and piles	Bridges decks and piles, roads	Bridges decks and piles, roads, tunnels

8.2.4 Costs

How much do these self-healing approaches cost? The additional costs for using self-healing agents will be presented, but it must be noted that the information given is purely indicative to have an order of magnitude, and that the prices can vary according to the country and economical situation.

The following calculations (**Table 8.5**) can be made considering:

- The additional cost per m³ of concrete;

- Only the cost of materials is considered;

- With 550 kg/m³ the dosage of cement in this project;

- The price of CSA was given by the manufacturer for a ready-mix concrete perspective;

- The price of CA is the average price mentioned in (Roig-Flores et al., 2021) converted in US dollars;

- The price of SAP comes from (Snoeck, 2015) converted in US dollars.

Table 8.5. Estimation of additional costs per m³ of concrete for the self-healing agents used in this project

Self-healing agent	Dosage ($\%\text{-}m_{cement}$)	Price ($/kg)	Total cost ($/m³)
CSA	3.33%	1.0 – 1.2	18 – 22
CA	2%	8.1	89
SAP	0.5%	3.6	9.9

In comparison, the additional costs for other self-healing approaches are shown thereafter, as estimated by Snoeck (2015), converted in US dollars. It must be noted that these costs only consider the cost of the materials and components and not the manufacturing costs, which would be significantly higher for the encapsulation techniques.

- Microcapsules containing polyurethane (3%-vol) = **763 $/m³**;

- Bacterial spores ($1 - 4\%\text{-}m_{cement}$) in microcapsules ($1 - 3\%\text{-}m_{cement}$), considering 300 kg/m³ of cement = **187 to 568 $/m³**;

- Microfibres (2% PVA) with SAP ($1\%\text{-}m_{cement}$), considering 571 kg/m³ of cement = **85 $/m³**.

It can be seen that the costs of the self-healing agents used in this project are significantly lower by one order of magnitude than the other self-healing approaches.

In any case, despite the higher initial cost of self-healing concrete compared to a normal concrete, the total life cycle cost of structure containing such material would be lower than normal or high strength concrete structures, if no repair is needed, as illustrated by **Figure 8.4**, from (van Breugel, 2007).
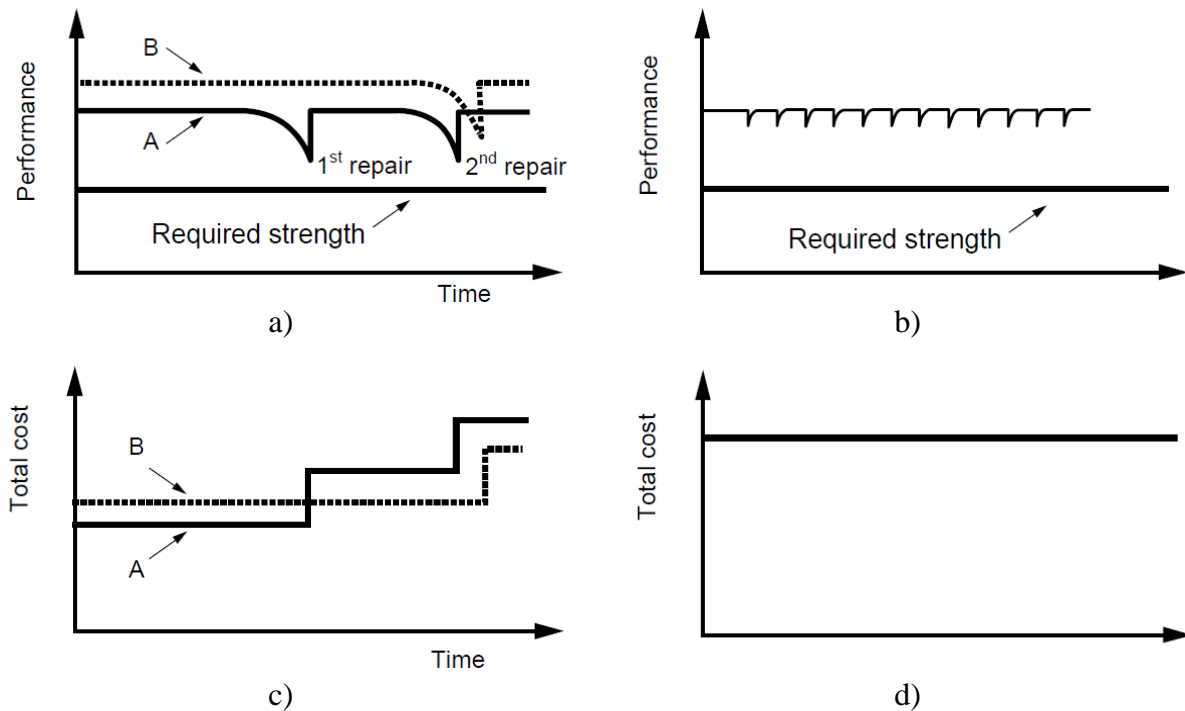

Figure 8.4. a) Conceptual performance for normal (A) and high strength (B) concrete structures and b) for self-healing concrete structure, and c) and d) their corresponding costs, from (van Breugel, 2007)

CHAPTER 9   CONCLUSIONS AND RECOMMENDATIONS

9.1 Objectives of the project

This research project aimed to evaluate the self-healing capacity of concrete containing various admixtures (crystalline admixture CA, expansive agent CSA, superabsorbent polymer SAP) alone and in combinations (CA+SAP and CA+CSA) under several expositions via a thorough characterisation (water permeability, mechanical recovery, visual observations and microscopic analyses).

The specific objectives of this project are reminded hereafter:

1. Develop and validate a new water permeability set-up adapted to concrete prisms with a flexural crack;

2. Evaluate the self-healing potential of concrete containing various admixtures under laboratory (water immersion, wet/dry cycles, air, water flow) and outdoor expositions with several characterisation methods (water permeability, mechanical recovery and microstructure analyses);

3. Evaluate the self-healing potential of concrete under repeated reloading;

4. Establish performance of concrete compositions, exposure conditions and experimental methods to improve and measure the self-healing capacity of concrete and deepen fundamental understanding of the phenomenon.

Three experimental programs were carried out corresponding to the first three specific objectives. The new knowledge and understanding of self-healing gathered in this project answered the fourth specific objective.

9.2 Conclusions

9.2.1 Testing methods to evaluate self-healing

In this research project, the self-healing capacity of a fibre reinforced concrete (FRC) was evaluated with water permeability test, mechanical recovery evaluations and visual observations of the crack closure on the same pre-cracked prism. Microscopic analyses (SEM-EDS) were also performed on healed crack surfaces. This is the first time that all these properties were determined on the same specimen.

The following conclusions can be drawn on the testing methods:

- The new water permeability set-up developed is robust. It provides repeatable and reliable results to evaluate self-healing of prisms having a flexural crack.

- Water permeability coefficient (K_w) slightly decreases with increasing pressure gradient from 20 to 40 kPa for specimens with K_w above $3\text{x}10^{-6}$ m/s. Below this threshold, the impact of the pressure gradient was negligible. This study of the impact of the pressure gradient allowed to select the adequate pressure gradient applied in the next experimental programs (30 kPa).

- Assessing self-healing of prisms via surface crack closure measurements (Closing Ratio) may lead to over- or underestimation of the self-healing process measured by water permeability test (Healing Ratio). Macroscopic observations of the healed cracks should thus be taken for qualitative assessment only.

- Contrary to surface crack measurements, K_w gives information on the whole crack volume and thus better characterise crack changes during self-healing. In addition, it directly gives information on durability recovery that could be expected on a structure. Therefore, water permeability measurement is the best evaluation method to evaluate concrete self-healing. Besides, water permeability results are easy to compare with the ones in literature.

- Mechanical recovery depends greatly on the loading procedure and recovery indexes selected, thus comparison with literature is difficult. Reference uncracked specimens

subjected to the same condition as cracked specimens are important to adequately determine the effect of self-healing. They are rarely considered in literature.

- Durability recovery measured by water permeability test (Healing Ratio) is not governed by the same parameters (density, distribution and type of healing products) as mechanical recovery measured by flexural tests (Strength Regain). As a consequence, the healing mechanical performance was not correlated to the durability performance. Partially healed cracks in terms of Healing Ratio can have a high Strength Regain.

- Additional microscopic analyses are required to better understand the healing process in the different and expositions.

- The methodology used in this project (water permeability and flexural recovery on the same specimen) enabled to assess thoroughly self-healing in concrete and to deepen fundamental understanding of the self-healing phenomenon. This methodology could inspire standard testing methods to evaluate self-healing.

9.2.2 Impact of the healing exposition

In Experimental Program 2 of this project, prisms were exposed in laboratory and outdoor conditions. The laboratory conditions consisted in water immersion, wet/dry cycles, air (only for the control mix) for 3 months and a continuous water flow test for around 1 week. The realistic outdoor exposure lasted for 1 year in Montreal climate.

The following conclusions can be drawn on these healing expositions:

- The healing exposition is the most influencing factors of self-healing. Its impact was visible through water permeability measures, mechanical recovery evaluations and microscopic analyses.

- The self-healing kinetics was rapid and then stabilised in water immersion, while it was more progressive in wet/dry cycles and slower in outdoor exposure.

- The expositions that most favoured self-healing in terms of final Healing Ratio were in the following order: wet/dry cycles (93%) > water immersion (84%) > outdoor exposure (71%).

The order was opposite when considering the Strength Regain: outdoor exposure (106%) > wet/dry cycles (99%) > water immersion (95%).

- The Healing Ratio is mostly influenced by the density of the healing products at macroscopic (external crack surfaces) and microscopic (crack faces analysed by SEM) scales. The expositions with respect to the densities were in the following order: wet/dry cycles (very dense products covering the whole external crack surfaces) > water immersion (dense products covering the whole external crack surfaces) > outdoor exposure (dense products not covering the whole external crack surfaces).

- The Strength Regain is mostly influenced by the type of healing products and their distribution inside the crack. The expositions with respect to the type of healing products and their distribution were in the following order: outdoor exposure (large calcite crystals and more healing products inside the crack) > wet/dry cycles (vaterite and calcite more present the external crack surfaces) > water immersion (ettringite and calcite more present at the external crack surface). More healing products were formed in depth in outdoor exposure because self-healing occurred more slowly. In wet/dry and water conditions, healing occurred more rapidly, hence the CO_2 and water were partly blocked to further penetrate into the crack.

- Continuous water flow test did not accelerate self-healing in comparison to water immersion. Different healing products were found under continuous water flow, mainly aragonite, in comparison to calcite and ettringite in water immersion.

- For the first time, time equivalence between a laboratory condition and the real outdoor condition was established. 25 days in laboratory wet/dry condition could represent 5 to 50 months outside depending on the FRC mix considered.

9.2.3 Influence of the self-healing agents

The Experimental Program 2 also aimed to investigate the impact of using various self-healing agents. Six FRC mixes were made, the control mix as well as mixes containing CSA, CA, SAP and the combinations CA+SAP and CA+CSA. The mixes containing SAP were adjusted with additional superplasticiser to compare the FRC mixes with similar mechanical performance.

The following conclusions can be drawn on these mixes containing self-healing agents:

- There were slight differences between the healing performance of the mixes in each exposition studied, for water permeability, Strength Regain observations and microstructure. Each healing agent provided globally some improvement compared to the control mix.

- The mix containing CSA presented in general high Healing Ratio (*HR*) (among the top 3 in all expositions) but lower Strength Regains (*SR*) (among the bottom 2).

- The mix containing CA was often among the top 3 regarding both *HR* and *SR*, except in water immersion where it showed the lowest *HR*. Besides, the CA mix presented the lowest initial flexural performance.

- The mixes containing SAP (SAP and CA+SAP) were less influenced by the exposure condition, due to the internal supply of water during drier periods. The SAP mix was mostly among the top 3 for both *HR* and *SR*. The CA+SAP mix was, on the other hand, often among the bottom 3.

- No synergetic effect was found in CA+SAP and CA+CSA mixes compared to the performances of the single admixtures (CA, SAP and CSA).

- The SAP and CA mixes showed the best healing performance regarding water permeability results under real outdoor exposure, while the control mix performed the worst.

- The CA, control and SAP mixes presented the best healing performance regarding Strength Regain in the outdoor exposure, while the CA+CSA mix performed the worst. As the CA mix presented the lowest initial flexural performance and the control mix ranked among the worst in other expositions, the SAP mix is considered the best candidate in terms of mechanical performance.

- Overall, the SAP mix demonstrated the best healing potential in real outdoor conditions regarding both durability and mechanical properties.

9.2.4 Self-healing under repeated reloading

In Experimental Program 3 of this project, repeated reloading (pre-cracking, two reloading and then final reloading up to failure) were carried out on a CA+CSA mix exposed in wet/dry cycles. The prisms were healed for 2 weeks and they were reloaded every 3 weeks. Two types of reloading were considered: up to the same $CMOD_{max}$ so that the maximal crack width does not change (simulating a structure under low traffic and magnitude), and up to CMOD+ΔCMOD (ΔCMOD = 0.2 mm) so that the crack gets wider at each reload (simulating a structure under high traffic and magnitude). Only the water permeability results were presented. Further analyses of the crack width and mechanical recovery evaluations will be completed during postdoc activities.

The following conclusions can be drawn on the impact of repeated reloading:

- Two phenomena occur at the same time with opposite effects: healing during wet/dry exposition and damage during reloading. The magnitude of the repeated damage dictates which effect will be greater.

- When reloaded up to $CMOD_{max}$ with no increase of the original crack width, the self-healing effect was superior to the damage effect. The self-healing of prisms reloaded led to an average $HR = 28\%$, above the one of reference reloaded prisms exposed in air ($HR = 12\%$). It is assumed that after more healing/cracking cycles, the HR would increase more.

- When reloading up to CMOD+0.2 mm with increasing the crack opening, the effect of healing was inferior to the damage effect. The water permeability coefficients exceeded K_{wi}, leading to negative $HR = -74\%$. It is assumed that after more repeated reloading, K_w would increase further. However, if the prisms were reloaded with a lower and more realistic widening of the crack with or with a prolonged healing period, prisms may reach positive values of HR after more healing/cracking cycles.

- In any case, repeated reloading slows down but does not prevent healing. Not all the healing products are broken with the repeated reloading, which means that the healing products are quite strong. This confirms the self-healing potential of structures deteriorating progressively.

9.3 Recommendations for further research

9.3.1 Testing methods to evaluate self-healing

The following recommendations for further research are proposed for the testing methods to evaluate self-healing:

- Modify the water permeability set-up to enable measuring permeability of prisms simultaneously to bending load to assess self-healing under more realistic condition.

- Use the water permeability device to measure permeability of other types of specimens representative of structural components, such as reinforced prisms (with rebar instead of fibres) or tie-specimens containing the self-healing agents, under constant and cyclic loading.

- Modify the water permeability device to enable measurements in parallel on several specimens. This would facilitate testing more specimens and conditions.

- Perform repeated reloading in other conditions:

    o   Perform realistic cyclic loading to simulate road traffic;

    o   For prisms exposed outdoor;

    o   Reloading procedures involving a more realistic crack opening increase, for example ΔCMOD = 0.05 – 0.1 mm instead of 0.2 mm.

- Perform 4-point bending tests instead of 3-point bending tests to evaluate if healed cracks reopen or new cracks form elsewhere during reloading.

- Perform complete analyses to examine with more accuracy the coverage of the healing products on the crack faces. After reloading, the crack faces can be separated and analysed with a microscope or with spray of phenolphthalein to observe the surface covered by calcium carbonate. This would confirm if healing products are less present inside the crack because of a rapid self-healing process.

- Perform other durability tests on healed specimens to determine how the healing products decrease the other transport or deterioration mechanisms:

- o Chloride penetration;

- o Carbonation;

- o Sulphate attack;

- o Freeze-thaw resistance (the SAP may be beneficial).

- Perform further microscopic analyses to better identify the healing products, such as thermogravimetric analysis (TGA) or X-ray diffraction analysis (XRD).

- Develop non-destructive tests for application on structures.

9.3.2 Healing conditions

The following recommendations for further research are proposed regarding the self-healing agents/approaches:

- Expose more specimens outdoor to assess self-healing during more than 1 year, assessing self-healing via non-destructive tests (water permeability, resonant frequency…).

- Perform wet/dry cycles with seawater to represent a condition of tidal zones of marine structures.

- Large-scale projects in real condition for a new structure or a repair, with SAP and CA as self-healing agents:

  - o Large-scale slabs kept outside near a structure to receive de-icing salts and that can be transported back in the laboratory for measurements and reloading;

  - o Large-scale structural elements made with self-healing concrete that are frequently monitored.

9.3.3 Self-healing agents/approaches

The following recommendations for further research are proposed regarding the self-healing agents/approaches:

- Develop cementitious pellets containing self-healing agents to enhance the self-healing capacity as the agents remain unhydrated (not consumed) before cracking.

- Evaluate the self-healing agents of this study but in strain-hardening materials (UHPFRC or ECC) that will only present microcracks in service conditions (inferior to 0.1 mm).

- Evaluate the self-healing capacity of other admixtures, such as MgO-based expansive agent that seems promising.

- Study the performance of other self-healing approaches with the methodology used in this project (water permeability and mechanical recovery on the same prism).

9.4 Publications derived from this thesis

The following papers were submitted or published from the research activities completed in this thesis.

9.4.1 International peer-reviewed journals

1. Lauch, K.-S., Desmettre, C., & Charron, J.-P. (2021). New water permeability set-up and factors affecting concrete self-healing. *Construction and Building Materials*, *294*. https://doi.org/10.1016/j.conbuildmat.2021.123595

2. Lauch, K.-S., Desmettre, C., & Charron, J.-P. (2021). Self-healing of concrete containing different admixtures under laboratory and outdoor expositions - Part 1: water permeability. *Submitted for publication in Cement and Concrete Composites*.

3. Lauch, K.-S., Charron, J.-P., & Desmettre, C. (2021). Self-healing of concrete containing different admixtures under laboratory and outdoor expositions - Part 2: mechanical behaviour. *Submitted for publication in Cement and Concrete Composites*.

9.4.2 International peer-reviewed conference

1. Lauch, K.-S., Desmettre, C., & Charron, J.-P. (2021). Self-healing of Fibre Reinforced Concrete Containing an Expansive Agent in Different Exposure Conditions. In P. Serna, A. Llano-Torre, J. R. Martí-Vargas, & J. Navarro-Gregori, *Fibre Reinforced Concrete: Improvements and Innovations* BEFIB, Cham.

REFERENCES

ACI-212. (2012). *Report on chemical admixtures for concrete*.

Al-Tabbaa, A., Litina, C., Giannaros, P., Kanellopoulos, A., & Souza, L. (2019). First UK field application and performance of microcapsule-based self-healing concrete. *Construction and Building Materials*, *208*, 669-685. https://doi.org/10.1016/j.conbuildmat.2019.02.178

Aldea, C.-M., Shah, S. P., & Karr, A. (1999). Effect of cracking on water and chloride permeability of concrete. *Journal of Materials in Civil Engineering*, *11*(3), 181-187.

Alghamri, R., & Al-Tabbaa, A. (2020). Self-healing of cracks in mortars using novel PVA-coated pellets of different expansive agents. *Construction and Building Materials*, *254*. https://doi.org/10.1016/j.conbuildmat.2020.119254

Anglani, G., Tulliani, J.-M., & Antonaci, P. (2020). Behaviour of pre-cracked self-healing cementitious materials under static and cyclic loading. *Materials*, *13*(5). https://doi.org/10.3390/ma13051149

Assmann, A. (2013). *Physical properties of concrete modified with superabsorbent polymers* Institut für Werkstoffe im Bauwesen der Universität Stuttgart].

Azarsa, P., Gupta, R., & Biparva, A. (2019). Assessment of self-healing and durability parameters of concretes incorporating crystalline admixtures and Portland Limestone Cement. *Cement and Concrete Composites*, *99*, 17-31. https://doi.org/10.1016/j.cemconcomp.2019.02.017

Beglarigale, A., Eyice, D., Tutkun, B., & Yazici, H. (2021). Evaluation of enhanced autogenous self-healing ability of UHPC mixtures. *Construction and Building Materials*, *280*. https://doi.org/10.1016/j.conbuildmat.2021.122524

Borg, R. P., Cuenca, E., Maria Gastaldo Brac, E., & Ferrara, L. (2018). Crack sealing capacity in chloride-rich environments of mortars containing different cement substitutes and crystalline admixtures. *Journal of Sustainable Cement-based Materials*, *7*(3), 141-159.

Breysse, D., & Gérard, B. (1997). *Transport of fluids in cracked media* (Report 16 - Penetration and permeability of concrete: barriers toorganic and contamining liquids, Issue. H. W. Reinhardt.

Buller, A. S., Abro, F. U., Lee, K. M., & Jang, S. Y. (2019). Mechanical recovery of cracked fiber-reinforced mortar incorporating crystalline admixture, expansive agent, and geomaterial. *Advances in Materials Science and Engineering*. https://doi.org/10.1155/2019/3420349

Cailleux, E., & Pollet, V. (2009). *Investigations on the development of self-healing properties in protective coatings for concrete and repair mortars* Second International Conference on Self-Healing Materials, Chicago, USA.

Canadian Standards Association. (2014). CSA A23.3 : Design of concrete structures. In.

Canadian Standards Association. (2019). CSA S6 : Canadian Highway Bridge Design Code. In.

Charron, J.-P., Denarié, E., & Bühwiler, E. (2007). Permeability of ultra high performance fiber reinforced concretes (UHPFRC) under high stresses. *Materials and Structures*, *40*, 269-277.

Charron, J.-P., Denarié, E., & Bühwiler, E. (2008). Transport properties of water and glucol in an ultra high performance reinforced concrete (UHPFRC) under high tensile deformation. *Cement and Concrete Research*, *38*, 689-698.

Cuenca, E., & Ferrara, L. (2017). Self-healing capacity of fiber reinforced cementitious composites. State of the art and perspectives. *KSCE Journal of Civil Engineering*, *21*(7), 2777-2789.

Cuenca, E., Tejedor, A., & Ferrara, L. (2018). A methodology to assess crack-sealing effectiveness of crystalline admixtures under repeated cracking-healing cycles. *Construction and Building Materials*, *179*, 619-632.

De Belie, N., Gruyaert, E., Al-Tabbaa, A., Antonaci, P., Baera, C., Bajare, D., Darquennes, A., Davies, R., Ferrara, L., Jefferson, T., Litina, C., Miljevic, B., Otlewska, A., Ranogajec, J., Roig-Flores, M., Paine, K., Lukowski, P., Serna, P., Tulliani, J.-M., Vucetic, S., Wang, J., & Jonkers, H. M. (2018). A review of self-healing concrete for damage management of structures. *Advanced Materials Interfaces*, 28 pages.

de Rooij, M., Van Tittelboom, K., De Belie, N., & Schlangen, E. (2013). *Self-healing phenomena in cement-based materials : state-of-the-art report of RILEM Technical Committee 221-SHC, Self-Healing Phenomena in Cement-Based Materials* (Vol. 11). Springer.

Delsol, S. (2012). *Evaluation du coefficient d'orientation dans les bétons renforcés de fibres métalliques* Ecole Polytechnique de Montréal].

Deng, H., & Liao, G. (2018). Assessment of influence of self-healing behavior on water permeability and mechanical performance of ECC incorporating superabsorbent polymer (SAP) particles. *Construction and Building Materials*, *170*, 455-465.

Desmettre, C. (2011). *Contribution à l'étude de la perméabilité du béton armé sous sollicitations statiques et cycliques* Ecole Polytechnique de Montréal].

Desmettre, C., & Charron, J.-P. (2011). Novel water permeability device for reinforced concrete under load. *Materials and Structures*, *44*, 1713-1723.

Desmettre, C., & Charron, J.-P. (2012). Water permeability of reinforced concrete with and without fiber subjected to static and constant tensile loading. *Cement and Concrete Research*, *42*, 945-952.

Desmettre, C., & Charron, J.-P. (2013). Water permeability of reinforced concrete subjected to cyclic tensile loading. *ACI Materials Journal*, *110*(1), 79-88.

Edvardsen, C. (1999). Water permeability and autogenous healing of cracks in concrete. *ACI Materials Journal*, *96*(4), 448-454.

Escoffres, P., Desmettre, C., & Charron, J.-P. (2018). Effect of a crystalline admixture on the self-healing capability of high-performance fiber reinforced concretes in service conditions. *Construction and Building Materials*, *173*, 763-774.

European Committee for Standardization. (2004). Eurocode 2 : calcul des structures en béton - Partie 1-1 : Règles générales et règles pour les bâtiments. In. Brussels.

European Committee for Standardization. (2005). EN 14651 : Test method for metallic fibered concrete - Measuring the flexural tensile strength. In *European Standard* (pp. 17).

Fattahi, S. (2015). *Etude de l'auto-cicatrisation de mortiers contenant des additions réactives* Université de Sherbrroke].

Ferrara, L., Ferreira, S. R., Krelani, V., Silva, F., & Toledo Filho, R. D. (2014a). Effect of natural fibres on the self healing capacity of high performance fibre reinforced cementitious composites. 3rd International RILEM Conference on Strain Hardening Cementitious Composites, Dordrecht, The Netherlands.

Ferrara, L., Krelani, V., & Carsana, M. (2014b). A "fracture testing" based approach to assess crack healing of concrete with and without crystalline admixtures. *Construction and Building Materials*, *68*, 535-551.

Ferrara, L., Krelani, V., & Moretti, F. (2016a). Autogenous healing on the recovery of mechanical performance of High Performance Fibre Reinforced Cementitious Composites (HPFRCCs): Part 2 - Correlation between healing of mechanical performance and crack sealing. *Cement and Concrete Composites*, *73*, 299-315.

Ferrara, L., Krelani, V., & Moretti, F. (2016b). On the use of crystalline admixtures in cement based construction materials: from porosity reducers to promoters of self healing. *Smart Material and Structures*, *25*, 17p.

Ferrara, L., Krelani, V., Moretti, F., Roig-Flores, M., & Serna Ros, P. (2017). Effects of autogenous healing on the recovery of mechanical performance of High Performance Fibre Reinforced Cementitious Composites (HPFRCCs): Part 1. *Cement and Concrete Composites*, *83*, 76-100.

Ferrara, L., Van Mullem, T., Cruz Alonso, M., Antonaci, P., Paul Borg, R., Cuenca, E., Jefferson, A., Ng, P.-L., Peled, A., Roig-Flores, M., Sanchez, M., Schroefl, C., Serna, P., Snoeck, D., Tulliani, J.-M., & De Belie, N. (2018). Experimental characterization of the self-healing capacity of cement based materials and its effects on the material performance: A state of the art report by COST Action SARCOS WG2 [Review]. *Construction and Building Materials*, *167*, 115-142.

Gagné, R., & Argouges, M. (2012). A study of the natural self-healing of mortars using air-flow measurements. *Materials and Structures*, *45*, 1625-1638.

Gérard, B., Breysse, D., Ammouche, A., Houdusse, O., & Didry, O. (1996). Cracking and permeability of concrete under tension. *Materials and Structures*, *29*(187), 141-151.

Ghosh, S. K. (2009). Self-healing materials : fundamentals, design strategies, and applications. In *Self-healing materials* (pp. 1-28). Wiley-VCH.

Gouvernement du Québec. (2021). *Normales climatiques 1981-2010*. Retrieved 2021-06-12 from https://environnement.gouv.qc.ca/climat/normales/climat-qc.htm

Gruyaert, E., Debbaut, B., Snoeck, D., Diaz, P., Arizo, A., Tziviloglou, E., Schlangen, E., & De Belie, N. (2016). Self-healing mortar with pH-sensitive superabsorbent polymers: testing of the sealing efficiency by water flow tests. *Smart Material and Structures*, *25*, 11 pages.

Gupta, R., & Biparva, A. (2015). Innovative test technique to evaluate "self-sealing" of concrete. *Journal of Testing and Evaluation*, *43*(5), 1091-1098. https://doi.org/10.1520/JTE20130285

Hamedanimojarrad, P., Adam, G., Ray, A., Vessalas, K., Thomas, P., & Nejadi, S. (2010). *A novel multi-functional expansive additive for drying shrinkage reduction in mortars* 21st Australian Conference on the Mechanics of Structures and Materials, Melbourne (Australia).

Hearn, N. (1998). Self-sealing, autogenous healing and continued hydration : what is the difference ? *Materials and Structures*, *31*, 563-567.

Herbert, E., & Li, V. (2013). Self-healing of microcracks in Engineered Cementitious Composites (ECC) under a natural environment. *Materials*, *6*, 2831-2845.

Homma, D., Mihashi, H., & Nishiwaki, T. (2009). Self-healing capability of fibre reinforced cementitious composites. *Journal of Advanced Concrete Technology*, *7*(2), 217-228.

Hong, G., & Choi, S. (2017). Rapid self-sealing of cracks in cementitious materials incorporating superabsorbent polymers. *Construction and Building Materials*, *143*, 366-375.

Hong, G., Song, C., & Choi, S. (2020). Autogenous healing of early-age cracks in cementitious materials by superabsorbent polymers. *Materials*, *13*(3). https://doi.org/10.3390/ma13030690

Huang, H., & Ye, G. (2015). Self-healing of cracks in cement paste affected by additional $Ca2+$ ions in the healing agent. *Journal of Intelligent Material Systems and Structures*, *26*(3), 309-320.

Ismail, M. (2006). *Etude des transferts et de leurs interactions avec la cicatrisation dans les fissures pour prolonger la durée de service des infrastructures (ponts, centrales nucléaires)* Institut National des Sciences Appliquées de Toulouse]. Toulouse (France).

Jaroenratanapirom, D., & Sahamitmongkol, R. (2011). Self-crack closing ability of mortar with different additives. *Journal of Metals, Materials and Minerals*, *21*(1), 9-17.

Jensen, O. M. (2008). Use of superabsorbent polymers in construction materials. 1st International Conference on Microstructure Related Durability of Cementitious Composites, Nanjing (China).

Jensen, O. M., & Hansen, P. F. (2001). Water-entrained cement-based materials I. Principles and theoretical background. *Cement and Concrete Research*, *31*, 647-654.

Jensen, O. M., & Hansen, P. F. (2002). Water-entrained cement-based materials II. Experimental observations. *Cement and Concrete Research*, *32*, 973-978.

Jiang, Z., Li, W., & Yuan, Z. (2015). Influence of mineral additives and environmental conditions on the self-healing capabilities of cementitious materials. *Cement and Concrete Research*, *57*, 116-127.

Jonkers, H. M. (2011). Bacteria-based self-healing concrete. *Heron*, *56*(1), 1-12.

Kim, J. S., & Schlangen, E. (2010). Superabsorbent polymers to stimulate self healing in ECC. 2nd International Symposium on Service Life Design for Infrastructure, Delft (The Netherlands).

Lachemi, M., Hossain, K. M. A., Ramcharitar, M., & Shehata, M. H. (2007). Bridge deck rehabilitation practices in North America. *Journal of Infrastructure Systems*, *13*, 225-234.

Lauer, K. R., & Slate, F. O. (1956). Autogenous healing of cement paste. *Journal of the American Concrete Institute*, *27*(10), 1083-1097.

Lee, H. X. D., Wong, H. S., & Buenfeld, N. R. (2016). Self-sealing of cracks in concrete using superabsorbent polymers. *Cement and Concrete Research*, *79*, 194-208.

Li, D., Chen, B., Chen, X., Fu, B., Wei, H., & Xiang, X. (2020a). Synergetic effect of superabsorbent polymer (SAP) and crystalline admixture (CA) on mortar macro-crack healing. *Construction and Building Materials*, *247*.

Li, G., Liu, S., Niu, M., Liu, Q., Yang, X., & Deng, M. (2020b). Effect of granulated blast furnace slag on the self-healing capability of mortar incorporating crystalline admixture. *Construction and Building Materials*, *239*. https://doi.org/10.1016/j.conbuildmat.2019.117818

Li, M., & Li, V. C. (2011). Cracking and Healing of Engineered Cementitious Composites under Chloride Environment. *ACI Materials Journal*, *108*(3). https://doi.org/10.14359/51682499

Li, V. (2003). On Engineered Cementitious Composites (ECC): A review of the material and its applications. *Journal of Advanced Concrete Technology*, *1*(3), 215-230.

Li, V., & Herbert, E. (2012). Robust self-healing concrete for sustainable infrastructure. *Journal of Advanced Concrete Technology*, *10*, 207-218.

Li, V. C., Wu, C., Wang, S., Ogawa, A., & Saito, T. (2002). Interface Tailoring for Strain-Hardening Polyvinyl Alcohol-Engineered Cementitious Composite (PVA-ECC). *ACI Materials Journal*, *99*(5). https://doi.org/10.14359/12325

Litina, C., Bumanis, G., Anglani, G., Dudek, M., Maddalena, R., Amenta, M., Papaioannou, S., Perez, G., Calvo, J. L. G., Asensio, E., Cobos, R. B., Pinto, F. T., Augonis, A., Davies, R., Guerrero, A., Moreno, M. S., Stryszewska, T., Karatasios, I., Tulliani, J.-M., Antonaci, P., Bajare, D., & Altabbaa, A. (2021). Evaluation of methodologies for assessing selfhealing performance of concrete with mineral expansive agents: An interlaboratory study. *Materials*, *14*(8). https://doi.org/10.3390/ma14082024

Lo Monte, F., & Ferrara, L. (2021). Self-healing characterization of UHPFRCC with crystalline admixture : Experimental assessment via multi-test/multi-parameter approach. *Construction and Building Materials*, *283*.

Mengel, L., Krauss, H.-W., & Lowke, D. (2020). Water transport through cracks in plain and reinforced concrete – Influencing factors and open questions. *Construction and Building Materials*, *254*.

Mignon, A., Graulus, G.-J., Snoeck, D., Martins, J., De Belie, N., Dubruel, P., & Van Vlierberghe, S. (2015). pH-sensitive superabsorbent polymers: a potential candidate material for self-healing concrete. *Journal of Materials Science*, *50*, 970-979.

Mönnig, S., & Lura, P. (2007). Superabsorbent polymers - An additive to increase the freeze-thaw resistance of high strength concrete. In Springer (Ed.), *Advances in Construction Materials* (pp. 351-358).

Mors, R. M., & Jonkers, H. M. (2019). Bacteria-based self-healing concrete: evaluation of full scale demonstrator projects. *RILEM Technical Letters*, *4*, 138-144.

Mousavi, S. S., Guizani, L., Bhojaraju, C., & Ouellet-Plamondon, C. (2021). The effect of air-entraining admixture and superabsorbent polymer on bond behaviour of steel rebar in pre-cracked and self-healed concrete. *Construction and Building Materials*, *281*, 122568. https://doi.org/https://doi.org/10.1016/j.conbuildmat.2021.122568

Mousavi, S. S., Ouellet-Plamondon, C. M., Guizani, L., Bhojaraju, C., & Brial, V. (2020). On mitigating rebar–concrete interface damages due to the pre-cracking phenomena using superabsorbent polymers. *Construction and Building Materials*, *253*, 119181. https://doi.org/https://doi.org/10.1016/j.conbuildmat.2020.119181

Namnoum, C. Y., Hilloulin, B., Grondin, F., & Loukili, A. (2021). Determination of the origin of the strength regain after self-healing of binary and ternary cementitious materials including slag and metakaolin. *Journal of Building Engineering*, 102739. https://doi.org/https://doi.org/10.1016/j.jobe.2021.102739

Nanayakkara, A. (2003). *Self-healing of cracks in concrete subjected to water pressure* Second International Symposium New Technologies for Urban Safety of Mega Cities, Tokyo (Japan).

Negrini, A., Roig-Flores, M., Mezquida-Alcaraz, E. J., Ferrara, L., & Serna, P. (2019). Effect of crack pattern on the self-healing capability in traditional, HPC and UHPFRC concretes measured by water and chloride permeability.*MATEC Web Conf. (France)* Concrete Solutions 2019 - 7th International Conference on Concrete Repair, 30 Sept.-2 Oct. 2019, France.

Nishiwaki, T., Koda, M., Yamada, M., Mihashi, H., & Kikuta, T. (2012). Experimental study on self-healing capability of FRCC using different types of synthetic fibers. *Journal of Advanced Concrete Technology*, *10*, 195-206.

Palin, D., Mo, Y., Wiktor, V., & Jonkers, H. M. (2019). An Improved Test for Generating Rapid, Accurate, and Reliable Crack Permeability Data for Cementitious Materials. *International Journal of Civil Engineering*, *17*(5), 645-652. https://doi.org/10.1007/s40999-018-0326-8

Park, B., & Choi, Y. C. (2018). Self-healing capability of cementitious materials with crystalline admixtures and super absorbent polymers (SAPs). *Construction and Building Materials*, *189*, 1054-1066.

Park, B., & Choi, Y. C. (2019). Investigating a new method to assess the self-healing performance of hardened cement pastes containing supplementary cementitious materials and crystalline admixtures. *Journal of Materials Research and Technology*, *8*(6), 6058-6073. https://doi.org/10.1016/j.jmrt.2019.09.080

Park, B., & Choi, Y. C. (2021). Effect of healing products on the self-healing performance of cementitious materials with crystalline admixtures. *Construction and Building Materials*, *270*.

Picandet, V., Khelidj, A., & Bellegou, H. (2009). Crack effects on gas and water permeability of concretes. *Cement and Concrete Research*, *39*, 537-547.

Quebec Ministry of Transport. (2013). *Quebec infrastructure plan PQI 2011-2016*.

Quebec Ministry of Transport. (2019). *General condition index* (QMT statistics, Issue.

Qureshi, T. S., & Al-Tabbaa, A. (2016). Self-healing of drying shrinkage cracks in cement-based materials incorporating reactive MgO. *Smart Material and Structures*, *25*, 16 pages.

Rajczakowska, M., Nilsson, L., Habermehl-Cwirzen, K., Hedlund, H., & Cwirzen, A. (2019). Does a high amount of unhydrated Portland cement ensure an effective autogenous self-healing of mortar? *Materials*, *12*(20). https://doi.org/10.3390/ma12203298

Rapoport, J., Aldea, C.-M., Shah, S. P., Ankenman, B., & Karr, A. (2002). Permeability of cracked steel fiber-reinforced concrete. *Journal of Materials in Civil Engineering*, *14*(4), 355-358.

Reinhardt, H. W., & Jooss, M. (2003). Permeability and self-healing of cracked concrete as function of temperature and crack width. *Cement and Concrete Research*, *33*, 981-985.

Roig-Flores, M., Formagini, S., & Serna, P. (2021). Self-healing concrete-What Is it Good For? *Materiales de Construcción*, *71*(341), e237. https://doi.org/10.3989/mc.2021.07320

Roig-Flores, M., Moscato, S., Serna, P., & Ferrara, L. (2015). Self-healing capability of concrete with crystalline admixtures in different environments. *Construction and Building Materials*, *86*, 1-11.

Roig-Flores, M., Pirritano, F., Serna, P., & Ferrara, L. (2016). Effect of crystalline admixtures on the self-healing capability of early-age concrete studied by means of permeability and crack closing tests. *Construction and Building Materials*, *114*, 447-457.

Sahmaran, M., Yildirim, G., Noori, R., Ozbay, E., & Lachemi, M. (2015). Repeatability and pervasiveness of self-healing in engineered cementitious composites. *ACI Materials Journal*, *49*(112), 513-522.

Sánchez, M., Faria, P., Ferrara, L., Horszczaruk, E., Jonkers, H. M., Kwiecień, A., Mosa, J., Peled, A., Pereira, A. S., Snoeck, D., Stefanidou, M., Stryszewska, T., & Zając, B. (2018). External treatments for the preventive repair of existing constructions: A review. *Construction and Building Materials*, *193*, 435-452. https://doi.org/https://doi.org/10.1016/j.conbuildmat.2018.10.173

Sangadji, S., Wiktor, V., Jonkers, H., & Schlangen, E. (2017). The Use of Alkaliphilic Bacteria-based Repair Solution for Porous Network Concrete Healing Mechanism. *Procedia Engineering*, *171*, 606-613. https://doi.org/https://doi.org/10.1016/j.proeng.2017.01.387

Schlangen, E., & Joseph, C. (2009). Self-healing processes in concrete. In S. K. Ghosh (Ed.), *Self-healing materials* (pp. 141-182). Wiley-VCH.

Schröfl, C., Mechtcherine, V., & Gorges, M. (2012). Relation between the molecular structure and the efficiency of superabsorbent polymers (SAP) as concrete admixture to mitigate autogenous shrinkage. *Cement and Concrete Research*, *42*, 865-873.

Selvarajoo, T., Davies, R. E., Gardner, D. R., Freeman, B. L., & Jefferson, A. D. (2020). Characterisation of a vascular self-healing cementitious material system: Flow and curing properties. *Construction and Building Materials*, *245*. https://doi.org/10.1016/j.conbuildmat.2020.118332

Sevcik, R., Sasek, P., & Viani, A. (2018). Physical and nanomechanical properties of the synthetic anhydrous crystalline $CaCO_3$ polymorphs: vaterite, aragonite and calcite. *Journal of Materials Science*, *53*(6), 4022-4033. https://doi.org/10.1007/s10853-017-1884-x

Sherir, M. A. A., Hossain, K. M. A., & Lachemi, M. (2016). Self-healing and expansion characteristics of cementitious composites with high volume fly ash and MgO-type expansive agent. *Construction and Building Materials*, *127*, 80-92.

Sherir, M. A. A., Hossain, K. M. A., & Lachemi, M. (2017a). Development and recovery of mechanical properties of self-healing cementitious composites with MgO expansive agent. *Construction and Building Materials*, *148*, 789-810.

Sherir, M. A. A., Hossain, K. M. A., & Lachemi, M. (2017b). The influence of MgO-type expansive agent incorporated in self-healing system of Engineered cementitious Composites. *Construction and Building Materials*, *149*, 164-185.

Shin, K. J., Bae, W., Choi, S.-W., Son, M. W., & Lee, K. M. (2017). Parameters influencing water permeability coefficient of cracked concrete specimens. *Construction and Building Materials*, *151*, 907-915. https://doi.org/10.1016/j.conbuildmat.2017.06.093

Sisomphon, K., Copuroglu, O., & Koenders, E. A. B. (2012). Self-healing of surface cracks in mortars with expansive additive and crystalline additive. *Cement and Concrete Composites*, *34*, 566-574.

Sisomphon, K., Copuroglu, O., & Koenders, E. A. B. (2013). Effect of exposure conditions on self healing behavior of strain hardening cementitious composites incorporating various cementitious materials. *Construction and Building Materials*, *42*, 217-224.

Snoeck, D. (2015). *Self-healing and microstructure of cementitious materials with microfibres and superabsorbent polymers* Universiteit Gent]. Ghent (Belgium).

Snoeck, D., & De Belie, N. (2016). Repeated autogenous healing in strain-hardening cementitious composites by using superabsorbent polymers. *Journal of Materials in Civil Engineering*, *28*(1), 11 pages.

Snoeck, D., Dewanckele, J., Cnudde, V., & De Belie, N. (2016). X-ray computed microtomography to study autogenous healing of cementitious materials promoted by superabsorbent polymers. *Cement and Concrete Composites*, *65*, 83-93.

Snoeck, D., Schaubroeck, D., Dubruel, P., & De Belie, N. (2014a). Effect of high amounts of superabsorbent polymers and additional water on the workability, microstructure and strength of mortars with a water-to-cement ratio of 0.50. *Construction and Building Materials*, *72*, 148 - 157.

Snoeck, D., Schrofl, C., & Mechtcherine, V. (2018). Recommendation of RILEM TC 260-RSC: testing sorption by superabsorbent polymers (SAP) prior to implementation in cement-based materials. *Materials and Structures/Materiaux et Constructions*, *51*(5). https://doi.org/10.1617/s11527-018-1242-8

Snoeck, D., Van Tittelboom, K., Steuperaert, S., Dubruel, P., & De Belie, N. (2014b). Self-healing cementitious materials by the combination of microfibres and superabsorbent polymers. *Journal of Intelligent Material Systems and Structures*, *25*(1), 13-24.

Tang, W., Kardani, O., & Cui, H. (2015). Robust evaluation of self-healing efficiency in cementitious materials - A review. *Construction and Building Materials*, *81*, 233-247.

Teall, O. D., R. ; Pilegis, M. ; Kanellopoulous, A. ; Sharma, T. ; Paine, K. ; Jefferson, A. ; Lark, R. ; Gardner, D. ; Al-Tabbaa, A. (2016). Self healing concrete full scale site trials. 11th fib International PhD Symposium in Civil Engineering, Tokyo (Japan).

Tsangouri, E., Lelon, J., Minnebo, P., Asaue, H., Shiotani, T., Van Tittelboom, K., De Belie, N., Aggelis, D. G., & Van Hemelrijck, D. (2019). Feasibility study on real-scale, self-healing concrete slab by developing a smart capsules network and assessed by a plethora of advanced monitoring techniques. *Construction and Building Materials*, *228*. https://doi.org/10.1016/j.conbuildmat.2019.116780

Tsukamoto, M., & Woener, J. D. (1991). Permeability of cracked fibre-reinforced concrete. *Darmstadt Concrete*, *6*, 123-135.

van Breugel, K. (2007). Is there a market for self-healing cement-based materials? First International Conference on Self-Healing Materials, Noordwijk aan Zee, The Netherlands.

Van Mullem, T., Anglani, G., Dudek, M., Vanoutrive, H., Bumanis, G., Litina, C., Kwiecień, A., Al-Tabbaa, A., Bajare, D., Stryszewska, T., Caspeele, R., Van Tittelboom, K., Jean-Marc, T., Gruyaert, E., Antonaci, P., & De Belie, N. (2020a). Addressing the need for standardization of test methods for self-healing concrete: an inter-laboratory study on concrete with macrocapsules. *Science and Technology of Advanced Materials*, *21*(1), 661-682. https://doi.org/10.1080/14686996.2020.1814117

Van Mullem, T., Gruyaert, E., Caspeele, R., & Belie, N. D. (2020b). First large scale application with self-healing concrete in Belgium: Analysis of the laboratory control tests. *Materials*, *13*(4). https://doi.org/10.3390/ma13040997

Van Mullem, T., Gruyaert, E., Debbaut, B., Caspeele, R., & De Belie, N. (2019). Novel active crack width control technique to reduce the variation on water permeability results for self-healing concrete. *Construction and Building Materials*, *203*, 541-551. https://doi.org/10.1016/j.conbuildmat.2019.01.105

Van Tittelboom, K., & De Belie, N. (2013). Self-healing in cementitious materials - A review. *Materials*, *6*(6), 2182-2217.

Van Tittelboom, K., De Belie, N., Lehmann, F., & Grosse, C. U. (2012). Acoustic emission analysis for the quantification of autonomous crack healing in concrete. *Construction and Building Materials*, *28*(1), 333-341. https://doi.org/10.1016/j.conbuildmat.2011.08.079

Van Tittelboom, K., De Belie, N., Van Loo, D., & Jacobs, P. (2011). Self-healing efficiency of cementitious materials containing tubular capsules filled with healing agent. *Cement and Concrete Composites*, *33*, 497-505.

Van Tittelboom, K., Wang, J., Araújo, M., Snoeck, D., Gruyaert, E., Debbaut, B., Derluyn, H., Cnudde, V., Tsangouri, E., Van Hemelrijck, D., & De Belie, N. (2016). Comparison of different approaches for self-healing concrete in a large-scale lab test. *Construction and Building Materials*, *107*, 125-137.

Van Tittelboom, K. G., E. ; Rahier, H. ; De Belie, N. (2012). Influence of mix composition on the extent of autogenous crack healing by continued hydration or calcium carbonate formation. *Construction and Building Materials*, *37*, 349-359.

Wang, J. Y., Soens, H., Verstraete, W., & De Belie, N. (2014). Self-healing concrete by use of microencapsulated bacterial spores. *Cement and Concrete Research*, *56*, 139-152. https://doi.org/10.1016/j.cemconres.2013.11.009

Wang, X., Fang, C., Li, D., Han, N., & Xing, F. (2018). A self-healing cementitious composite with mineral admixtures and built-in carbonate. *Cement and Concrete Composites*, *92*, 216-229.

Wang, X., Huang, Y., Huang, Y., Zhang, J., Fang, C., Yu, K., Chen, Q., Li, T., Han, R., Yang, Z., Xu, P., Liang, G., Su, D., Ding, X., Li, D., Han, N., & Xing, F. (2019). Laboratory and field study on the performance of microcapsule-based self-healing concrete in tunnel engineering. *Construction and Building Materials*, *220*, 90-101. https://doi.org/10.1016/j.conbuildmat.2019.06.017

Wang, X., Xing, F., Zhang, M., Han, N., & Qian, Z. (2013). Experimental Study on Cementitious Composites Embedded with Organic Microcapsules. *Materials*, *6*(9), 4064-4081. https://www.mdpi.com/1996-1944/6/9/4064

Wiktor, V., & Jonkers, H. M. (2012). *The potential of bio-based repair system to increase the durability of repaired concrete structures* Second International Conference on Microstructural-related Durability of Cementitious Composites, Amsterdam, The Netherlands.

Yang, Y., Lepech, M. D., Yang, E.-H., & Li, V. C. (2009). Autogenous healing of engineered cementitious composites under wet–dry cycles. *Cement and Concrete Research*, *39*(5), 382-390. https://doi.org/https://doi.org/10.1016/j.cemconres.2009.01.013

Yildirim, G., Khiavi, A. H., Yeilmen, S., & Sahmaran, M. (2018). Self-healing performance of aged cementitious composites. *Cement and Concrete Composites*, *87*, 172-186. https://doi.org/10.1016/j.cemconcomp.2018.01.004

Zohuriaan, J., & Kabiri, K. (2008). Superabsorbent polymer materials : a review. *Iranian Polymer Journal*, *17*(6), 451 - 477.

APPENDIX A CALCULATION OF REYNOLDS NUMBER

The use of Darcy's law implies the validity of several assumptions: incompressible laminar flow, steady state equilibrium and homogeneous porous material. To verify the laminar state of the flow, the Reynolds number can be calculated with **Eq. A.1**, with ρ = the density of water (kg/m³), v = the flow velocity (m/s), L = the characteristic length (m) and μ = the dynamic viscosity of water (Pa s).

$$Re = \frac{\rho \, v \, L}{\mu} \qquad\qquad \textbf{(A.1)}$$

The velocity was determined with the highest flow rate recorded in this project (Q_{max} = 3.95x10^{-6} m³/s), divided by the cross-section exposed to the water flow (which is 96 x 96 mm²), while the characteristic length is the average crack width at the notch root. For the experimental program in this research, the following values have thus been considered:

- $\rho = 1000$ kg/m³

- $\mu = 1\text{x}10^{-3}$ Pa s

- $v = 4.29\text{x}10^{-4}$ m/s

- $L = 0.41\text{x}10^{-3}$ m

The Reynolds number is hence equal to:

$$Re = \frac{1000 \,.\, 4{,}29.\, 10^{-4} \,.\, 0{,}41.\, 10^{-3}}{10^{-3}} = 0.18 \qquad\qquad \textbf{(A.2)}$$

This value is way below the limit where the flow is considered laminar (Re < 2000).

APPENDIX B MACROSCOPIC OBSERVATIONS (EXPERIMENTAL PROGRAM 2)
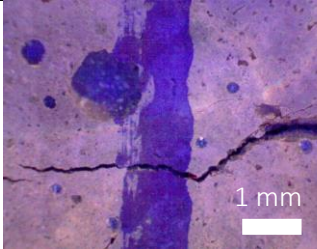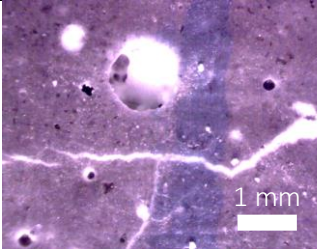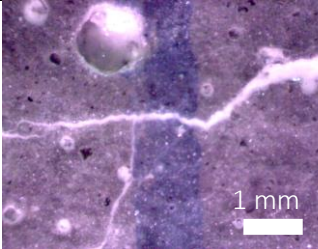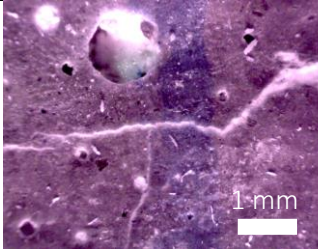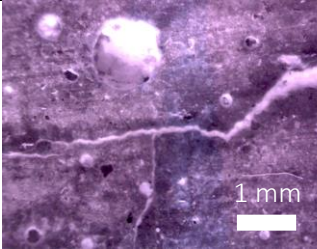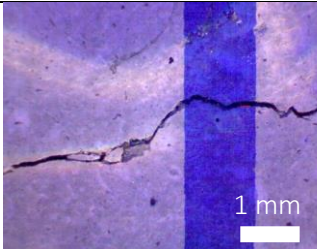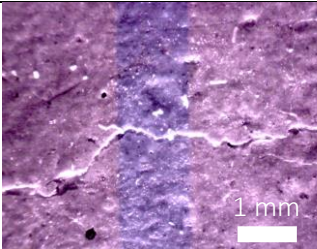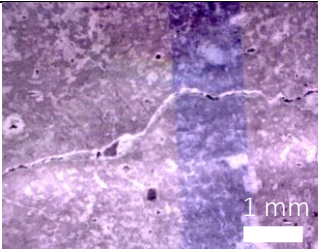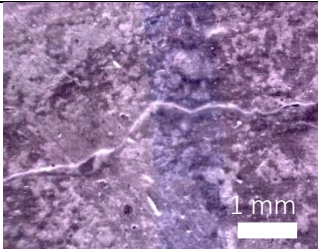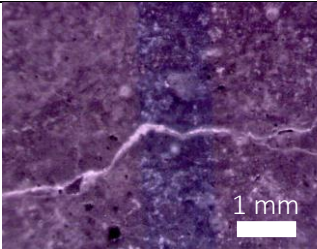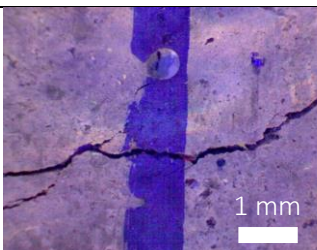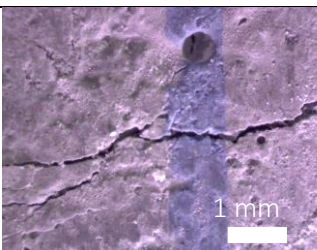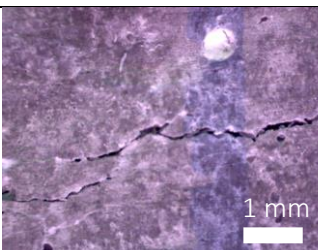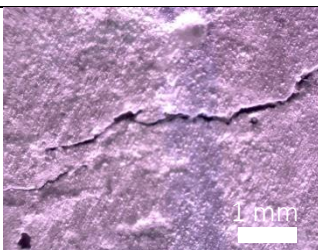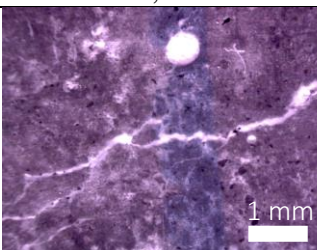
	Initial	11 days	25 days	2 months	3 months
a) Water	$w_i = 0.15$ mm	$HR = 96\%$	$HR = 98\%$	$HR = 99\%$	$HR = 99\%, SR = 89\%$
b) Wet/dry	$w_i = 0.15$ mm	$HR = 90\%$	$HR = 90\%$	$HR = 93\%$	$HR = 95\%, SR = 98\%$
b) Air	$w_i = 0.17$ mm	$HR = 22\%$	$HR = 21\%$	$HR = 37\%$	$HR = 39\%, SR = 95\%$

Figure B.1. Evolution of crack closure for sections of cracks of the control mix: a) prism C1 (face 2) under water immersion, b) prism C12 (face 1) in wet/dry cycles and c) prism C3 (face 1) in ambient air
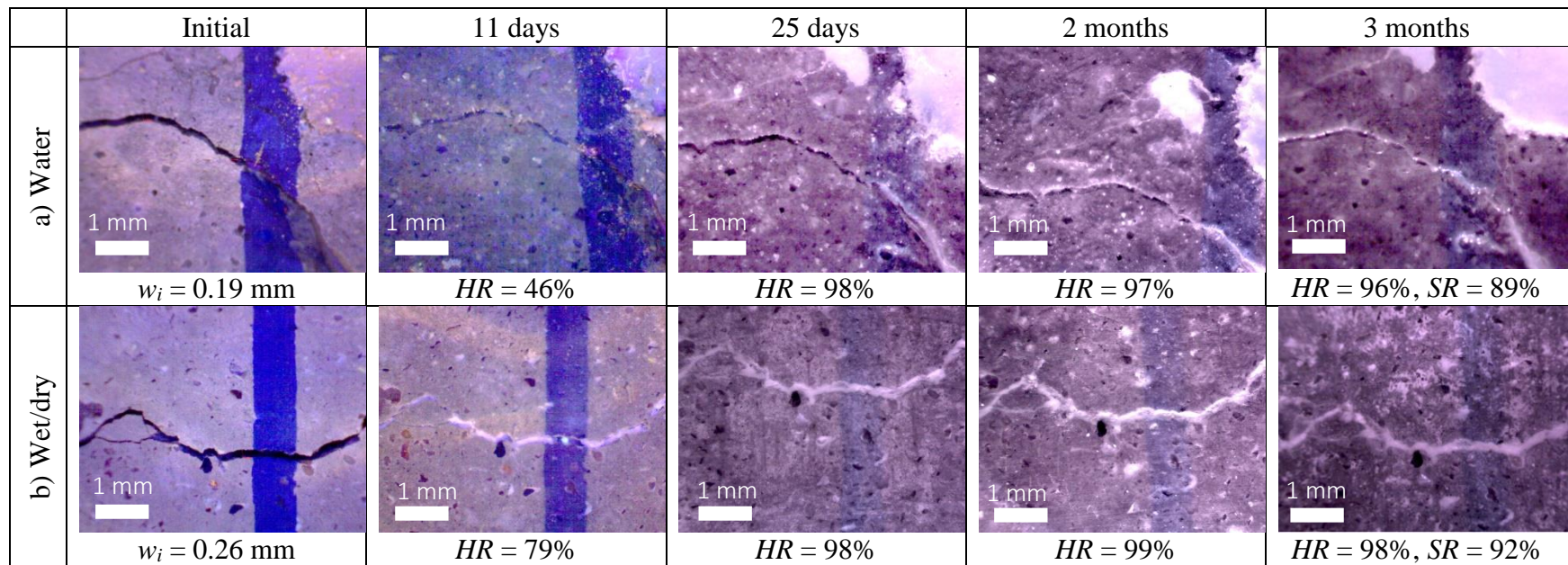
	Initial	11 days	25 days	2 months	3 months
a) Water	1 mm	1 mm	1 mm	1 mm	1 mm
	$w_i = 0.19$ mm	$HR = 46\%$	$HR = 98\%$	$HR = 97\%$	$HR = 96\%$, $SR = 89\%$
b) Wet/dry	1 mm	1 mm	1 mm	1 mm	1 mm
	$w_i = 0.26$ mm	$HR = 79\%$	$HR = 98\%$	$HR = 99\%$	$HR = 98\%$, $SR = 92\%$

Figure B.2. Evolution of crack closure for sections of cracks of the CSA mix: a) prism C7 (face 2) under water immersion and b) prism C2 (face 2) in wet/dry cycles

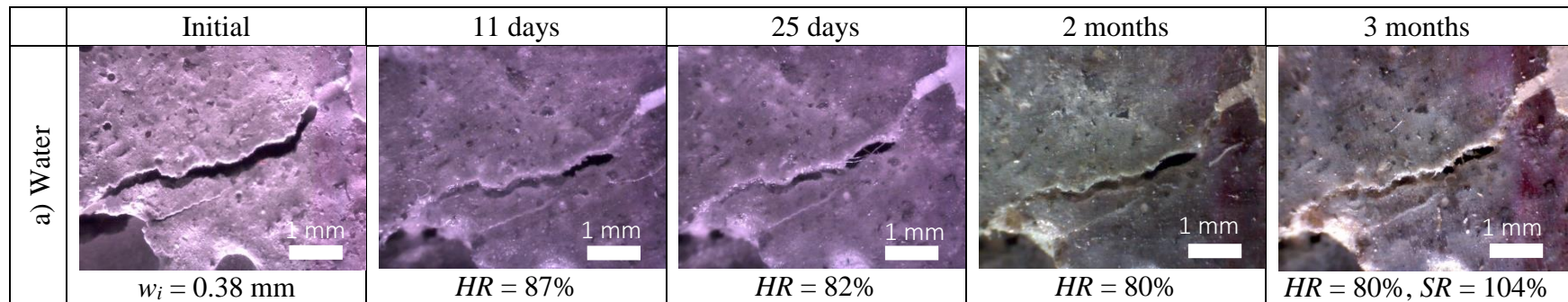|	Initial	11 days	25 days	2 months	3 months
a) Water	1 mm	1 mm	1 mm	1 mm	1 mm
	$w_i = 0.38$ mm	$HR = 87\%$	$HR = 82\%$	$HR = 80\%$	$HR = 80\%$, $SR = 104\%$

Figure B.3. Evolution of crack closure for sections of cracks of the CA mix: a) prism C4 (face 2) under water immersion and b) prism C5 (face 2) in wet/dry cycles

$w_i = 0.36$ mm	$HR = 69\%$	$HR = 86\%$	$HR = 91\%$	$HR = 97\%$, $SR = 100\%$

Figure B.3. Evolution of crack closure for sections of cracks of the CA mix: a) prism C4 (face 2) under water immersion and b) prism C5 (face 2) in wet/dry cycles (cont.)
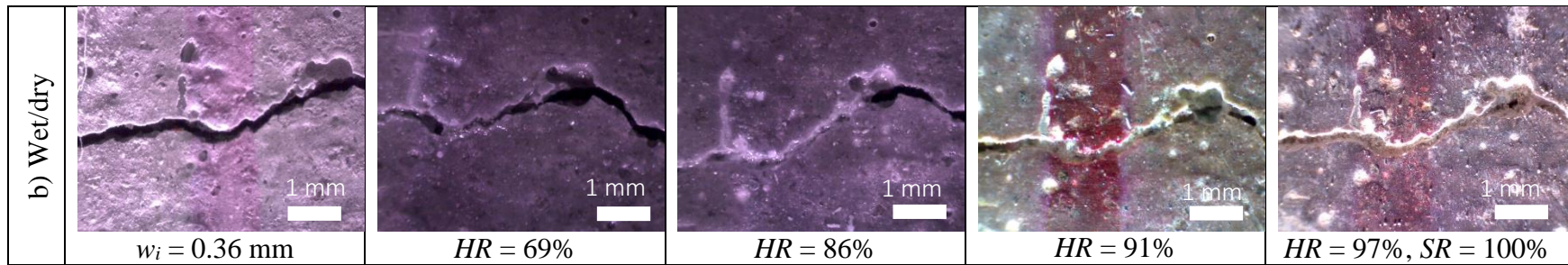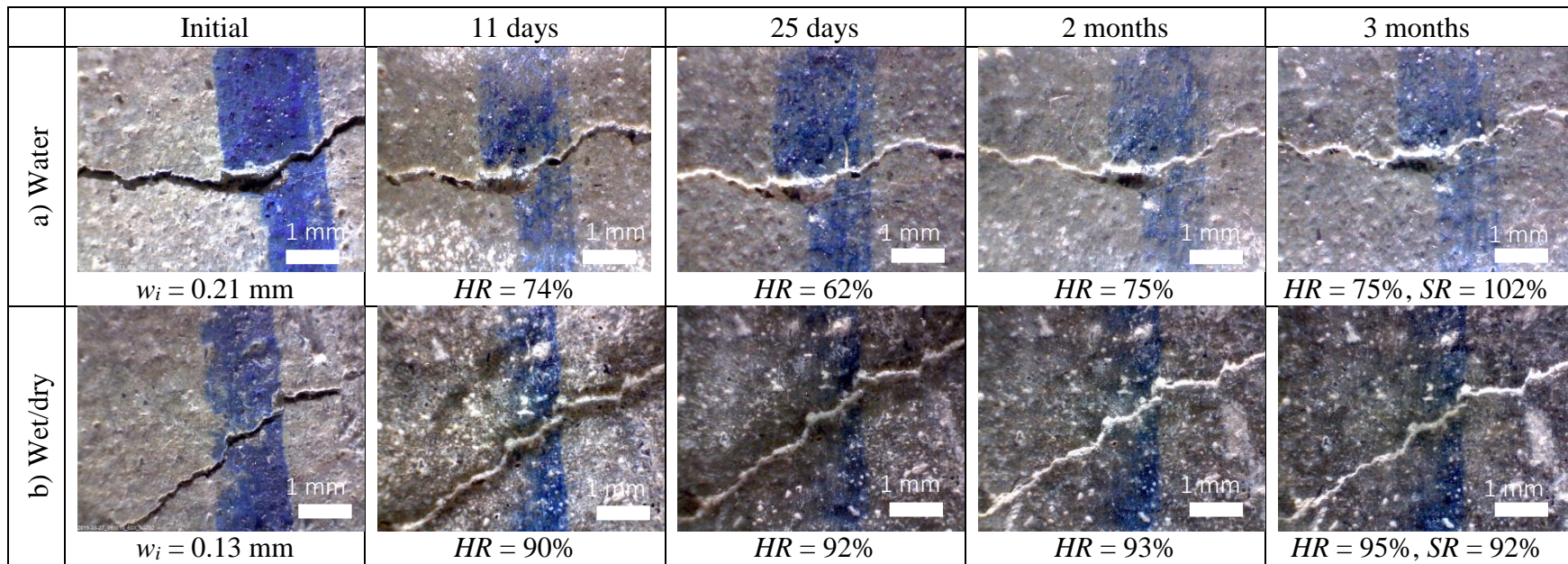

	Initial	11 days	25 days	2 months	3 months
a) Water	$w_i = 0.21$ mm	$HR = 74\%$	$HR = 62\%$	$HR = 75\%$	$HR = 75\%$, $SR = 102\%$
b) Wet/dry	$w_i = 0.13$ mm	$HR = 90\%$	$HR = 92\%$	$HR = 93\%$	$HR = 95\%$, $SR = 92\%$

Figure B.4. Evolution of crack closure for sections of cracks of the SAP mix: a) prism C1 (face 1) under water immersion and b) prism C2 (face 1) in wet/dry cycles
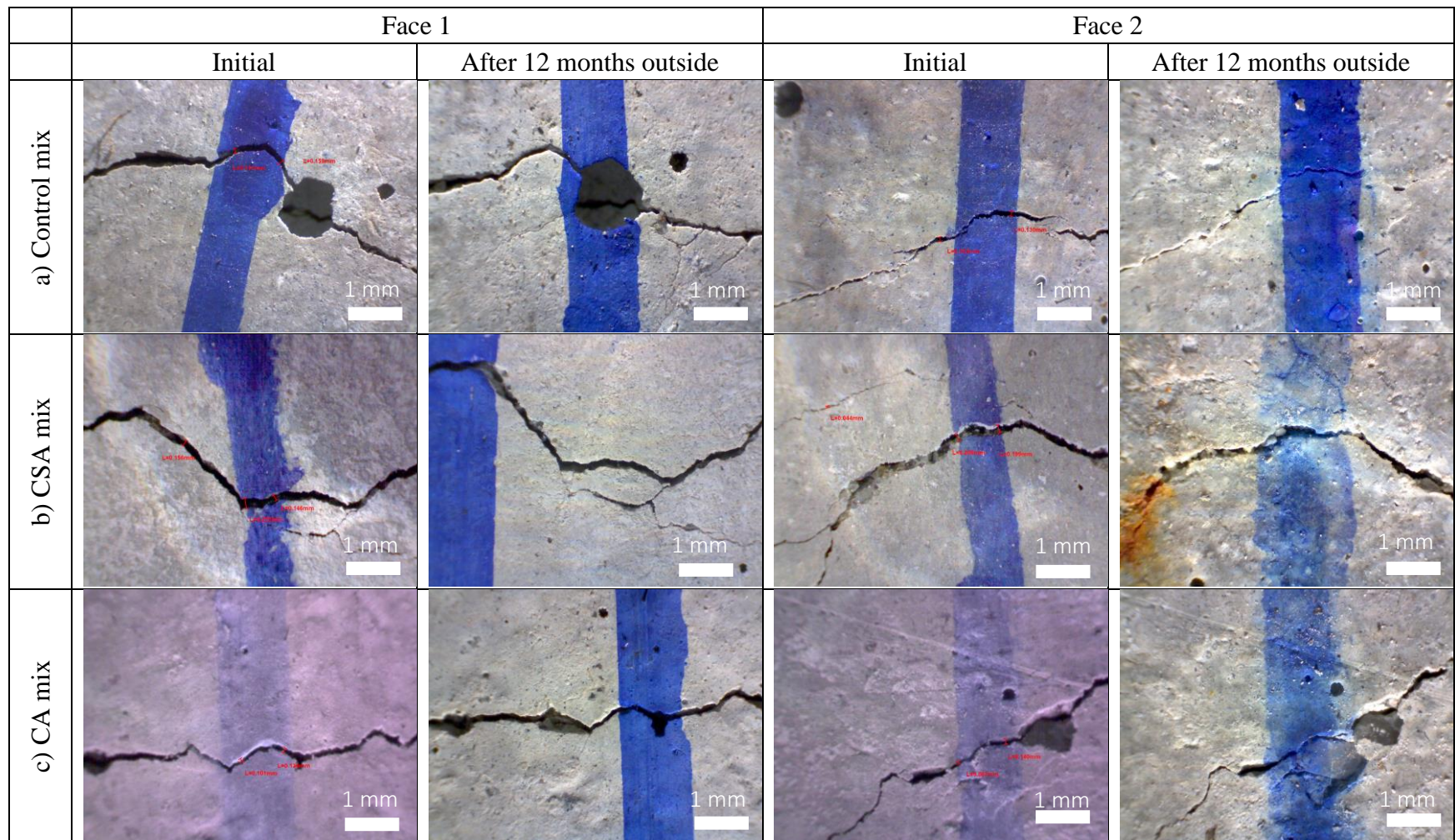
Figure B.5. Macroscopic pictures of cracks at face 1 and face 2 before and after healing in outdoor exposure for: a) control, b) CSA, c) CA and d) SAP mixes
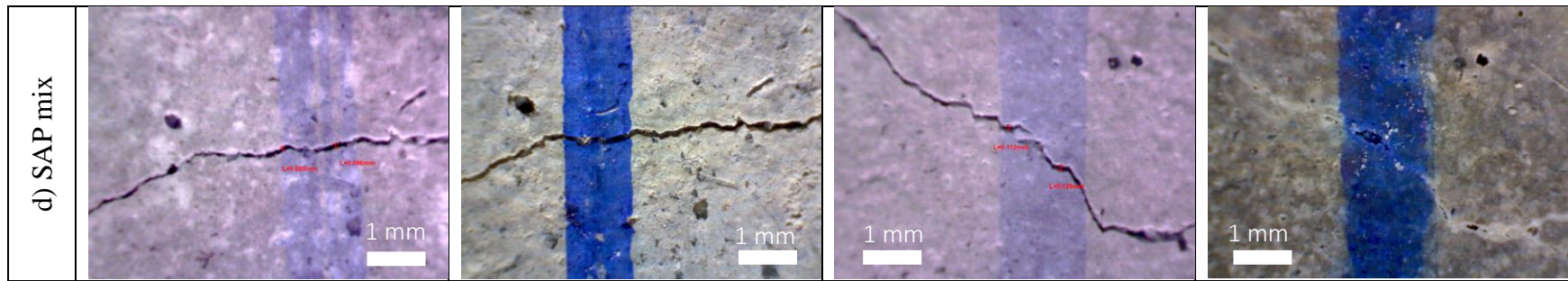
Figure B.5. Macroscopic pictures of cracks at face 1 and face 2 before and after healing in outdoor exposure for: a) control, b) CSA, c) CA and d) SAP mixes (cont.)

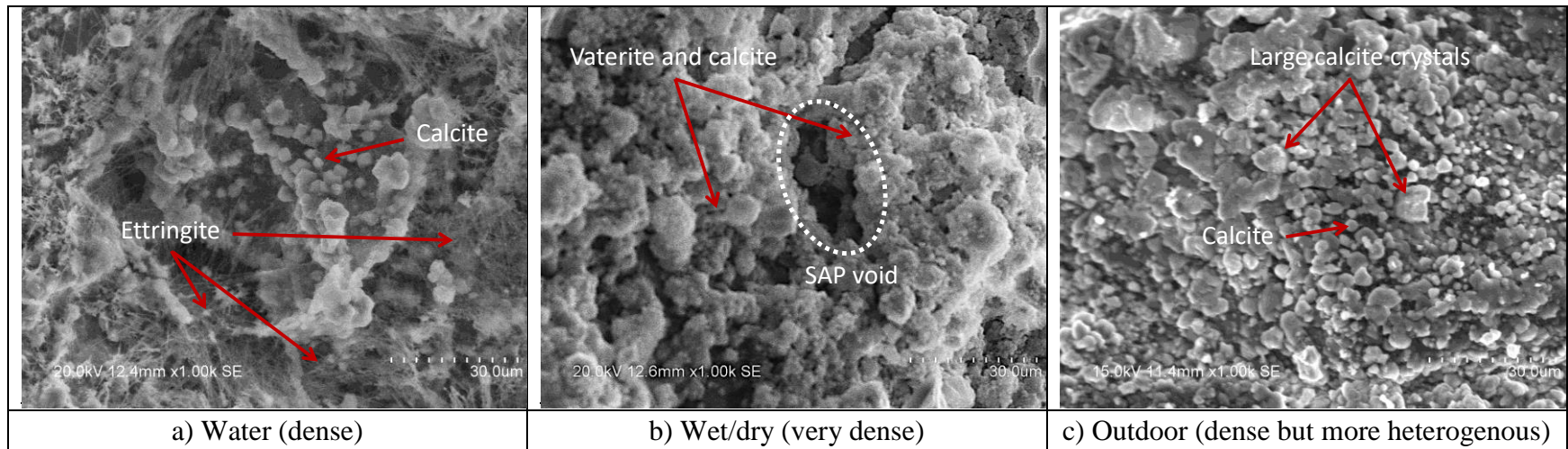# APPENDIX C MICROSCOPIC ANALYSES (EXPERIMENTAL PROGRAM 2)

| a) Water (dense) | b) Wet/dry (very dense) | c) Outdoor (dense but more heterogenous) |

Figure C.1. Summary of different healing products and densities found (example for the SAP mix) in a) water, b) wet/dry and c) outdoor expositions (X 1000 magnification)
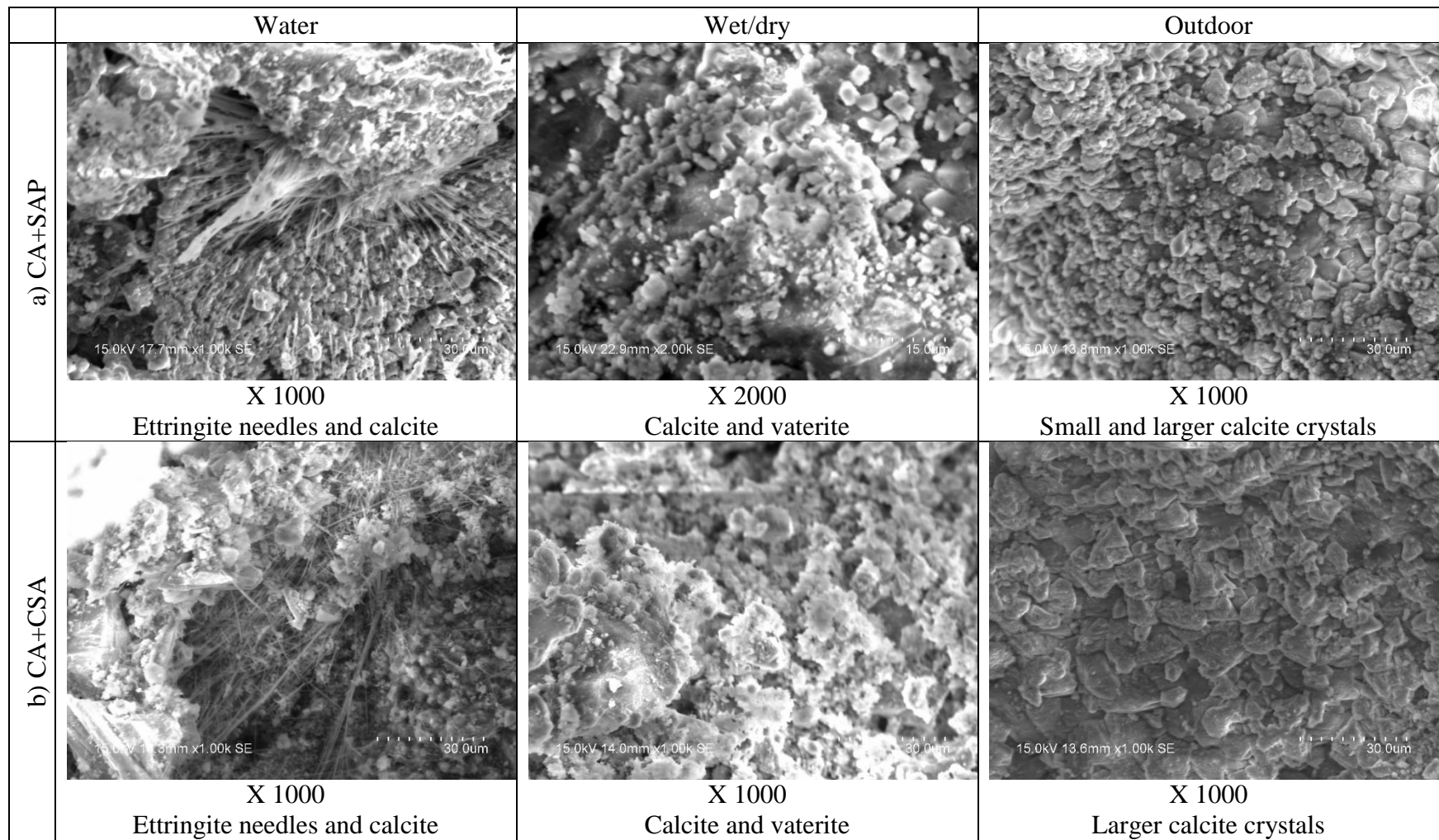
Water	Wet/dry	Outdoor
X 1000	X 2000	X 1000
Ettringite needles and calcite	Calcite and vaterite	Small and larger calcite crystals
X 1000	X 1000	X 1000
Ettringite needles and calcite	Calcite and vaterite	Larger calcite crystals

a) CA+SAP

b) CA+CSA

Figure C.2. Microstructure in water, wet/dry and outdoor exposures for a) CA+SAP and b) CA+CSA mixes